

METHODS IN IMAGE PROCESSING TO IMPROVE UNDERSTANDING OF
LASER INDUCED FLUORESCENCE RESPONSE IN MOSS
TO METAL AND ENVIRONMENTAL STRESS

A DISSERTATION SUBMITTED TO THE GRADUATE DIVISION OF THE
UNIVERSITY OF HAWAI'I AT MĀNOA IN PARTIAL FULFILLMENT
OF THE REQUIREMENTS FOR THE DEGREE OF

DOCTOR OF PHILOSOPHY

IN

EARTH AND PLANETARY SCIENCES

AUGUST 2023

By

Kelly Truax

Dissertation Committee:

Henrietta Dulai, Chairperson

Anupam Misra

Milton Garces

Wendy Kuhne

Celia Smith

Keywords: Moss, Bryophyte, Metal Contamination, Environmental Contamination, Metal
Detection, Laser Induced Fluorescence, Image Processing

Acknowledgments

A great deal of effort and expertise went into developing the techniques laid out as part of this work and I would be amiss to not recognize the many people who made it possible. As a part of work funded by the Consortium for Monitoring, Technology, and Verification (MTV) and in partnership with the University of Michigan, I am grateful to have been brought on to work on a proposal they deemed of great interest to the Department of Energy (DOE) and the National Nuclear Security Administration (NNSA). MTV allowed me to attend many conferences and workshops, build dialogue and relationships, and develop professionally in ways that often pushed me to give back, not only to those who came before me, but also those who are certain to follow. To Sarah Pozzi, Shaun Clarke, Courtney Wagner, and John Rodriguez, thank you for the tireless work you put into the consortium and its mission to educate and provide opportunities for students. I'd also like to thank Laura Tovo and Wendy Kuhne from SRNL for their wonderful ideas when I started out and to those members at LLNL who provided fantastic ideas for me to explore with our new laser system. I also want to say thank you to all of the people over the years who asked questions, provided ideas, or just genuinely wanted to know more. It helped me tremendously to be thoughtful about not just how I talk about my work, but to understanding the importance of knowing who the work is for and that it should be shared. There are too many of you to name individually, but please know each of you shaped not only the research but my experiences.

To my committee members for coming along with me on this journey, I offer a thank you that is most definitely not big enough for all of the experience and wisdom you have offered. Whether it be talking professional development and signal processing with Milton Garces, learning the in's and out's of emission and excitation with Anupam Misra, or thinking about the broader applications of the technique in terms of future endeavors with Wendy Kuhne each was important to my graduate degree and the end product of this dissertation. Without Anupam we wouldn't have even had a project to begin with, and many of the experiments in this work came out of the things we've learned together and he has been willing to share. Wendy also played quite a role during my Master's Thesis to shape many of the ideas we ended up pursuing as research in the following pages. To Celia Smith and her graduate students (Scott Van De Verg and Angela Richards Donà), I have to offer not only thanks but extreme awe at what you do. I've only begun to scratch the surface of the mysteries of botany and your boundless knowledge has helped to spark new ideas, confirm old experiments, and open a whole world of possibilities. My only regret is how little time we've had and the great fun I'm sure we could have concocted just to see what was possible.

To the staff and faculty of EPS and HIGP who have been friends, colleagues, and mentors, thank you for teaching me to slow down sometimes and look around me and this beautiful community. To

Kathleen Ruttenberg who treated my queries and comprehensive examination with enthusiasm and care. You directly impacted the way I think about writing papers for journals and reigniting my passion for geochemistry. To Peter Englert who gave me a great first semester and taught me that the right answer is only as useful as the skills we build to get to it. To Garrett who put me on the path to integrating coding into my work and continues to advocate for the students and department. To Gary Huss who made the Nuclide Chart not only interesting but useful for understanding the world around us. To Eric Gaidos who was the fearless leader of a collaborative paper that gave me my first taste at publication. To Lily, Arlene, Chad, Jason, Susan, Anela, and Lori, thank you for answering my questions, helping me navigate travel and expenses, and overall, just being willing to talk about anything and everything. Finally, I like to say thank you to Jasper Konter who passed away last Summer. Though he is no longer with us, he was the first professor I had in class after coming to Hawai'i and his welcoming presence set the tone for all the positive people and experiences I would have in the 4 years to follow. I still forget every once in a while that you're gone, and will get hopeful I'll see you in the hallway as we cross paths on the way to the lab. Just know I've always got a friendly smile and wave waiting for you.

I was proud to serve as a graduate representative and liaison between faculty and students towards a department that embraces each of us while also being humble enough to know where we could improve. Even though my work was well outside the scope of most students, everyone was helpful, supportive, and curious. Especially my fellow graduate students who were happy to talk all things research and non-research related. Thank you for making me laugh and for constantly reminding me that even if things are difficult, we're in this together and that makes us stronger. To Kei, Sarah, Jonathan, Shirin, and Wyatt, thanks for including me in your cohort and talking code with me whenever I found myself stuck. I only hope that I have been able to support you as much as you have supported me while at UHM. To Haley Currier, thanks for jumping on board with my project with both feet and even creating new ideas. I'm very proud to have been able to work with you and hope that your continued experiences only grow. To Sarah Obra Nakata, thanks for finding the work interesting enough to spend a whole REU working with me and always laughing along. You widened my experience working with undergraduates and taught me what works well for supporting those taking on projects for the first time.

To my friends and family, I apologize. When I finished my Master's I'm sure many of you thought I had stopped talking about moss, but instead I doubled down. Thank you to my parents, Dennis and Jeanie, for always cheering me on when I was struggling to find the confidence in my own voice. Thank you for always telling me it was okay to get cake when times were hard and for reminding me to get cake and celebrate the wins. I often get focused on what comes next and you helped me remember the milestones I passed to get here. To my sister Courtney who just received her Doctorate in Nursing this past December. Thanks for saying I inspired you to finally get that final degree and for the healthy

competition to the finish line. Congrats on the win and the degree. Thank you to my friends who week in and week out gave me a space and time to separate from my work and have a little fun. To the girls I've lived with in our shared living house, (TK, Jade, Arielle, Ana, Yuka, and Shae) thanks for reminding me to eat, relax, and go to the beach sometimes. It doesn't mean I followed the advice, but you made the ride all the more memorable. I'll miss all of you and our Pink House. To Russell who supported me in moving to Hawai'i to get a degree and keeps reminding me how wonderful the world can be, I can't say thank you enough. The fact that you stuck it through the highs and lows and still enjoy my company baffles me every day. Thanks for always inspiring me look at things from a different perspective and for embracing my flaws.

And finally, and perhaps most importantly I want to thank my advisor, Henrietta Dulai. I often feel I was pushing you this way and that way trying to get things done at an absurd pace. Thank you for reminding me to slow down and, not only take a second look, but to allow time for new ideas and questions to arise. You were right. It always led to a better product in the end. I'm also sorry it took so long for me to realize how you process and interpret data. It was a fantastic learning experience for me to rethink not only how I talk about my work, but how I present and show the findings. I still love tables and color coding, but there are so many other ways to describe data. Thank you for supporting me when I wanted to take on new projects and skills. Thanks for the long talks about work, the department, or just to check in. Coming to the end I do wish we had more time to work on things, more ideas to explore, more challenges to tackle. Not that we haven't done enough, but because what was done and the journey there were an absolute pleasure. Truly, thank you for taking a chance on me 4 years ago to pick up a new project and run with it and to follow along. I promise next time I'll work harder not to drag you around.

With that there's only one more thanks to give, and that is to whomever reads this work. Thanks for taking the time. I hope you find it interesting and that don't hesitate to reach out should you want to know more.

-Kelly Truax

Funding: This work was funded by the Consortium for Monitoring, Technology, and Verification under Department of Energy National Nuclear Security Administration award number DE-NA0003920.

Abstract

The ability to detect, measure, and locate the source of contaminants or radionuclides is of ongoing interest. There are many techniques for modeling atmospheric transport, sampling near sites of known contamination, and monitoring locations of interest. A widely-used tool for identification and bioremediation comes in the form of vegetation that can serve as indicators of recent and historic events. Large scale vegetation sampling, however, can be costly and labor-intensive, making a non-invasive in-situ technique an attractive alternative. Laser induced fluorescence (LIF) emission is quickly gaining efficacy as a tool to excite biologically-critical molecules, such as chlorophyll, and thereby observe the health of plants and algae. Such techniques are comparable to spectrophotometry, but with the potential benefit of being portable. The technique presented here uses images collected of LIF in moss (*Thuidium plicatile*) using a CMOS camera to identify the presence of different metals in healthy and impaired tissues. RGB data from each image is recorded and used to create density histograms of each color channel's relative abundance of pixels where a specific color corresponds to a decimal code value ranging from 0 to 255. Changes in these histograms correlate to shifts in chlorophyll emission and help in the positive identification of very small tissue concentrations at nmol per cm² levels of copper, zinc, and lead (Cu, Zn, Pb), as well as mixtures of metals. The research focuses on applications of the technique to compare metal contamination to background levels in moss tissues as well as to photoperiod and environmental stressors. Testing included a chlorophyll specific laser system (Semi-conductor diode 445 nm and 462 nm) alongside a Yg:ND pulsed system (355 nm and 532 nm).

Abbreviations

CoCoBi – Color Compact Biofinder; developed by Misra et al. (2021) for future NASA missions to remotely detect biological materials. It uses a 532nm green laser and 355nm UV laser that fire in tandem at nanosecond pulses. It is designed to use nanosecond laser pulses with a compact color CMOS camera as the detector to collect time-resolved images of fluorescence emission by plant tissues.

Chl – Chlorophyll. Often used in the text to refer to chlorophyll -a, -b, a/b ratio, or total chlorophyll content per unit area or weight of tissue.

Chl-SL – Chlorophyll Specific Laser system; can use either a 445 nm blue laser (Chl-a specific) or 462 nm blue laser (Chl-b specific) with or without bandpass filter (650 nm for chl-b and 670 nm for Chl-a). Uses the same CMOS camera from the CoCoBi as a detector to collect images of fluorescence emission responses.

CMOS – Complementary Metal Oxide Semiconductor camera with transistors at every pixel translating light to electrons using about 100x less power than a CCD camera. Though more cost effective, they have less light sensitivity and are more susceptible to the introduction of noise.

Cu – copper

CuCl₂ – copper chloride

DI – deionized water

DOE – U.S. Department of Energy

DTW – Dynamic Time Warping; method for finding the distance between two curves and calculating the path that minimizes the cumulative distance between those points

DCV – Decimal Code Values

LIF – laser induced fluorescence; the technique of using a laser to excite particles which release energy when they return to a stable state which appears in different wavelengths of light, also known as fluorescence emission.

LLNL – Lawrence Livermore National Laboratory

MTV – Consortium for Monitoring Technology and Verification (University of Michigan)

N - nitrogen

Nd:YAg – Neodymium-doped yttrium aluminum garnet crystal (Nd:Y₃Al₅O₁₂) that is used as a lasing medium for solid-state lasers.

NNSA – National Nuclear Security Administration

Pb - lead

Pb(NO₃)₂ – lead nitrate

RGB – red-green-blue; specifically, in reference to color spectrum or decimal codes as they pertain to red, green, and blue color channels.

SRNL – Savannah River National Laboratory

Zn – zinc

ZnCl₂ – zinc chloride

Data Availability

The code created as part of this research is open to the public for use. Though it was developed in MATLAB® the work is translational to use in Python by using Scikit-learn's library. A GitHub repository has been created for the Dissertation work with individual branches for each research chapter. At this time, all data including images have been uploaded as compressed folders on the University Google Drive associated with ktuax@hawaii.edu. Hard copies of the images have been stored for future use and can be provided per request should the original versions be inaccessible. If the Google Drive is no longer active, please refer to updates on GitHub regarding author communication and data availability.

Google Drive –

https://drive.google.com/drive/folders/1CFIU4aufgV62G_XvzIM717GSxZXbcWNd?usp=drive_link

GitHub – https://github.com/KTruax/Truax_PhD_2023.git

Note on Moss Species

Thuidium plicatile is a moss species indigenous to Hawai'i (Staples et al., 2004) and the one chosen to be used for experimentation and observation. The specific specimen used was collected from O'ahu along the Wa'ahila Ridge Trail. A frond-like species in appearance, *Thuidium plicatile* is similar in appearance to the invasive *Hypnum plumaeforme* Wilson (Crum & Mueller-Dombois 1968; Hoe 1974) which is not recorded as being present on O'ahu (Staples et al., 2004). *Thuidium plicatile* Mitt. and *Thuidium plicatile* Mitt. var. *brevifolium* E.B. Bartram are more broadly recognized as synonyms of *Thuidium cymbifolium* Dozy & Molk (Hoe 1974; Touw, 2001). *Thuidium* is the genus of moss in the family *Thuidiaceae* so named for the fronds appearing to look like small cedar trees with creeping, branching and pinnate leaves. 191 accepted species names are known in the genus *Thuidium* with all existing in temperate to tropical climates (The Plant List, 2013; World Flora Online, 2023). With that knowledge, if you are encouraged to work with a moss species you do not have to rely solely upon *Thuidium plicatile* as a means of conducting research as there are many other species in existence.

TABLE OF CONTENTS

ACKNOWLEDGEMENTS	ii
ABSTRACT	v
ABBREVIATIONS	vi
DATA AVAILABILITY	viii
NOTE ON MOSS SPECIES	viii
TABLE OF FIGURES	xii
TABLE OF TABLES	xv
<u>1 INTRODUCTION</u>	<u>1</u>
1.1 MOTIVATIONS FOR RESEARCH	1
1.2 HEAVY METALS AND MOSS AS A BIOMONITOR	1
1.3 LIF AND THE ROLE OF CHLOROPHYLL	3
1.4 OUTLINE OF DISSERTATION	4
<u>2 LASER INDUCED FLUORESCENCE FOR MONITORING ENVIRONMENTAL CONTAMINATION IN VEGETATION</u>	<u>5</u>
2.1 ABSTRACT	5
2.2 INTRODUCTION	5
2.3 METHODOLOGY	8
2.3.1 LABORATORY PROCEDURE	9
2.3.2 IMAGING USING THE CoCoBi	11
2.3.3 DATA ANALYSIS	11
2.4 RESULTS	15
2.4.1 ANALYSIS METHOD COMPARISON AND PARAMETER OPTIMIZATION	15
2.4.2 SINGLE COLOR ANALYSIS USING DENSITY DIFFERENCE	21
2.4.3 TWO COLOR ANALYSIS USING DTW	24
2.4.4 MULTI-COLOR RATIOS AS A MEANS OF STRESSOR DETERMINATION	26
2.5 DISCUSSION	29
2.6 CONCLUSION	33
<u>3 COMPARISON OF TWO LASER SYSTEMS TOWARD AN IMPROVED TECHNIQUE USING LIF TO MONITOR CHLOROPHYLL RESPONSE IN MOSS</u>	<u>34</u>
3.1 ABSTRACT	34
3.2 INTRODUCTION	34
3.3 METHODOLOGY	37
3.3.1 LABORATORY CULTIVATION AND CU TREATMENT	38
3.3.2 LASER SYSTEMS AND LIF TECHNIQUE	38
3.3.3 CHEMICAL ANALYSIS	41

3.3.4	DATA ANALYSIS	43
3.4	RESULTS	44
3.4.1	COMPARISON OF IMAGE ANALYSIS METHODS	44
3.4.2	COMPARISON OF CoCoBi AND CHL-SL RESULTS	48
3.4.3	METAL AND CHLOROPHYLL EXTRACTION	51
3.5	DISCUSSION	54
3.6	CONCLUSION	57

4 EXPLORING NATURAL VARIABILITY OF CHLOROPHYLL AND CU UPTAKE IN MOSS USING LIF **59**

4.1	ABSTRACT	59
4.2	INTRODUCTION	59
4.3	METHODOLOGY	62
4.3.1	LABORATORY CULTIVATION AND CU TREATMENT	62
4.3.2	LASER SYSTEMS AND LIF TECHNIQUE	63
4.3.3	CHEMICAL ANALYSIS	65
4.3.4	DATA ANALYSIS	67
4.4	RESULTS	70
4.4.1	PREPROCESSING APPROACH COMPARISON	70
4.4.2	COMPARISON OF LIF APPROACHES APPLIED TO FRONDS	72
4.4.3	COMPARISON OF LIF ANALYSIS TO CHL-SL AND SET FRONDS	78
4.4.4	CHLOROPHYLL EXTRACTION AND SET RESULTS	80
4.5	DISCUSSION	85
4.6	CONCLUSION	88

5 CONCLUSION **89**

5.1	SUMMARY	89
5.2	FUTURE WORK	91

6 APPENDIX **92**

6.1	APPENDIX A	92
6.1.1	COMPARISON OF IMAGES COLLECTED USING THE BIOFINDER AND THE CoCoBi	92
6.1.2	PRELIMINARY TESTING TO CHARACTERIZE Pb AND Zn RESPONSE IN MOSS	93
6.1.3	MIRACLE-GRO NUTRIENTS	95
6.1.4	DENSITY DIFFERENCE CODE	95
6.1.5	COMPARISON OF 24 VS 12-HOUR PLOTS OF DATA	96
6.1.6	NOTES ON GAIN LEVEL AND METHODS USED WHEN COLLECTED IMAGES WITH GREEN LASER	97
6.1.7	UV LASER SUMMARY	98
6.1.8	TABLES ASSOCIATED WITH FIGURES IN MAIN TEXT	108
6.2	APPENDIX B	117
6.2.1	IMAGE ANALYSIS RESULTS FOR ALL LASER WAVELENGTHS AND COMPARISON METHODS	117
6.2.2	TABLES CORRESPONDING TO APPENDIX 6.2.1 FIGURES	126

6.2.3	TABLES CORRESPONDING TO FIGURES IN MAIN BODY	139
6.2.4	ADDITIONAL METAL AND CHLOROPHYLL PLOTS	145
6.3	APPENDIX C	148
6.3.1	IMAGE ANALYSIS RESULTS FOR ALL LASER WAVELENGTHS AND COMPARISON METHODS	148
6.3.2	CHLOROPHYLL AND METAL RESULTS	156
7	REFERENCES	158

TABLE OF FIGURES

FIGURE 2.1: IMAGES OF MOSS SAMPLES	13
FIGURE 2.2: IMAGES OF A TRIAL COLLECTED FROM ONE SESSION BEING COMPARED TO A SINGLE MASTER MEAN CONTROL AND TO MULTIPLE CONTROL IMAGES	14
FIGURE 2.3: SINGLE-COLOR DENSITY DIFFERENCE COMPARISON OF IMAGES OF MOSSES	18
FIGURE 2.4: SINGLE-COLOR DTW COMPARISON OF IMAGES OF MOSSES	19
FIGURE 2.5: TWO-COLOR DTW COMPARISON OF THE METAL GROUP TO THE CONTROL	20
FIGURE 2.6: SINGLE COLOR DENSITY DIFFERENCE	22
FIGURE 2.7: WELCH T-TEST RESULTS OF SINGLE COLOR DENSITY DIFFERENCE	24
FIGURE 2.8: TWO-COLOR DTW	25
FIGURE 2.9: WELCH T-TEST RESULTS OF TWO COLOR DTW	26
FIGURE 2.10: USE OF COLOR RATIOS FROM DENSITY DIFFERENCE	27
FIGURE 2.11: PLOTTED RATIOS OF DENSITY DIFFERENCE	28
FIGURE 3.1: COCOBI AND CHL-SL SIDE BY SIDE FOR DIRECT COMPARISON OF THE SIZE AND FLEXIBILITY OF SET-UP FOR BOTH SYSTEMS.	39
FIGURE 3.2: IMAGES OF THE SAME MOSS SAMPLE TAKEN BY VARIOUS COMBINATIONS OF LASER SYSTEMS	40
FIGURE 3.3: COMPARISON OF MOSS RESPONSE TO BOTH LASERS OF THE COCOBI	45
FIGURE 3.4: COMPARISON OF MOSS RESPONSE TO THE CHL-A LASER	46
FIGURE 3.5: COMPARISON OF MOSS RESPONSE TO THE CHL-B LASER	47
FIGURE 3.6: COMPARISON OF 3 LASER SYSTEMS	49
FIGURE 3.7: MOSS TRAY IMAGES COMPARED TO THE CONTROL AND VALIDATED USING A WELCH T-TEST	50
FIGURE 3.8: CHLOROPHYLL EXTRACTION RESULTS	53
FIGURE 3.9: METAL EXTRACTION RESULTS	53
FIGURE 3.10: CHLOROPHYLL EXTRACTION VERSUS METAL EXTRACTION DRY WEIGHT	54
FIGURE 3.11: CHL-B LASER RESULTS COMPARED TO CHLOROPHYLL EXTRACTION RESULTS OF A/B RATIO AND DRY WEIGHT METAL EXTRACTION.	57
FIGURE 4.1: COMPARISON OF FROND IMAGES USING THE COCOBI, CHL-A, AND CHL-B LASERS.	64
FIGURE 4.2: DENSITY DIFFERENCE AND DTW RESULTS FOR 10 TRAY 3 CONTROL IMAGES COMPARED TO ALL SAMPLES WITHIN THE CONTROL	70
FIGURE 4.3: THE FOUR PLOTS SHOW HISTOGRAMS OF THE SAME IMAGE	72
FIGURE 4.4: COMPARISON OF MOSS RESPONSE TO BOTH LASERS OF THE COCOBI	73
FIGURE 4.5: COMPARISON OF MOSS RESPONSE TO THE CHL-A LASER	74
FIGURE 4.6: COMPARISON OF MOSS RESPONSE TO THE CHL-B LASER	76
FIGURE 4.7: COMPARISON OF 3 LASER SYSTEMS	77
FIGURE 4.8: COMPARISON OF TWO COLOR DTW IMAGE ANALYSIS RESULTS	78
FIGURE 4.9: IMAGES OF SINGLE FROND FOR CHLOROPHYLL EXTRACTION AND A PAIR OF FRONDS FOR METAL EXTRACTION	79
FIGURE 4.10: COMPARISON OF TWO COLOR DTW RVB RESULTS	79
FIGURE 4.11: CHLOROPHYLL EXTRACTION RESULTS	84
FIGURE 4.12: METAL EXTRACTION RESULTS	84
FIGURE 4.13: CHL-B LASER RESULTS COMPARED TO CHLOROPHYLL EXTRACTION RESULTS OF A/B RATIO AND DRY WEIGHT METAL EXTRACTION	85
FIGURE A.1: COMPARISON OF MOSS IMAGED USING THE BIOFINDER AND THE COCOBI	92
FIGURE A.2: 48 HOUR RESPONSE LIF RESPONSE OF CU TREATED MOSS OBSERVED USING THE COCOBI	93
FIGURE A.3: PLOTS OF CU, PB, AND ZN RESPONSE AT MULTIPLE DOSING LEVELS OBSERVED USING THE COCOBI	95
FIGURE A.4: COMPARISON OF DENSITY DIFFERENCE ANALYSIS	96

FIGURE A.5: SINGLE-COLOR DENSITY DIFFERENCE COMPARISON OF IMAGES OF MOSSES COLLECTED USING ONLY THE GREEN LASER	97
FIGURE A.6: SINGLE-COLOR DTW COMPARISON OF IMAGES OF MOSSES COLLECTED USING ONLY THE GREEN LASER	97
FIGURE A.7: TWO-COLOR DTW COMPARISON OF IMAGES OF MOSSES COLLECTED USING ONLY THE GREEN LASER	98
FIGURE A.8: SINGLE-COLOR DENSITY DIFFERENCE COMPARISON OF IMAGES OF MOSSES COLLECTED USING ONLY THE UV LASER	99
FIGURE A.9: SINGLE-COLOR DTW COMPARISON OF IMAGES OF MOSSES COLLECTED USING ONLY THE UV LASER	100
FIGURE A.10: TWO-COLOR DTW DIFFERENCE COMPARISON OF IMAGES OF MOSSES COLLECTED USING ONLY THE UV LASER	100
FIGURE A.11: SINGLE COLOR DENSITY DIFFERENCE ANALYSIS FOR ALL COLOR CHANNELS OF IMAGES TAKEN JUST THE UV LASER.	101
FIGURE A.12: COLOR RATIOS FROM DENSITY DIFFERENCE ANALYSIS OF IMAGES COLLECTED USING THE UV LASER	104
FIGURE A.13: SINGLE-COLOR DENSITY DIFFERENCE COMPARISON OF IMAGES OF MOSSES COLLECTED USING BOTH LASERS TREATED WITH METALS TO THE CONTROL.	106
FIGURE A.14: SINGLE-COLOR DTW COMPARISON OF IMAGES OF MOSSES COLLECTED USING BOTH LASERS TREATED WITH METALS TO THE CONTROL.	107
FIGURE A.15: TWO-COLOR DTW COMPARISON OF IMAGES OF MOSSES COLLECTED USING BOTH LASERS TREATED WITH METALS TO THE CONTROL.	107
FIGURE B.1: COMPARISON OF MOSS RESPONSE TO ALL LASERS OF THE COCOBI USING SINGLE-COLOR DENSITY DIFFERENCE IMAGE ANALYSIS.	117
FIGURE B.2: COMPARISON OF MOSS RESPONSE TO ALL LASERS OF THE COCOBI USING SINGLE-COLOR DTW IMAGE ANALYSIS.	118
FIGURE B.3: COMPARISON OF MOSS RESPONSE TO ALL LASERS OF THE COCOBI USING TWO-COLOR DTW IMAGE ANALYSIS.	119
FIGURE B.4: COMPARISON OF MOSS RESPONSE TO ALL FILTER OPTIONS ON THE CHL-A LASER USING SINGLE-COLOR DENSITY DIFFERENCE IMAGE ANALYSIS.	120
FIGURE B.5: COMPARISON OF MOSS RESPONSE TO ALL FILTER OPTIONS ON THE CHL-A LASER USING SINGLE-COLOR DTW IMAGE ANALYSIS.	121
FIGURE B.6: COMPARISON OF MOSS RESPONSE TO ALL FILTER OPTIONS ON THE CHL-A LASER USING TWO-COLOR DTW IMAGE ANALYSIS.	122
FIGURE B.7: COMPARISON OF MOSS RESPONSE TO ALL FILTER OPTIONS ON THE CHL-B LASER USING SINGLE-COLOR DENSITY DIFFERENCE IMAGE ANALYSIS.	123
FIGURE B.8: COMPARISON OF MOSS RESPONSE TO ALL FILTER OPTIONS ON THE CHL-B LASER USING SINGLE-COLOR DTW IMAGE ANALYSIS.	124
FIGURE B.9: COMPARISON OF MOSS RESPONSE TO ALL FILTER OPTIONS ON THE CHL-B LASER USING TWO-COLOR DTW IMAGE ANALYSIS.	125
FIGURE B.12: CHLOROPHYLL EXTRACTION VERSUS METAL EXTRACTION WET WEIGHT	147
FIGURE B.13: CHL-A MOSS CONTENT VERSUS CHL-B MOSS CONTENT OVER THE DURATION OF THE EXPERIMENT. BLACK CIRCLES REPRESENT EACH MOSS TRAY AT TIME 0 WHEN DOSED WITH CU.	147
FIGURE C.1: COMPARISON OF MOSS RESPONSE TO ALL LASERS OF THE COCOBI USING SINGLE-COLOR DENSITY DIFFERENCE TO COMPARE ALL COLOR CHANNELS (R,G,B).	148
FIGURE C.2: COMPARISON OF MOSS RESPONSE TO ALL LASERS OF THE COCOBI USING SINGLE-COLOR DTW TO COMPARE ALL COLOR CHANNELS (R,G,B).	149
FIGURE C.3: COMPARISON OF MOSS RESPONSE TO ALL LASERS OF THE COCOBI USING TWO-COLOR DTW TO COMPARE ALL COLOR CHANNELS (R,G,B).	150

FIGURE C.4: COMPARISON OF MOSS RESPONSE TO ALL FILTER OPTIONS FOR THE CHL-A LASER USING SINGLE-COLOR DENSITY DIFFERENCE TO COMPARE ALL COLOR CHANNELS (R,G,B).	151
FIGURE C.5: COMPARISON OF MOSS RESPONSE TO ALL FILTER OPTIONS FOR THE CHL-A LASER USING SINGLE-COLOR DTW TO COMPARE ALL COLOR CHANNELS (R,G,B).	152
FIGURE C.6: COMPARISON OF MOSS RESPONSE TO ALL FILTER OPTIONS FOR THE CHL-A LASER USING TWO-COLOR DTW TO COMPARE ALL COLOR CHANNELS (R,G,B).	153
FIGURE C.7: COMPARISON OF MOSS RESPONSE TO ALL FILTER OPTIONS FOR THE CHL-B LASER USING SINGLE-COLOR DENSITY DIFFERENCE TO COMPARE ALL COLOR CHANNELS (R,G,B).	154
FIGURE C.8: COMPARISON OF MOSS RESPONSE TO ALL FILTER OPTIONS FOR THE CHL-B LASER USING SINGLE-COLOR DTW TO COMPARE ALL COLOR CHANNELS (R,G,B).	155
FIGURE C.9: COMPARISON OF MOSS RESPONSE TO ALL FILTER OPTIONS FOR THE CHL-B LASER USING TWO-COLOR DTW TO COMPARE ALL COLOR CHANNELS (R,G,B).	156
FIGURE C.10: CHLOROPHYLL EXTRACTION RESULTS OF TOTAL CHL, CHL-A AND -B, AND CHL A/B RATIO, COMPARED TO TWO COLOR DTW (RVB) RESULTS	156
FIGURE C.11: METAL EXTRACTION RESULTS OF CU WET WEIGHT OF FRONDS COLLECTED EVERY 24 HOURS COMPARED TO CHL-A AND CHL-B TWO COLOR DTW RESULTS.	157

TABLE OF TABLES

TABLE 2.1: DOSING FOR THE 11 MOSS TRAYS OVER 7 DAYS SEPARATED BY GROUP.	10
TABLE 2.2 – NATURAL OR INTERNATIONAL GUIDELINES FOR METAL CONTENT IN SOIL, WATER, AND AIR	31
TABLE 2.3 – EXAMPLES OF MEASURED WET AND DRY DEPOSITION VALUES FOR CU, ZN, AND PB	31
TABLE 3.1: RESULTS FROM CHLOROPHYLL EXTRACTION	51
TABLE 3.2: RESULTS FROM METAL EXTRACTION	52
TABLE 4.1: RESULTS FROM CHLOROPHYLL EXTRACTION	81
TABLE 4.2: RESULTS FROM METAL EXTRACTION	83
TABLE A.1: TOTAL DOSE ACCUMULATION OVER 48 HOURS	93
TABLE A.2: WELCH’S T-TEST APPLIED TO THE DENSITY DIFFERENCE ANALYSIS	101
TABLE A.3 VALUES CALCULATED FROM DENSITY DIFFERENCE ANALYSIS OF IMAGES COLLECTED USING A UV LASER	105
TABLE A.4: VALUES FOR ALL TRIALS CALCULATED FROM USING THE DENSITY DIFFERENCE	108
TABLE A.5: WELCH’S T-TEST APPLIED TO THE DENSITY DIFFERENCE ANALYSIS	109
TABLE A.6: VALUES FOR ALL TRIALS CALCULATED FROM USING THE DTW	111
TABLE A.7: WELCH’S T-TEST APPLIED TO THE DTW ANALYSIS	113
TABLE A.8: RATIO VALUES OF MULTI-COLOR DENSITY DIFFERENCE COMPARISON	115
TABLE B.1: COMPARISON OF MOSS RESPONSE TO ALL LASERS OF THE COCOBI USING SINGLE- COLOR DENSITY DIFFERENCE IMAGE ANALYSIS.	126
TABLE B.2: COMPARISON OF MOSS RESPONSE TO ALL LASERS OF THE COCOBI USING SINGLE- COLOR DTW IMAGE ANALYSIS.	127
TABLE B.3: COMPARISON OF MOSS RESPONSE TO ALL LASERS OF THE COCOBI USING TWO-COLOR DTW IMAGE ANALYSIS.	129
TABLE B.4: COMPARISON OF MOSS RESPONSE TO ALL FILTER OPTIONS FOR THE CHL-A LASER USING SINGLE-COLOR DENSITY DIFFERENCE IMAGE ANALYSIS.	130
TABLE B.5: COMPARISON OF MOSS RESPONSE TO ALL FILTER OPTIONS FOR THE CHL-A LASER USING SINGLE-COLOR DTW IMAGE ANALYSIS.	131
TABLE B.6: COMPARISON OF MOSS RESPONSE TO ALL FILTER OPTIONS FOR THE CHL-A LASER USING TWO-COLOR DTW IMAGE ANALYSIS.	133
TABLE B.7: COMPARISON OF MOSS RESPONSE TO ALL FILTER OPTIONS FOR THE CHL-B LASER USING SINGLE-COLOR DENSITY DIFFERENCE IMAGE ANALYSIS.	134
TABLE B.8: COMPARISON OF MOSS RESPONSE TO ALL FILTER OPTIONS FOR THE CHL-B LASER USING SINGLE-COLOR DTW IMAGE ANALYSIS.	136
TABLE B.9: COMPARISON OF MOSS RESPONSE TO ALL FILTER OPTIONS FOR THE CHL-B LASER USING TWO-COLOR DTW IMAGE ANALYSIS.	137
TABLE B.10: COMPARISON OF MOSS RESPONSE TO ALL ANALYSIS METHOD USING BOTH LASERS OF THE COCOBI.	139
TABLE B.11: COMPARISON OF MOSS RESPONSE TO ALL ANALYSIS METHOD USING THE CHL-B FILTER WITH THE CHL-A LASER.	140
TABLE B.12: COMPARISON OF MOSS RESPONSE TO ALL ANALYSIS METHOD USING THE CHL-B FILTER WITH THE CHL-B LASER.	142
TABLE B.13: MOSS TRAY IMAGES COMPARED TO THE CONTROL AND VALIDATED USING A WELCH T-TEST	143

1 INTRODUCTION

1.1 MOTIVATIONS FOR RESEARCH

The research is funded and motivated by the goals of the U.S. Department of Energy (DOE) and the U.S. National Nuclear Security Administration (NNSA) to develop new technologies that can aid in the detection or deterrence of nuclear proliferation activities. The work has been a collaboration with the University of Michigan and National Laboratories (SRNL and LLNL) as a part of the Consortium for Monitoring, Technology, and Verification (MTV). The objective of this project was the development and testing of a novel remote sensing technology applicable for the observation of biota. It was determined that this methodology would use laser induced fluorescence (LIF) emission, from chlorophyll in living plants, and image processing for rapid detection of heavy metal or radionuclide presence in the environment due to mining, industry, or contamination events. The ultimate goals were to determine the feasibility of the technique, and if successful, further develop methods for remote sensing, and provide a baseline evaluation of the effectiveness and future applications that are possible with current technology.

1.2 MOSS AS A BIOMONITOR OF HEAVY METAL CONTAMINATION

Metal distribution in the environment from anthropogenic sources have long been a concern, but regulations within the last few decades have made monitoring of industry, mining, and urban development more important. Heavy metals in high concentrations can be bound in soil and desorb into water long after their deposition thereby making monitoring of more recent accumulation(s) challenging (Stankovic, 2014; Norgate et al., 2007). Focusing on atmospheric deposition of these metals of interest can help to distinguish current events in the environment from historic ones (Berg et al., 1995; Wolterbeek, 2002; Stankovic, J.D., 2018). Biota have been used since the 1960's for monitoring bioaccumulation with living plant communities in impacted areas specifically serving not only as indicators of metal toxicity and contamination, but also as habitat health and bioremediation monitors (Tremper et al. 2004). One group of biomonitors are mosses, which have been traditionally used to measure atmospheric deposition of heavy metals in regions that can support growth of natural moss communities.

Mosses have long been used as cost effective monitors of environmental change because moss are resilient to various contamination sources, large surface to weight ratio, distribution throughout differing environments, and simple tissue structure (Sun et al., 2009; Serbula et al. 2012; Suchara et al. 2011). Their lack of a true root system limits heavy metal accumulation to atmospheric deposition across their photosynthetic surface (Berg & Steinnes, 1997; Degola et al., 2014). Specific metal accumulation varies with moss surface area and molecular differences in cell wall composition (Chakraborty & Paratkar, 2006; Sarkar et al., 2009; Stanković et al., 2018; Petschinger et al., 2021). Essential micro-nutrients such as Cu, Zn, and Ni are typically preferentially taken up and incorporated into cellular structures because of their importance in metabolic processes, while non-essential elements like Pb and Hg could be adsorbed as particulate matter on the surface, bound to chelating sites in the cell wall, or absorbed and deposited in and around cells (Vázquez et al., 1999b; Macedo-Miranda et al., 2016). Non-essential metals are usually toxic to plants in any amount, but high levels of essential micro-nutrients have also been shown to also alter chloroplasts and total chlorophyll content (Nagajyoti et al., 2010; Krzesłowska, 2011; Choudhury & Panda, 2005; Tremper et al., 2004; Sun et al., 2009). High levels of Cu were consistently found across studies to cause change in chlorophyll content and affect the ratio of Chl -a and -b (*Thuidium delicatulum* (L.) Mitt., *Thuidium sparsifolium* (Mitt.) Jaeg., and *Ptychanthus striatus* (Lehm. & Linderb.); Shakya et al., 2008). These changes in Chl have been documented using spectrophotometry, PAM (Pulse-Amplitude-Modulation), and laser induced fluorescence (Truax et al., 2020; Truax et al., 2022).

Previous work (Truax et al., 2022) focused on developing a proof-of-concept methodology applying image analysis of LIF response in mosses could identify Cu contamination in those living tissues. That work specifically used the “Standoff Biofinder” (Misra, 2018), which was a pulsed Nd:YGa dual laser system (green 532 nm excitation laser and UV 355 nm excitation laser) fired at a nanosecond rate. It was found that differentiation of Cu concentrations at varying $\mu\text{mol}/\text{cm}^2$ levels was possible based on comparison of color histograms of treated moss to control samples. However, those levels of Cu tested would only be found in the most contaminated sites. It was determined that future work, now presented here, would focus on determining the best methods to improve the application of LIF to detect metal accumulation in mosses while improving sensitivity detection to nmol/cm^2 levels.

1.3 LIF AND THE ROLE OF CHLOROPHYLL

Inducing fluorescence emission in chlorophyll has been used widely to evaluate plant physiology and characterize photosynthetic efficiency (Krause & Weis, 1991; Kolber et al., 2005). Chlorophyll content can play a large role in the ability to monitor changes within a plant due to stressors or physiological factors (Chappelle et. al., 1984). The degree of fluorescence, or intensity, depends on both the light source and the properties of the sample's molecular structure (Valeur & Berberan-Santos, 2011). Of the available portable technology, pulse amplitude modulation (PAM) is the most commonly used for leaf-level investigations, but remains impractical for application to remote sensing (Schreiber et al. 1986; Schreiber & Bilger 1993; Schreiber, 2004; Brooks & Niyogi, 2011; Haidekker et al., 2022). When considering alternatives, lasers can be used to produce a broad range of wavelength excitations making lasers excellent sources of light for inducing fluorescence emission of Chl (Valeur & Berberan-Santos, 2011; Silvia & Utkin, 2018).

Laser induced fluorescence (LIF) emission is still a relatively new technique being applied in the biological sciences to monitor shifts in photosynthetic physiology and chlorophyll-a light harvesting in plants, corals, and algae (Brach, 1977; Buschmann 2007). Fluorescence emission is induced via laser excitation beam that allows capture of the short life-time fluorescence emission of living plant material. The laser excites molecules using electromagnetic radiation which is absorbed and quickly released as a spontaneous emission of light at lower energy levels but larger values for wavelength (Kinsey, 1977; Maarek & Kim, 2001). LIF offers the ability for in-situ non-destructive measurements without the need for close-up devices, such as PAM, or reliance on long distance satellite information. This non-invasive technique shows promise as a complement to traditional sampling while allowing for repeated measurements of the same habitat. In the case of this research, a CMOS camera is used in place of a spectrometer increasing the flexibility in placement relative to the laser (side-by-side), compact size, and reduced cost with limited loss of sensitivity. The benefits in LIF when compared with near-infrared spectroscopy are LIF's non-destructive method, portability, and the ability to take measurements under daylight at considerable distance (Gameiro, 2016; García-Sánchez et al., 2017; Marques de Silva, 2018; Tan et al., 2019).

1.4 OUTLINE OF DISSERTATION

The following dissertation will outline three experiments conducted to better understand response by the moss, *Thuidium plicatile*, to background contaminate exposure using LIF paired with image analysis. Original work from a Master's Thesis (Truax et al., 2020) developed a method to detect contaminants using LIF to observe responses by this moss to Cu treatment. The work of this dissertation extends that foundational work to explore the feasibility of incorporating LIF into laboratory or field work with the benefit of reducing labor and costs from more traditional sampling and chemical analysis techniques. The second chapter focuses on multiple stressors and metal types while also introducing new methods for comparison between treated and untreated trials. The third chapter delves into the development and application of a chlorophyll specific laser design, while also comparing the new system to the originally used "CoCoBi" (Misra et al. 2021). The final chapter adapts previous techniques to new image data in the form of individual moss fronds to better understand the natural variability of chlorophyll response within the moss species. Finally, the major conclusions and suggestions for future applications will be discussed.

2 LASER INDUCED FLUORESCENCE FOR MONITORING ENVIRONMENTAL CONTAMINATION IN VEGETATION

2.1 ABSTRACT

The ability to detect, measure, and locate the source of contaminants, especially, heavy metals and radionuclides is of ongoing interest. A common tool for contaminant identification and bioremediation comes in the form of vegetation that can serve as indicators of recent and historic pollution. However, large scale sampling can be costly and labor-intensive. Hence, non-invasive in-situ techniques such as laser induced fluorescence (LIF) are becoming useful and effective ways to observe the health of plants and algae through the excitation of organic molecules, e.g. chlorophyll, through indirect measurement. Such techniques are comparable to spectrophotometry but with the potential benefit of being portable. This research supports image analysis of LIF through comparison with traditional, destructive methods to assess efficacy. The technique presented utilizes images collected of LIF emission in moss to identify different metals known to be present at different dosing concentrations. Analysis through image processing of LIF response was key to positive identification of Cu, Zn, Pb, and a mixture of the metals at nmol/cm² levels. Specifically, the RGB values from each image were used to create density histograms of each color channel's relative pixel abundance at each decimal code value. These histograms were then used to compare color shifts linked to the successful identification of contaminated moss samples. Photoperiod and extraneous environmental stressors had minimal impact on the histogram color shift when compared to metals.

2.2 INTRODUCTION

Heavy metal contamination in the environment from anthropogenic sources has long been a concern, and newer, more strict regulations call for frequent and rigorous monitoring. Heavy metals in high concentrations have been shown to bind with soil and be released into water long after their release and deposition, hence making monitoring of more recent contaminant accumulation more challenging (Stankovic, 2014; Norgate et al., 2007). Focusing on atmospheric deposition of these metals of interest can help to distinguish current events in the environment from historic ones (Berg et al., 1995; Wolterbeek, 2002; Stankovic, J.D., 2018). Observation of biota have been used since the 1960's for monitoring metals through

bioaccumulation, with local plant communities specifically serving as habitat monitors and tests for success of bioremediation (Tremper et al. 2004). One commonly employed biomonitor are mosses, which have traditionally aided in the monitoring of the atmospheric deposition of heavy metals derived from their lack of a true root system to accumulate historic contaminants from underlying soils (Berg & Steinnes, 1997; Degola et al., 2014).

Mosses are a resilient group of genera with a simple cellular structure and are found in a wide variety of biomes (Sun et al., 2009; Serbula et al. 2012; Suchara et al. 2011). Though mosses are good accumulators of environmental contaminants, uptake of a specific metal accumulation varies with moss surface area and molecular differences in cell wall composition (Chakraborty & Paratkar, 2006; Sarkar et al., 2009; Stanković et al., 2018; Petschinger et al., 2021). Micro-nutrients such as Cu, Zn, and Ni are preferentially acquired and incorporated into cellular structures because of the need in metabolic processes; non-essential elements such as Pb and Hg may not be absorbed but adsorbed but end up trapped as particulate matter on the surface, bound to chelating sites, or deposited outside of cells (Vázquez et al., 1999b; Macedo-Miranda et al., 2016). Non-essential metals are usually toxic to plants in even in low levels (ppm, nmol), but high levels of micro-nutrients have been shown to also alter chloroplasts and total chlorophyll content (Nagajyoti et al., 2010; Krzesłowska, 2011; Choudhury & Panda, 2005; Tremper et al., 2004; Sun et al., 2009). High levels of Cu were consistently found across studies to cause change in chlorophyll content and affect the ratio of chl -a and -b (Shakya et al., 2008). These changes in chlorophyll have been documented in mosses and other plants using spectrophotometry (Vernon, 1960; Jeffery et al., 1997; Han et al., 2014; Sun et al., 2021), Pulse-Amplitude-Modulation (PAM; Schreiber, 2004; Brooks & Niyogi, 2011; Haidekker et al., 2022), and laser induced fluorescence (LIF; Truax et al., 2022).

Though the literature denotes changes in chlorophyll level as a result of metal stress (Nagajyoti et al., 2010; Shakya, 2008), shifts in chlorophyll content have also been documented to occur in plants due to environmental factors (Lavrov et al., 2012; Gameiro et al. 2016; Peters et al., 2018). Al-Radady et al. showed that physical stress can affect the efficiency of plant tissues to retain elements (1993). Documentation of chlorophyll fluorescence has aided in the detection of stress conditions in plants (Lichtenthaler, 1988; Subhash, 1997; Yang-Er, 2019) and LIF techniques have been shown sensitive enough to measure N level differences in field grown corn receiving different treatments of N fertilization (McMurtrey, 1994). Experiments have also

detected shifts in red fluorescence emission associated with severe drought (Lavrov et al., 2012) and the effects of water stress from overwatering (Gameiro et al. 2016). Each of these parameters are likely to affect plants during *in-situ* analysis making it necessary for any monitoring method to be able to distinguish between metal induced stress and environmental effects from water stress, drought, and nutrient introduction. Another inherent factor affecting plants is length of photoperiod and seasonal changes (Lefsrud et al., 2006), which can differ across geographic locations and times of year affecting plant growth and efficiency of nutrient accumulation (Peters et al., 2018). This paper sets out to document how metal induced stress is distinguishable from environmental variance, by testing for these features.

Laser induced fluorescence (LIF) emission is an emerging technique applied in the biological sciences to monitor shifts in photosynthetic physiology and chlorophyll-a/-b in plants, and algae (Brach, 1977; Buschmann 2007). In this work, fluorescence is induced via a pulsed laser at a rate of nanoseconds to capture the short life-time fluorescence of organic material. The laser excites molecules using electromagnetic radiation which is absorbed and quickly emitted as a spontaneous emission of light of lower energy and of a specific wavelength (Kinsey, 1977; Maarek & Kim, 2001). The lasers used are commonly ND:YAg solid state lasers that combine lower cost with higher power efficiency. LIF offers the ability for *in-situ* non-destructive measurements without the need for close-up devices, such as PAM, or reliance on long distance satellite information that come with their own shortcomings (Manzar et al., 2019; Papenfus et al., 2020). LIF could replace traditional sampling and allow for larger scale, repeated measurements of the same habitat. The benefits of LIF when compared to near-infrared (near-IR) spectroscopy are that near-IR is a non-destructive method, uses portable instruments, and can take measurements at considerable distance under daylight without having to account for the impact of reflectance from the angle of the sun (Gameiro, 2016; García-Sánchez et al., 2017; Marques de Silva, 2018; Tan et al., 2019).

Previous work (Truax et al., 2020) strove to develop a method to identify Cu contamination in moss tissues using the LIF response coupled with image analysis. The effort employed the “Standoff Biofinder” (Misra, 2018), which was a pulsed Nd:YGa dual laser system (green 532 nm excitation laser and UV 355 nm excitation laser) fired at a nanosecond rate. It was found that differentiation of Cu concentrations at varying $\mu\text{mol}/\text{cm}^2$ levels was possible based on comparison of color histograms of treated moss samples to those of control samples. However,

that proof-of-concept work was limited to testing of only one metal, Cu, at concentrations 2-3 magnitudes above common environmental levels of concern. Therefore, while it proved the feasibility of applying LIF to metal detection in mosses, improved sensitivity would be required to reach detection at nmol/cm² levels.

For this study, adjustments were made to the design and functionality of the laser system to prevent power loss, improve reflectivity in the laser lens, and block unwanted wavelengths with the addition of a short pass filter to the upgraded CMOS camera. These adjustments improved LIF detection limits of Cu to the nmol/cm² level, well within environmental detection levels of interest. This improved system was renamed “CoCoBi”, for Color Compact Biofinder (Misra, 2021), and has been documented to detect 1 ppm of chlorophyll in ethanol from a single laser pulse excitation. The unit can be used effectively from up to a 3 m distance with a field view of 60 cm. The system can also distinguish between biofluorescence and mineral luminescence using time-gated measurements. Further information on the improved sensitivity of the CoCoBi versus the Biofinder for Cu, Zn, and Pb can be found in Appendix A (6.1.1).

One goal of this research was to demonstrate the applicability of the CoCoBi at environmentally relevant (nmol/cm²) Cu levels. Efforts expanded to applying the methodology to other metals and to observe if multiple environmental stressors, such as drought and length of photoperiod, could affect the moss response and image analysis. Cu was used for its known response, but Zn and Pb were also included because they are known to have been released from industrial, mining, and highway sources (Nriagu 1996; WHO 2007). Another reason for examining these heavy metals, specifically, arises from the frequent detection of heavy metals in trace metal assessments conducted for environmental and public health (Wong et al., 2006).

2.3 METHODOLOGY

The research is divided into three parts based on the methods developed previously (Truax 2022). Part one focuses on the laboratory treatment and care of the moss samples. Part two uses LIF and captures color images of the moss response. Images were then analyzed in part three to quantify the moss response for comparison of stressed samples to a control.

2.3.1 Laboratory Procedure

The moss *Thuidium plicatile* is a moss species endemic to Hawai'i (Staples et al., 2004; see Notes on Moss Species) and was collected along the Wa'ahila Ridge Trail and State Recreational Area (21.307°, -157.797°) on February 15, 2021. The forested area represents an uncontaminated environment that sits along the Southeastern part of the Ko'olau mountain range beneath the Honolulu Watershed Forest Reserve. The samples were washed and cleaned of forest litter before being placed on trays which were moved within a laboratory grow tent for incubation. Moss samples throughout the time were kept at a temperature of 18-20°C, 50-60% relative humidity, and 14-17 W/m² ambient light to simulate a shaded area (1400-1800 lux; daylight = 32000 lux; overcast = 1000 lux), with a default daylight length of 10 hours. Experiments began in May and ran through June of 2021 for a total of 4 weeks.

Three metals of interest (Cu, Zn, and Pb) were administered individually and as a mixture of the three metals for comparison. Three environmental stressors of interest were selected and included drought, overwatering (drowning), and high nutrient regime. The effects of long (14 hr), short (6 hr), and dark (0 hr) photoperiods were also tested. With the inclusion of a control, preparation of samples was conducted two weeks before experiments in May leading to the separation of moss onto eleven different plastic trays. Each tray contained moss covering an area of 316 cm² (7 in x 7 in) which were then placed in the grow tent. A two-week acclimation period prior to the start of the experiment was implemented for moss physiological responses to laboratory conditions and transplantation to trays to stabilize.

During the experimentation period, each tray of moss was removed from the tent for ~0.5 hours for treatment and imaging after which it was immediately returned. On non-treatment days all moss (save the drought sample) were given 30 mL of distilled water (DI). DI was added on non-treatment days to maintain a constant watering regime ensuring that any moss response recorded was the result of experimental addition of metals, nutrients, or a stress response. The length of the experiment was seven days total including a control day and treatment with metal three times at increasing levels of toxicity with 48 hours between treatments. For the three increasing levels of doses, Cu, Zn, and Pb were administered at 1, 10, and 100 nmol/cm² every 48 hours, respectively. Compounds of CuCl₂, ZnCl₂, and Pb(NO₃)₂ were chosen for testing. The trial treated with the mixture of metals used the combination of the three metals at each of the three doses. Wetting of the samples always occurred within five minutes prior to imaging.

The nitrified sample was given a single dose of nutrients on the first day of the experiment (Miracle-Gro AeroGarden Liquid Plant Food 4-3-6; Appendix A – 6.1.3). The drought sample ceased to receive water on the first day of the experiment to watch the effect of withholding water over the course of a week. The overwatered sample received 30 mL of DI each morning before imaging and again before imaging 12hrs later, totaling twice as much watering as all other samples. Photoperiods for all samples were kept at 10 hours except for the long photoperiod (14 hrs), the short photoperiod (6 hrs), and the dark photoperiod (no light) treatments. Each of the photoperiod samples were given one week under their new light conditions before their first imaging. Table 2.1 outlines the treatments for each sample over the 7 days of the experiment. Only a maximum of 4 trials were run per week breaking the experiment into three sample groups: those treated with metals, changing environmental conditions, and finally photoperiod conditions. The control trial was imaged during the same experimental period as the “environmental condition” group.

Table 2.1: Dosing for the 11 moss trays over 7 days separated by group. If not specified, the photoperiod is 10hrs. All DI, individual and combined metal solutions were 30 mL.

Group	Tray	Day 1	Day 2	Day 3	Day 4	Day 5	Day 6	Day 7
Control		DI	DI	DI	DI	DI	DI	DI
Metals	Copper	DI	1 nmol/cm ²	DI	10 nmol/cm ²	DI	100 nmol/cm ²	DI
	Zinc	DI	1 nmol/cm ²	DI	10 nmol/cm ²	DI	100 nmol/cm ²	DI
	Lead	DI	1 nmol/cm ²	DI	10 nmol/cm ²	DI	100 nmol/cm ²	DI
	Mix	DI	1 nmol Cu/cm ² 1 nmol Zn/cm ² 1 nmol Pb/cm ²	DI	10 nmol Cu/cm ² 10 nmol Zn/cm ² 10 nmol Pb/cm ²	DI	100 nmol Cu/cm ² 100 nmol Zn/cm ² 100 nmol Pb/cm ²	DI
Environmental	Nutrients	4-3-6 3 mL diluted with 27 mL DI	DI	DI	DI	DI	DI	DI
	Drought	N/A	N/A	N/A	N/A	N/A	N/A	N/A
	Flood	2xDI	2xDI	2xDI	2xDI	2x DI	2xDI	2xDI
Photoperiod	Long	DI 14hr	DI 14hr	DI 14hr	DI 14hr	DI 14hr	DI 14hr	DI 14hr

	Short	DI 6hr						
	Dark	DI N/A						

2.3.2 Imaging using the CoCoBi

Each group of moss samples was imaged starting on day 1 to collect a baseline control for each tray. Moss receiving metal solutions were dosed on days 2, 4, and 6 before imaging. The nitrified sample received excess nutrients on day 1, while all other environmental group samples maintained the same treatment throughout the 7 days of the experiment. The moss trays were always imaged after wet deposition when applicable, and imaging was conducted every 12 hours. In the case of the overwatered sample, wetting occurred before all imaging sessions. Imaging was conducted in 30-minute windows in order of trial number and those imaging times were held consistent for each sample between 6 and 8 am and 6 and 8 pm.

Further details of the laser system are described in Misra et al. (2021) but in short: the CoCoBi is a dual laser system that uses both green and UV lasers. Images were collected with the Baumer Camera Explorer software which allows the CMOS camera to be synchronized with the 112 ns pulses of the Nd:YAg laser. Baumer Camera Explorer allowed for the adjustment of the camera's exposure, gain, and time delay (Misra et al., 2018). Images were taken at 3 gain levels (5, 10, and 15) when using both lasers. Images were also collected for the green laser and UV laser individually and the results for each can be found in Appendix A (6.1.6-7), respectively. The stand the CoCoBi sits on does not allow for a top down position for imaging (90° from the horizontal plane). This results in an angle of 60° being used which allows for five shots to be taken of the front of each moss tray (each corner and the center), and then the tray was rotated 180° so the back of the moss could be imaged, producing 10 images in total.

2.3.3 Data Analysis

2.3.3.1 Single-color comparison

Once the images were collected, RGB (Red, Green, and Blue) pixels within each image were extracted to create density histograms of the relative abundance of each decimal code value from 0 to 255 for each color channel. The decimal code abundances were then normalized using

the total pixel count to create a percent abundance curve (Figure 2.1). Once calculated, the profiles of these histograms were then used to assess the difference between curves (density difference; Figure 2.1).

$$Difference = 1 - (\sum \min|trial(x), control(y)|) \quad \text{Eq. 1}$$

Where x represents the color intensities for the corresponding trial, and y represents the same for the control images (Swain & Ballard, 1992). An alternative method was also used to dynamically time warp one curve to fit another (DTW; Jekel et al., 2018).

$$D(i, j) = |x(i) - y(j)| + \min \begin{cases} D(i + 1, j) \\ D(i + 1, j + 1) \\ D(i, j + 1) \end{cases} \quad \text{Eq 2.}$$

Where x and y represent strings of data and i and j represent the length of each string so that $D(i, j)$ equals the best alignment distance between all data points along the lengths of x and y (Jekel et al., 2018). Sample images of mosses from the metal group trays before treatments and all control sample images from the week of experimentation were included for comparison. This experiment captured 10 images per tray per day of the experiment and had a total of 193 control images sampled in total.

Two methods of analysis were conducted to determine performance of a control mean against the using all individual control images. Since the pool included 193 images, we evaluated if the added processing time of individual comparisons would produce a more robust result when considering stress or metal identification. The developed workflow relies upon batch processing of the individual images stored in organized folders. Functions created in MATLAB® (2021a) access the data stored in these folders and process them to extract RGB color histograms. From these histograms, the individual trials can be compared to the control for each day of the

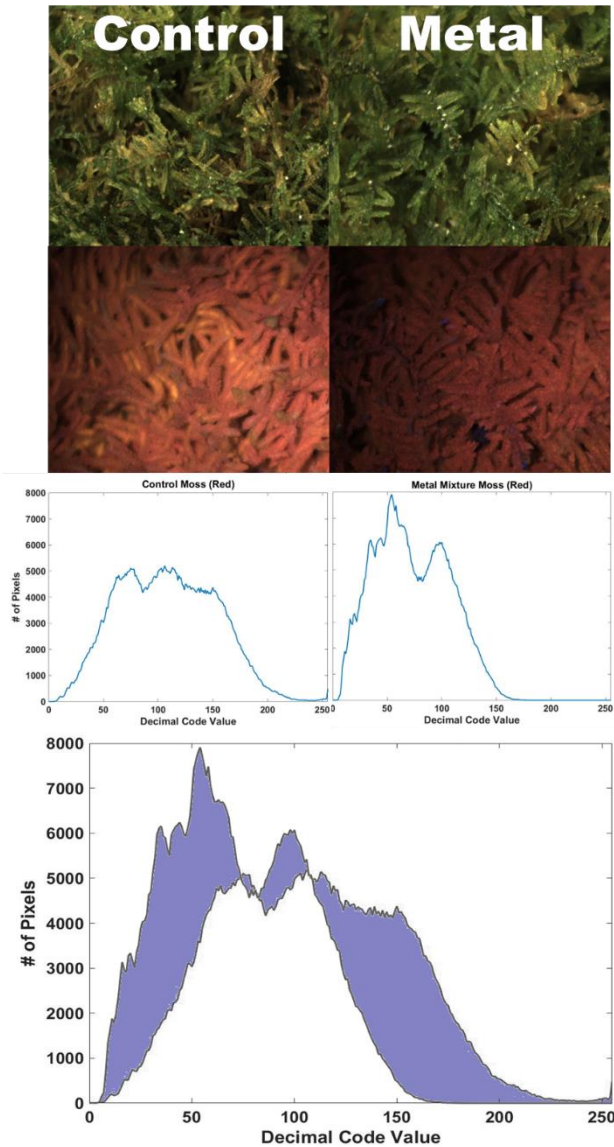


Figure 2.1: Images of moss samples (from top to bottom) showing matching samples under natural light and LIF with a control sample on the left and a contaminated sample on the right. From LIF images color histograms of the red color channel are plotted and then compared using the density difference method overlapping the two curves and finding the areas of difference (bottom plot), or using the DTW method (not shown) to find the minimal direction of change needed in the x/y direction.

experiment using either the density difference or DTW method. From these comparisons, a trial mean, standard deviation of the sample images, and standard error of the trial mean can be calculated for each day for each trial and stored in arrays for further use. The major difference in the organization of the data for analysis is how images are compared between treated and control samples.

The first method uses what is termed here as a “master mean method” (MMM). Put simply, all 193 control images are processed to extract their RGB histograms which are then stored in 3 tables based on color. Then, the mean and standard deviation for each decimal code value within the color tables are found for the 193 images. These values are then stored to be used for comparison to all trials of the experiment as a singular mean histogram of all control samples. Thereby, the 10 treated moss images collected every 12 hours for each trial can be compared to the one control master mean (Figure 2.2a). The second method, termed “batch mean method” (BMM), also stores the RGB histograms within a table but creates another function to compare all 10 images of a single day treated trial to all 193 images of the control to find all possible iterations of difference (Figure 2.2b). The mean, standard

deviation, and standard error of the trial mean are then found after analysis is complete for the density difference or DTW methods of comparison.

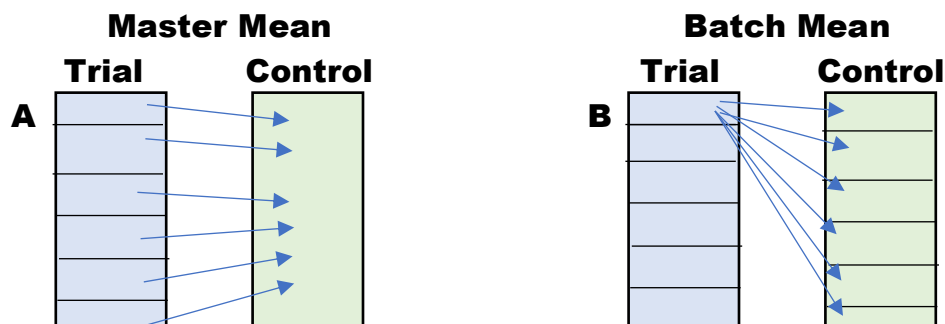


Figure 2.2: (A) Shows individual images of a trial collected from one session being compared to a single master mean control. (B) Shows individual images of a trial collected from one session being compared to multiple control images. Example MATLAB® code for density difference calculations can be found in Appendix A (6.1.4).

Theoretically, the batch mean method should yield better specificity in differentiating metal contamination from the natural variability of the plant. The master mean method is limited by the already small 10-image sample pool which could allow for potential outliers to have a larger impact on reported distribution and error. However, for real time application, the batch mean method requires far more computational resources and could prove to have only marginally improved results for slower processing times. Comparison of the mean and median for both methods was used as a first check for possible outliers, with a tolerance interval of 99% set for the observed population. Errors were also calculated to show the natural variation that exists across all control moss samples. The mean and standard deviation for each day were used to compare all trials to the control using a Welch's t-test to check if two populations of images are similar enough that we cannot reject that they are the same. The t-test was used for each color channel for each trial in comparison to the control based on day of the trial.

2.3.3.2 Multi-color comparison

One drawback of using the density difference method to find differences between images is that it can only be used to compare single-color histograms. It was found that DTW could be used for both single- and two-color analysis which improved the sensitivity of detection and separation of individual samples from each other and the control (Truax et al., 2020). Because of

the use of the improved CoCoBi LIF system, DTW was used again for two-color analysis. Previous work had only explored the two-color combination of red and green color channels. To observe the possible reaction of moss to a variety of stressors, all 3 two-color combinations were considered in this analysis (RvG, GvB, RvB).

However, even this approach does not allow for the use of all information from the three available color channels. Thus, to improve upon previous methods and to determine if change amongst the three color channels was due to a specific stressor, a new method was developed for testing. Single-color differences derived using both density difference and DTW methods were extracted for each color channel (R,G,B) for each trial image on each day of the experiment and compared with its control. This calculated difference is represented in Eq. 3, 4, and 5 for each color variable as R_D , G_D , and B_D , where $_D$ denotes the color histogram difference. Each individual color difference (R_D , G_D , and B_D) was then divided by the sum of all 3 color differences, representing the total color difference between treated and control images.

$$\frac{R_D}{(R_D + G_D + B_D)} \quad \text{Eq. 3}$$

$$\frac{G_D}{(R_D + G_D + B_D)} \quad \text{Eq. 4}$$

$$\frac{B_D}{(R_D + G_D + B_D)} \quad \text{Eq. 5}$$

The resulting ratios represent the relative color change as a fraction of the total change. This was done for all trials, including the control. The mean of each color ratio was calculated to observe if a pattern of separation was discernable within the data. A Welch's t-test was used to quantitatively determine if any color ratio pattern for a given trial deviated from the control across the 7-day experiment. Deviation from the control is only recorded as true if it exceeds a confidence interval of 99%.

2.4 RESULTS

2.4.1 Analysis method comparison and parameter optimization

As a first step, images from trials treated with metals were compared to the control images collected every 12 hours to assess what laser settings and which image analysis method,

master or batch mean method, provided the best sensitivity for stressor identification (to see a comparison of 12 hour response and 24 hour response see Appendix A -6.1.5). In Figure 2.3, LIF images were processed for each metal tested using the density difference method against both the control master mean method (MMM) and batch mean method (BMM). Apparent from all tests is that all treated trials show larger differences on the days of treatment. All three colors show similar trends in their response whether using MMM or BMM. However, comparison across these two methods show slight, but important differences. For example, some 0-day controls show significant difference from control mean when using MMM, while this does not occur with BMM. This phenomenon in MMM is undesirable as it may produce some false positive interpretation. Use of the MMM shows good separation from the control when identifying exposure to the combination of metals, but is much less consistent for Pb and Cu, and, overall, the least effective in identifying Zn exposure. Identification of Zn using LIF is only reliable when using the 355 nm UV laser. For all other metals, results obtained using a combination of both lasers appear similar to those produced from just using the 532 nm green laser (consistent with Truax et al., 2020), except for Cu, where the green laser plots seem to have a decrease in sensitivity. These plots and further analysis of similarities and differences of results using the green and UV lasers individually can be found in Appendix A (6.1.6-7). All gains used with both lasers (5, 10, 15) provide good results, though the lower gain level of 5 may introduce less noise by reducing oversaturation in the images. And while a gain of 5 may reduce oversaturation of the images collected, a gain of 10 appears to show better sensitivity and further separation from the control samples when attempting to identify all metals tested (Figure 2.3). The blue color channel appears to have the best separation from the control for identifying dosing of each metal, with green being the next best, followed by red.

In comparison to the density difference method, single-color DTW analysis (Figure 2.4) applied to the same data (both laser; gain of 10) appears very similar to the density difference profiles but are more muted and less separated from the control. The plots of MMM and BMM approaches are similar to each other and lack distinction for all but the mixture of metals regardless of laser type. The DTW technique does have one benefit in being highly effective for identifying the presence of a combination of metals. Though single-color DTW application failed to effectively identify individual metal response, two-color DTW analysis (Figure 2.5) proved not only to have distinct levels of separation from the control for each metal but also good

separation at environmentally relevant levels. Due to it using two colors for the analysis a gain of 5 was favored to limit the potential for increased oversaturation in the data. As with the density difference method, MMM and BMM have similar profiles, with BMM showing better sensitivity when compared to the control. Of the combinations of color channels tested, red versus green and green versus blue produced the best separation of metal exposure from the control. As with density difference, profiles are similar between images taken with both lasers and just the green laser, but with both lasers having better separation when compared to the control. The lowest gain tested with UV (15) shows useful profiles as well, but just as with the green laser, it does not perform better than both lasers at any gain level except when considering Zn. Further discussion of Zn results using UV can be found in Appendix A (6.1.7).

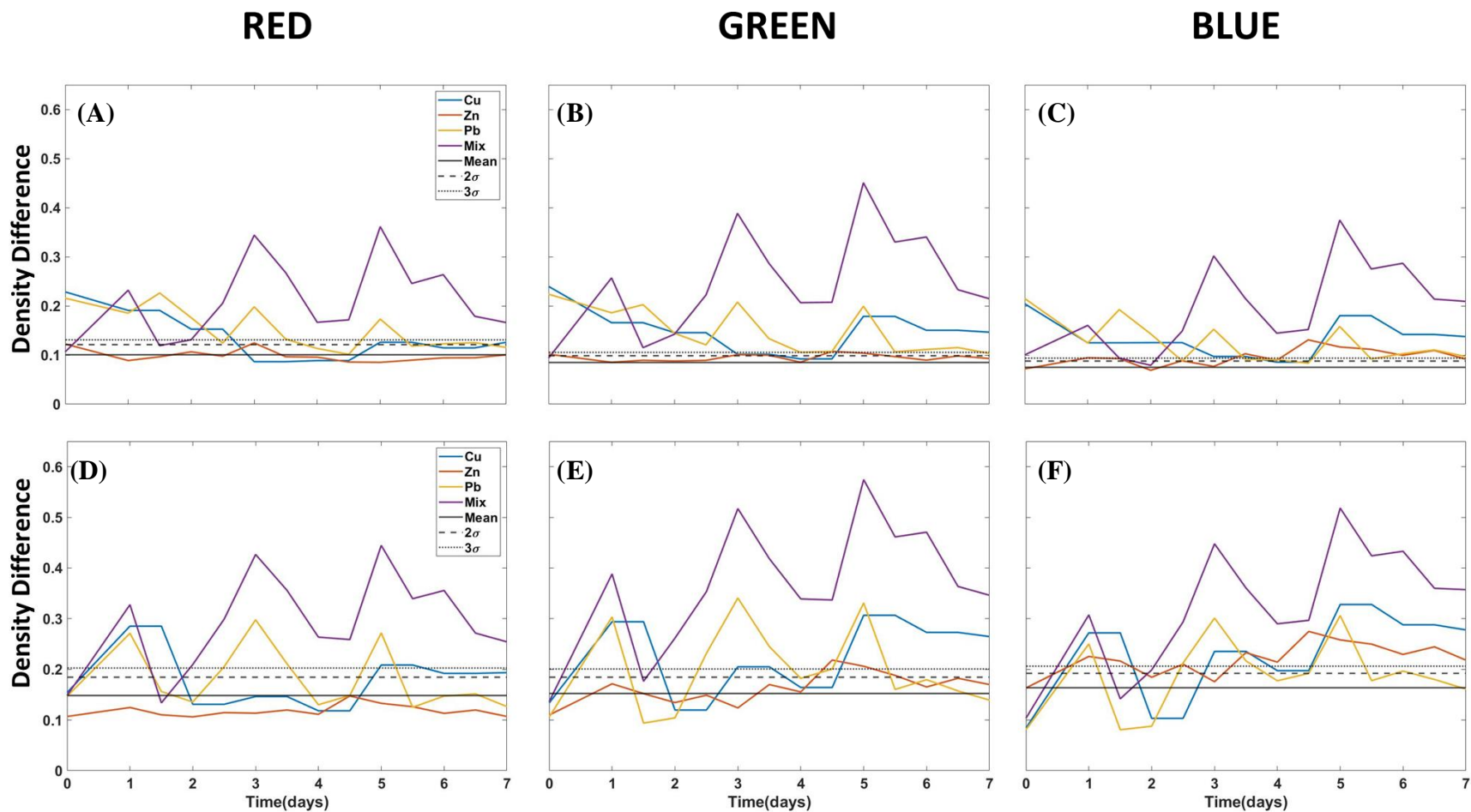


Figure 2.3: Single-color density difference comparison of images of mosses treated with metals to the control. Plots are sorted first by analysis method and then by color (R,G,B) using a master mean (MMM; A, B, and C) or batch control method (BMM; D, E and F). X-axis for all figures is in time (days) and the y-axis is the difference between images of metal treated and control moss as determined by individual colors. Purple (metal mix), yellow (Pb), blue (Cu), and orange (Zn).

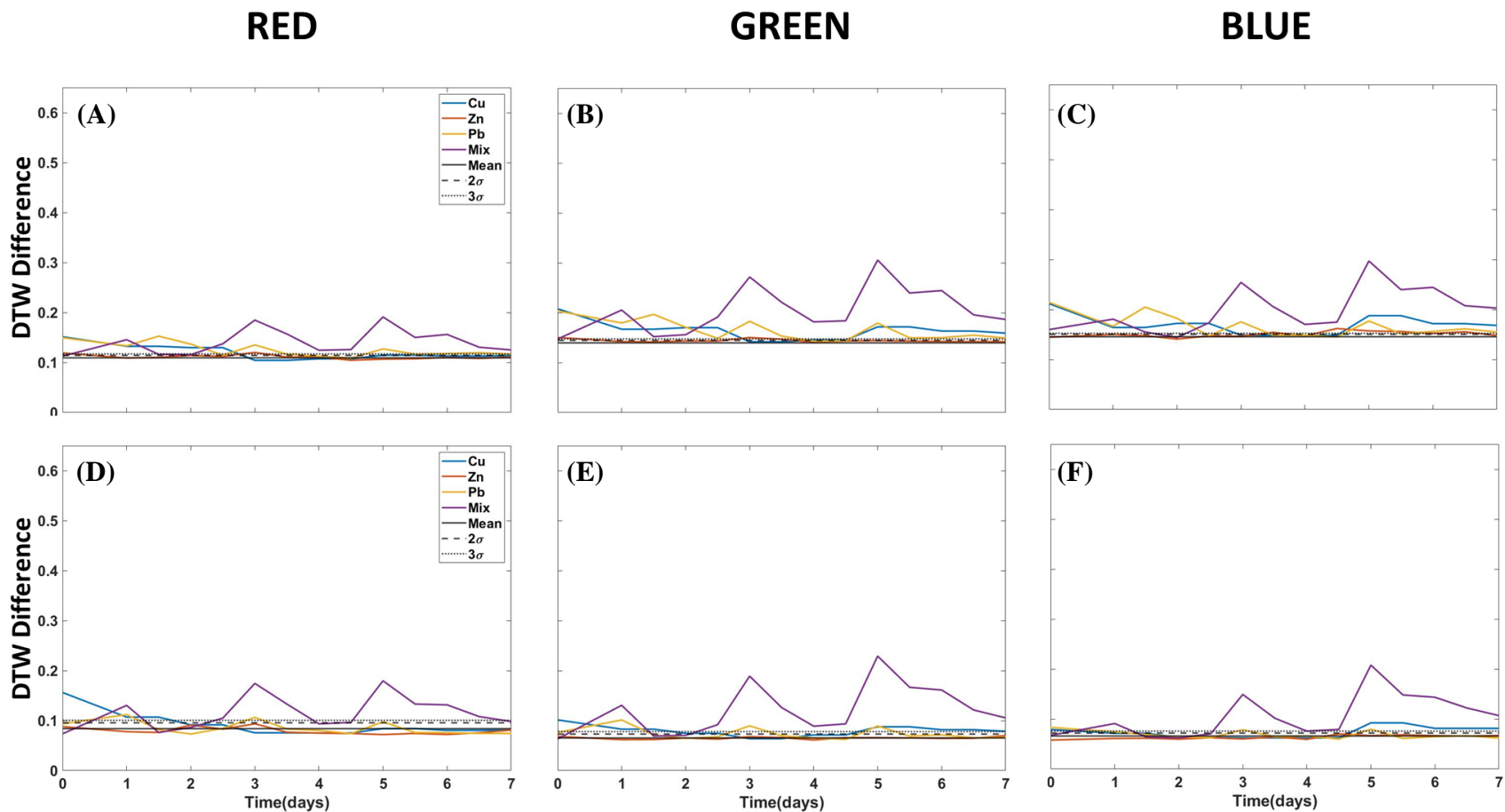


Figure 2.4: Single-color DTW comparison of images of mosses treated with metals to the control. Plots are sorted first by analysis method and then by color (R,G,B) using a master mean (MMM; A, B, and C) or batch control method (BMM; D, E and F). X-axis for all figures is in time (days) and the y- axis is the difference between images of metal treated and control moss as determined by individual colors. Purple (metal mix), yellow (Pb), blue (Cu), and orange (Zn).

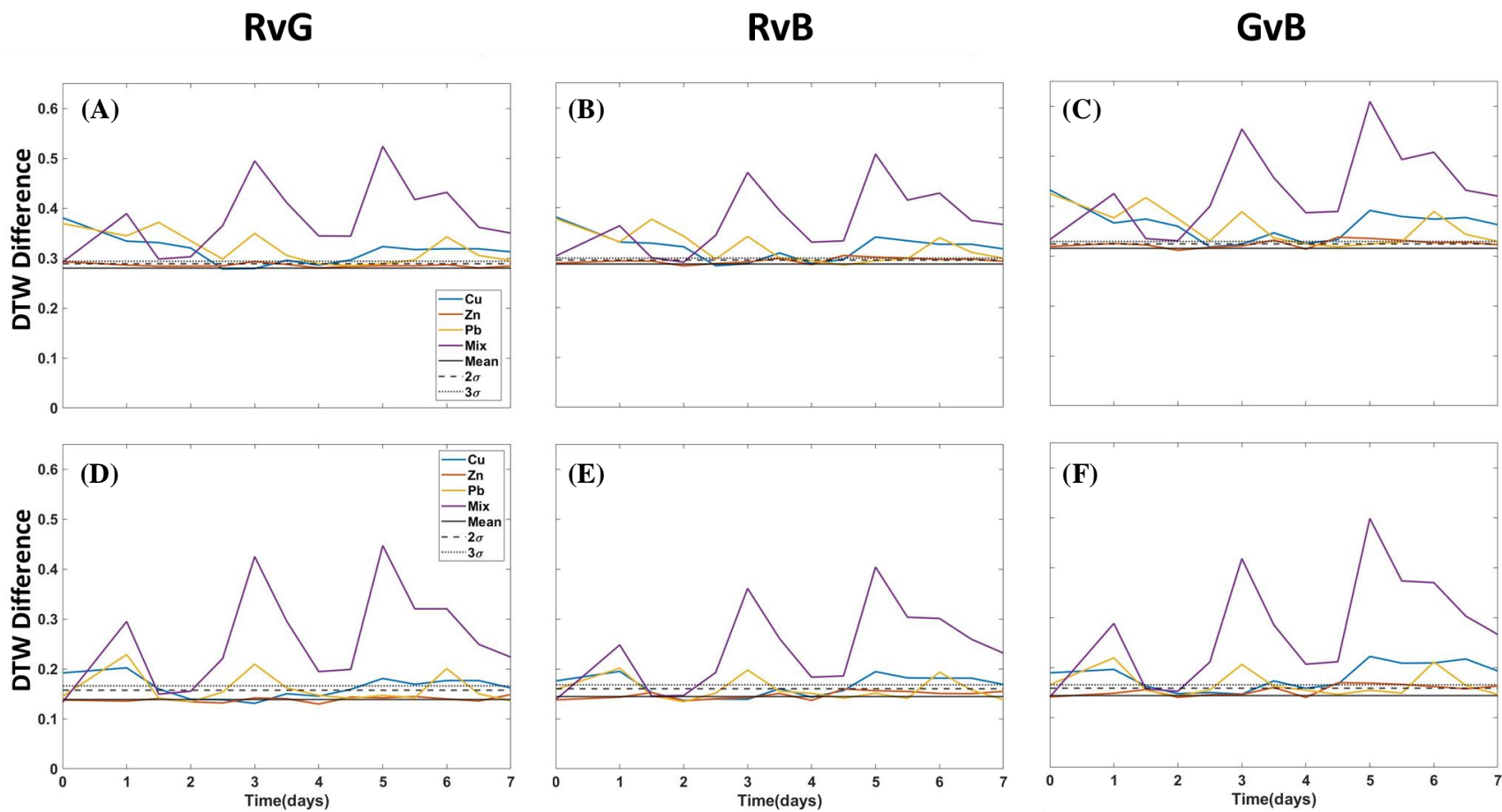


Figure 2.5: Two-color DTW comparison of the metal group to the control. Plots are sorted first by analysis method and then by color (R,G,B) using a master mean (MMM; A, B, and C) or batch control method (BMM; D, E and F). X-axis for all figures is in time (days) and the y-axis is the difference between images of metal treated and control moss as determined by individual colors. Purple (metal mix), yellow (Pb), blue (Cu), and orange (Zn).

After reviewing the metal identification results using single- and two-color analysis methods, it was determined that use of BMM for single-color density difference analysis and two-color DTW provided the best separation of differences from the control for metal identification. Of the lasers and gains compared (Figures 2.3-5), single-color analysis using the density difference method was most effective when employing both lasers at a gain of 10. Two-color analysis using DTW was found optimal with both lasers at a gain of 5. The optimized analysis methods and laser parameters were applied to evaluate the effect of the two environmental stressor groups tested during 7-day experiment: environmental stressors and variable photoperiod. A Welch's t-test was applied to each color channel in each trial compared to the control for each day of the experiment to observe if significant difference in images from stressed plants and control could be statistically determined. This is done in addition to determining if a trial deviates from the confidence interval of the control throughout the course of the experiment.

2.4.2 Single color analysis using Density Difference

Experimental testing of three stress groups (metals contamination, environmental stress, and photoperiod length) using images collected from both lasers at a gain of 10 (Figure 2.6; Appendix A - 6.1.8) reveal that in R and G colors of images of mosses affected by environmental stressors show little deviation from the control sample. Long periods of overwatering or of excess nutrients resulted in a RGB profile change, but results of mean and variance show the results either fall within the control's natural variation or slightly rise above the 99% confidence interval. When comparing the three color channel results, R appears the least separated from the control when observing metals with G having the greatest deviation. However, the green color channel also shows an increasing deviation from the control for over-wetting and nutrients eventually over time crossing the control 3σ threshold that is not present in the red color channel. The blue color channel shows the same deviation for over-wetting, with nutrients showing a consistent separation from control after the moss received a single dose. Drought appears to have the least deviation from the control until the final day of the experiment, and prolonged testing would be needed to determine a response representative of in-situ seasonal drought conditions.

The effects of photoperiod length seem to have a greater separation of images from control than environmental stressors, with shorter photoperiod having the least deviation in red

and green color channels (Figure 2.7 panels G, H, I). Long and dark photoperiods have similar deviations for red and green color channels, but a larger separation from the control is apparent in the blue channel (Figure 2.6I). The blue color channel also appears most responsive to all metal treatment days during the experiment (days 1, 3, and 5; Figure 2.6C). Photoperiod and metals were not tested together therefore it is uncertain how their profiles would be presented if both occurred simultaneously. It is unknown if the profiles would respond with the same degree of difference from the control causing the metal and photoperiod stressors to overlap and be indistinguishable. The alternative is that the degree of difference from the control for both stressors would combine to create a larger separation, with the profiles stacking to create a new profile that would be distinct from metal or photoperiod individually.

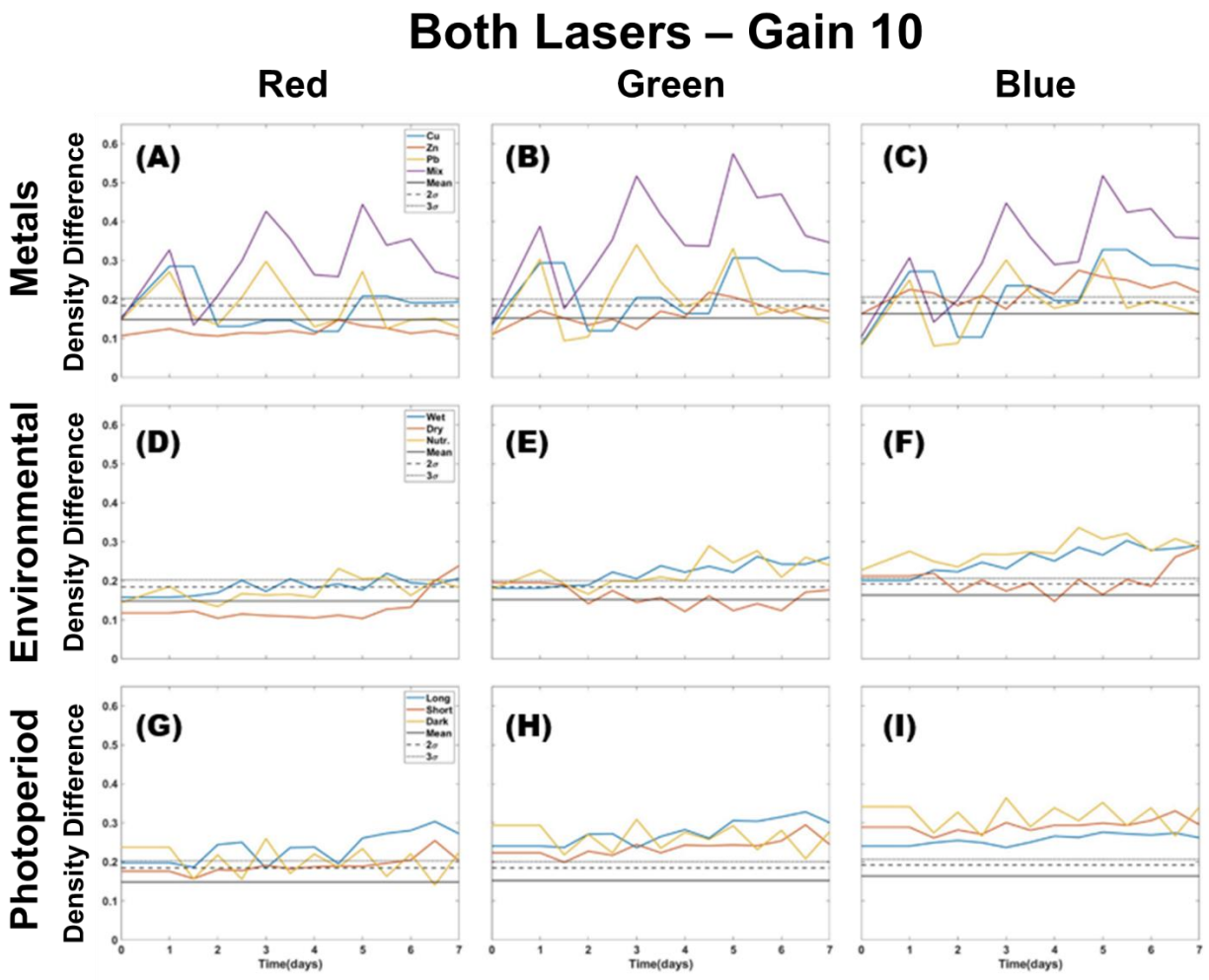


Figure 2.6: Single color density difference using BMM analysis for all color channels of images taken using both lasers, of metal, environmental, and photoperiod trials with the control mean and confidence intervals included.

The Welch t-test results in Figure 2.7 (Table in 6.1.8) suggest that image processing using the blue color channel presents statistically significant deviation from the control for all stressor types. Statistically significant difference between both the green and blue channels from the control can be found in Cu profiles for each treatment day and for Zn on the first day of dosing. Lead shows separation in all color channels on all dosing days whereas the mixture of metals shows separation every day after the first dose in all color channels. Over-wetting, drought, and nutrients have lower “t” values when using the red color channel and only separate from the control on some days in blue and green color channels. As observed visually in Figure 2.6, the t-test confirms that photoperiod length profiles could negatively interfere with metal identification by overlapping with similar statistical difference when compared to the control in all color channels.

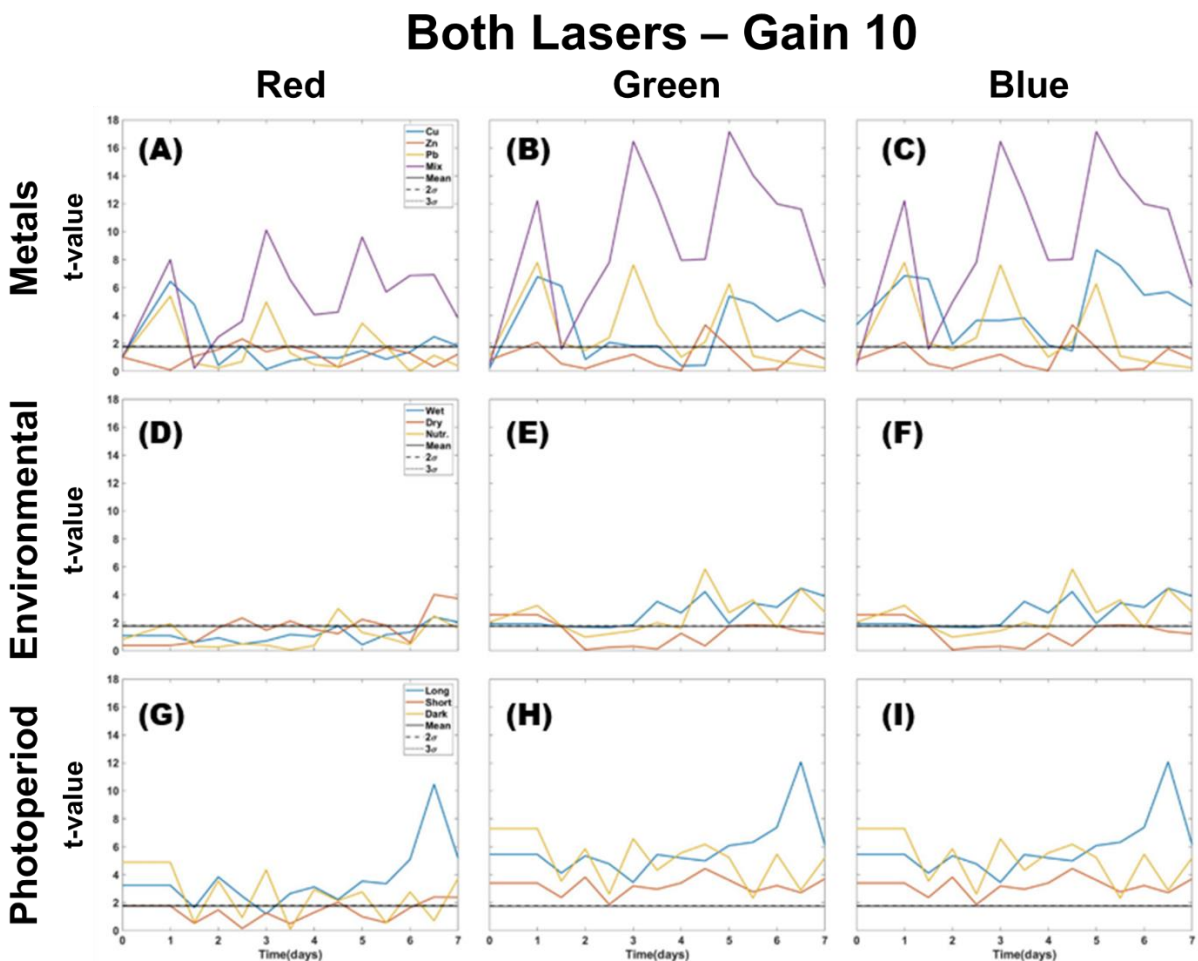


Figure 2.7: Welch t-test results of single color density difference values (Figure 6) for all color channels of images taken using both lasers, of metal, environmental, and photoperiod trials with the t-value included.

2.4.3 Two color analysis using DTW

Figure 2.8 (Table in 6.1.8) shows the profiles for images processed using the two-color DTW analysis using both lasers at a gain of 5. All environmental and photoperiod stressors are mostly bound within the natural variation of the control. It is apparent that the presence of metal can be revealed through statistical difference in all of the color combinations (RvG, RvB, or GvB) with the exception of Zn. Zn shows deviation only in GvB but this overlaps with trends observed in environmental or photoperiod tests. Cu differs from controls in RvG and RvB, and the mixture of metals will show deviation in all three colors. Environmental and photoperiod stressors almost always show only one two-color deviation (save for day 5). It is hinted that the shorter and dark photoperiods may deviate in GvB while the long photoperiod in RvG. These results would suggest that use of both lasers is still the most optimal for metal detection. Between single-color density difference analysis and two-color DTW, DTW proves to provide clear identification of metals without interference due to environmental or photoperiod effects. The mixture of metals is easy to observe and separate out from the individual metal doses. There does appear to be an initial response on the first treatment day (day 1) for Pb, Cu, and the mixture of metals, but Cu is more distinguishable in GvB whereas Pb stays constant in its profile throughout the color combinations. The most significant observation that can be made is that the environmental and photoperiod profiles do not show large variation and only minimally separate from the control if at all. Deviation is more likely in the RvB and GvB for environmental stressors, while photoperiod may be more pronounced, though slightly, in RvG and GvB. This could indicate that environmental stressors are more likely to be distinguishable through the blue color channel while photoperiod can be identified using the green color channel. Metals can be identified regardless of color channel and will present with a similar profile which is not observed with the other stressor types.

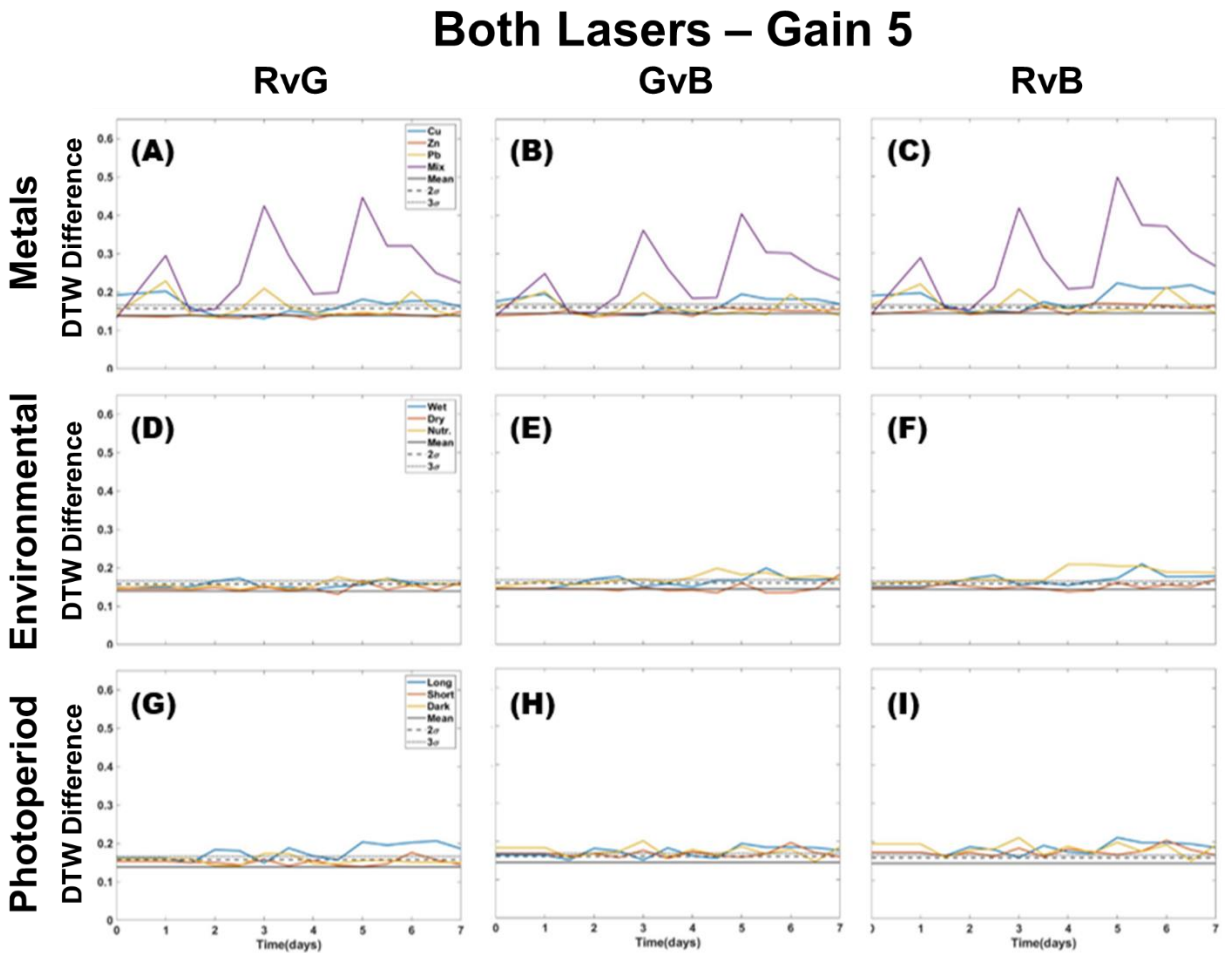


Figure 2.8: Two-color DTW using BMM analysis for all color channels of images taken using both lasers, of metal, environmental, and photoperiod trials with the control mean and confidence intervals included.

The Welch's t-test was also applied to the two color DTW values and can be seen in Figure 2.9 (Table in 6.1.8). From the plotted profiles it can be observed that use of DTW is more effective than density difference at minimizing the observed deviation of environmental or photoperiod stressors from the control. The nutrients appear to deviate in RvB and GvB while the long photoperiod deviates in RvG and GvB. Again, we see the presence of deviation for environmental stressors when the blue color channel is present and in photoperiod treatments when the green color channel is present. This method is quite effective for delineating between a mixture of metals and individual metal profiles. However, it might be difficult to determine if a stressor was caused by nutrients or Cu. Lead and Zn are almost impossible to identify. Therefore, this approach may be best applied when trying to determine if there is a presence of multiple metals within a given sample.

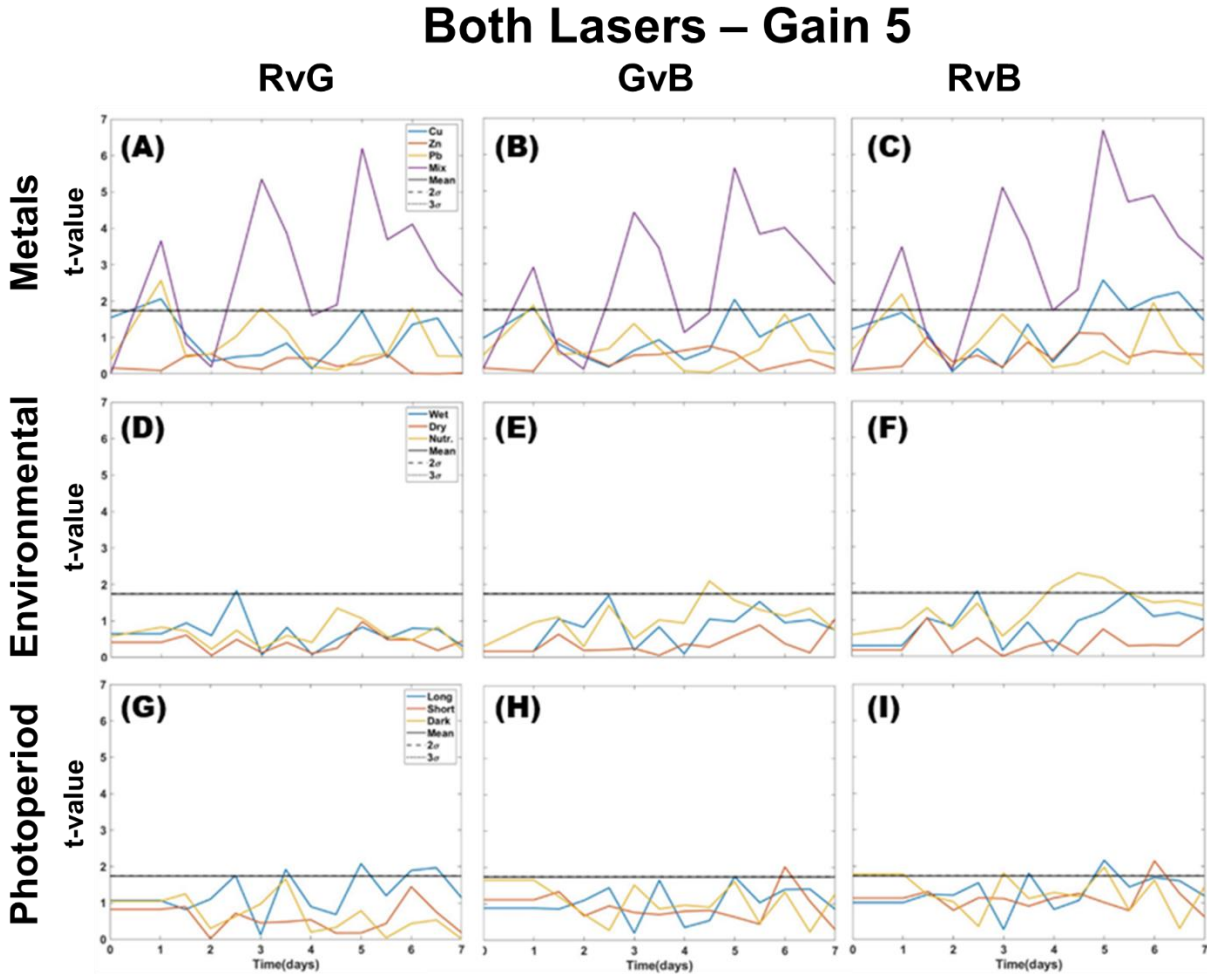


Figure 2.9: Welch t-test results of two color DTW values (Figure 2.8) for all color channels of images taken using both lasers, of metal, environmental, and photoperiod trials with the t-value included.

2.4.4 Multi-color ratios as a means of stressor determination

Multi-color analysis has the potential to capture the relationship between all color channels and is hypothesized to be at least as valuable as two-color analysis for individual metal differentiation. A contribution from each color to the overall image change in comparison to a control can be expressed as a fraction or percent of a single-color change within the sum of all color changes. We also derived this ratio for the control by applying BMM using the 10 images collected each day for the control sample taken during the 7-day experiment and comparing it to the total number of control images (193) as was done with the other trials. The color fraction relationship is shown as bar graphs on Figure 2.10 (6.1.8), which shows the results for each trial from the density difference analysis of both lasers at a gain of 10. The short and dark

photoperiods, high nutrient regime, and over-wetting all show a similar pattern of increasing fraction of contribution from red (lowest), to green, and finally to blue (highest). The long photoperiod and the control show even contribution from all three colors. The long photoperiod does appear to have a slightly larger contribution from green while the control has a slightly larger contribution to the overall image change from the blue color. With time, the images for the drought treatment change from green to red dominated change, while blue color change contribution stays about the same. The metal profiles are the most distinct, with Zn showing the largest change contributed by blue color and decreasing red contribution. Pb and Cu start with red color change domination, which shifts over time to green and blue. The mixture of metals maintains a higher contribution from change in the green channel and is distinct from all other trials.

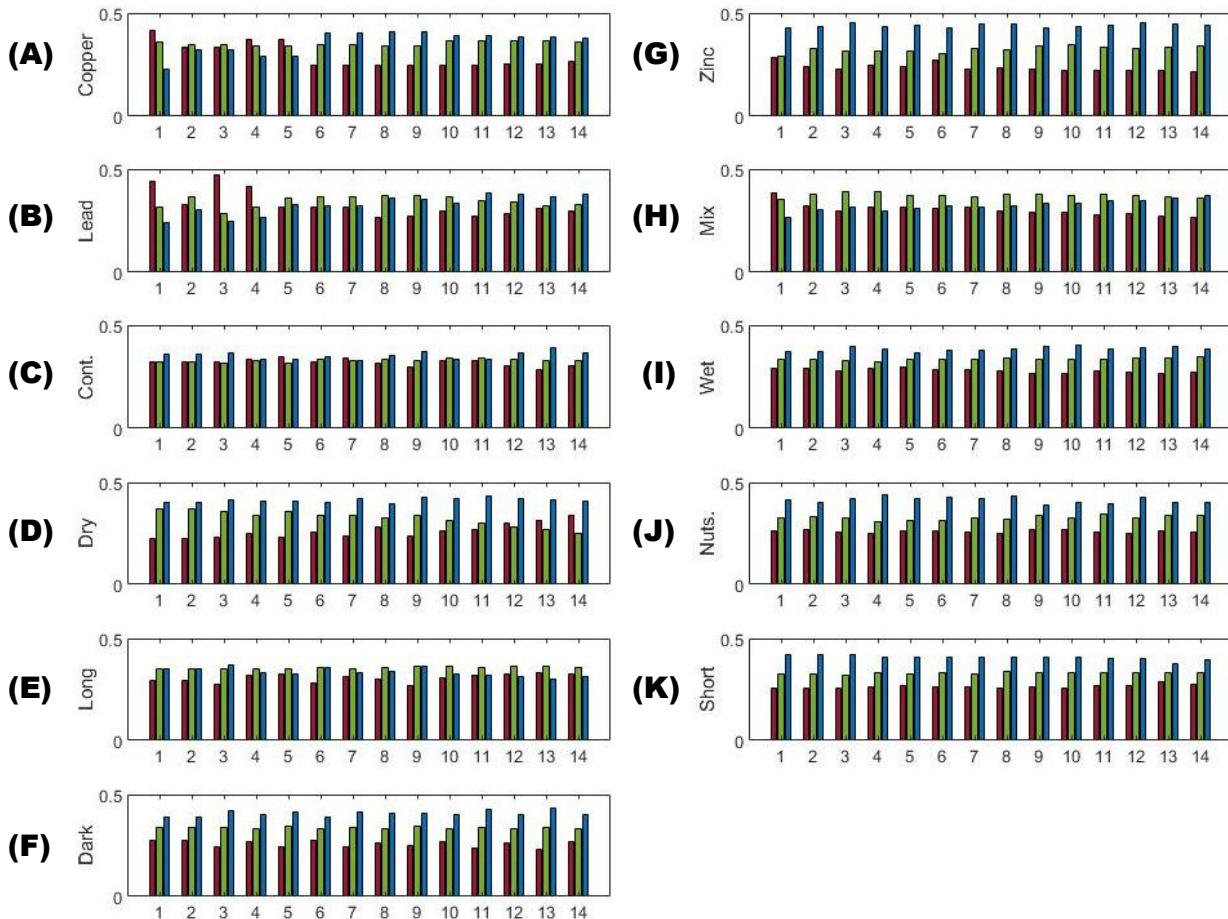


Figure 2.10: Use of color ratios from density difference (both lasers) analysis to compare the 11 trials using BMM. Values used are listed in Appendix A (6.1.8) and calculated from dividing individual color channels (R,G,B) by the sum of their difference from the control.

Plotting these ratio values (Figure 2.11; 6.1.8) confirm that the highest fraction of green and blue channel contribution to overall change is associated with metal contamination of Cu, Pb, and the mix. Zn only deviates in the blue channel which heavily overlaps with all photoperiods and environmental stressors except over-wetting, which is most similar to the control and the long photoperiod which may interfere with metal identification. These results are more straight forward than the one-color analysis using the density difference method, but both show valuable information that combined could make separation between stressor types easier.

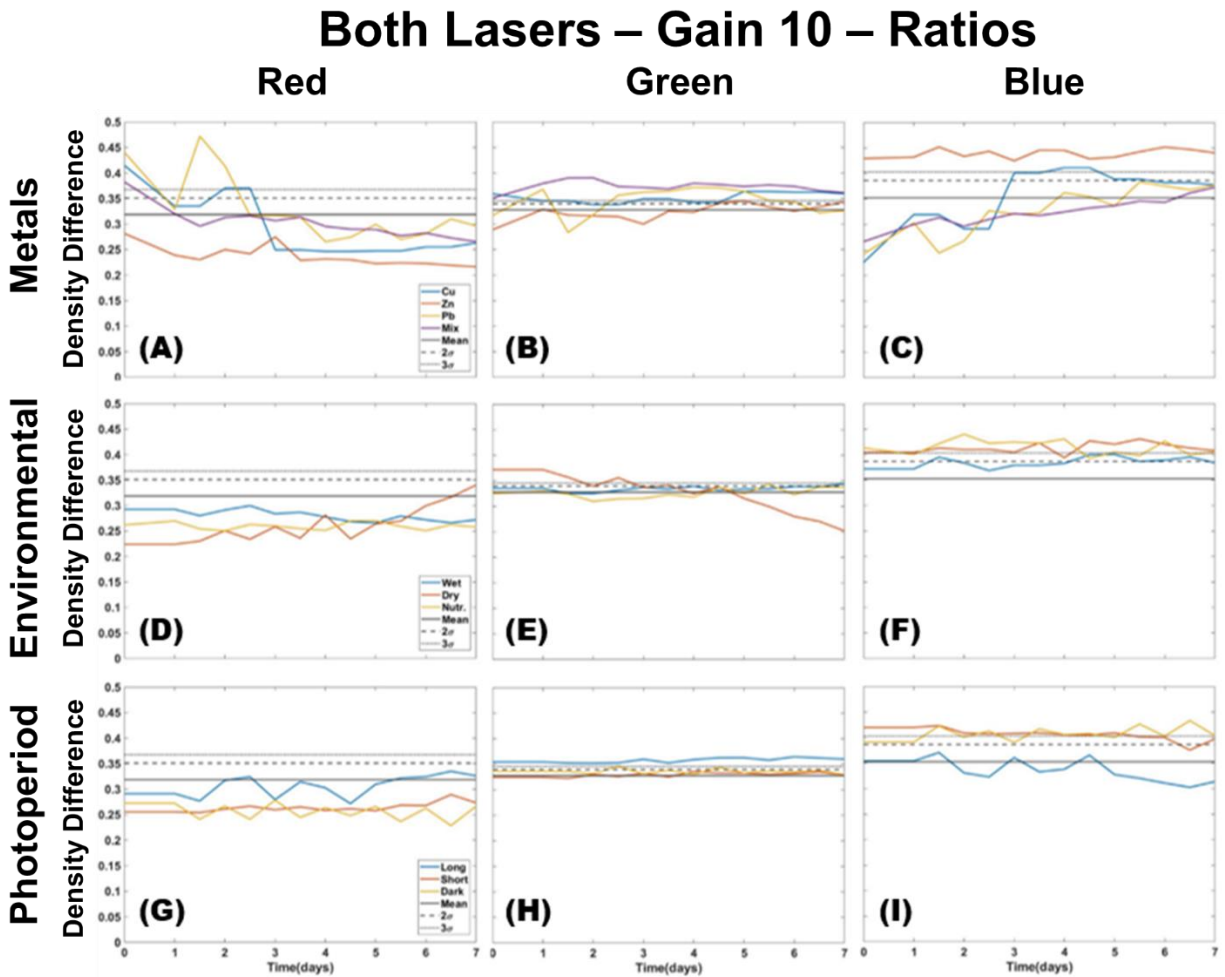


Figure 2.11: Plotted ratios of density difference for individual color fraction of the total difference. Values match those found in Figure 2.10.

2.5 DISCUSSION

The presented experiments illustrate that with carefully tailored methodology (laser combination, gain setting, and color analysis method), it is possible to use LIF to identify metal contamination in moss at environmental levels (nmol/cm^2) even when compared to plants put under environmental stress. From the various settings tested, the system using both lasers proved to have the best sensitivity to all metals compared to just the individual lasers. All tested gain levels produced comparable results, but images produced at lower gain levels may be preferable to ensure that oversaturation and the addition of noise are reduced in the collected images. All analysis (Figures 2.3-5) demonstrates that the BMM approach of using individual images that are compared to a batch of control measurements is more effective than using MMM when comparing trials to the mean of the control. The former method produces better separation of images of treated samples from the images of control samples. As for the applicability of R, G, and B colors, the blue color channel appeared to be the most sensitive in providing separation from not only the control, but also from individual dosing days when observing the metal group. The red channel was the least sensitive, but this is theorized to result from the overlap between trials associated with natural chlorophyll fluorescence (red). Therefore, separation in green and blue color channels proves to be very useful for the identification of metal contamination.

Using both lasers, capturing images at a gain of 10, and using BMM for single color density difference analysis allows for detection of multiple stressors. The parameters are not sensitive to environmental stressors but photoperiod in Figure 2.6 showed major overlap with individual metals which could create difficulty in identification. Metals and photoperiod were not tested on the same sample so it is uncertain if they would have additive effects. T-test confirms that the photoperiod length could cause interference with any metal identification, but the metals themselves have a 2 or 3 color deviation from the control on dosing days. When considering color ratios, green channel separation from the control is associated with Cu and Pb metal contamination (Figure 2.10 and 2.11). Zn is difficult to discern as it overlaps with the elevated blue channel which is more consistent with environmental or photoperiod stressors. Using a Welch t-test combined with color ratios makes it possible to distinguish the type of stressor present (metal, environmental, photoperiod) when using DTW with two-color analysis, but lacks enough specificity to distinguish individual metals.

Single-color DTW analysis (Figure 2.4) had muted profiles with similar distributions seen with the density difference analysis, but single color DTW lacked clear distinction between stressors and the control. Due to the lack of differentiation between metal trials, single-color DTW was not used for comparison of environmental or photoperiod stressors as it was deemed the results would prove to be inconclusive. The only case where single-color DTW is recommended may be when attempting to distinguish whether a single metal or multiple metals are present in a given sample. Therefore, single-color DTW was not explored in the same depth as single-color density difference or two-color DTW analysis.

Two-color DTW results shown in Figure 2.8 have environmental and photoperiod profiles that rarely deviate from the natural variation of the control. However, plotting the t-test values for each two-color combination proved useful in separating a combination of metals from other stressor types (Figure 2.9). Much as with density difference we can observe that photoperiod and environmental stressors mostly only deviate in one of the two-color combinations. Zn is still difficult to identify, though a RvG and GvB combined deviation may be an indicator of Zn presence. Repeated experiments would be needed for validation. Cu shows early deviation in RvG and RvB at lower treatment levels and at higher dosing deviates instead in the RvB and GvB. This is distinct from Pb and the mixture of metals which deviate from the control in all color combinations. Because of their similar deviation it is possible that identifying Pb from the mixture of metals would be difficult and understanding of the response of other metal combinations is unknown at this time.

The levels of metals used for treatments were well within the range detectable in areas of concern like industrial, mining, or roadway sites. From the metals tested, Pb has the strictest environmental limits based on international guidelines to protect human health (Table 2.2). Pb is toxic and shows a strong response in moss regardless of the experimental settings and analysis methods. Zinc on the other hand could only be detected at a much higher threshold, which may hint that larger doses are needed for plants to be affected but the difficulty in detecting the treatment levels of Zn tested are acceptable as they are low enough to not be of concern to public health. It is also important to note that though there may be a particular concentration of metal accumulated in soil or solution that does not mean a 100% uptake will occur in any given plant. Our focus was mainly on atmospheric deposition, though overland transport can be administered

through wet or dry deposition. Values for measured accumulation documented by EPA ambient air quality monitoring programs or via studies into vegetation have been compiled into Table 2.3.

Table 2.2 – Natural or international guidelines for metal content in soil, water, and air

	Cu	Zn	Pb
Soil	50-140 mg/kg	10-300 mg/kg	5-30 mg/kg
Water	-	-	10 lg/L .001-.06 mg/L (uncontaminated)
Air	-	-	0.5 lg/m ³ 4-20 mg/g (dust)
Lowest Level Tested	0.34 mg/m ²	-	-
Highest Level Tested	34 mg/m ²	-	-

*Bardi, 2010; WHO, 2007; Serbula, 2008

Table 2.3 – Examples of measured wet and dry deposition values for Cu, Zn, and Pb

Wet Deposition		
Cu	Zn	Pb
0.49-2.2 mg/m ² /yr New Jersey (Reinfelder et al., 2005)	2.41 mg/m ² /yr Gary, Indiana (Willoughby, 1995)	1.06 mg/m ² /yr Gary, Indiana (Willoughby, 1995)
0.70 mg/m ² /yr Reston, Virginia (Conco et al., 2004)		2.20 mg/m ² /yr Chicago, Illinois (Vermette et al., 1995)
1.06 mg/m ² /yr Chicago, Illinois (Colman et al., 2001)		
0.8±0.7 mg/m ² /yr Urban China Pan and Wang (2015)		
4.7 mg/m ² /yr Hong Kong, China Pan and Wang (2015)		
14.6 mg/m ² /yr Singapore Pan and Wang (2015)		
Dry Deposition		
Cu	Zn	Pb
3.65 mg/m ² /yr Michigan (Paode et al, 1998)		1.10 mg/m ² /yr Michigan (Paode et al, 1998)
21.9 mg/m ² /yr Chicago, Illinois (Paode et al, 1998)		25.55 mg/m ² /yr Chicago, Illinois (Paode et al, 1998)

Based on these reported values, detection of Pb and Cu are assumed to be possible with this technique. Some of the treatment levels represent a yearly deposition inventory that would

match a single dose administered in our experiment. However, previous work has shown the single dose or cumulative treatments provide similar results (Truax et al., 2022). Consideration would then need to be given to a plant, such as moss, that would have a long enough life span to monitor long term accumulation as well as the potential to record inputs from more recent events. Many of these values (mg/m²; mg/L) provide a baseline level from which to assume anthropogenic contamination in industrialized, urban areas, or near highways. Mixtures of metals are easy to identify but the metals themselves will continue to prove to be difficult to identify. It is recommended that other metals, combinations, and overlaps between metals and other stressors should be further explored to better understand the LIF response recorded in mosses. Other studies have implemented comparison to transpiration or photosynthetic rate which would help confirm that stress is being induced via any one trial tested (Lichtenthaler et al., 1990; Buschmann, 2007; Marques da Silva, 2018). It would also help to gauge how much stress a particular moss might be under before, during, and after experimentation.

There are several studies looking at the impact of environmental stressors on the health and response of plants. These responses can be highly variable based on the type of vegetation and the environmental factors at play in a particular ecosystem. Vascular plants often have more complex responses to stress than more simplistic nonvascular plants like mosses. Understanding how each may respond through changes in photosynthetic efficiency could greatly improve the broad application of the LIF technique (Swoczyna et al., 2022). Even amongst taxonomically close species like bryophytes, there can be drastic differences in response to temperature and precipitation directly affecting pigment and health (Rastogi et al., 2020; Świsłowski et al., 2021a). Though there are numerous studies looking at the resiliency and benefit of using moss as bioaccumulators and the time of accumulation, but there are far fewer that question natural environmental factors that could impact plant health outside of agriculture. The only consistent metrics appear to be based on water availability which appear to more greatly impact moss than even the harshest of climates (Malenovský et al., 2015; Świsłowski et al., 2021b). There could be room for experiments that lead to a better understanding of the effect such conditions may have on photosynthetic rate and plant capacity for metal accumulations in the case of bioremediation.

With respect to metal location within plant tissues, it is possible in future work to explore chlorophyll concentration and potential a/b ratio changes. This could help to inform if shifts in

captured fluorescence color in images are due to stress, metals, or both. If Zn is sequestered into lipid structures instead of within chlorophyll itself, then that would have a direct impact on the fluorescence response recorded. Pairing these methods with a more chlorophyll specific laser system could also help document if changes are specific to different metals and aid in the understanding of active organic reactions in addition to plant health (i.e., microbial activity; Segura et. al, 2009; Chaudhry et al., 2021). Future work aims to explore the impact of these stressor specifically to chlorophyll-a and -b in order to better understand plant response through LIF. Continued use of the density difference and DTW methods will be key to measuring differences from control samples and monitoring the effectiveness of the technique moving forward.

2.6 CONCLUSION

After testing several types of stressors in mosses and capturing the results via images of LIF, distinctions can be made between heavy metal stress, environmental stressors, and changes in photoperiod. Use of both the UV and green lasers is still the optimal when used with density difference and DTW analysis. Density difference is best used for single-color analysis with t-test verification of deviation from the control. DTW is most effective for two-color analysis and clear separation of metals from other stressors. Three color analysis using ratios and raw difference values allows us to separate out individual metals from each other or distinguish between similar responses between stressor types observed using density difference or DTW. Further exploration of the combined effect of photoperiod with metal stress is of interest. Metal identification at nmol/cm^2 levels is possible, though Zn and Cu are more difficult to distinguish at 1 nmol/cm^2 which is within acceptable environmental background levels for those metals. Pb and a mixture of metals, however, can be detected at such low thresholds which are a high risk compared to Zn and Cu. The detection limits documented in this research are still within the range of levels known to impact plant and human health and could be used as a tool for early detection monitoring. Future work strives to adapt the technique for field use for multiple types of vegetation to monitor the environmental health of plants and to aid in the detection of contaminate sources.

3 COMPARISON OF TWO LASER SYSTEMS TOWARD AN IMPROVED TECHNIQUE USING LIF TO MONITOR CHLOROPHYLL RESPONSE IN MOSS

3.1 ABSTRACT

Laser induced fluorescence (LIF) is an emerging technique for studying a broad spectrum of organic processes. Previous work has been successful in using LIF (CoCoBi; Nd:YGa pulsed laser system) to identify metal contamination and environmental stress in mosses. However, there are several metabolic processes in plants that can result in a fluorescence response as a result of metal contamination or other changes in chlorophyll content. To better understand these responses the research set out to compare two laser systems, the CoCoBi and a newly developed Chl-SL, to determine which was best for identifying the presence of Cu at environmentally relevant levels. The Chl-SL has two blue lasers (445 and 462 nm) to excite moss samples at the peak absorption for chl-a and -b. Both laser systems employ a CMOS camera to capture the short lifetime fluorescence as images that are then processed for comparison to a control trial. Three trays of moss were dosed with increasing levels of Cu (1, 10, and 100 nmol/cm²) and fronds were collected from each to conduct metal and chlorophyll extraction for validation of LIF results. As expected, the CoCoBi has a more variable result from image analysis while both the Chl-A and Chl-B lasers perform better. Image analysis compared with chlorophyll content revealed a decrease in chl a/b ratio at the time of dosing when using higher doses of Cu. This would support that metal stress has an initial impact on chlorophyll response and that it can be documented using LIF.

3.2 INTRODUCTION

Excess levels of heavy metals in the environment are a continuing concern to the health of ecosystems and human populations (Giannakoula et al., 2021). High concentrations of essential metals (Cu, Zn, etc.) can be just as toxic as non-essential heavy metals (Pb, Hg, etc.) leading to negative physiological response and growth inhibition in plants (Vázquez et al., 1999a; Nagajyoti et al., 2010; Krzesłowska, 2011; Heckathorn et al., 2004; Hall, 2002). These metals can continue to accumulate in the environment over time, creating higher risks of contamination in soil and water and thus a need for remediation (Stankovic, 2018; Norgate et al.,

2007; Zhang et al., 2018). Copper (Cu) is one such essential micronutrient that exists naturally in the environment but is also used for industrial and agricultural purposes (Nagajyoti et al., 2010; Giannakoula et al., 2021). High concentrations of Cu can be toxic to plants, and though necessary for metabolic processes can cause damage to cellular structures in excess (Heckathorn et al., 2004; Hall, 2002; Rocchetta & Küpper, 2009).

Many methods rely on chlorophyll monitoring as an indicator of plant health, as chlorophyll is considered the most important acceptor and emitter of visible light energy through the photosynthetic processes (Chappelle et al., 1985). Use of fluorescence offers an opportunity to monitor plant stress and metal contamination through effects on biochemical and physiological effect that directly impact photosynthetic efficiency. This efficiency is determined through measurement of fluorescence, where energy transfer to chlorophyll occurs due to the compact nature of chloroplast structure (Chappelle et al., 1984). Fluorescence is defined as the short lifetime emission of light due to absorption of a wavelength followed by an emission returning a molecule to its ground energy state (Chappelle et al., 1985; Fedotov et al., 2019; Lakowicz, 2006; Jameson, 2014). Changes due to stress may result in a significant decrease in chlorophyll content and activity, and, therefore, result in observable changes to fluorescence response (Chappelle et al., 1984; Hedimbi, Singh, & Kent, 2012).

Truax (2022) and others (Lakowicz, 2006; Jameson, 2014; Yang-Er et al., 2019) show that metals can bind to chlorophyll and produce specific fluorescence signatures. However, other proteins within plants can also incorporate or be affected by metals, and fluoresce within the visible region (Jameson, 2014; Chappelle et al., 1985), leading to the potential for multiple signatures to be recorded depending on the type and wavelength of the laser used to induce emission. Previous work used the Color Compact Biofinder (CoCoBi; Misra et al. 2021) due to its sensitivity in detecting the short lifetime fluorescence of pigments in living systems. Though effective in determining the presence of contamination in vegetation (Truax et al., 2022), the CoCoBi's strength of detecting a broad range of organic molecules using two pulsed lasers fired at nano second rates (355 nm UV and 532 nm Green) means color changes likely result from other pigments or molecular interaction and not just limited to chlorophyll response (Gunther et al., 1991; Jeffrey et al., 2003). It is hypothesized that a better metal to chlorophyll specificity and determination of contaminant presence could be achieved using imaging targeted specifically

towards changes in chlorophyll-a and -b. Thus, the development and testing of a new system that focuses on chlorophyll absorption bands could aid LIF research.

Experimentally induced fluorescence emission by chlorophyll has long and widely been used to evaluate plant physiology and characterize photosynthetic efficiency through electron transport (Krause & Weis, 1991; Kolber et al., 2005). The degree of fluorescence, or intensity, depends on the properties of the molecular structure (Valeur & Berberan-Santos, 2011). Of the available technology, pulse amplitude modulation (PAM) is the most commonly used, but remains impractical for application to remote sensing at a distance (Schreiber et al. 1986; Schreiber & Bilger 1993; Schreiber, 2004; Brooks & Niyogi, 2011; Haidekker et al., 2022). Lasers can be used to produce a broad range of wavelengths making them excellent sources of light for inducing fluorescence. Semiconductor diodes have become increasingly popular due to their broad application and low cost compared to pulsed solid state or gas-tube systems (Valeur & Berberan-Santos, 2011; Silvia & Utkin, 2018).

Chlorophyll content and photosynthetic efficiency can play a large role in the use of LIF and the ability to monitor changes associated with stressors or physiological factors (Chappelle et al., 1984). Israsena Na Ayudhya et al. (2015) conducted experiments using ferns to demonstrate the primary absorption bands for chlorophyll-a and -b. The higher absorption bands are typically used in red or near-IR (650-710 nm) but the corresponding emission bands are light sensitive and require close proximity to the sample of interest (Buschmann, 2007). We propose, instead, to use the lower (blue) wavelengths of 445 nm and 462 nm (Chl-a and -b) presented by Israsena Na Ayudhya et al. (2015; Brach et al., 1977), which will produce emissions in the visible red region (650 nm for Chl-b and 670 nm for Chl-a) and can be documented with the same CMOS camera previously used with the CoCoBi (Misra et al., 2021). These blue wavelengths have been historically used in both pulsed and continuous forms to study chlorophyll photosynthetic efficiency (Kolber et al., 2005).

Previous research was focused on determining if the new image analysis techniques when paired with the CoCoBi could be effective in identifying stress in moss (Truax et al., 2022). More specifically, if the methods could be used to delineate a specific stressor type (metals, environmental, photoperiod) or metal (Cu, Zn, Pb, Mix). It was possible using a combination of techniques to delineate metal contamination at environmentally relevant levels (nmol/cm^2) from other stressor types. In some cases, it was even possible to identify contamination as Cu or Pb.

However, responses from the plants exposed to Zn or other stressor types produced similar deviation from the control and lead to the desire to create a system that may be more chlorophyll specific to determine if it can improve the sensitivity, link changes in chlorophyll to metal treatment, and limit the contributing biological factors found in a variety of plant types.

The objective of the current research was to determine the best laser wavelengths for use in monitoring chlorophyll response to the addition of excess Cu at environmentally relevant levels (nmol/cm²) for inducing changes in plant response. Previous literature suggests that increasing metal exposure results in decreasing Chl-a/b ratios in moss (Shakya et al., 2008). Hence the hypothesis in this work is that changes in plants observed by chlorophyll specific LIF techniques will be correlated with copper and chlorophyll levels measured directly after their extraction from plants. The work also allows for further expansion of previous by using the same moss species and Cu treatment levels to prove the reproducibility and mechanism of the LIF technique paired with image processing methods. Color histograms are produced from the collected images of LIF and compared to a control to determine if statistical deviation from an untreated control plant is present in a given sample. Chemical analysis of chlorophyll-a and -b content, as well as metal accumulation within the plant were conducted to validate any observed analytical trends found in each of the laser systems tested.

3.3 METHODOLOGY

This work builds on previous work and complements LIF by the direct evaluation of treated moss by chemical analysis of chlorophyll and Cu after their extraction from the plants. This work helps validate the findings in Truax 2022 using the CoCoBi, and applies methods developed in Truax 2020 to compare the evolution of the different laser systems used (Standoff Biofinder – Misra et al., 2018; CoCoBi – Misra et al., 2021). The research is divided into four parts with the first focused on laboratory treatment and cultivation of the moss samples. Part two uses LIF to capture color images of the moss response to various treatments from part one. Part three includes chemical analysis of chlorophyll and Cu extracted from the treated moss samples. Finally, in part four, LIF images are processed to quantify moss response to observed absorbed Cu concentrations and respective measured chlorophyll levels.

3.3.1 Laboratory Cultivation and Cu Treatment

The moss collected for experimentation, *Thuidium plicatile*, is an endemic moss species to Hawai‘i (Staples et al., 2004; see Notes on Moss Species) and can be found on the island of O‘ahu along the Wa‘ahila Ridge Trail and State Recreational Area (21.307°, -157.797°). The shaded area sits along the Southeastern part of the Ko‘olau mountains and represents an uncontaminated environment where the species can be found year-round. After collection, moss samples were washed and cleaned of forest litter before being placed on three different trays each covering an area of 587 cm² (7in. x 13in.). These trays were then placed within a laboratory grow tent with an average temperature of 18-20°C, 50-60% relative humidity, and 14-17 W/m² ambient light (1400-1800 lux), with a day length of 10 hours. Two weeks were allotted for plant acclimatization to the grow tent before beginning experiments.

The experiment was run over a 72-hour period with each moss tray being imaged every 8 hours. The first 24-hour period included no Cu treatments in order to record a baseline control for each tray before dosing. At the 24-hour mark (or time 0) each tray received a single dose of Cu with the Tray 1 receiving 1 nmol/cm², Tray 2 10 nmol/cm², and the Tray 3 100 nmol/cm². Moss response was then monitored by LIF for another 48 hours. A wire grid was constructed to divide the moss trays into 10 equal partitions from which multiple images could repeatedly be taken of the same sample space on a given moss tray. After imaging, a single frond and a pair of fronds were selected once a day (every 24 hours starting with the control) from each of the 10 partitions on each moss tray. The single frond was imaged and then underwent chlorophyll extraction (3.3.3.1). The pair of fronds underwent the sequential elution technique (SET) for metal extraction (3.3.3.2). Once fronds had been imaged, the trial tray was returned to the grow tent accounting for no more than half an hour of time away from the grow tent.

3.3.2 Laser Systems and LIF Technique

This study compares LIF using the CoCoBi (Misra et al., 2021) and a newly designed chlorophyll specific laser system (Chl-SL). Both systems use the same CMOS camera that is integrated with the Baumer Camera Explorer software which allows the user to control camera settings and capture images for later analysis. The CoCoBi is a pulsed Nd:YGa dual laser system (green 532 nm excitation laser and UV 355 nm excitation laser) fired at a nanosecond rate (112 ns). The Chl-SL system uses two semi-conductor diode lasers at the 445 nm and 462 nm wavelengths (these are continuous). The CoCoBi has integrated time synchronized pulses

which allow it to image at any time of day, while the new system prototype does not have this feature. In order to keep comparisons fair between the two units, imaging was only done in the dark. With the caveat that if successful, the Chl-SL system can be improved by the addition of the pulsed feature hence daytime use.

A diffuser was tested on all systems to spread the laser beams into a uniform illumination across the surface of the moss sample. But the filters with the CoCoBi did not allow enough light through for effective image analysis. Thus, the filters are only employed with the new laser system. The new system also has the option of using band pass filters at the 650 nm and 670 nm wavelengths to capture emission specific to Chlorophyll-a and -b. These band pass filters heavily limit the fluorescence signatures to a 10 nm wide range of light on the spectrum that are received by the camera sensors. By limiting the wavelengths of light that are measured we can ensure that the received signal is associated with a chlorophyll emission and not another biological reaction. Figure 3.1 shows an image of the CoCoBi and new Chl-SL side by side. Figure 3.2 shows each of the lasers and filter options.

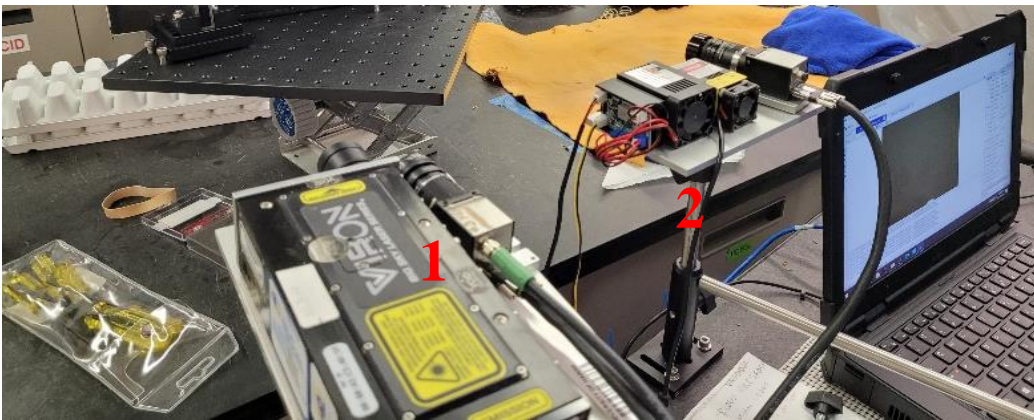


Figure 3.1: Bottom left (1) shows the CoCoBi and middle right (2) shows the Chl-SL allowing a direct comparison of the size and flexibility of set-up of both systems. Chl-SL is more compact and represents a transition towards a lighter more mobile LIF system. Both lasers are connected to a computer using the Baumer Camera Explorer software to capture images.

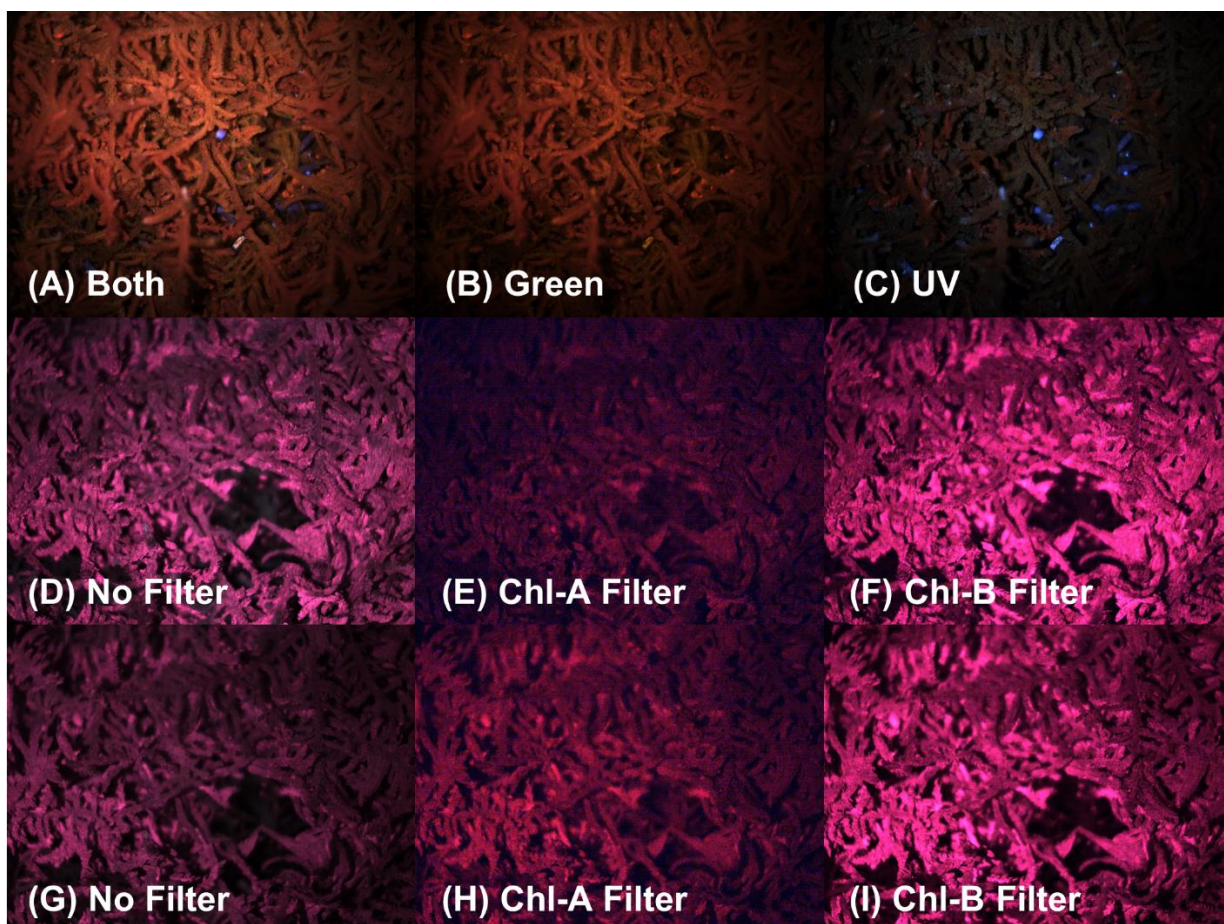


Figure 3.2: Images of the same moss sample taken by various combinations of laser systems as follows: (A) CoCoBi using both lasers. (B) the Green 532 nm CoCoBi laser. (C) The CoCoBi 355 nm laser. (D) Chl-a 445 nm laser without a filter. (E) Chl-a laser with 670 nm Chl-a bandpass filter. (F) Chl-a laser with 650 nm Chl-b bandpass filter. (G) Chl-b 462 nm laser without a filter. (H) Chl-b laser with 670 nm Chl-a bandpass filter. (I) Chl-b laser with 650 nm Chl-b bandpass filter.

Each tray of moss was divided into 10 sections using a wire grid. Samples were imaged starting day 1 (time = -24 hours) to collect a baseline control for each tray. Metal dosing occurred 24 hours later on day 2 before imaging (time=0). The moss trays were always imaged after wet deposition when applicable (every 24 hours). When not dosed with metal, moss trays were only given 50 mL of DI. Imaging was conducted every 8 hours in 30-minute windows in order of trial number. Imaging times were held consistently for each sample between 5-8 am, 1-4 pm, and 9-12 pm. Images were collected by integrating the Baumer Camera Explorer software with the CMOS cameras paired both the CoCoBi and the Chl-SL. Images (Figure 3.2) were collected using just the 532 nm green laser, just the 355 nm UV laser, and both lasers in tandem for the

CoCoBi. The Chl-SL collected images using the 445 nm laser with no filter, 445 nm with the 650 nm filter, 445 nm with the 670 nm filter, 462 nm laser with no filter, 462 nm with the 650 nm filter, and the 462 nm with the 670 nm filter. The 650 nm band pass filter corresponds to the maximum emission peak for chlorophyll-b while the 670 nm band pass filter corresponds to chlorophyll-a (Israsena Na Ayudhya et al., 2015). Preliminary testing was conducted to determine optimal camera settings to streamline sampling to a single image per laser and/or filter combination limiting each of the 10 collected sample areas on a tray to having 9 images each.

3.3.3 Chemical Analysis

To assess the actual metal uptake and chl changes in the plants corresponding to the observed LIF results, traditional chemical analysis was also conducted. Chlorophyll and metals were extracted from moss fronds every 24 hours after laser imaging throughout experimentation (starting at time 0). Metal concentrations absorbed by the plants were measured using the sequential elution technique (Pérez-Llamazares et. al., 2010) followed by ICP-MS analysis (ICP-MS, Thermo-Fisher Element 2, University of Southern Mississippi Center for Trace Analysis). Chlorophyll extraction from a single frond (Hu et. al., 2013) was followed by spectrophotometry (Hewlett Packard Diode Array Spectrophotometer; Caesar et. al., 2018) allowing for the measurement of Chl-a and -b in DMF.

3.3.3.1 Sequential Elution Technique (SET)

The effectiveness of the Cu treatment was assessed by the direct measurement of Cu inventory in moss. After imaging each day, 10 pairs of fronds were removed from each tray corresponding to the 10 imaged areas of the treated moss. The fronds were each cut 2 cm from the tip, weighed, and then leached using a sequential elution technique (SET) to extract metal from the surface of moss as well as its extra- and intracellularly bound Cu content (Brown & Wells, 1988; Vázquez et. al., 1999a). Frond pairs were shaken in 10 mL of DI for 30 seconds to remove any unbound metals. The fronds were then removed from the DI water, dried, and immersed in 10 mL of 10 mM ethylenediaminetetraacetic acid (EDTA) solution (Pérez-Llamazares et. al., 2010). Fronds were submerged and shaken in EDTA solution for 45 minutes. The process was then repeated in a fresh fraction of 10 mL of EDTA for 30 minutes. The two EDTA fractions were combined for extracellular Cu analysis. Samples were then blotted dry, weighed, then dried in a furnace at 50°C for 24 hours before cooling for 24 hours in a desiccator.

The dry weight of cooled fronds was recorded and, finally, samples were submerged in 10 mL of 1M HNO₃ for 30 minutes of shaking to induce partial digestion and release of intracellular Cu fractions.

All samples were then analyzed for copper content (DI, EDTA, and HNO₃). The individual DI water, EDTA, and nitric acid fractions were analyzed for Cu concentration using a sector-field inductively coupled plasma–mass spectrometer (ICP–MS, Thermo-Fisher Element 2) at the University of Southern Mississippi Center for Trace Analysis (CETA). A self-aspirating nebulizer (Elemental Scientific, Omaha, NE, USA) with low-flow (100 µL/min) and Teflon spray chamber was utilized. Cu-63 was determined in medium resolution and calibration was conducted using external standards made in 0.16 M ultrapure nitric acid. These were then checked against standard reference waters from the U.S. Geological Survey. There was also an in-house consistency standard measured to ensure a sensitivity check, long-term stability, and instrumental drift correction. Cu analysis was also conducted for solution blanks of DI, EDTA, and HNO₃ and time 0 control non-treated fronds to determine baseline Cu concentrations.

3.3.3.2 Chlorophyll Extraction Method

To assess chlorophyll content and physiological response a protocol used for chlorophyll extraction in water lettuce was adapted for the moss samples (Moran & Porra, 1980; Porra, 2002; Inskeep & Bloom, 1985). After imaging, 10 single fronds were removed from each tray corresponding to the 10 imaged areas of the treated moss. Each moss frond was measured from the tip to a distance of 2 cm at which point they were cut with a sterilized razor blade. The samples were then weighed before being placed within a plastic sample tube. Once all fronds were measured and weighed, 2 mL of DMF (N-Dimethylformamide) was added to each sample. Initial testing showed that 1 mL DMF was needed for each cell layer of a sample, and the moss species was deemed to be 2 cell layers thick (Petschinger et al., 2021). DMF is more effective at limiting the continued degradation of chlorophyll than ethanol or acetone, and can be used (when kept cold) for longer periods of time after extraction is initially conducted (Porra, 2002; Hu et al., 2013).

Samples were then capped, wrapped in aluminum foil, and immediately placed within a cooler with ice packs to limit the amount of light exposure. All samples were given 48 hours before they were measured by spectrophotometry for Chl-a and -b using a 1 mL cuvette. The

cuvette was washed with DMF before 1 mL of DMF was used to calibrate the spectrophotometer (Hewlett Packard Diode Array Spectrophotometer). Measuring of samples was then conducted with cuvette cleaning and recalibration process conducted every 30 samples. Altogether 120 samples were analyzed using values of $E^{663.8}$ and $E^{646.8}$ collected for each frond and used to determine *Chl a* (Eq. 1), *Chl b* (Eq. 2), and *Chl a+b* (Eq. 3) at $\mu\text{g/ml}$ levels (Porra, 2002). These were then adjusted for per mg wet weight of the original frond. Because fronds were immediately put into DMF after weighing a dry weight is not available.

$$[\text{Chl } a] = 12.00 E^{663.8} - 3.11 E^{646.8} \quad \text{Eq.1}$$

$$[\text{Chl } b] = 20.78 E^{646.8} - 4.88 E^{663.8} \quad \text{Eq.2}$$

$$[\text{Chl } a + b] = 17.67 E^{646.8} + 7.12 E^{663.8} \quad \text{Eq.3}$$

3.3.4 Data Analysis

3.3.4.1 Single-color comparison

As with Truax 2022, RGB (Red, Green, and Blue) pixels were extracted from each image to create density histograms based on decimal code value from 0 to 255 for each color channel. These histograms were then normalized using total pixel count to create percent abundance curves. These curves were then used to calculate the difference between treated samples and the control by either using the density difference method found in Eq. 4.

$$\text{Difference} = 1 - (\sum \min|trial(x), control(y)|) \quad \text{Eq. 4}$$

where x represents the color intensities for the corresponding trial, and y represents the same for the control images (Swain & Ballard, 1992). Or, difference can be calculated using dynamic time warping to fit one curve to another (DTW):

$$D(i, j) = |x(i) - y(j)| + \min \begin{cases} D(i + 1, j) \\ D(i + 1, j + 1) \\ D(i, j + 1) \end{cases} \quad \text{Eq. 5}$$

where x and y represent strings of data and i and j represent the length of each string so that $D(i, j)$ equals the best alignment distance between all data points along the lengths of x and y (Jekel et al., 2018). Sample images of moss from the metal group trays before treatments and all control

sample images from the week of experimentation were included for comparison. The 10 images collected from each tray were batch processed by comparing them to all of the collected control images (30).

3.3.4.2 **Multi-color comparison**

Both density difference and DTW can be used to compare single-color histograms, but only DTW can be used for two-color analysis which has been shown to improve contaminant detection and separation of individual samples from the control (Truax et al., 2022). All two-color combinations (RvG, GvB, RvB) were calculated for the collected images. A mean and standard deviation to 3σ were determined for the control and used to compare if any color channel shows a significant deviation from the control's variability. A Welch's T-test was also applied to quantitatively confirm that any one sample population effectively deviated from the control.

3.4 RESULTS

3.4.1 Comparison of image analysis methods

Initial analysis of images collected using the CoCoBi are compiled in Figure 3.3 which shows method of analysis by single- or two-color comparison. Though images were collected using the green and UV lasers independently (Appendix B – 6.2.1; tables 6.2.2), using both lasers in tandem continues to provide the most consistent response when observing Cu using LIF in moss. The three analysis methods (density difference, single color DTW, and two color DTW) are in good agreement, with single color DTW (Figure 3.3 D-F) showing a narrower range for natural variability in the control for all color channels when compared to density difference (Figure 3.3 A-C). DTW shows Tray 1 as the only sample with deviation from the control at time 0 when Cu treatment was administered and later at time 40 hours. However, Tray 2 and Tray 3 do not show any deviation from the control even though they have higher metal doses. This may indicate that the organic response is not Cu or chlorophyll specific, or is the result of metal interaction with lipid or protein structures, or that this laser system is not suitable for consistent detection of the plant response to Cu dosing. Two-color DTW (Figure 3.3 G-I)

matches the results of the single-color analysis, and confirms the consistent response between all color channels. All tables corresponding to figures can be found in Appendix B (6.2).

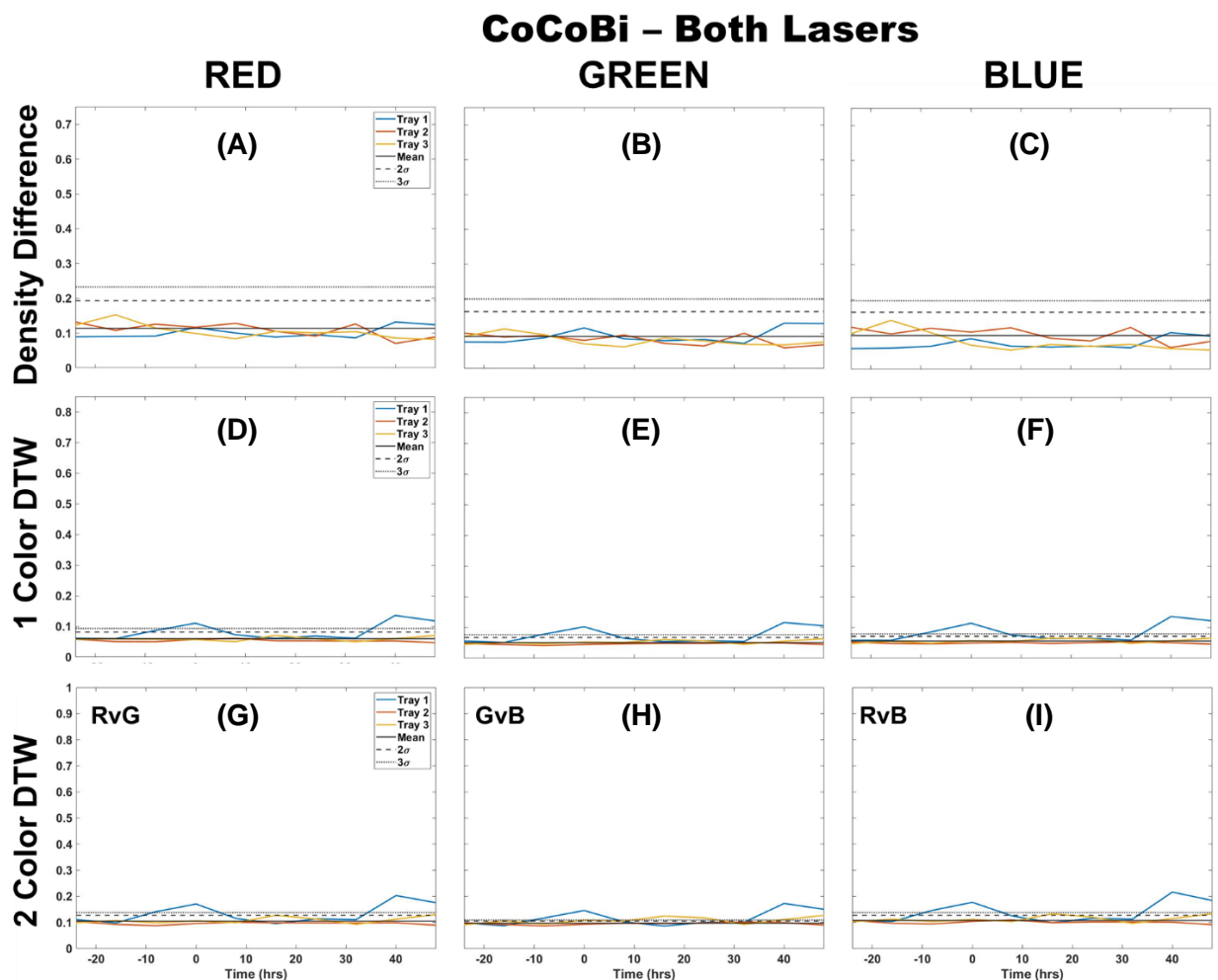


Figure 3.3: Comparison of moss response to both lasers of the CoCoBi using three image analysis methods: (A-C) single-color density difference, (D-F) single-color DTW, and (G-I) two-color DTW. Images were collected every 8 hours over three days. Control images were collected for the first 24 hours. At time 0 three Cu treatments were given at 1 nmol/cm^2 for Tray 1 (blue), 10 nmol/cm^2 for Tray 2 (red), and 100 nmol/cm^2 for Tray 3 (yellow).

Figure 3.4 is a comparison of the same analysis methods using the Chl-A laser (445 nm) with the Chl-B bandpass filter (650 nm). Results using the Chl-A laser with the Chl-A filter and with no filter can be found in Appendix B (6.2.1). Results from the Chl-A filter are comparable to the Chl-B filter but with less separation from the control. Use of no filter introduces a broader spectrum of light resulting in acceptance of all fluorescence wavelengths to the camera including those that may not be chlorophyll specific. Of the three analysis methods, the density difference

(Figure 3.4 A-C) shows the largest range of natural variability for the control and only a clear response to Cu in Trays 2 and 3 in the blue color channel. Single color DTW (Figure 3.4 D-F) condenses the control variability range allowing for observed response of Tray 2 and Tray 3 in all three color channels. Though the blue color is again the most prominent with significant deviation from control, the green shows response at both the 0 and 24 hour marks while red shows a response at 24 but only above the 2σ . Two color DTW (Figure 3.4 G-I) provides nice separation from control in multiple color combinations, but shows no separation of Tray 1 which is a low dose of Cu that would exist in natural background levels. However, the deviation at the higher doses at 10 and 100 nmol/cm² is significant.

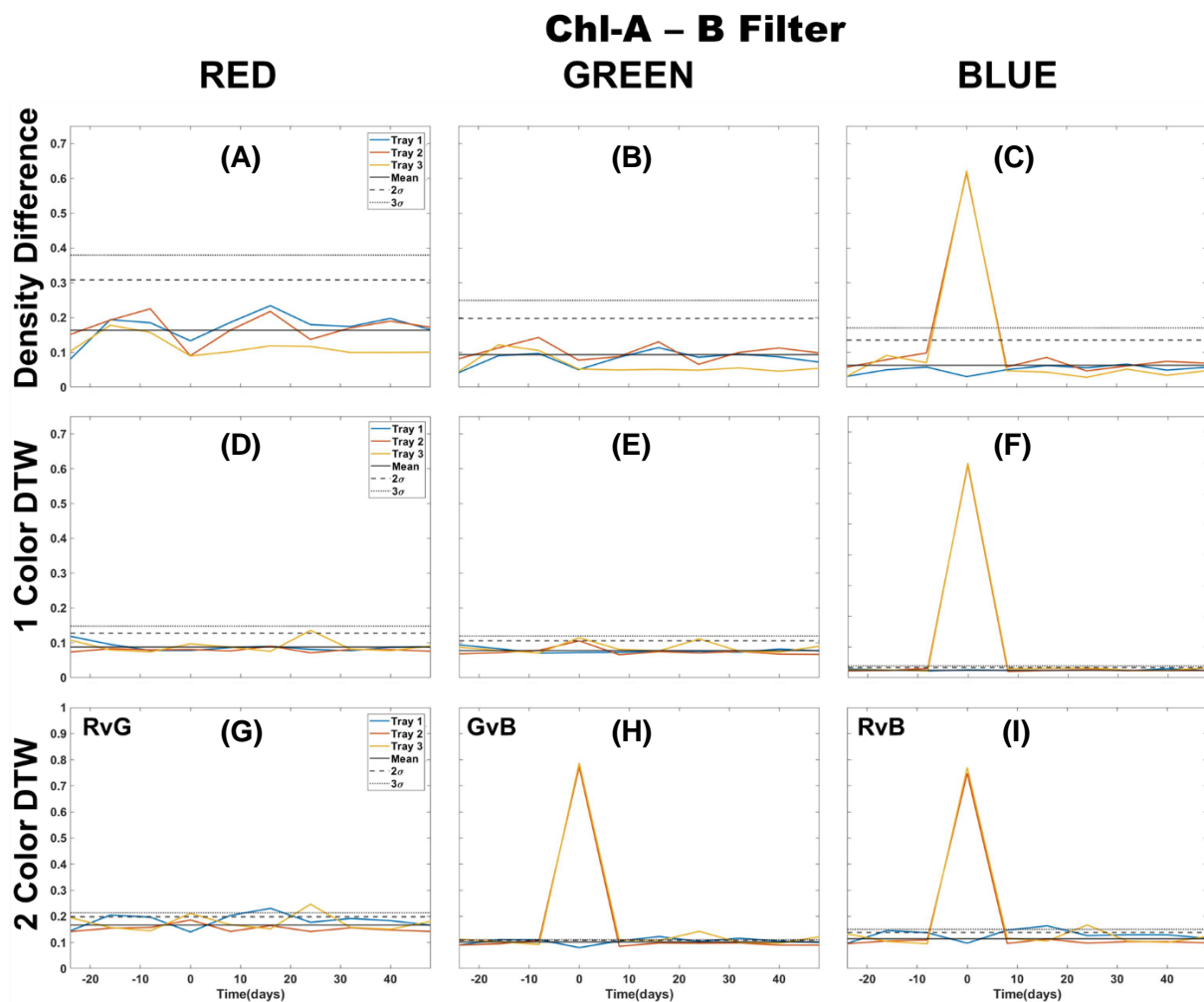


Figure 3.4: Comparison of moss response to the Chl-A laser (445 nm) with the Chl-B filter (650 nm) of the Chl-SL system using three image analysis methods: (A-C) single-color density difference, (D-F) single-color DTW, and (G-I) two-color DTW. Images were collected every 8 hours over three days. Control images were collected for the first 24 hours. At time 0 three Cu treatments were given at 1 nmol/cm² for Tray 1 (blue), 10 nmol/cm² for Tray 2 (red), and 100 nmol/cm² for Tray 3 (yellow).

As with the Chl-a laser, Figure 3.5 shows comparison using the Chl-b laser (462 nm) with the Chl-b bandpass filter (650 nm) (corresponding analysis of the Chl-a filter and no filter are located in Appendix B). Profiles of all three analysis methods using Chl-b are similar to the Chl-a laser results (Figure 4), but show no deviation from the control above 2σ except at dosing of Cu at time 0 in trays 2 and 3. Density difference (Figure 3.5 A-C) again has a larger range for control variability and shows dips in each tray at the 0 and 24 hours which could be indicative of natural day/night cycling. This is not apparent in single color DTW (Figure 3.5 D-F) which only varies from the control in the blue color channel. Two color DTW (Figure 3.5 G-I) supports single color analysis of the blue color channel impact on profiles, but unlike Chl-a there is no deviation from the control of tray 1 in any of the profiles.

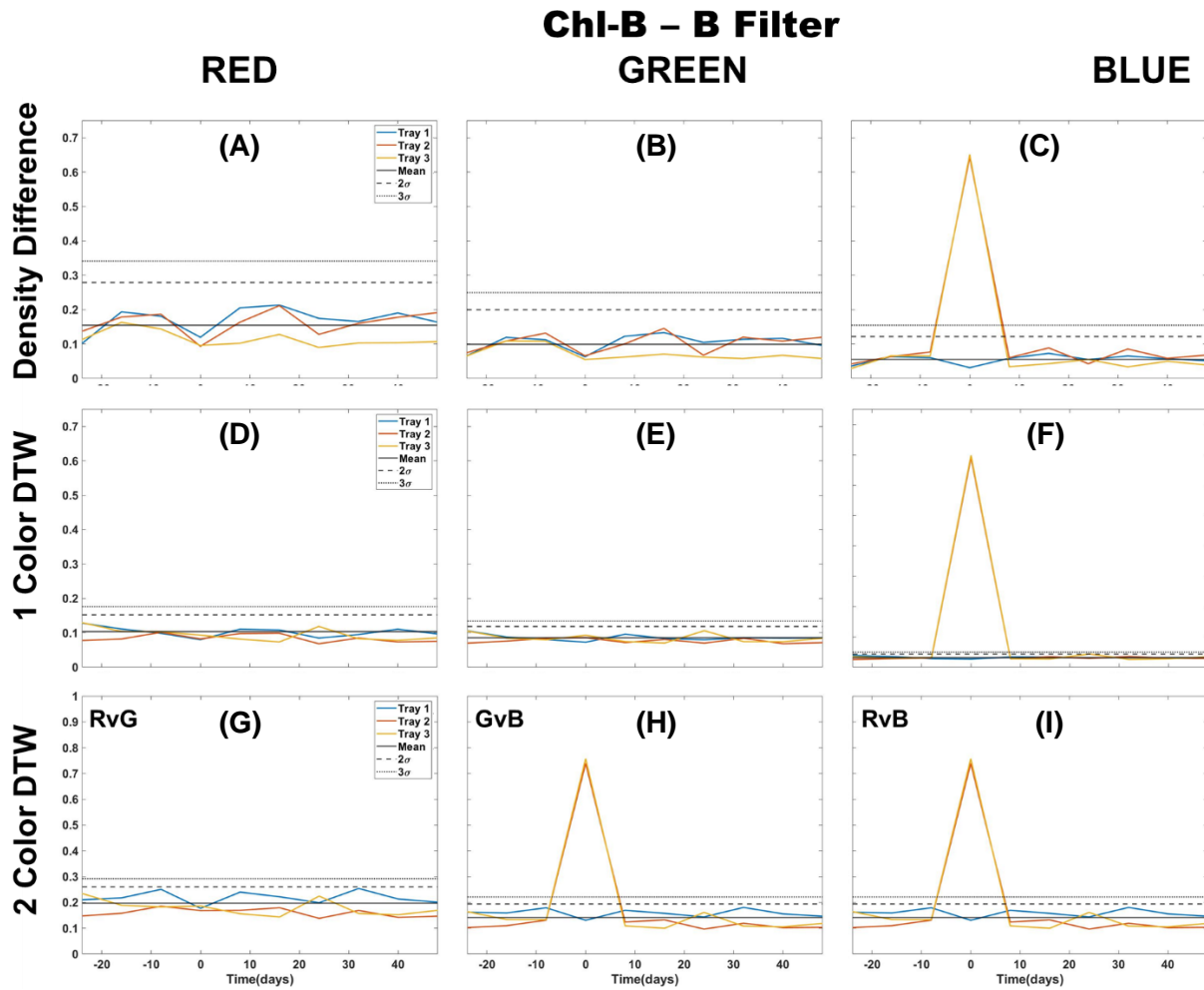


Figure 3.5: Comparison of moss response to the Chl-B laser (462 nm) with the Chl-B filter (650 nm) of the Chl-SL system using three image analysis methods: (A-C) single-color density difference, (D-F) single-color DTW, and (G-I) two-color DTW. Images were collected every 8 hours over three days.

Control images were collected for the first 24 hours. At time 0 three Cu treatments were given at 1 nmol/cm² for Tray 1 (blue), 10 nmol/cm² for Tray 2 (red), and 100 nmol/cm² for Tray 3 (yellow).

3.4.2 Comparison of CoCoBi and Chl-SL results

When observing the results of each laser system, analysis in the blue color channel reveals the best and most consistent separation of Cu dosed moss images from the control. Thus, we can compare the individual lasers and analysis methods to each other to observe any similarities or differences in Figure 3.6. The lack of separation from the control of images collected with the CoCoBi (Figure 3.6 A,D,G) is more prominent when compared to the chlorophyll specific laser wavelengths with only the lowest dosed (1 nmol/cm²) Tray 1 showing separation from the control. The Chl-A and Chl-B lasers (both using the B-filter) are in good agreement with Trays 2 and 3 deviating at the time of dosing (time 0). This may confirm that the response recorded by the CoCoBi regardless of analysis method is not Cu or chlorophyll specific. The profiles of Chl-A (Figure 3.6 B,E,H) and Chl-B (Figure 3.6 C,F,I) are similar between all analysis methods with the clearest separation between the two lasers' results in the two color DTW analysis. Difference determined by single color DTW is more difficult to identify, but it is clear in two color DTW that statistically significant deviation from the control only occurs in Trays 2 and 3 at the time of Cu dosing when using the Chl-A or B lasers.

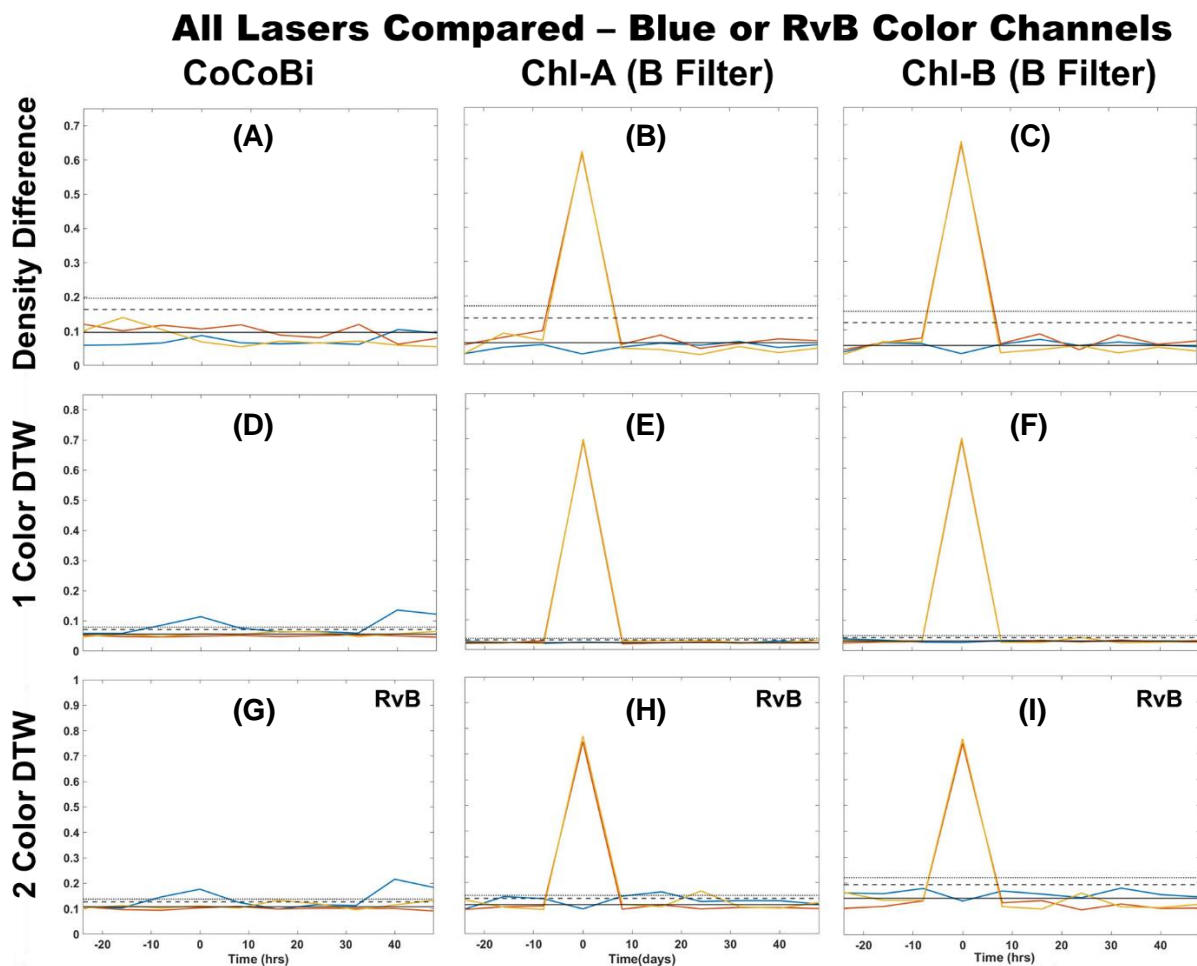


Figure 3.6: Comparison of 3 laser systems (CoCoBi – A,D,G; Chl-A – B,E,H; Chl-B – C,F,I) and 3 analysis methods (density difference – A,B,C; single color DTW – D,E,F; two color DTW – G,H,I) in the blue or RvB color channel. Images were collected every 8 hours over three days. Control images were collected for the first 24 hours. At time 0 three Cu treatments were given at 1 nmol/cm² for Tray 1 (blue), 10 nmol/cm² for Tray 2 (red), and 100 nmol/cm² for Tray 3 (yellow).

To provide validation and specificity to the results in Figure 3.6, a Welch T-test was used to compare all analysis methods by a common metric (t-value) and a potential to provide separation between individual Trays (Figure 3.7). The CoCoBi t-values show more separation from the control than observed in Figure 3.6, yet the patterns are inconsistent between analysis methods and further underline the non-specificity of the CoCoBi system. The density difference has more subtle deviation from the control with separation at time 0 when looking at Tray 3. However, all Trays show better separation the longer time passes from Cu treatment. Both DTW methods are punctuated with numerous and, perhaps unspecific, moss response which do not match dosing at time 0 or any day-night cyclical pattern. When looking at the Chl-A and Chl-B

lasers results while using the Chl-B filter, they are again in good agreement between analysis methods. However, the Chl-A results show higher Tray 3 response than Tray 2 for both single color analysis methods, while Chl-B only shows this for density difference. When using two-color DTW the Chl-A laser appears to show larger separation between trays and some low-level detection 24 hours after dosing. Chl-B could be just as useful regardless of analysis method and provides the ability to determine levels of Cu treatment for detection when using both simple analysis and when comparing t-value results.

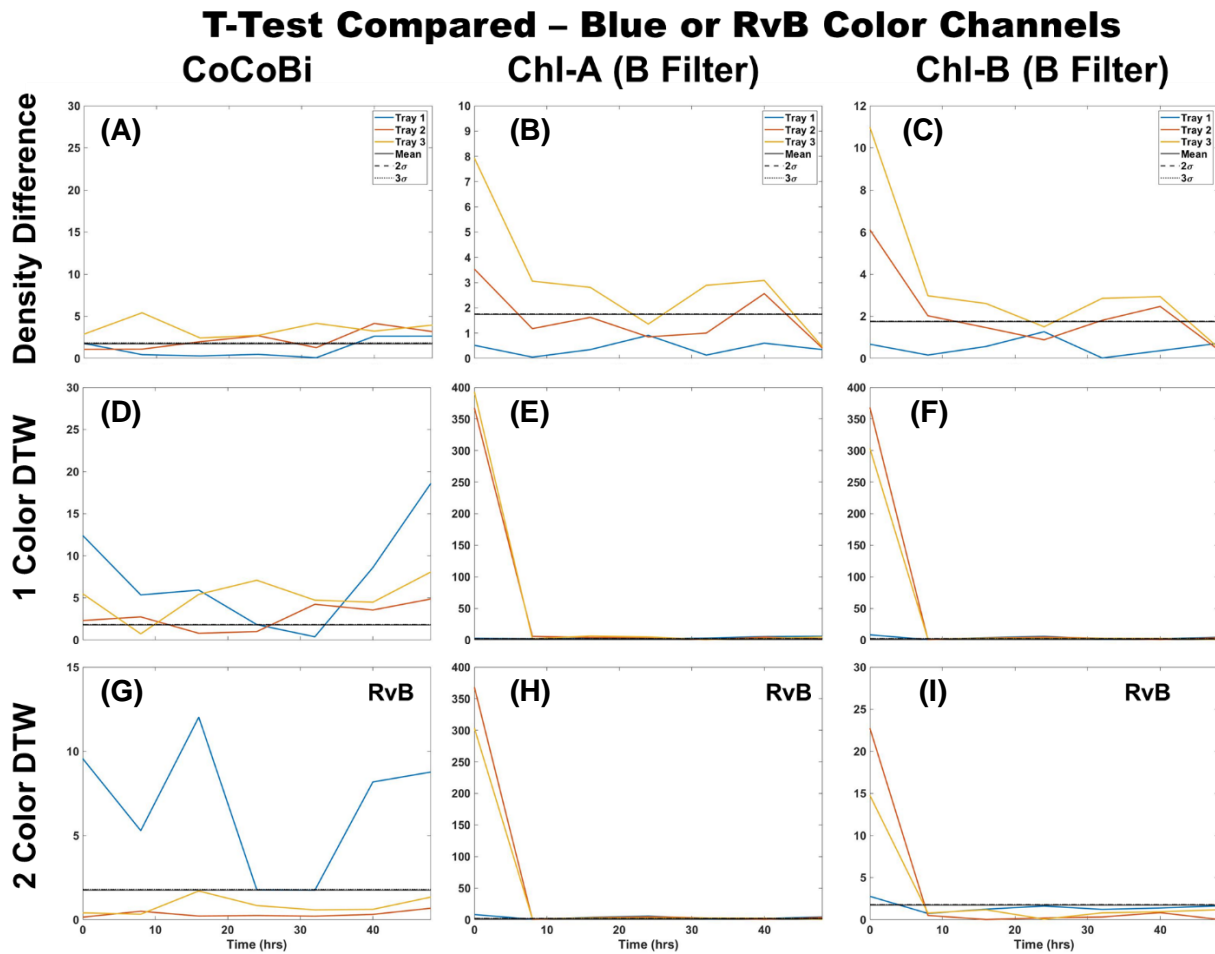


Figure 3.7: Moss tray images compared to the control and validated using a Welch t-test plotted as shown. Time starts at the initial dosing (time 0) and continues 48 hours) to compare the 3 laser systems (CoCoBi – A,D,G; Chl-A – B,E,H; Chl-B – C,F,I) and 3 analysis methods (density difference – A,B,C; single color DTW – D,E,F; two color DTW – G,H,I) in the blue or RvB color channel.

3.4.3 Metal and Chlorophyll Extraction

It is clear that the CoCoBi is outperformed by the more consistent results shown by the Chl-SL lasers. The results of the two color DTW analysis using RvB for Chl-A and Chl-B lasers were used to compare to the chlorophyll and metal extraction results. Mean and standard deviation for these values can be found in Table 3.1 (chlorophyll extraction) and Table 3.2 (metal extraction). Figure 3.8 compares both Chl-SL lasers with use of the Chl-B filter to the chlorophyll extraction results of chlorophyll a/b ratio. Plots of chl-a, chl-b, and total chl can be found in Appendix B (6.2) due to their similarity to chlorophyll a/b ratio. Most of the image analysis results show the points clustered below the 0.2 DTW difference level with only the Cu dosed Tray 2 and 3 at time 0 separated at the top for all plots. Between Chl-A and Chl-B lasers, the most significant difference is the clustering of values on non-dosing days. 24-hour Tray 3 results fall above the control for the Chl-A laser, while the control sits above the same sample in the Chl-B laser results. Of each of the chlorophyll extraction values, a/b ratio shows the greatest distinction between possible metal dosing levels, however all results have a broad standard deviation which may result from higher variability in individual frond absorption of Cu. Nevertheless, it is clear that Tray 2 and 3 chl a/b ratios at time 0 plot on the lower end of the ratio ranges and are the only results that are significantly different from the control using LIF.

Table 3.1: Results from chlorophyll extraction. Values shown are the mean and standard deviation of 10 fronds collected every 24 hours for each tray including the control. These are Chl-a (nm) and Chl-b (nm) measurements taken with a spectrophotometer and calculated by using the equations detailed in (Porra, 2002). Each value is adjusted for by weight (mg) of a 2 cm section of frond measured before chlorophyll extraction.

Tray 1	Chl a	Chl b	Total Chl	Chl a/b Ratio
Control	3.983+-0.731	1.542+-0.277	5.526+-1.007	1.710+-0.569
0	2.432+-0.839	0.989+-0.360	3.425+-1.187	0.852+-0.465
24	3.391+-1.339	1.279+-0.485	4.670+-1.822	1.218+-0.572
48	2.366+-0.872	0.871+-0.329	3.238+-1.200	1.182+-0.395
Tray 2				
Control	4.081+-1.582	1.536+-0.593	5.616+-2.174	1.381+-1.341
0	3.332+-1.218	1.371+-0.473	4.703+-1.690	1.093+-0.558
24	3.247+-0.959	1.210+-0.369	4.458+-1.326	1.121+-0.231
48	3.904+-1.589	1.442+-0.579	5.346+-2.167	1.365+-0.914
Tray 3				
Control	3.474+-2.089	1.310+-0.807	4.784+-2.895	1.357+-0.509
0	2.295+-0.771	0.905+-0.291	3.201+-1.059	0.714+-0.207
24	2.209+-1.124	0.819+-0.422	3.029+-1.544	1.184+-0.316
48	3.204+-1.634	1.184+-0.656	4.390+-2.289	1.656+-0.545

Table 3.2: Results from metal extraction. Values shown are of the mean and standard deviation of the wet and dry weight of pairs of fronds. 10 sets of fronds for each tray were collected and Cu extracted using SET every 24 hours. Values are adjusted to account for weight (g) of moss pairs and shown in nmol/g and mg/kg levels.

	Total Cu nmol/g				Total Cu mg/kg	
	ww	std	dw	std	dw	std
Tray 1						
Control	56.91	23.11	259.61	79.77	0.0164	0.0051
0	89.32	23.95	295.78	-11.76	0.0188	0.0008
24	63.09	15.82	274.84	-12.71	0.0175	0.0008
48	76.17	14.12	275.42	-22.66	0.0175	0.0014
Tray 2						
Control	28.14	6.73	114.96	-31.06	0.0073	0.0020
0	162.09	54.71	1321.33	469.21	0.0834	0.0298
24	186.70	73.85	1108.80	230.38	0.0705	0.0146
48	244.30	63.80	1205.04	314.53	0.0766	0.0200
Tray 3						
Control	25.36	4.43	121.36	-18.93	0.0077	0.0012
0	1881.11	444.89	13525.22	3581.74	0.8595	0.2277
24	1859.52	862.25	11349.63	4483.73	0.7212	0.2849
48	1636.30	475.54	9723.26	3238.96	0.6179	0.2058

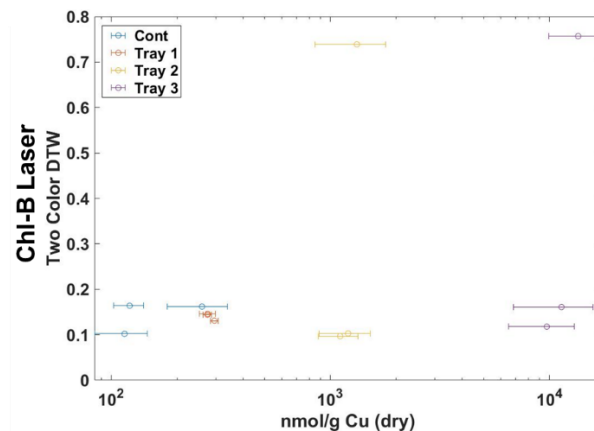
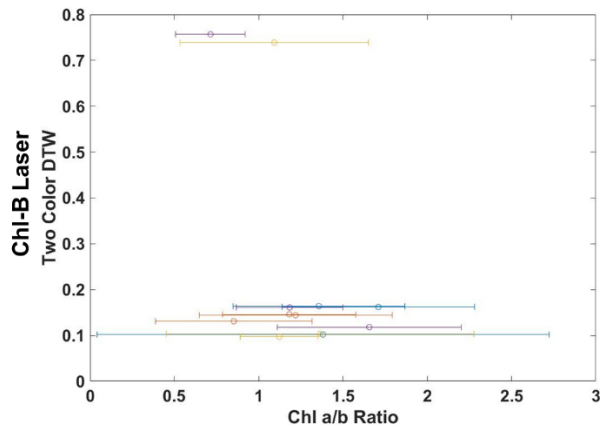
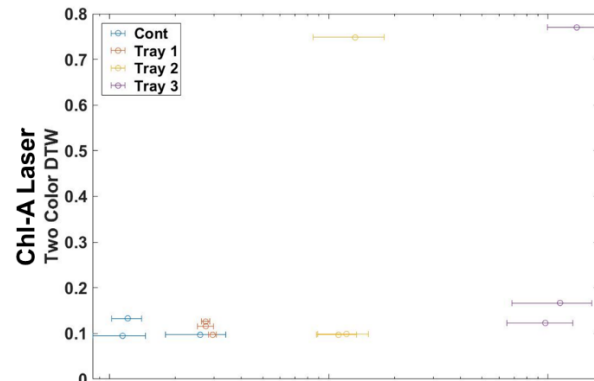
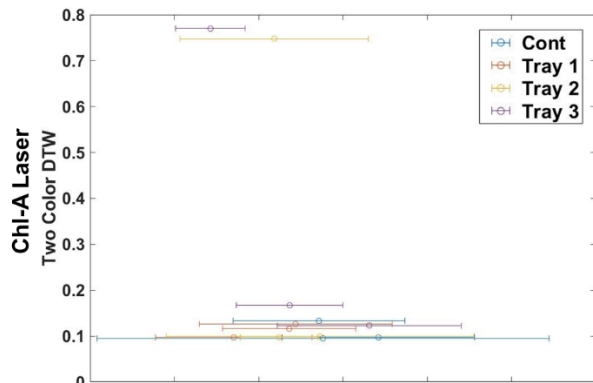


Figure 3.8: Chlorophyll extraction results as a/b ratio, compared to two color DTW results from images collected using the Chl-A (top) and Chl-B lasers (bottom) using the B filter. (Total Chl, chl-a and -b can be found in Appendix B

Figure 3.9: Metal extraction results and dry weight of 10 pairs of fronds collected every 24 hours compared to Chl-A and Chl-B two color DTW results.

Two color DTW analysis was also compared to Cu values taken from metal extraction for moss dry weight (Figure 3.9; wet weight in Appendix B – 6.2.4). The distributions of metal content for both laser wavelengths are similar with slight variation of the control and Tray 1 when observing DTW versus total metal content (nmol/g). Interestingly, there appears no direct correlation between DTW analysis and metal results for samples analyzed 24 and 48 hours after dosing. Both Tray 2 and 3 samples collected after Cu dosing at time 0 are well separated at the top of the plots from the rest of the images. However, the same Cu levels can be seen with lower DTW for samples collected from Trays 2 and 3 at 24 and 48 hours after dosing. It seems that the LIF response is immediate and short-term without long-term effects even though Cu content in the plants stays elevated (Cu does not get eliminated or otherwise removed from plants). When plotting metal results against chlorophyll values in Figure 3.10 (dry weight), some trends appear. Tray 3, most notably, has consistently lower chlorophyll values while also having the highest metal content. The plots do not show a direct correlation between doses of metal and chlorophyll change but both metrics could be useful for understanding plant response as chlorophyll is affected by metal content. Metal does appear to have an impact on initial chlorophyll response with lower chl-a and -b at the time of dosing (time 0 symbols highlighted by black outline) with a quick return to a more normal range seen in the control samples. Even with overlap in Cu content between Tray 1 and the control this shift can be observed.

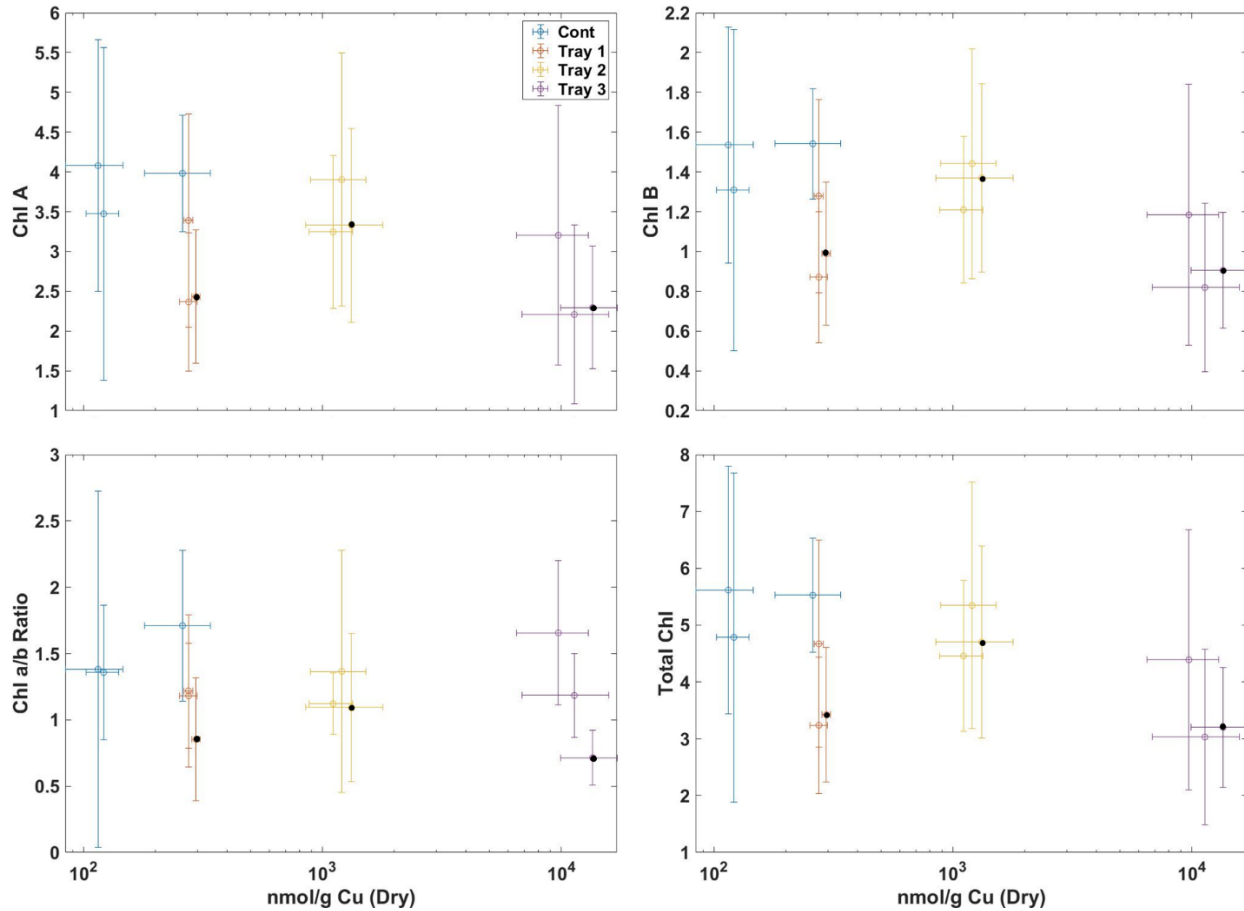


Figure 3.10: Chlorophyll extraction versus metal extraction dry weight collected every 24 hrs. Time 0 samples are marked with a black circle.

3.5 DISCUSSION

Comparison of the laser systems regardless of image analysis method has confirmed that the use of a laser wavelength more suited for maximum chlorophyll absorption, and therefore emission, is preferable to the broad organic application of the previously used CoCoBi (Figure 3.3). Both the Chl-A (445 nm; Figure 3.4) and Chl-B (462 nm; Figure 3.5) blue lasers tested in this work showed consistent response at time of metal dosing whether using the single color density difference or DTW, or two color DTW analysis. Using either laser without a filter tends to introduce indistinct observations of moss response that cannot be directly linked to chlorophyll. It is recommended that use of either the Chl-A (670 nm) or Chl-B (650 nm) bandpass filter be utilized to limit measurement of fluorescence wavelength to those in the red

spectrum associated with chlorophyll response. Of the filters used, the B filter appears to narrow the range of the control moss natural variability when compared to the A filter.

Of the three image analysis methods (Figure 3.6), all are in good agreement when it comes to observing the Cu dose administered at time 0 for Trays 2 and 3 which have toxicity levels above what would naturally be found in environmental background. When comparing single color analysis, DTW has more statistical deviation from the control than the density difference regardless of the laser used. DTW is not only preferred for its single color analysis, but also for two color analysis which enhances the results sometimes recorded in two different color channels. Of the color channels used (R,G,B), the blue color channel consistently showed the highest response with occasional signatures separating from the control in the green color channel when using the Chl-A laser. Though there was a small response recorded 24 hours after dosing, it is assumed to be a delayed metabolic process due to the high level of Cu from the treatment to moss on Tray 3. Two color DTW provides better separation from the control with less variability than single color DTW, allowing for definitive identification when using RvB.

Use of the blue color channel and RvB allowed for comparison and validation that both Chl-A and Chl-B lasers outperform the CoCoBi when it comes to identifying immediate changes in chlorophyll content after dosing. It also made it much easier to compare the chlorophyll specific lasers and their subtle differences. When applying a Welch t-test (Figure 3.7) it is also observed that the Chl-A consistently identifies each tray in order of its toxicity when using single color analysis. The Chl-B results could be seen as preferable because the only response recorded is at the time of Cu dosing and thus no other response could be interpreted over the course of the experiment. It is greatly separated from the other two trays, but shows promise in being able to separate out toxicity levels by degree of two-color DTW difference from a control.

Both lasers were compared to metal and chlorophyll extraction results (Figures 3.8-9; Tables 3.2-3) and show clear separation of the Tray 2 and 3 two color DTW results from all other values at the time of Cu treatment. It can be seen more prominently how using the Chl-B laser with the B filter results in all other samples collected staying below the DTW control threshold. Even though the data distribution and degree of variation from Chl-A laser results are similar, DTW values overlap with the control making it more difficult to discern any patterns. It can be noted for both lasers that the higher toxicities are shifted towards lower a/b ratio values with Tray 3 presenting with lower sample variability than other trials. The control appears to

have the broadest range of chl a/b ratios of all moss observed. It could be stated that high deviation in DTW from the control would match lower chl a/b ratios (or any metric), but we cannot state that a lower chl a/b ratio is indicative of Cu toxicity or metal response.

Moss dry weights were collected for metal analysis and compared to the chlorophyll specific lasers. As with chlorophyll extraction, distribution of the data appears similar and it is clear to see the separation of the DTW values at time 0 for Trays 2 and 3. However, the degree of metal contamination does not appear to correlate to the recorded moss response at times 24 and 48. All Tray 3 samples collected are very high in Cu, but only the initial dose shows any separation from the other samples when looking at DTW. This is the same for tray 2 samples even though their mean Cu content is 10x lower. They are both quite separate from Tray 1 and the control, and yet we cannot state that the recorded response is directly related to the level of metal present in a moss sample. We can however, observe that the level of Cu within a moss stays roughly the same over time from a singular dose.

Finally, metal and chlorophyll extractions results were compared to each other to look for possibility of correlation. It is observed that Trays 2 and 3 are clearly separated from all other samples, clustering within their own groups. When comparing chlorophyll metrics, it becomes apparent that all show the same lower shift correlating to higher toxicity that was observed when comparing chlorophyll content to DTW results. It confirms that there may be a relationship between increased Cu toxicity and decreased a/b ratio. To visualize this with image analysis using the Chl-B laser, the data was combined in Figure 3.11. What results is a delineation between the dosing time 0 and all other samples with a clear relationship with lower a/b ratio. Therefore, it can be expected that a large DTW deviation from the control will be associated with an initial dosing event but not a historical one when using moss and Chl-SL systems. Figure 3.11 could also be interpreted to indicate that there is a large range of chl a/b ratios in healthy plants, but the ratio could actually increase if a high level of Cu is bioavailable within the plant. Meaning, initial Cu toxicity could cause a stress response and shift to reduction in chlorophyll-a, but long-term toxicity may actually improve chl-a production in the case of Cu.

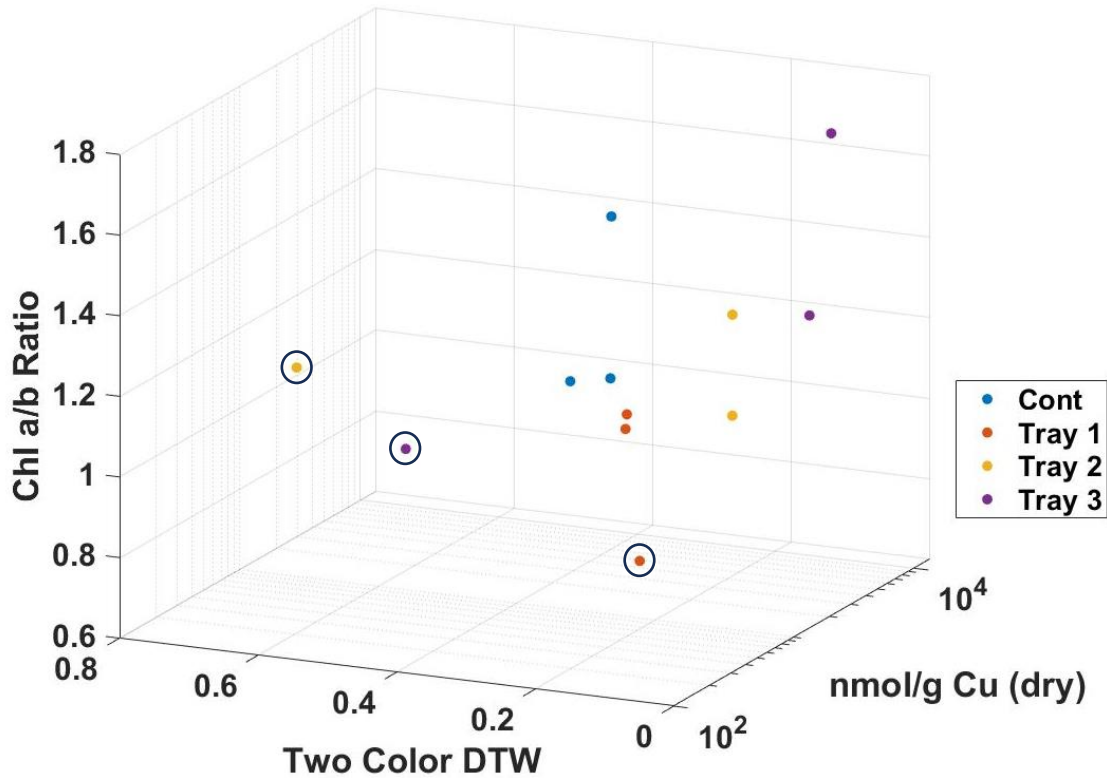


Figure 3.11: Chl-B laser results (x-axis) compared to chlorophyll extraction results of a/b ratio (y-axis) and dry weight metal extraction (z-axis). Black circles are placed around time 0 results.

It is recognized here that 12 data points make it challenging to definitively make broad claims about the application of the Chl-SL beyond the promise that it shows for detecting initial events of metal pollution. Of the data presented, each is representing 10 fronds or frond pairs analyzed for chlorophyll or Cu content. Previous work had great success in imaging moss mats to assess potential for the presence of metals in a given sample. However, to better understand the impact of chlorophyll content or individual metal absorption the broad variability of the fronds themselves must be better understood. Perhaps this will reveal more trends than the 12 data points presented in this work. Future work should focus on a more complete understanding of moss response variability and its impacts on the LIF technique.

3.6 CONCLUSION

The work presented set out to compare two laser systems, the CoCoBi and Chl-SL, to determine which was best for identifying the presence of Cu at environmentally relevant levels

while focusing on chlorophyll response in plants. Three trays of moss were dosed with increasing levels of Cu (1, 10, and 100 nmol/cm²) and fronds were collected from each to conduct metal and chlorophyll extraction. Results showed that both laser wavelengths used as part of the Chl-SL (445 and 462 nm) showed consistent moss response at the time of dosing. The CoCoBi, however, was more variable and appeared to respond to metabolic processes separate from chlorophyll. Though the Chl-a and Chl-b lasers performed similarly regardless of analysis method, the Chl-b laser showed only deviation at the time of dosing. It is recommended that the Chl-b bandpass filter (670 nm) be used regardless of laser type to reduce the recorded natural variability of the control. All analysis methods in the blue color channel were highly effective, but single and two color DTW provides better specificity than the density difference method. A Welch t-test allows for better separation of individual trials and enhances the effectiveness of two color DTW. It is not possible to say the metal content is directly linked to deviation of DTW from the control, but initial dosing does appear to cause a shift in chlorophyll a/b ratio. Long term metal content could result in a higher a/b ratio by comparison. A larger DTW value is also associated with lower a/b ratio, but a/b ratio does not guarantee deviation from the control. Work will continue to look at individual fronds to understand if their response to Cu toxicity follows the same observed results found looking at moss mats. Testing with other metals and plant species is also of great interest.

4 EXPLORING NATURAL VARIABILITY OF CHLOROPHYLL AND CU UPTAKE IN MOSS USING LIF

4.1 ABSTRACT

Chlorophyll has long been used as a natural indicator of plant health and photosynthetic efficiency. Laser induced fluorescence (LIF) is an emerging technique for understanding broad spectrum organic processes and has more recently been used to monitor chlorophyll response in plants. Previous work has focused on developing a LIF technique for imaging moss mats to identify metal contamination with the current focus shifting towards application to moss fronds and aiding sample collection for chemical analysis. Two laser systems (CoCoBi a Nd:YGa pulsed laser system and the Chl-SL with two blue continuous semiconductor diodes) were used to collect images of moss fronds exposed to increasing levels of Cu (1, 10, and 100 nmol/cm²) using a CMOS camera. The best methods for preprocessing of images was conducted before analysis of fluorescence signatures were compared to a control. The Chl-SL system performed better than the CoCoBi with dynamic time warping (DTW) proving the most effective for image analysis. Manual thresholding to remove lower decimal code values improved data distributions and proves whether using one or two fronds in an image. Higher DTW difference from the control correlates to lower chlorophyll a/b ratios and higher metal content indicating that LIF with the aid of image processing can be an effective technique for identifying Cu contamination shortly after an event.

4.2 INTRODUCTION

Bryophytes have long been used as bioindicators of heavy metal accumulation in the environment due to various anthropogenic sources (Bates, 1992; Jiang et al., 2018). Of the species commonly used, mosses are the most widely distributed across differing elevations and climates. Mosses have a simple non-vascular structure, lacking true roots enabling them to accumulate most of their nutrients from the atmosphere (Aboal et al., 2010; Bidwell et al., 2019). Because they are often only one or two cell-layers thick, mosses have a high ion exchange affinity due to their lack of a protective epidermis leading to absorption of both inorganic and organic compounds (Gjengedal & Steinnes, 1990; Gonzalez & Pokrovsky, 2014). When

compared to vascular plants, mosses consistently prove more effective in metal accumulation (Jiang et al., 2018). The use of moss for environmental sampling has been validated through chemical analysis (Nagajyoti et al., 2010; Stankovic et al., 2014) and proved to be valuable for large-scale surveys (Szczepaniak & Biziuk, 2003; Ram et al., 2015) by being capable of absorbing nutrients and contaminants directly from the atmosphere.

A good bioindicator is defined as an organism that can successfully provide new information about the quality of a given environment (Van Dobben et al., 2001) while also capable of monitoring potential pollutants and their temporal and spatial distributions (de Temmerman, et al., 2005). To be an effective biomonitor, a plant species must be capable of detecting changes over time in the environment and help in source identification (Kuang, et al., 2007). Because mosses can be found on every continent and over a vast array of ecosystems, they are uniquely capable of surviving in harsh and often highly polluted areas (Wang, et al., 2008; Cui et al., 2009). Mosses also benefit from being a species that can withstand repeated sampling and potential to provide annual growth segments for continuous monitoring of both recent and historical heavy metal accumulation (Čeburnis et al., 2002; Van Dobben et al., 2001; Wang et al., 2008; Dragovič and Mihailovič, 2009).

However, the accumulation of heavy metal pollutants can occur through several different mechanisms depending on the moss species and physiological mechanisms for ionic exchange. Some particulates can become trapped on the surface of cells due to negatively charged anionic sites, others are incorporated into cellular walls, while higher affinity metals are more likely to be used in metabolic processes within the cell itself (Van Dobben et al., 2001; Blagnytė & Paliulis, 2010). Metal retention efficiency has been documented to decrease in the order of $Cu > Pb > Ni > Zn$, with Cu and Pb showing the strongest correlation between metal concentration and atmospheric deposition (Rosman, et al., 1998; Čeburnis et al., 1999). Pb's toxicity even in small doses is well known for its potential health concerns both to humans and the environment, but even an essential micronutrient like Cu can be harmful in high concentrations (Heckathorn et al., 2004; Hall, 2002; Rocchetta & Küpper, 2009). Because of its high affinity and need for use in metabolic processes, Cu provides a key example of metal behavior to best understand and document physiological response. Though mosses are more cost effective than atmospheric collectors and able to accumulate wide ranges of heavy metals (Gatziolis et al., 2016; Rai, 2016; Jiang et al., 2018), the sampling and chemical analysis can be laborious and time consuming. We

propose that environmental sampling could be expedited by the addition of remote sensing using laser induced fluorescence (LIF).

Use of chlorophyll fluorescence to evaluate plant physiology and characterize photosynthetic efficiency has long been used to determine vascular structure and metabolic processes (Krause & Weis, 1991; Kolber et al., 2005; Valeur & Berberan-Santos, 2011). Lasers can be used as a primary source for inducing fluorescence in plants (Valeur & Berberan-Santos, 2011; Silvia & Utkin, 2018) to monitor chlorophyll content and monitor changes due to metal or environmental stress (Chappelle et. al., 1984; Israsena Na Ayudhya et. al., 2015; Yang-Er et al., 2019). Changes in chlorophyll can be documented by shifts in the short lifetime fluorescence emission of light corresponding to the absorption of laser wavelength by a molecule during its ground energy state (Lakowicz, 2006; Hedimbi, Singh, & Kent, 2012; Jameson, 2014; Fedotov et al., 2019). It has been documented in the literature that metals can bind to chlorophyll and protein structures to produce specific fluorescence signatures (Jeffrey et al., 1995; Lakowicz, 2006; Jameson, 2014; Yang-Er et al., 2019).

Success using LIF has been recorded in previous work using the Color Compact Biofinder (CoCoBi; Misra et al., 2018; Misra et al., 2021; Truax et al., 2022) which uses two nanosecond pulsed lasers fired in tandem (355 nm UV and 532 nm Green) to detect a broad range of organic molecule responses using a CMOS camera. However, the low selectivity of that technique does not allow for direct identification of the process responsible for the fluorescence response. Thus, a chlorophyll specific laser system (Chl-SL) was developed that focuses on chlorophyll absorption by using laser wavelengths of 445 nm and 462 nm (Chl-a and -b) which produce emissions in the visible red region (650 nm for chl-b and 670 nm for chl-a) and can be documented with the same CMOS camera previously used with the CoCoBi (Misra et al., 2021; Israsena Na Ayudhya et al., 2015).

Previous work (Truax et al., 2022) has focused on image analysis of moss mats using LIF. To better understand chlorophyll and metal content this study will instead shift to individual frond analysis and sample preparation techniques to determine the effectiveness of LIF of both the CoCoBi and Chl-SL on a smaller scale. As with any plant, moss fronds can have a high level of variation in chlorophyll content and therefore fluorescence response even amongst healthy samples. To effectively evaluate and compare images collected using LIF, more traditional chemical analysis of chlorophyll and metal extraction with all be used for validation. It is

expected that the technique can help provide identification of Cu contamination within moss samples and find correlation to chlorophyll content and metal accumulation while creating a methodology that is reproducible. The ultimate goal is to provide a method of sampling individual fronds that are highly representative of a contaminated moss mat identified using LIF in the environment. We recognize that LIF is limited in its specificity compared to traditional destructive techniques of metal content analysis, but through this study we demonstrate that LIF can help to find and sample target areas in a way that complements traditional bioassay approaches through targeted sampling at potential contaminated sites.

4.3 METHODOLOGY

The work adapts the methods developed in previous studies (Truax et al., 2020; Truax et al., 2022) on moss mats and applies them to individual moss fronds that were collected, imaged, and used for chemical analysis of chlorophyll and Cu content. The research is divided into four parts with the first focused on laboratory treatment and cultivation of the moss mats from which individual fronds were later collected. Part two uses LIF of the CoCoBi and Chl-SL to capture color images of moss frond response to various Cu treatments. Part three details the chemical analysis procedures for chlorophyll and Cu extracted from each frond or frond pair. Finally, LIF images of fronds are processed to quantify moss response to observed absorbed Cu concentrations and corresponding measured chlorophyll levels.

4.3.1 Laboratory Cultivation and Cu Treatment

Thuidium plicatile, is an endemic moss species to Hawai'i (Staples et al., 2004; see Notes on Moss Species) and can be found on the island of O'ahu along the Wa'ahila Ridge Trail and State Recreational Area (21.307°, -157.797°). The moss has been consistently used in previous work (Truax et al., 2022) for its known response to LIF and uncontaminated environment along the Southeastern part of the Ko'olau mountains. Moss mats were collected, taken to the lab, and rinsed and cleaned of forest litter before being divided onto three trays each covering with an area of 587 cm² (7in. x 13in.). The trays were then placed within a laboratory grow tent which maintained an average temperature of 18-20°C, 50-60% relative humidity, and 14-17 W/m² ambient light (1400-1800 lux), with a day length of 10 hours. An acclimatization period of two weeks was allotted before beginning tests.

The experiment was conducted over 72-hours allowing for collection of moss fronds from each tray to be imaged every 24 hours (4 in total). A wire grid was constructed to divide the moss trays into 10 equal partitions from which frond samples were selected for imaging and later chemical analysis. The first 24-hour frond sampling was used to record normal control response for each tray before Cu treatments. At the 24-hour mark (or time 0) each tray received a single dose of Cu with Tray 1 receiving 1 nmol/cm², Tray 2 10 nmol/cm², and Tray 3 100 nmol/cm². Fronds were collected within 10 minutes of Cu dosing and chemical analysis began within 30 minutes of Cu dosing. Frond collection, imaging, and chemical analysis were repeated for the next two 24-hour intervals (24 hours and 48 hours after Cu dosing). A single frond and pair of fronds were collected from each of the 10 partitions on each tray of moss. The single frond was imaged and then underwent chlorophyll extraction (4.3.3.1). The pair of fronds underwent sequential elution technique (SET) for metal extraction (4.3.3.2). Once fronds were imaged, the trial tray was returned to the grow tent accounting for no more than half an hour of time outside of the grow tent.

4.3.2 Laser Systems and LIF Technique

Two laser systems were used to record LIF response in the moss fronds. Both systems have been tested to evaluate LIF in moss mats, but neither have been utilized for documenting moss frond response. The CoCoBi (Misra et al., 2021) and a newly designed chlorophyll specific laser system (Chl-SL) both use the same CMOS camera which can be integrated with the Baumer Camera Explorer software allowing the user to control camera settings and capture LIF images for later analysis. The CoCoBi is a pulsed Nd:YGa dual laser system (green 532 nm laser and UV 355 nm laser) fired at a nanosecond rate (112 ns). The Chl-SL system uses two semi-conductor diode lasers at the 445 nm and 462 nm wavelengths which are continuous. The CoCoBi has integrated time synchronized pulses which allows it to image at any time of day, while the new system prototype does not have this feature. In order to keep methods for comparison even between the two units, imaging was only done in the dark.

A diffuser was mounted on each laser system to provide uniform illumination across the surface of the moss sample. Filters can be used with the CoCoBi to limit the wavelength passing to the sample to either the green or UV laser. The Chl-SL has the option of using a Chl-A bandpass filter (670 nm) or a Chl-B bandpass filter (650 nm) to capture emission specific to

chlorophyll-a and -b. These bandpass filters heavily limit the fluorescence signatures to a 10 nm wide range of light on the spectrum that are received by the camera sensors. By limiting the wavelengths of light that are measured we can ensure that the received signal is due to a chlorophyll emission and not another organic reaction. Figure 4.1 shows images of the same moss frond collected using both laser systems with all possible filter options.

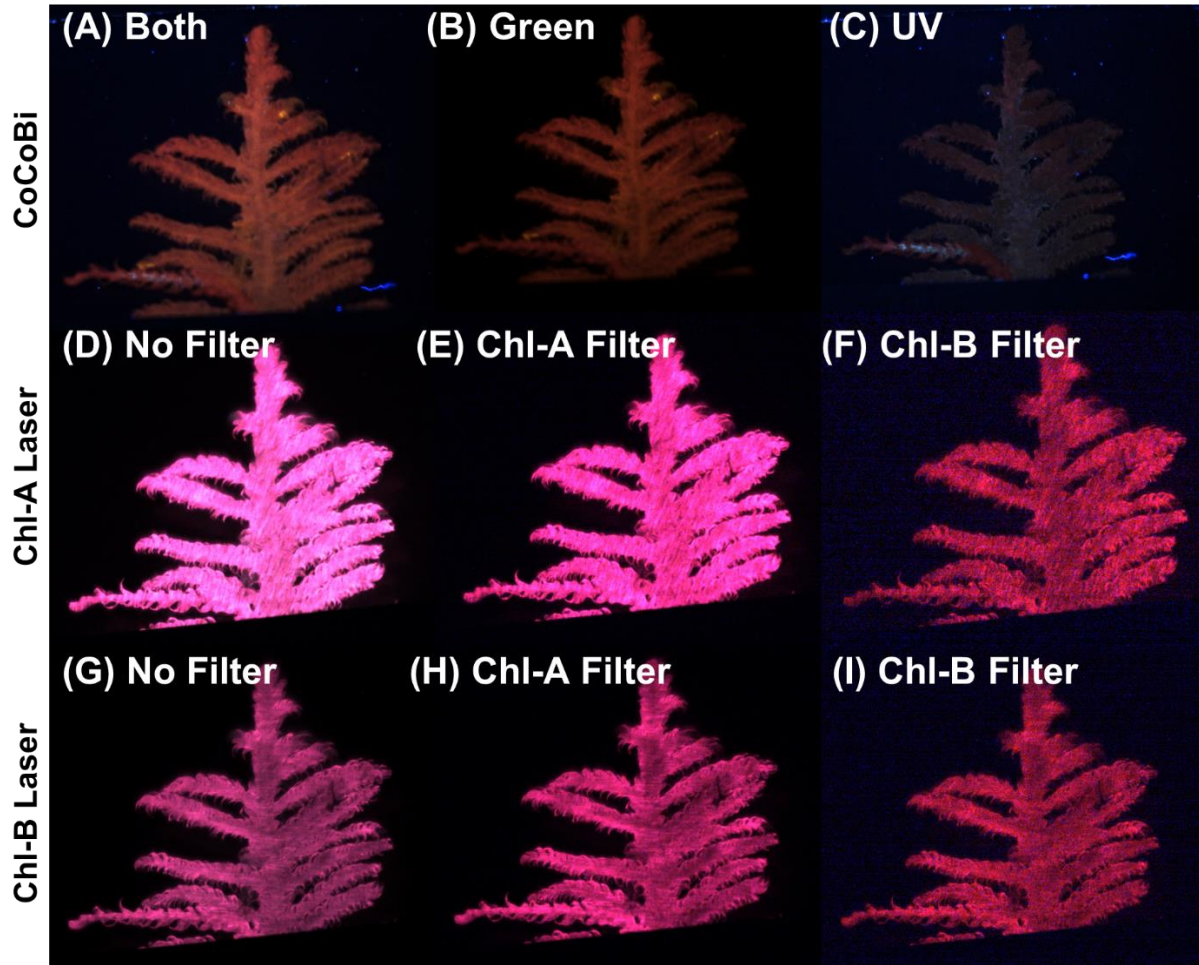


Figure 4.1: (A) Shows CoCoBi using both lasers. (B) Shows only the Green 532 nm CoCoBi laser. (C) The CoCoBi 355 nm laser. (D) Chl-A 445 nm laser without a filter. (E) Chl-A laser with 670 nm Chl-A bandpass filter. (F) Chl-A laser with 650 nm Chl-B bandpass filter. (G) Chl-B 462 nm laser without a filter. (H) Chl-B laser with 670 nm Chl-A bandpass filter. (I) Chl-B laser with 650 nm Chl-B bandpass filter.

Each tray of moss was divided into 10 sections using a wire grid from which a single frond and pair of fronds were selected. Samples were placed between two glass plates taped to allow only a 2-cm wide gap to remain visible. Fronds were carefully placed between these glass

plates with the tip of the sample at the top of the 2-cm window and placed over a black oxidized aluminum sheet. After imaging, the same 2-cm section was cut off for chemical analysis. A control baseline for each tray was collected on the first day of the experiment. Metal dosing occurred 24 hours later (at time 0 on day 2) with repeated imaging on days 3 and 4 (24 and 48 hours after dosing). Moss trays were always imaged after wet deposition and when not dosed with metal trays were only given 50 mL of DI. Imaging of moss fronds was conducted every 24 hours in 30-minute windows in order of trial number followed by a 30-minute window for chemical analysis to begin. Imaging times were held consistently for each sample between 1-4 pm. Images were collected by integrating the Baumer Camera Explorer software with the CMOS cameras paired both the CoCoBi and the Chl-SL. Images were collected using just the 532 nm green laser, just the 355 nm UV laser, and both lasers in tandem for the CoCoBi. The Chl-SL collected images using the 445 nm laser with no filter, 445 nm with the 650 nm filter, 445 nm with the 670 nm filter, 462 nm laser with no filter, 462 nm with the 650 nm filter, and the 462 nm with the 670 nm filter. The 650 nm band pass filter corresponds to the maximum emission peak for chlorophyll-b while the 670 nm band pass filter corresponds to chlorophyll-a (Israsena Na Ayudhya et al., 2015). Preliminary testing was conducted to determine optimal camera settings to streamline sampling to a single image per laser and/or filter combination limiting each of the 10 collected sample areas on a tray to having nine images each (Figure 4.1).

4.3.3 Chemical Analysis

To assess LIF results, Cu uptake and changes in chlorophyll were measured using traditional chemical analysis. Chlorophyll and metals were extracted from moss fronds every 24 hours after laser imaging throughout experimentation (starting at time 0). Metal concentrations absorbed by the plants were measured after using the sequential elution technique (Pérez-Llamazares et. al., 2010) followed by ICP-MS analysis (ICP-MS, Thermo-Fisher Element 2, University of Southern Mississippi Center for Trace Analysis). Chlorophyll extraction of a single frond (Hu et. al., 2013) was followed by spectrophotometry (Hewlett Packard Diode Array Spectrophotometer; Caesar et. al., 2018) allowing for the measurement of Chl-a and -b.

4.3.3.1 Sequential Elution Technique (SET)

At the start of the experiment 10 pairs of fronds were selected from each of the three moss trays corresponding to 1 of the 10 grid sections. After imaging, the top 2 cm from the tip of

the fronds cut, weighed, and leached using the sequential elution technique (SET) to extract metal from the surface of moss as well as its extra- and intracellularly bound Cu content (Brown & Wells, 1988; Vázquez et. al., 1999a). Frond pairs were shaken in 10 mL of DI for 30 seconds to remove any unbound metals. The fronds were then removed, dried, and immersed in 10 mL of 10 mM ethylenediaminetetraacetic acid (EDTA) solution (Pérez-Llamazares et. al., 2010). Fronds were submerged and shaken in EDTA solution for 45 minutes followed by another 30 minutes in a fresh fraction of 10 mL of EDTA. The two EDTA fractions were combined for extracellular Cu analysis. Samples were then blotted dry, weighed, and then dried in a furnace at 50°C for 24 hours before cooling for 24 hours in a desiccator. The dry weight of cooled fronds was recorded and, finally, samples were submerged in 10 mL of 1M HNO₃ for 30 minutes of shaking to induce partial digestion and release of intracellular Cu fractions.

All samples were then analyzed for copper content (DI, EDTA, and HNO₃). The individual DI water, EDTA, and nitric acid fractions were analyzed for Cu concentration using a sector-field inductively coupled plasma–mass spectrometer (ICP–MS, Thermo-Fisher Element 2) at the University of Southern Mississippi Center for Trace Analysis (CETA). A self-aspirating nebulizer (Elemental Scientific, Omaha, NE, USA) with low-flow (100 µL/min) and Teflon spray chamber was used. Cu-63 was determined in medium resolution and calibration was conducted using external standards made in 0.16 M ultrapure nitric acid. These were then checked against standard reference waters from the U.S. Geological Survey. There was also an in-house consistency standard measured to ensure a sensitivity check, long-term stability, and instrumental drift correction. Cu analysis was also conducted for solution blanks of DI, EDTA, and HNO₃ to determine baseline Cu concentrations.

4.3.3.2 Chlorophyll Extraction Method

Protocol used for chlorophyll extraction in water lettuce was adapted to determine chlorophyll content for moss samples (Moran & Porath, 1980; Porra, 2002; Inskeep & Bloom, 1985). 10 individual fronds were collected from the 10 grided areas on each tray after imaging. Moss fronds were cut 2 cm from the tip with a sterilized razor blade before being weigh. Samples were then placed within a plastic sample tube and 2 mL of DMF (N-Dimethylformamide) was added to each sample. Initial testing showed that 1 mL DMF was needed for each cell layer of a sample, and the moss species was deemed be 2 cell layers thick

given volume needed for full chlorophyll extraction within 48 hours (Petschinger et al., 2021). DMF is more effective at limiting the continued degradation of chlorophyll than ethanol or acetone, and can be used (when kept cold) for longer periods of time after extraction is initially conducted (Porra, 2002; Hu et. al., 2013).

Samples were then capped, wrapped in aluminum foil, and immediately placed within a cooler with ice packs to limit the amount of light exposure before finally being placed within a freezer. After 48 hours, each sample was measured by spectrophotometry for chl-a and -b using a 1 mL cuvette. The cuvette was rinsed with DMF before 1mL of DMF was used to calibrate the spectrophotometer (Hewlett Packard Diode Array Spectrophotometer). Measuring of samples was then conducted with cuvette cleaning and recalibration between every 30 samples. Altogether 120 samples were analyzed using values of $E^{663.8}$ and $E^{646.8}$ collected for each frond and used to determine *Chl a* (Eq. 1), *Chl b* (Eq. 2), and *Chl a+b* (Eq. 3) at $\mu\text{g/ml}$ levels (Porra, 2002). These were then adjusted for per mg wet weight of the original frond.

$$[Chl a] = 12.00 E^{663.8} - 3.11 E^{646.8} \quad \text{Eq.1}$$

$$[Chl b] = 20.78 E^{646.8} - 4.88 E^{663.8} \quad \text{Eq.2}$$

$$[Chl a + b] = 17.67 E^{646.8} + 7.12 E^{663.8} \quad \text{Eq.3}$$

4.3.4 Data Analysis

4.3.4.1 Image Preprocessing

Previous work with moss masses required minimal to no preprocessing of images collected using LIF due to the sample filling the full view of the CMOS camera. Moss fronds, however, are collected with a black background creating a large number of decimal code values at or near 0 (black). To assess the LIF response of a given frond and compare it to other frond samples requires that only the pixels associated with moss be considered. Two approaches were taken and will be compared for both effectiveness at capturing changes in images of moss fronds, and to determine their computational demand. The first is a manual method of thresholding that removes decimal code values (DCV) at intervals of 5 starting at 0 and increasing to 10% (25) of the available decimal code values (256) regardless of color channel.

The second method applies automatic thresholding which either can be applied to each color channel or can be applied to a grayscale version of the original LIF image. Previous work

has seen great benefit from working with color images and comparing plant response in all three color channels (R,G,B). Intuitively, it is expected that a grayscale image will produce less viable results. Automatic thresholding or multi-thresholding relies upon segmentation of light and dark regions within an image and benefits from contrasts between high and low intensities. High counts of pixels will create a distinct peak when displaying the image as a histogram. If these high abundance pixel regions are bound by DCV of low counts then the image can be segmented into classes defined by the high pixel count peaks. Each peak correlates to a range of DCV within the image so that a noisy or complex image may be difficult to segment. An image with only two or three peaks are much easier to identify and remove the peak we would associate with the background (low DCV). Single color or grayscale histograms of an image work best with this method to evaluate for variances in the foreground and background pixels based on DCV (Otsu, 1979; Zhang & Hu, 2008; Bangare et al., 2015). The variance within the foreground and background pixels helps to establish a threshold of high and low pixel values within the image. Once this threshold is found, the image can be shifted to binary where all pixels below the threshold are given a value of 0 and pixels above the threshold are given a 1. As such, pixels recoded at 0 can be removed from the data set while those with a 1 are retained (Bangare et al., 2015).

The challenge of using thresholding for image segmentation is that it is highly dependent on the difference between pixel intensities. Shadows, poor resolution images, and boundary regions can all cause valuable data to be lost or accidentally included because of uncertain delineation for a given threshold (Otsu, 1979). The fronds provide high contrast with their dark background and it is expected that thresholding will prove beneficial for this type of data. Though masks can be created, thresholding does not require them to classify pixels within an image but the option is available as are multiple thresholds within a given image (Zhang & Hu, 2008; Bangare et al., 2015). Because the established methodology of image analysis (Truax et al., 2022) already uses color histograms for comparison, thresholding either manually or automatically should prove effective. already collected from the sample LIF images used for density difference and DTW comparison.

4.3.4.2 Single-color comparison

After preprocessing, analysis of LIF in moss fronds was done by extracting RGB (Red, Green, and Blue) pixels from each image to create density histograms based on decimal code value for each color channel. These histograms were then normalized using the total pixel count to create percent abundance curves. These curves were then used to calculate the difference between treated samples and the control by either using the density difference method found in Eq. 4

$$Difference = 1 - (\sum \min|trial(x), control(y)|) \quad \text{Eq. 4}$$

where x represents the color intensities for the corresponding trial, and y represents the same for the control images (Swain & Ballard, 1992). Or, difference can be calculated using dynamic time warping to fit one curve to another (DTW):

$$D(i, j) = |x(i) - y(j)| + \min \begin{cases} D(i + 1, j) \\ D(i + 1, j + 1) \\ D(i, j + 1) \end{cases} \quad \text{Eq. 5}$$

where x and y represent strings of data and i and j represent the length of each string so that $D(i, j)$ equals the best alignment distance between all data points along the lengths of x and y (Jekel et al., 2018). Sample images of moss fronds were compared to control images collected for each tray 8, 16, and 24 hours before Cu dosing. These are included in the results as negative values before time 0 (dosing).

4.3.4.3 Multi-color comparison

Both density difference and DTW can be used to compare single-color histograms, but only DTW can be used for two-color analysis which has been shown to improve contaminant detection and separation of individual samples from the control (Truax et al., 2022). All two-color combinations (RvG, GvB, RvB) were calculated for the collected images. A mean and standard deviation to 3σ were determined for the control and used to compare if any color channel shows a significant deviation from the control's variability regardless of analysis method.

4.4 RESULTS

4.4.1 Preprocessing Approach Comparison

To evaluate the benefits of using either manual or automatic thresholding in preprocessing of frond images, 10 control images from Tray 3 were compared to all 30 control images of fronds collected from all three trays. Figure 4.2 shows single color comparison analysis using density difference and DTW to compare the same images with no alteration (0 pixels removed; 0 DCV), images with removal of pixels in ranges of DCV at intervals of 5 (5, 10, 15, 20, 25), images with automatic thresholding for each color channel (TH), and images converted to grayscale before automatic thresholding is applied (MLT). The expectation is to see little difference among the controls but the results reveal that density difference performs more poorly when any level of thresholding is applied, but is most impacted by automatic thresholding which would result in varying number of DCV removal between each image. When manually removing DCV, 10-25 perform approximately the same with slight increases in separation between frond samples with increasing DCV removal. Separation between samples is not necessarily negative, but control samples are expected to be in a narrower range of difference, which would optimally mean less variability in the control, hence easier separation of metal dosed samples. At the same time 0 DCV removal results in less difference in images due to their similarly black background.

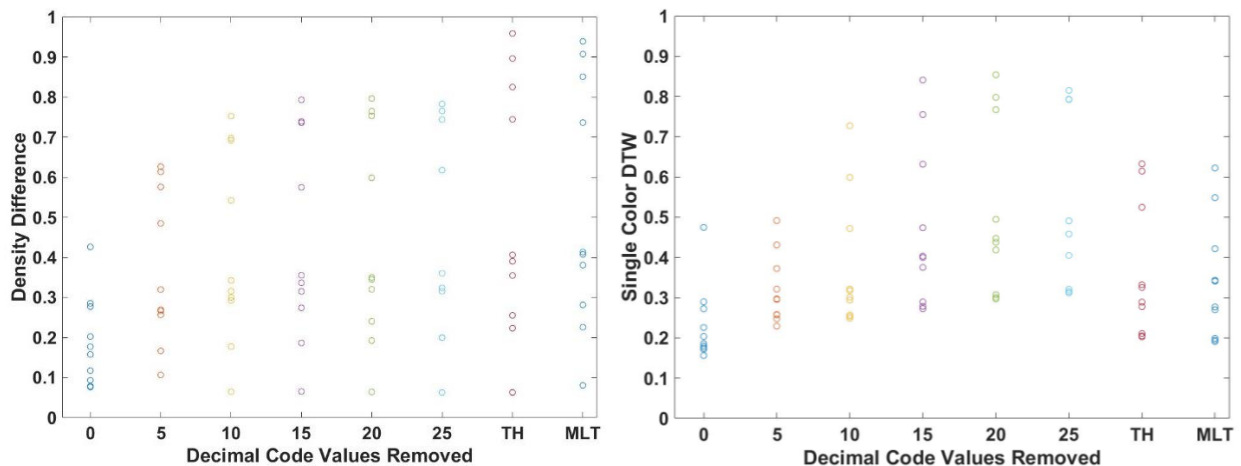


Figure 4.2: (A) Shows 10 density difference results of Tray 3 control images compared to all samples within the control (Tray 1, 2, and 3) while (B) shows DTW results for the same data. Manual thresholding was applied to compare the effect of analysis techniques. Decimal code values were removed in increments of 5 from 0 to 25 for manual thresholding. Automatic thresholding (TH and

MLT) adjusted the decimal code removal on an image-by-image basis. All results are for the blue color channel, while MLT shows results of a grayscale version of the original image.

Single color DTW performs much better which is likely due to it being less affected by a fixed comparison of the x-axis of image histograms. This is most notable when looking at the distribution of points at TH and MLT. Where these were the worst performing methods for density difference, they are quite good by comparison and outperform the high manual thresholding levels. It is interesting to observe that in both cases the 0 and 5 DCV removal have a narrow range for control images. In this case, being too narrow could be a result of too many pixels located in lower DCV which skews the data distribution by given too much emphasis in curve fitting to the more abundant regions dominated by the black background. This can be compared in Figure 4.3 showing color histograms of 0, 10, 20 DCV removed, and automatically set threshold (TH) images. With 0 DVC removed histogram profiles of all three color channels are dominated by low DCVs. At the removal of 10 DVC we see profiles for all three colors including their full peak curve. After removal of 20 DVC both red and blue color channels still include their full DCV curve associated with the frond, but green is cut off right before its peak. TH is similar to 20 with the green channel being cut short. To preserve all color channels for analysis and comparison it was decided that frond images would be manually thresholded at 10 DCV. The results are reasonably in agreement at this threshold for both single color analyses. Another reason for manually thresholding is due to automatic thresholding being very computationally demanding and taking 6-10 times longer to process the same number of images without the potential for only minimal improvement in comparison of treated and untreated samples. Though MLT performs well with DTW and is not computationally demanding, it requires a grayscale version of the image and thus makes multi-color comparison impossible to perform.

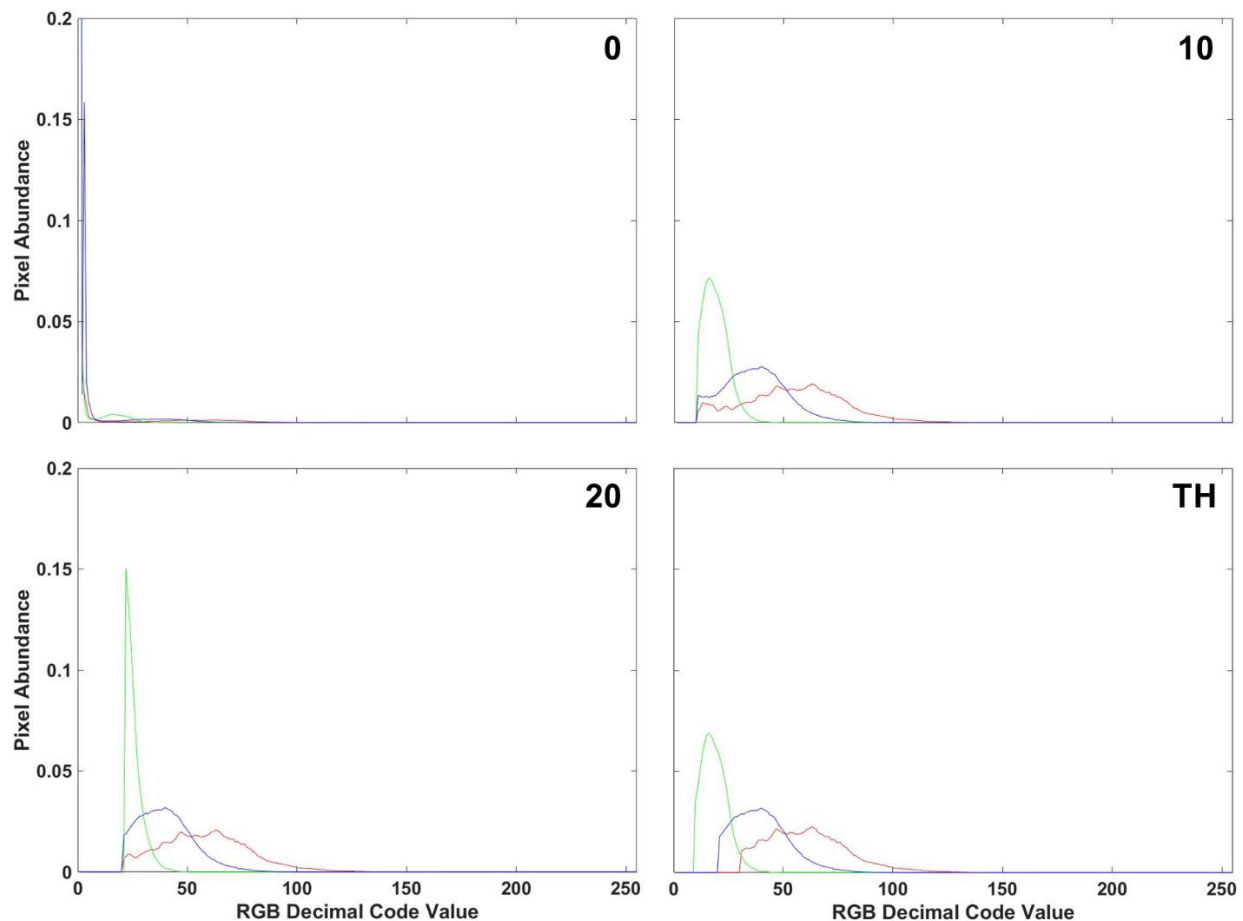


Figure 4.3: The four plots show histograms of the same image with varying number of decimal code values removed ranging from 0, 10, 20, and an automatic threshold (TH) at 30.

4.4.2 Comparison of LIF approaches applied to fronds

Analysis of fronds was limited initially to comparing only those images from which chlorophyll was extracted (single fronds). Pairs of fronds imaged for metal extraction were withheld from this initial analysis to be used for validation of the technique at a later step. Fronds were imaged using both laser systems (CoCoBi and Chl-SL) with results for all color channels and all analysis methods shown for the CoCoBi in Figure 4.4. The CoCoBi consistently shows better results when using the green and UV laser in tandem though results for the lasers used individually can be found in Appendix C (6.3). When considering analysis methods, two color DTW shows no deviation from the control at any point during the experiment save one control sample for Tray 1. Both single color analysis methods show a deviation in the red and blue color channels 24 hours after metal dosing for Tray 3 with no deviation in the green color channel. Of these methods, density difference appears to perform least well, as expected (4.5.1) with several

samples from all three trays deviating from the 3σ confidence interval of the control when looking at the red color channel. The blue color channel only deviates in Tray 3 24 hours after dosing. Single color DTW is in good agreement indicating that the CoCoBi may be measuring a metabolic response to the introduction of Cu 24 hours after the initial dosing. However, when further inspecting images collected with the CoCoBi, the blue channel response appears linked to a change in the tips of the fronds which could indicate a growth response in the moss and not being specific to chlorophyll fluorescence.

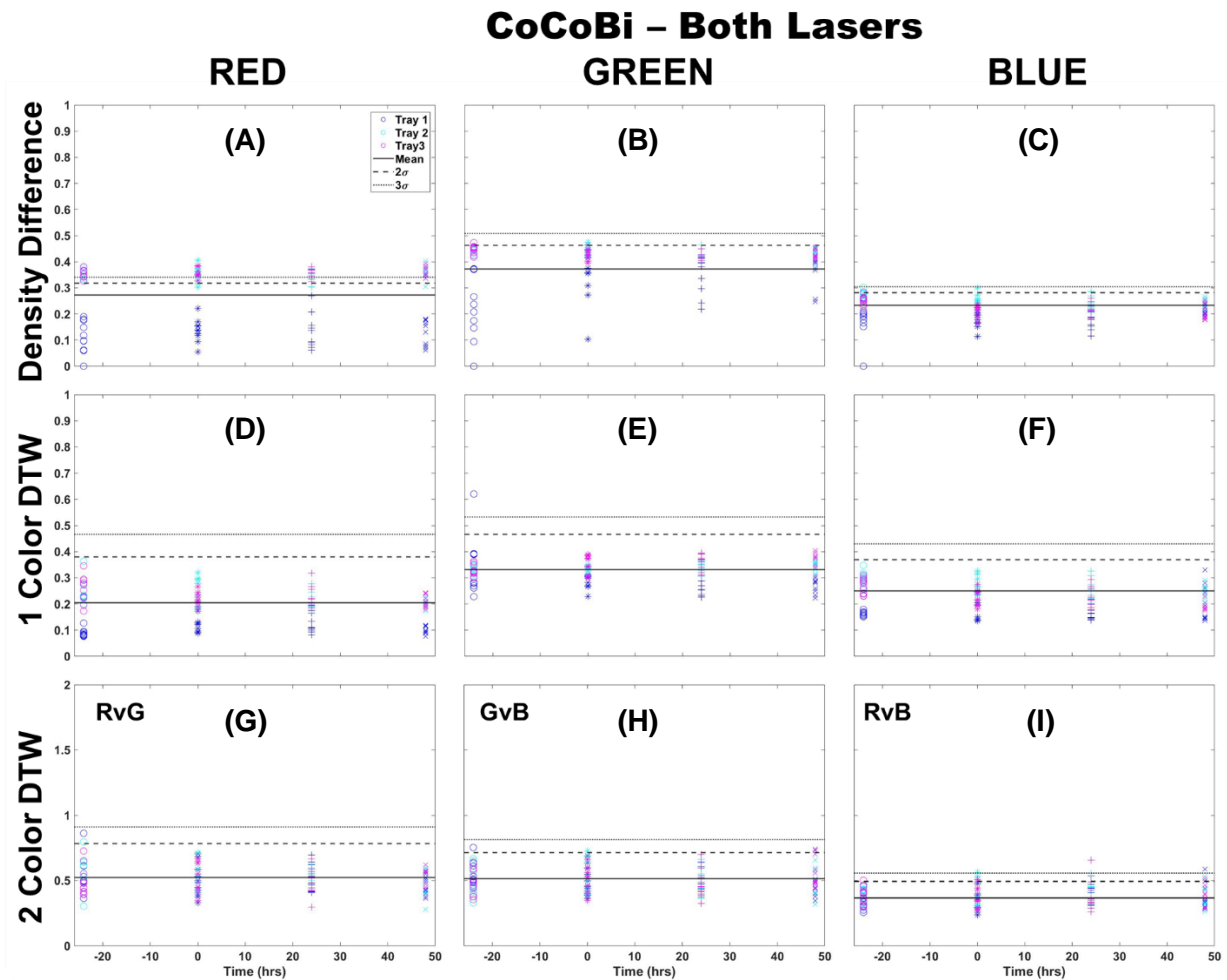


Figure 4.4: Comparison of moss response to both lasers of the CoCoBi using three image analysis methods: (A-C) single-color density difference, (D-F) single-color DTW, and (G-I) two-color DTW. Images of fronds were collected every 24 hours over three days. At time 0 three Cu treatments were given at 1 nmol/cm^2 for Tray 1 (blue), 10 nmol/cm^2 for Tray 2 (cyan), and 100 nmol/cm^2 for Tray 3 (magenta).

When using the Chl-A laser, application of the Chl-B filter improved image analysis results for all methods by providing better separation from the control samples and between trays

(Figure 4.5). Chl-A laser results with no laser and with the Chl-A filter can be found in Appendix C. Again, it can be observed that results using density difference are varied between color channels and between trays, and time since Cu dosing. The blue color channel is the most representative of the deviation expected of Cu dosing with clear separation using both single color and two color analysis methods with only the higher dosed Trays 2 and 3 separating from the control. There is almost no deviation in single color DTW for red and green color channels, but two color DTW reveals good separation from the control at time 0 and some separation of individual fronds from Trays 2 and 3 at 24 hours after dosing. The results here, however, are still muddled when considering red channel results, especially for two color analysis of red versus green (RvG) where there is separation from the control by some samples before dosing occurs.

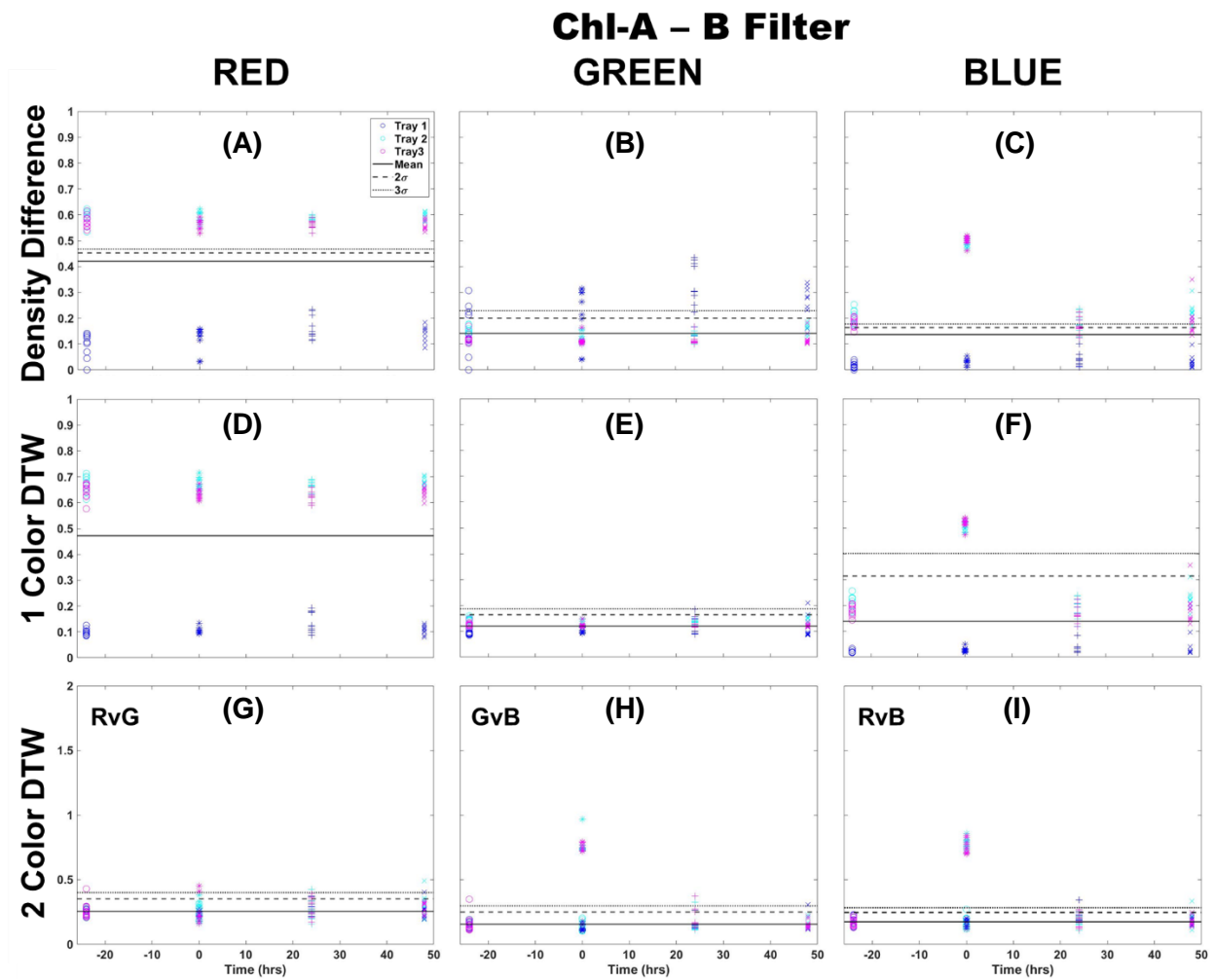


Figure 4.5: Comparison of moss response to the Chl-A laser (445 nm) with the Chl-B filter (650 nm) of the Chl-SL system using three image analysis methods: (A-C) single-color density difference, (D-F) single-color DTW, and (G-I) two-color DTW. Images of fronds were collected every 24 hours over

three days. At time 0 three Cu treatments were given at 1 nmol/cm² for Tray 1 (blue), 10 nmol/cm² for Tray 2 (cyan), and 100 nmol/cm² for Tray 3 (magenta).

The Chl-B laser with application of the Chl-B filter improves upon the results in Figure 4.5 regardless of analysis method. It can be seen in Figure 4.6 that the density difference method still shows wide variability between samples and separation from the control 3 σ before and after Cu dosing. However, it does show a change in the same distribution of points when comparing the blue color channel to red and green. Again, single color DTW performs better, but still has a few samples that deviate from the control in each of the color channels. The separation at the time of dosing (time 0) is well represented in the blue color channel while the red and green show an outlier from the general population results. Two color DTW shows good separation in both GvB and RvB for Trays 2 and 3. It also appears to show separation between the two dosing levels in GvB with Tray 3 samples slightly higher than those of Tray 2. There are still a few responses 24 and 48 hours later, but the initial Cu dosing is well separated and distinguishable from these perhaps prolonged metabolic processes. Though quite similar, the Chl-B laser with Chl-B filter (Figure 4.6) may provide slightly better specificity to individual frond response than observed with the Chl-A laser with Chl-B filter (Figure 4.5).

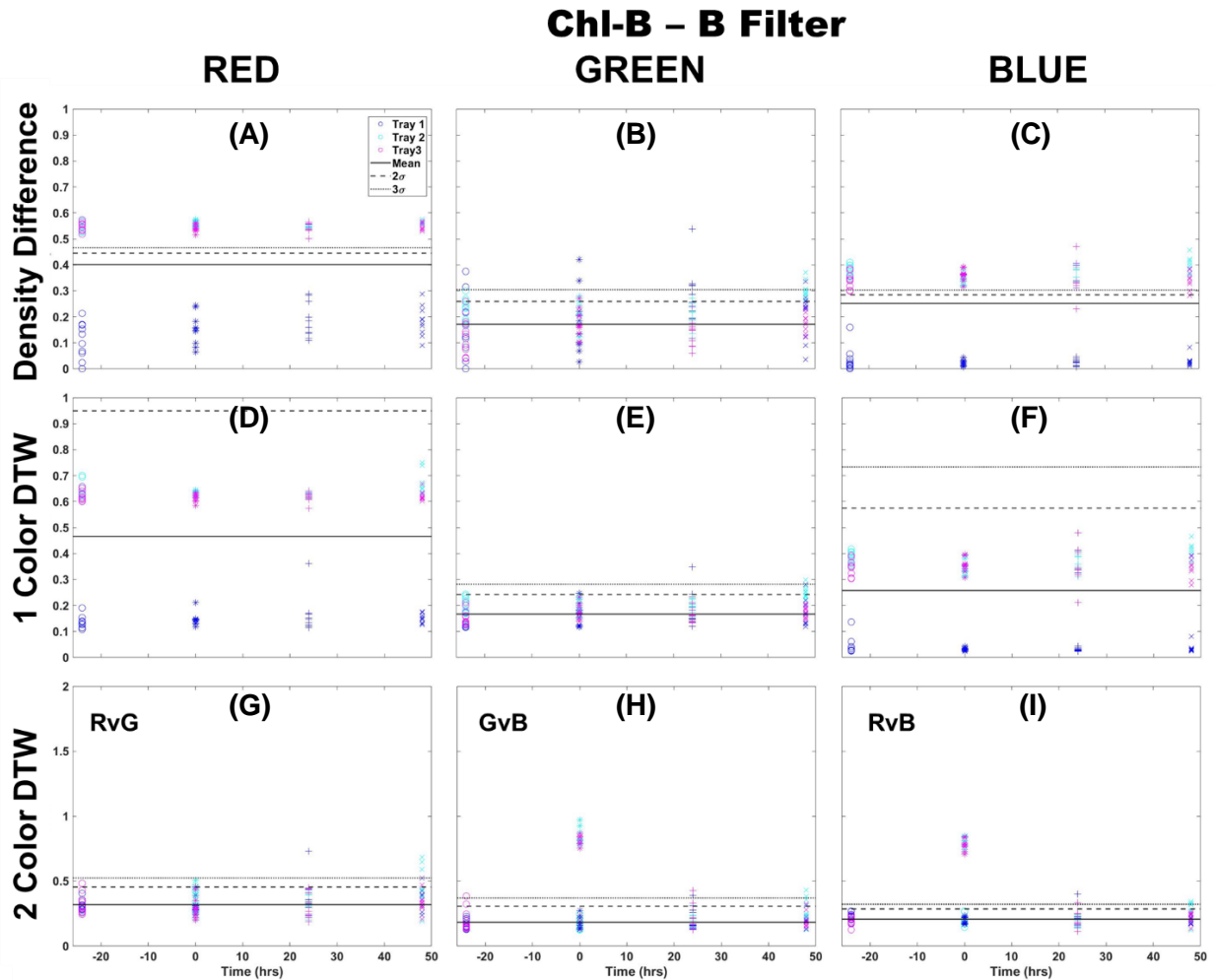


Figure 4.6: Comparison of moss response to the Chl-B laser (462 nm) with the Chl-B filter (650 nm) of the Chl-SL system using three image analysis methods: (A-C) single-color density difference, (D-F) single-color DTW, and (G-I) two-color DTW. Images of fronds were collected every 24 hours over three days. At time 0 three Cu treatments were given at 1 nmol/cm² for Tray 1 (blue), 10 nmol/cm² for Tray 2 (cyan), and 100 nmol/cm² for Tray 3 (magenta).

In Figure 4.7, all blue color channel or two color RvB results from each of the laser systems (Figures 4.4-6) are compiled for direct comparison. The 24 hour response after Cu dosing recorded by the CoCoBi is especially prominent here for Tray 3, but not well documented using the chlorophyll specific lasers. The Chl-A and Chl-B results show differing ranges for healthy chlorophyll response, but are in good agreement for separation at the time of Cu dosing (time 0). Upon closer inspection, Chl-A regardless of analysis method shows tightly condensed ranges for Tray 2 and 3 results at time 0 while Chl-B shows better separation from the control 3 σ for both DTW analysis of single and two colors while also showing good separation between individual fronds. Regardless of laser, density difference performs poorly when compared to

DTW even if overall distributions of points are similar. In Figure 4.8 Chl-A laser results of two color DTW are plotted to compare manual thresholding at 10 DCV and automatic thresholding. Automatic thresholding is in good agreement with manual method results, but show less separation from the control. Due to the computational demand and marginal observed improvement in analysis results, manual thresholding at 10 DCV is deemed to outperform automatic thresholding at this time. Because Chl-B results have better separation between individual frond samples, it's two color DTW results will be compared to chlorophyll and metal extraction.

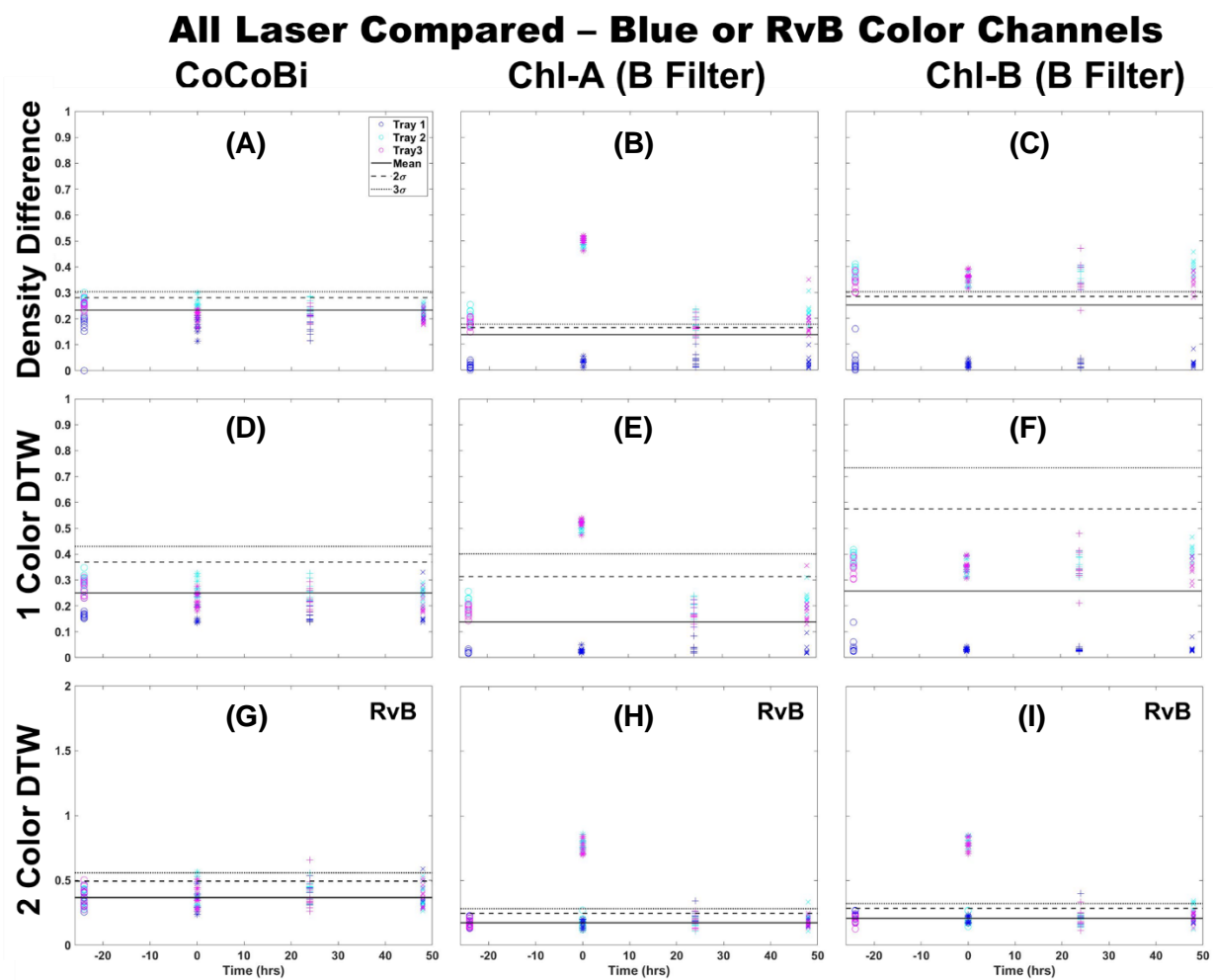


Figure 4.7: Comparison of 3 laser systems (CoCoBi – A,D,G; Chl-A – B,E,H; Chl-B – C,F,I) and 3 analysis methods (density difference – A,B,C; single color DTW – D,E,F; two color DTW – G,H,I) in the blue or RvB color channel. Images of fronds were collected every 24 hours over three days. At time 0 three Cu treatments were given at 1 nmol/cm² for Tray 1 (blue), 10 nmol/cm² for Tray 2 (cyan), and 100 nmol/cm² for Tray 3 (magenta).

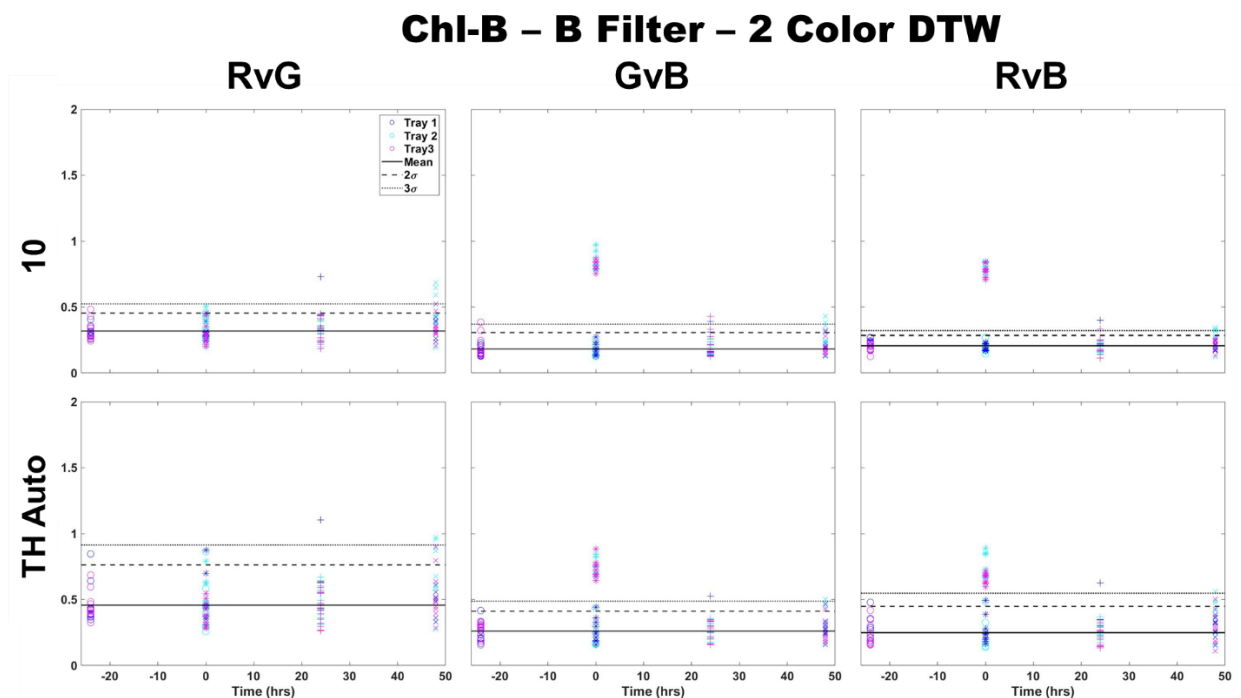


Figure 4.8: Comparison of two color DTW image analysis results using manual thresholding at 10 decimal code values and automatic thresholding for the Chl-B laser fitted with the Chl-B filter.

4.4.3 Comparison of LIF analysis to Chl-SL and SET fronds

Before comparison to chemical analysis results, two-color DTW was also applied to images collected of pairs of fronds for metal extraction. Figure 4.9 shows a visual comparison of how images look for a single frond collected for chlorophyll extraction and a pair of fronds collected for metal extraction. Figure 4.10 applies two-color DTW to images collected for both chemical analysis techniques for both the Chl-A and Chl-B lasers while using the Chl-B filter. There are subtle differences between images of single and pairs of fronds, but overall, the distribution of samples is very similar regardless of laser or number of fronds within the image analyzed. Pairs of fronds may show less separation between individual samples when compared to single fronds, but their degree of difference using two color DTW is in the same area. The range of the control is more similar between the Chl-A and Chl-B laser when observing frond pairs, but is minimally shifted when comparing single versus pairs for the Chl-B laser. These results give us confidence that the technique of two color DTW applied to images that have undergone thresholding of 10 DCV is repeatable for future samples, and easily adaptable to samples of different shapes and sizes.

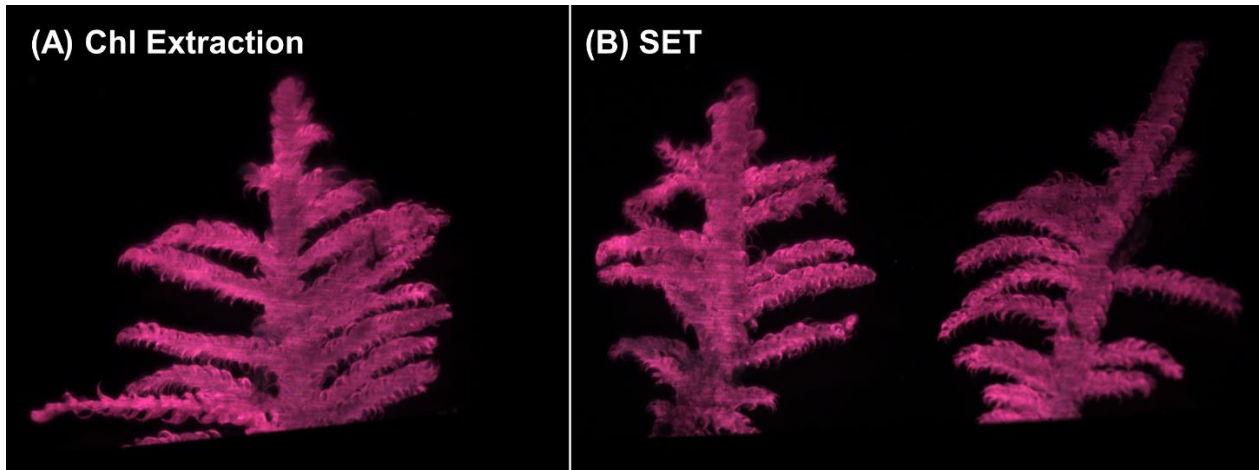


Figure 4.9: (A) Shows an LIF image collected of a single frond that later underwent chlorophyll extraction while (B) shows an LIF image of a pair of fronds that underwent metal extraction.

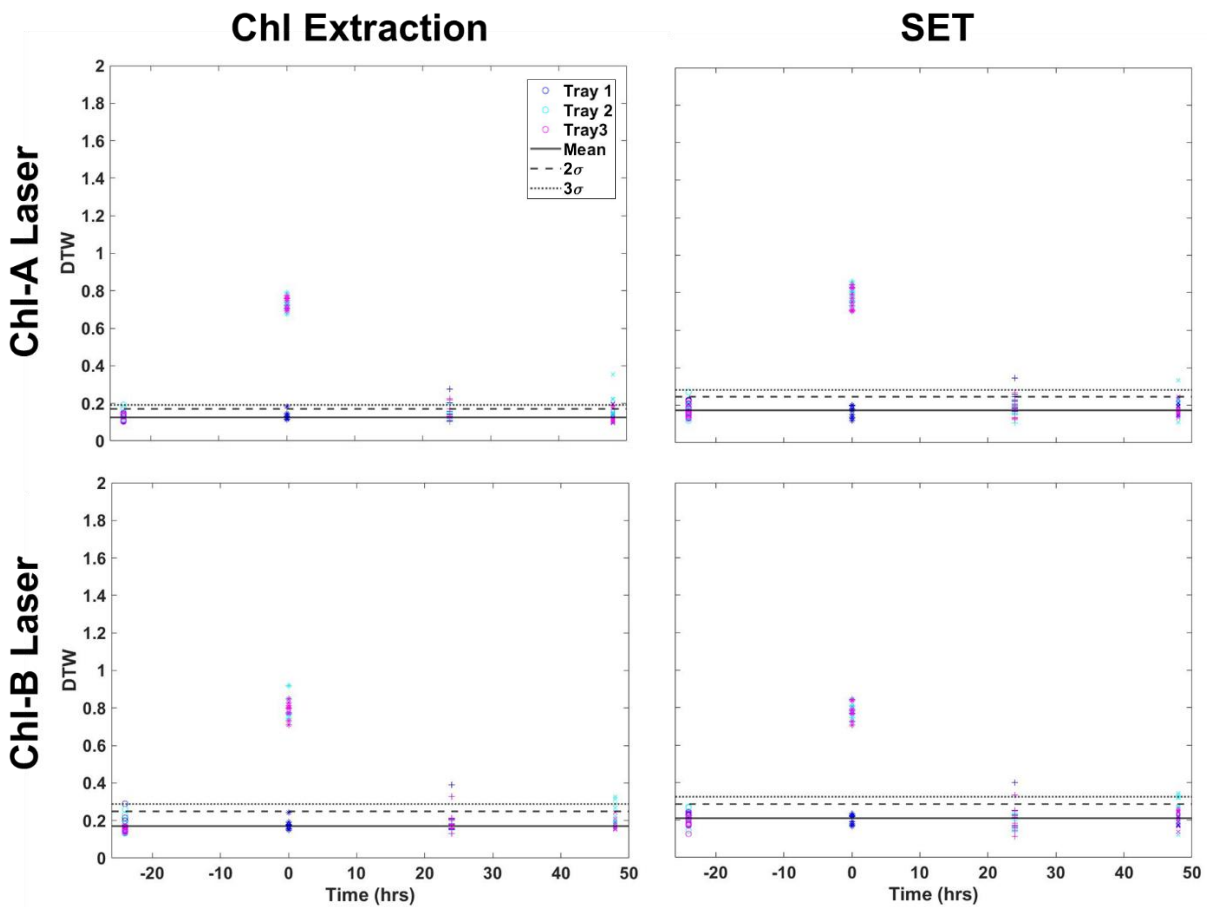


Figure 4.10: Comparison of two color DTW RvB results for both the Chl-A and Chl-B lasers with Chl-B filter when applied to single fronds from chlorophyll extraction and pairs of fronds collected for metal extraction (SET).

4.4.4 Chlorophyll Extraction and SET Results

Table 4.1 shows results of chlorophyll extraction for single fronds collected over the 72 hours of the experiment, while Table 4.2 shows Cu concentrations for both wet and dry weight. It should be noted that while chlorophyll content was measured for all fronds, only 5 samples from each tray collected before Cu dosing (control) were sent for metal analysis via ICP-MS (15 in total). In Figure 4.11, two color RvB DTW results are plotted against Chl a/b ratio for individual fronds while Figure 4.12 shows DTW analysis plotted against Cu dry weight values (nmol/g) for pairs of fronds. Plots of chl-a and -b, total chlorophyll, and chl versus metal content can be found in Appendix C. Chlorophyll results show a more compacted distribution of points when using the Chl-A Laser. Though Chl-B data is sparser there is still clear separation for samples not collected on the same day of Cu dosing. Samples collected on non-dosing days all stay below 0.5 difference and all none deviating points are below 0.3. There does appear to be correlation between a lower chl a/b ratio and Cu dosing with Tray 3 almost all below 1 in Figure 4.11, but the broad distribution of points appears between 0.5 and 3. Metal analysis results show the same clear separation above 0.7 DTW difference for samples collected after Cu dosing, but metal content does not appear directly correlated with deviation from the control in DTW. The control samples are clustered within the same region, with some deviation by Tray 2 and 3 at 24 and 48 hours after dosing. However, there are several Tray 3 samples collected 24 hours after dosing that still have high Cu content but are not observed to deviate. Therefore, it is possible to estimate that contamination is present in a given frond based on DTW, but high Cu levels separate for the initial dosing event do not correlate to high DTW difference.

Table 4.1: Results from chlorophyll extraction. Values shown are for 10 fronds collected every 24 hours from each tray including a control. These on Chl-a (nm) and Chl-b (nm) measurements taken with a spectrophotometer and calculated by using the equations detailed in (Porra, 2002). Each value is adjusted for by weight (mg) of a 2 cm section of frond measured before chlorophyll extraction.

Tray 1	Chl-a /mg	Chl-b /mg	Total Chl/mg	Chl a/b per mg	Tray 2	Chl-a /mg	Chl-b /mg	Total Chl/mg	Chl a/b per mg	Tray 3	Chl-a /mg	Chl-b /mg	Total Chl/mg	Chl a/b per mg
Cont 1	4.526	1.714	6.241	1.585	Cont 1	3.121	1.204	4.324	1.463	Cont 1	2.214	0.853	3.068	0.763
Cont 2	4.112	1.609	5.722	1.163	Cont 2	4.576	1.672	6.248	1.841	Cont 2	2.738	0.974	3.712	1.102
Cont 3	4.662	1.806	6.468	2.797	Cont 3	2.773	1.043	3.816	0.519	Cont 3	5.369	2.025	7.395	2.299
Cont 4	3.250	1.193	4.443	1.574	Cont 4	7.293	2.751	10.044	3.432	Cont 4	5.131	1.920	7.050	1.473
Cont 5	3.355	1.319	4.674	1.364	Cont 5	2.934	1.123	4.058	1.104	Cont 5	3.711	1.403	5.115	1.659
Cont 6	2.525	1.028	3.552	1.505	Cont 6	3.998	1.488	5.486	1.118	Cont 6	9.147	3.505	12.652	2.295
Cont 7	4.226	1.615	5.841	2.763	Cont 7	3.174	1.183	4.357	0.703	Cont 7	2.278	0.882	3.160	1.330
Cont 8	5.012	1.928	6.940	1.659	Cont 8	4.185	1.608	5.793	0.875	Cont 8	3.920	1.601	5.521	1.314
Cont 9	4.484	1.770	6.253	1.240	Cont 9	3.907	1.453	5.360	1.381	Cont 9	2.705	0.974	3.679	1.478
Cont 10	4.434	1.711	6.146	2.255	Cont 10	7.278	2.735	10.014	5.027	Cont 10	1.870	0.680	2.549	0.755
T0 - 1	1.206	0.476	1.682	0.780	T0 - 1	2.273	0.926	3.199	0.638	T0 - 1	1.836	0.830	2.665	1.030
T0 - 2	2.477	0.930	3.407	0.652	T0 - 2	1.707	0.701	2.408	0.606	T0 - 2	1.615	0.650	2.265	0.574
T0 - 3	3.395	1.268	4.663	0.673	T0 - 3	3.953	1.614	5.567	0.710	T0 - 3	2.533	1.016	3.549	0.598
T0 - 4	3.682	1.641	5.324	0.896	T0 - 4	4.240	1.725	5.966	2.081	T0 - 4	2.111	0.859	2.970	0.842
T0 - 5	2.219	1.177	3.396	0.798	T0 - 5	5.225	2.129	7.354	2.191	T0 - 5	3.441	1.344	4.785	1.042
T0 - 6	1.689	0.619	2.308	0.577	T0 - 6	5.779	2.248	8.027	0.918	T0 - 6	4.022	1.509	5.531	1.026
T0 - 7	3.561	1.435	4.996	1.288	T0 - 7	2.881	1.140	4.021	0.735	T0 - 7	1.754	0.628	2.382	0.610
T0 - 8	2.339	0.943	3.282	0.889	T0 - 8	2.877	1.227	4.104	1.426	T0 - 8	2.915	1.177	4.092	0.564
T0 - 9	1.809	0.731	2.540	0.570	T0 - 9	3.632	1.554	5.186	1.359	T0 - 9	1.810	0.698	2.508	0.590
T0 - 10	3.429	1.351	4.780	2.192	T0 - 10	2.849	1.245	4.095	1.482	T0 - 10	1.999	0.745	2.744	0.533
T24 - 1	2.640	0.992	3.632	1.792	T24 - 1	3.702	1.354	5.056	1.642	T24 - 1	3.520	1.385	4.905	1.474
T24 - 2	3.615	1.332	4.947	1.144	T24 - 2	2.681	0.998	3.679	1.238	T24 - 2	5.275	1.926	7.201	1.621
T24 - 3	3.551	1.389	4.940	0.635	T24 - 3	2.152	0.784	2.936	0.995	T24 - 3	1.799	0.742	2.542	0.607
T24 - 4	2.755	1.065	3.819	0.871	T24 - 4	2.626	1.043	3.669	1.054	T24 - 4	2.161	0.792	2.952	0.964
T24 - 5	2.348	0.892	3.240	2.005	T24 - 5	2.702	0.981	3.682	1.399	T24 - 5	2.777	1.056	3.833	1.129

T24 - 6	4.465	1.756	6.221	0.636	T24 - 6	2.525	0.945	3.470	0.794	T24 - 6	1.498	0.549	2.047	1.581
T24 - 7	4.559	1.709	6.268	1.427	T24 - 7	3.311	1.188	4.499	0.971	T24 - 7	1.677	0.596	2.272	1.294
T24 - 8	6.657	2.401	9.059	2.490	T24 - 8	4.602	1.652	6.254	1.174	T24 - 8	1.712	0.668	2.380	0.954
T24 - 9	1.710	0.632	2.341	1.183	T24 - 9	4.462	1.729	6.191	0.977	T24 - 9	1.812	0.606	2.419	1.128
T24 - 10	3.957	1.480	5.437	1.186	T24 - 10	5.013	1.936	6.949	1.191	T24 - 10	1.770	0.623	2.393	1.556
T48 - 1	3.472	1.248	4.721	1.042	T48 - 1	2.278	0.842	3.120	0.790	T48 - 1	3.160	1.087	4.246	2.463
T48 - 2	3.517	1.366	4.883	1.219	T48 - 2	3.055	1.088	4.143	1.279	T48 - 2	2.013	0.680	2.693	1.346
T48 - 3	2.692	1.003	3.696	1.251	T48 - 3	4.375	1.672	6.047	0.561	T48 - 3	6.490	2.480	8.970	1.415
T48 - 4	1.996	0.752	2.748	0.987	T48 - 4	8.229	3.007	11.236	3.755	T48 - 4	3.291	1.265	4.556	1.702
T48 - 5	2.413	0.868	3.281	2.236	T48 - 5	3.986	1.475	5.461	1.201	T48 - 5	2.946	1.123	4.070	1.347
T48 - 6	2.091	0.762	2.853	0.985	T48 - 6	3.117	1.206	4.323	1.434	T48 - 6	2.559	0.867	3.426	2.726
T48 - 7	2.889	1.005	3.894	1.326	T48 - 7	3.473	1.269	4.742	1.526	T48 - 7	6.746	2.636	9.383	1.876
T48 - 8	3.817	1.434	5.251	1.499	T48 - 8	4.453	1.666	6.119	0.964	T48 - 8	3.498	1.307	4.806	0.801
T48 - 9	2.055	0.783	2.839	1.133	T48 - 9	3.218	1.168	4.386	2.727	T48 - 9	2.642	1.082	3.724	2.134
T48 - 10	0.733	0.262	0.995	0.681	T48 - 10	5.311	1.919	7.231	1.523	T48 - 10	1.785	0.644	2.429	1.651

Table 4.2: Results from metal extraction. Values shown are of wet and dry weight of pairs of fronds. 10 sets of fronds for each tray were collected and Cu extracted using SET every 24 hours. Values are adjusted to account for weight (g) of moss pairs and shown in nmol/g and mg/kg levels.

Tray 1	ww	dw	Tray 2	ww	dw	Tray 3	ww	dw
Control 1	0.135	0.657	Control 1	0.073	0.270	Control 1	0.027	0.169
Control 2	0.047	0.232	Control 2	0.028	0.147	Control 2	0.043	0.261
Control 3	0.049	0.215	Control 3	0.023	0.129	Control 3	0.040	0.107
Control 4	0.058	0.258	Control 4	0.037	0.218	Control 4	0.042	0.290
Control 5	0.050	0.358	Control 5	0.034	0.233	Control 5	0.030	0.201
Time 0 - 1	0.090	0.304	Time 0 - 1	0.210	1.524	Time 0 - 1	2.124	14.470
Time 0 - 2	0.113	0.409	Time 0 - 2	0.261	2.136	Time 0 - 2	2.258	11.109
Time 0 - 3	0.126	0.524	Time 0 - 3	0.099	0.965	Time 0 - 3	1.351	11.039
Time 0 - 4	0.079	0.352	Time 0 - 4	0.176	1.061	Time 0 - 4	2.106	13.178
Time 0 - 5	0.098	0.387	Time 0 - 5	0.286	2.420	Time 0 - 5	1.593	12.760
Time 0 - 6	0.084	0.390	Time 0 - 6	0.069	0.434	Time 0 - 6	1.613	10.272
Time 0 - 7	0.060	0.346	Time 0 - 7	0.180	1.648	Time 0 - 7	2.065	15.628
Time 0 - 8	0.185	0.480	Time 0 - 8	0.133	1.094	Time 0 - 8	0.989	8.377
Time 0 - 9	0.059	0.334	Time 0 - 9	0.121	1.195	Time 0 - 9	2.396	18.085
Time 0 - 10	0.108	0.275	Time 0 - 10	0.195	1.578	Time 0 - 10	2.426	21.176
Time 24 - 1	0.135	0.531	Time 24 - 1	0.173	0.790	Time 24 - 1	2.047	12.101
Time 24 - 2	0.083	0.387	Time 24 - 2	0.184	0.891	Time 24 - 2	0.894	6.601
Time 24 - 3	0.068	0.331	Time 24 - 3	0.122	0.965	Time 24 - 3	3.789	18.376
Time 24 - 4	0.059	0.337	Time 24 - 4	0.207	1.541	Time 24 - 4	1.480	10.655
Time 24 - 5	0.095	0.355	Time 24 - 5	0.158	1.458	Time 24 - 5	1.495	7.566
Time 24 - 6	0.032	0.251	Time 24 - 6	0.426	1.659	Time 24 - 6	2.727	19.670
Time 24 - 7	0.063	0.279	Time 24 - 7	0.199	1.103	Time 24 - 7	2.184	12.659
Time 24 - 8	0.067	0.356	Time 24 - 8	0.236	1.400	Time 24 - 8	0.696	5.298
Time 24 - 9	0.050	0.367	Time 24 - 9	0.170	1.370	Time 24 - 9	2.138	13.261
Time 24 - 10	0.088	0.399	Time 24 - 10	0.101	0.753	Time 24 - 10	1.254	8.152
Time 48 - 1	0.091	0.457	Time 48 - 1	0.181	1.022	Time 48 - 1	2.285	13.269
Time 48 - 2	0.101	0.358	Time 48 - 2	0.233	1.148	Time 48 - 2	0.983	6.900
Time 48 - 3	0.058	0.361	Time 48 - 3	0.188	1.114	Time 48 - 3	2.035	11.327
Time 48 - 4	0.056	0.276	Time 48 - 4	0.440	2.323	Time 48 - 4	1.148	6.357
Time 48 - 5	0.089	0.289	Time 48 - 5	0.214	1.199	Time 48 - 5	1.719	10.314
Time 48 - 6	0.127	0.408	Time 48 - 6	0.208	1.254	Time 48 - 6	1.722	5.176
Time 48 - 7	0.064	0.297	Time 48 - 7	0.257	0.760	Time 48 - 7	2.124	10.785
Time 48 - 8	0.063	0.333	Time 48 - 8	0.242	1.107	Time 48 - 8	1.814	14.474
Time 48 - 9	0.098	0.361	Time 48 - 9	0.249	1.470	Time 48 - 9	0.755	5.778
Time 48 - 10	0.124	0.457	Time 48 - 10	0.339	1.497	Time 48 - 10	1.886	13.694

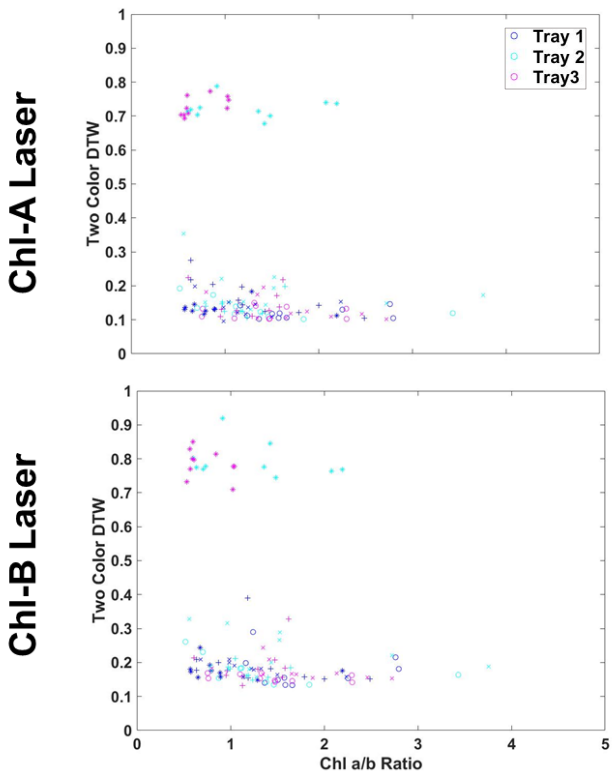


Figure 4.11: Chlorophyll extraction results of chl a/b ratio, compared to two color DTW results from images collected using the Chl-A (top) and Chl-B lasers (bottom) using the B filter. (Total Chl, chl-a and -b can be found in Appendix B)

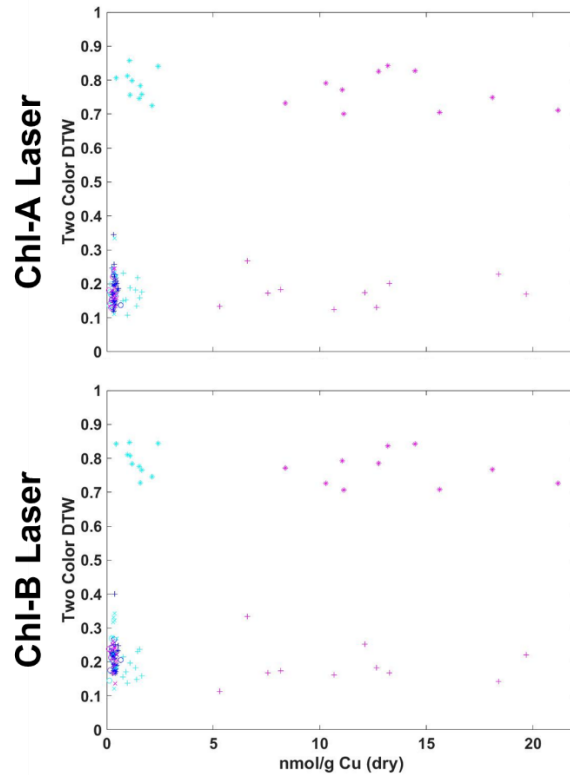


Figure 4.12: Metal extraction results of Cu dry weight of fronds collected every 24 hours compared to Chl-A and Chl-B two color DTW results.

Because chlorophyll and metal extraction are both destructive processes, it was not possible in this case to analyze the same fronds for both chlorophyll and Cu content. However, an attempt was made in Figure 4.13 to make a rough comparison using single frond results and matching Cu extraction values to the already plotted Chl a/b ratio. What results is a clear separation of points below and above 0.5 two color DTW difference. Those above 0.5 were fronds collected from Trays 2 and 3 on the same day as Cu dosing while all other data below 0.5 were either collected before dosing (control) or after dosing (24 and 48 hours later). Though the amount of Cu absorbed by the fronds is quite variable their response using DTW is consistent. Most notable would be that the shift in Chl a/b ratio to below 1 is correlated to this high initial Cu dose, while over time the moss shifts to a higher Chl a/b ratio. In fact, the Tray 1 and Tray 2 Cu doses could prove beneficial to long term moss health by increasing chlorophyll production. At this time, DTW applied to image analysis appears valuable to being able to detect Cu

contamination within moss frond sample shortly after a pollution event, but is less valuable after 24 hours. Though degree of DTW cannot specify the level of contamination it can indicate a minimum threshold and range of contamination above the background since no Tray 1 samples deviated through the experiment. DTW was also able to help document correlation to shift in chlorophyll content due to the introduction of metal.

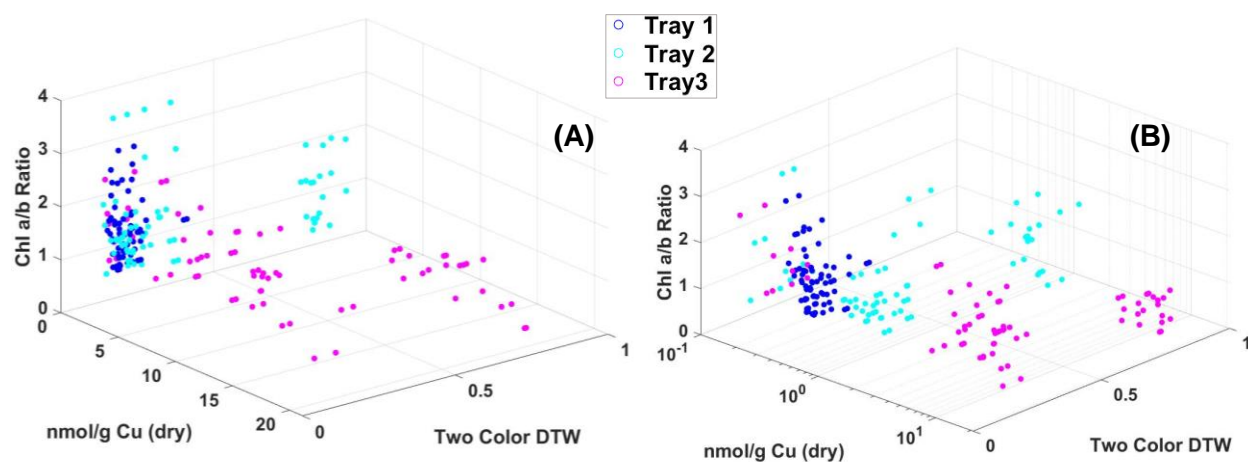


Figure 4.13: (A) Chl-B laser results (x-axis) compared to chlorophyll extraction results of a/b ratio (y-axis) and dry weight metal extraction (z-axis). (B) Shows the same data with a logarithmic scale for Cu.

4.5 DISCUSSION

Previous work applied image analysis of LIF image strictly to moss mats that filled the full view of the CMOS camera utilized in both the CoCoBi and Chl-SL. Though the CoCoBi has been successful in determining the presence of Pb and delineating the moss reaction to metal versus environmental stressors, it's application towards other metals such as Cu and Zn have been inconsistent with the level of metal dosing. Thus, the Chl-SL system was developed for testing if more chlorophyll specific lasers such as the Chl-A (445 nm) and Chl-B (462 nm) used in this work would prove to be better at detecting Cu contamination above environmental background. Techniques for single- and two color image analysis were also applied here to moss fronds to aid in determination if moss mat techniques could be used for targeted sampling of moss fronds that would be representative of identified contamination and aid in complementing of more traditional chemical analysis through chlorophyll and metal extraction.

To achieve image analysis, preprocessing of images was necessary to remove the dominant pixel counts at low decimal code values (DCV) which are a result of the black

aluminum oxide sheets that are used as a non-reflective background during the experiment. Several manual and auto thresholding levels were applied to the images and then evaluated by single color analysis for their effective removal without loss of valuable fluorescence information from frond samples. It was determined that a thresholding and removal of the first 10 DCV vastly improved results of DTW which is a technique not impeded by changes in x or y-axis and only concerned with finding the best fit between two curves. Density difference however was greatly impacted, which lead to similar distributions of data when compare to single and two color DTW, but poor separation when compared to control fronds. Though auto thresholding shows promise, it ultimately was far too computationally demanding when applied to multiple color channels for the potentially minimal benefit of better sample identification of Cu dosing. Using a grayscale version of the image for thresholding is not as computational demanding, but limits the use of multiple color channels for evaluation without any improved results for Cu dosing identification.

When comparing the different laser systems, the Chl-SL performs better than the CoCoBi whether using the Chl-A or Chl-B laser. Density difference performs poorly regardless of laser or filter systems in use, but both single and two color DTW perform well. Use of the Chl-B filter with either Chl laser provides a better separation of frond samples from time 0 at Cu dosing than without a filter or with the Chl-A filter. This is most likely because it is best at capturing the maximum absorption of Chl-B reaction to metal stress while also overlapping with the more dominant Chl-A absorption and emission region (Israsena Na Ayudhya et al., 2015). Though both lasers perform well, the Chl-B laser may offer the potential to separate out not only an event of metal contamination above background levels, but also to distinguish between individual levels of contamination. Whether applied to single fronds or pairs of fronds, the lasers when fitted with the Chl-B filter and with images preprocessed to remove the first 10 DCV are effective at detecting fronds immediately after Cu dosing using single or two color DTW analysis.

Evaluation of chlorophyll and metal analysis when compared to DTW results for both Chl lasers shows distributions of fronds into to sections. In the first section are those DTW images of fronds that deviated from the control at the time of Cu dosing and the second are all other samples. In the case of chlorophyll a/b ratio, DTW difference above 0.5 correlates to the initial Cu dose with Tray 2 samples below and a/b ratio of 2 and all Tray 3 samples with the

higher dose of 100 nmol/cm² falling below an a/b ratio of 1. This would indicate that the initial Cu dose may result in moss fronds responding with either a decrease in chl-a, an increase in chl-b, or both. It can be noted that a lower a/b ratio (2 or lower) can be expected of images collected that produce a DTW difference above 0.5. However, a lower a/b ratio is still present in uncontaminated samples and thus a separation of samples based solely on chlorophyll a/b ratio is not possible. Similarly, metal analysis reveals separation of Trays 2 and 3 from all other samples based on their Cu levels, but only those samples collected on the Cu dosing day deviate in DTW above 0.5. Tray 3 values at 24 and 48 hours after dosing still have high levels of Cu content and yet do not deviate from the control when observing DTW analysis of images. Thus, DTW deviation can help to determine a threshold of Cu contamination soon after an event, but will not detect metal contamination already present in the plant.

It is considered a success that techniques previously only applied to moss mats have been adapted and proven here to be applicable to individual fronds as well. It is believed that the single or two color DTW analysis can be used for analysis of any fluorescence response to aid in evaluation and determination of difference from a control sample. More-over, the removal of the first 10 DCV for RGB images appears as useful if not more than automatic thresholding with the benefit of being computationally much faster to complete. The ability to test the manual thresholding on single fronds and validate its effectiveness when applied to pairs of fronds gives us confidence that the technique can be used for any sample where the background may contribute a dominant number of pixels. More testing is needed for application to backgrounds that are not uniform or may have depth challenges. It is believed that automatic thresholding could aid with such data sets, but must be improved before feasibly applied for reasonable evaluation time. If information for multiple colors is not needed or desired, the automatic thresholding should be quite useful and efficient if the provided image is in grayscale.

Future work would like to further validate the results in this research and also explore the response of moss to other metals of interest with the new Chl-SL system. Application to other plant types, specifically aquatic or vascular plants is of great interest to understand differences in fluorescence signature between species. It could also be of interest to explore if the specific levels of chl-a and chl-b can be determined within a given image collected with LIF. At this time, the image processing technique have proved useful in validating that LIF can be used to identify Cu contamination shortly after an event without confusing it for background level or

historic events. The technique, with limited modification through image preprocessing, can be used on either moss mats or moss fronds with valuable results.

4.6 CONCLUSION

The work compared LIF and image processing techniques previously used only on moss mats to evaluate chlorophyll and Cu content on moss fronds with the intent to develop a method to complement more traditional laboratory measurements. Manual thresholding was necessary as an image preprocessing step by removing the first 10 decimal code values of each color channel (RGB). Both single and two color DTW analysis to compare images to the control were effective at identifying samples immediately after Cu dosing. When compared to chlorophyll extraction, the higher DTW difference of time 0 Cu dosed fronds correlated to lower chlorophyll a/b ratios. Metal content above the dosing level of 10 nmol/cm² were also disguisable at time 0 using DTW. However, high metal content and low chlorophyll a/b ratios do not correspond directly to DTW difference. But, DTW difference does correlate to lower chlorophyll a/b ratios and higher metal content. Future work should re-assess preprocessing techniques and apply them to other plant and leaf types to understand various fluorescence response. The methodology of LIF paired with DTW image analysis is validated through comparison to chemical analysis to identify immediate moss response of Cu dosing. As the results of identification using DTW are only tied to high metal toxicity and changes in chlorophyll the technique could prove useful as an aid for field and laboratory work as an initial indicator of metal contamination.

5 CONCLUSION

5.1 SUMMARY

The dissertation's focus was on the development and testing of a novel remote sensing technology for potential application in the field for monitoring metal contamination in the environment through using LIF to measuring changes in moss response. The work continued building on the methodology outlined in Truax et al. (2022) and was adapted for use with different metals, environmental stressors, and sample sizes. Because the LIF technique captures fluorescence via a CMOS camera, the need for determination of the best image processing techniques with wide application became one of the primary focuses of the work. It was also important to compare the different LIF systems used over the course of the research to understand which wavelengths would prove most effective when observing chlorophyll changes in plants.

Chapter 2 was dedicated to testing the newly improved CoCoBi and its sensitivity levels at the nmol/cm² level for multiple metals and environmental stressors. As with the Master's research (Truax et al., 2020) use of both lasers in tandem proves the most effective application for image collection and analysis. Batch processing of images helped to increase the volume of data collected from a limited number of samples with minimal computational demand. Use of the density difference method of single color analysis and DTW for two-color analysis proved best for either separating metals from environmental stressors or separating metals from changes in photoperiod. Development of three-color analysis using ratios helped to confidently identify metals from other stressor types. Most notably by showing deviation in more than one color channel for metal contamination by Pb and a mixture of metals, versus only deviation in the blue color channel for other stressor types. Zn and Cu were less consistent and understanding their response is important since they are essential nutrients to plants.

Chapter 3 strove to compare two laser systems and see if it were possible to validate response previously recorded by the CoCoBi in Chapter 2 when using the same Cu dosing experiment. The CoCoBi was compared to the Chl-SL with traditional chemical analysis included to determine if the fluorescence responses observed by either system were linked to chlorophyll response. The CoCoBi was inconsistent in its results with limited deviation from the control. In contrast, the Chl-SL lasers tested (445 nm and 462 nm) performed very well with similar

response at the time of Cu dosing regardless of the analysis method used for comparison. Regardless of the laser used, it is recommended that the 670 nm bandpass filter be used to reduce the signal received by the CMOS camera. Of the analysis methods, both single and two color DTW provide better specificity than density difference. The blue color channel was the most responsive to change corresponding to Cu dosing. Results of chemical analysis compared to DTW reveal that high Cu content and low chl a/b ratio are associated with observed deviation from the control. However, high Cu content and/or low chl a/b ratio do not guarantee deviation from the control.

Chapter 4 took interest in applying image processing techniques that would allow for previous methodologies to be translated to use with individual moss fronds instead of the previously tested moss mats. Manual thresholding proved as a necessary image preprocessing step needed to remove the first 10 DCV from each color channel within the image. Regardless of the degree of thresholding density difference proved an ineffective method when applied to moss fronds. However, both single and two color DTW were effective at identifying samples shortly after Cu dosing. Those samples with the initial Cu dose of 10 nmol/cm² or more were easily distinguished from other samples. As with Chapter 3, DTW deviation from the control correlated very well with high Cu content and low a/b ratio, but these factors do not guarantee a detectable fluorescence responds. It is believed that the manual thresholding methods could easily be applied to other sample shapes and types with similar results.

Review of the presented work provides only a sample of the potential that LIF and image processing have to aid in understanding metabolic response in plants. With multiple wavelengths, there have been success in metal identification, stressor identification, and understanding of plant response to metal exposure. Though the long-term response to heavy metal contamination may not be monitored through LIF, a recent change in the environment could easily be detected. The remote sensing and non-destructive nature of the methodology allows for repeated monitoring of the same sample or habitat. Though its specificity towards level of metal contamination is only above the background, the promise of LIF as an aid in reducing the need for laborious sample collection is there. The small size and cost of the Chl-SL could make it well suited as a hand held, laboratory, or future drone technology for monitoring plant health and environmental contamination.

5.2 FUTURE WORK

Many of the techniques presented are relatively new due their combination together in trying to understand complex processes. With each answer that was uncovered through the experiments, several more questions followed. If the work were to continue within the scientific community, there are several future paths that could be explored. The combined effect of photoperiod and metal stress is of interest. Climate or season were not fully explored and could vary vastly depending on species. With that, only one bryophyte was explored as part of this work, but there are many out there with varying responses, chlorophyll content, and metal uptake as bioaccumulators. Though not presented here, work with vascular plants and water ferns has been conducted with success both in hydroponics and soil substrate. However, these were not as robust in their testing and offer more questions about fluorescence response, the role of soil chemistry, nutrient cycling, and metal accumulation in various plant structures. Though the CoCoBi was less effective for use with moss, it was valuable for detecting metal contamination versus environmental stressors. It was also very good at detecting the presence of Pb. The Chl-SL performed well and has been applied to multiple vegetation types with promising results. However, the current laser setup is small and low power limiting its optimal working range within 2 m. For adaptation to drone deployment, more powerful units will be required which could lead to a higher payload than desired. The fast nature of the analysis means real-time application is possible, but was not integrated into the work as of yet. Though currently all available code is in MATLAB, it is quite translational to Python with plans of shifting the work over for more accessibility.

6 APPENDIX

6.1 APPENDIX A

6.1.1 Comparison of images collected using the Biofinder and the CoCoBi

Figure A.1 shows images captured of Cu dosing response in moss using the Biofinder ($\mu\text{mol}/\text{cm}^2$) and the CoCoBi (nmol/cm^2) for comparison. Figure A.2a shows a plot comparing moss treated with Cu at nmol/cm^2 Cu to a control sample using the CoCoBi and analyzed with the methods from Truax et al. (2020) over a 48-hour period. Dosing was determined based on the previous single dose response using the Biofinder at $1.5 \mu\text{mol}/\text{cm}^2$. Three treatment levels, each one exponentially lower than the previous concentration (150, 15, 1.5 nmol/cm^2), were tested using the CoCoBi and their separation from the control is shown in Figure A.2b. 15-150 nmol/cm^2 Cu doses are easily identified, but 1.5 nmol/cm^2 , which would fall within background environmental levels, overlaps with the control images.

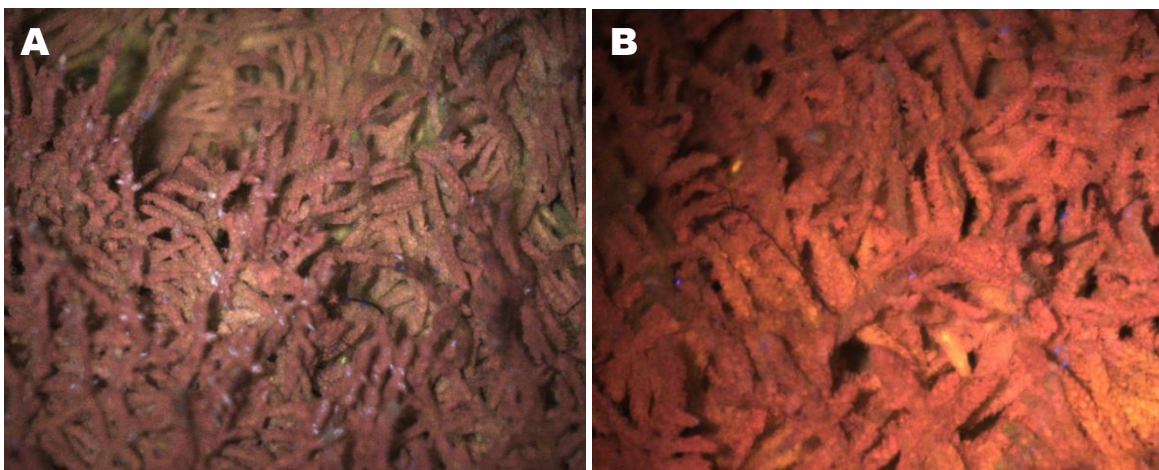


Figure A.1: Image A shows moss with $1.5 \text{ mmol}/\text{cm}^2$ Cu dose collected using the Biofinder. Image B shows moss with $0.15 \text{ mmol}/\text{cm}^2$ Cu dose collected using the CoCoBi. While both show a red biofluorescence of chlorophyll, the red response is more pronounced when using the CoCoBi at a lower Cu dose.

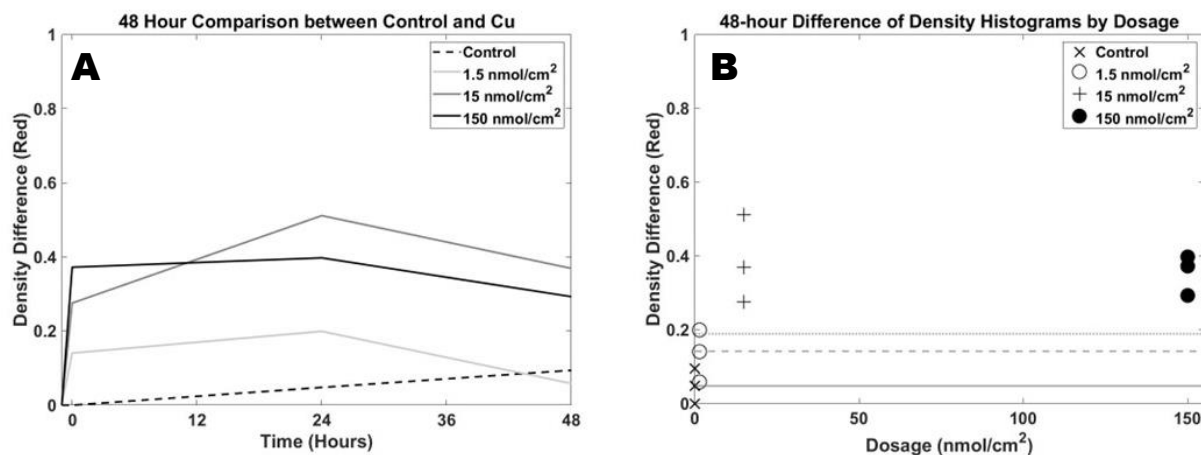


Figure A.2: Plot A displays Cu treated moss at different nmol/cm² Cu levels and a control sample (DI only) using images collected from the CoCoBi. Note the clear separation between Cu treated moss from the control. Plot B reveals that separation at 15-150 nmol/cm² is clearly distinguishable from the control, but 1.5 nmol/cm² would be more difficult to identify though well within normal environmental levels.

6.1.2 Preliminary testing to characterize Pb and Zn response in moss

Preliminary exploration of the response of Pb and Zn in moss using LIF was conducted as a part of the research conducted in Truax et. al. (2020), but has never been published. The results of the 96-hour experiment show metal content in Table A.1 where Pb had an increasing absorption over time, while Cu and Zn remained either constant with dose or decreased slightly. Figure A.3 displays images of Cu, Pb, and Zn treated moss with analysis for each color channel compared to a control over 48 hours after dosing of each metal. Pb does not separate from the control to the same degree as Cu, but is distinguishable. Zn on the other hand is only distinguishable upon dosing and observing the blue channel. The results of the work showed promise in detecting and identifying different metals and could benefit from the greater sensitivity of the CoCoBi, thus becoming a focal point of the research presented as part of this work.

Table A.1: Total dose accumulation over 48 hours after first treatment of moss using Cu, Pb, and Zn measured in $\mu\text{mol/g}$ dry weight for dosing at $1.5 \mu\text{mol/cm}^2$ levels. Values represent total metal accumulated in two fronds sampled from moss masses. Metal extraction was conducted using the sequential elution technique (SET) to separate out the surface, extra-, and intracellular accumulated metals (Brown and Wells, 1988; Vázquez et. al., 1999a; Pérez-Llamazares et al., 2010). Each reported

value is represented by 1 pair of fronds except the Cu 0 and 48 hour which were comprised of 3 pairs of fronds.

Time	Cu	Pb	Zn
0 hour (1st dose)	70.46 ± 13.5	70.8	154.2
24 hours	61.99	167.5	108.7
48 hours (2nd dose)	169.78 ± 13.9	194.8	312.5
72 hours	170.45	280.3	174.3

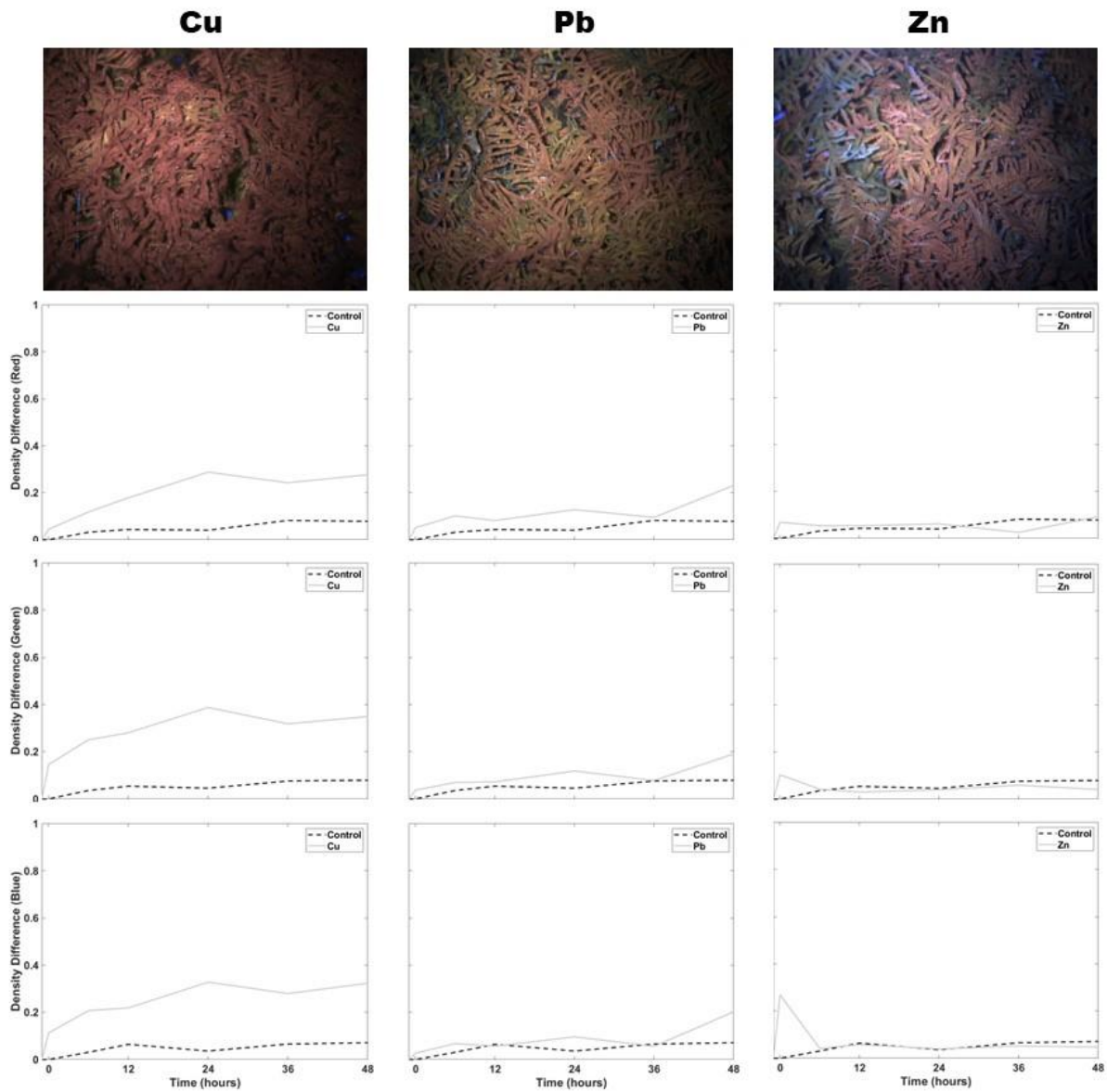


Figure A.3: The first column represents the image analysis of the response of moss to a $1.5 \mu\text{mol}/\text{cm}^2$ dose of Cu over 48 hours when compared to a control samples. The second column is the response of moss to a $1.5 \mu\text{mol}/\text{cm}^2$ dose of Pb over 48 hours. The third column is the response of moss to a $1.5 \mu\text{mol}/\text{cm}^2$ dose of Zn over 48 hours. The first row shows images of moss exposure using the Biofinder. The second row represents analysis using the red color channel. The third row is the green color channel, and the final row is the blue color channel.

6.1.3 Miracle-Gro Nutrients

Miracle-Gro AeroGarden Liquid Plant Food 4-3-6	
Total Nitrogen	4%
1% Ammoniacal Nitrogen	
3% Nitrate Nitrogen	
Available Phosphate (P_2O_5)	3%
Soluble Potash(K_2O)	6%
Calcium (Ca)	1%
Magnesium (Mg)	0.5%
0.5% Water-Soluble Magnesium	
Derived from: Potassium Nitrate, Calcium Nitrate, Mono Potassium Phosphate, Ammonium Nitrate, Magnesium Sulfate	

6.1.4 Density Difference Code

```
n = 10 Trial Images
j(:,1) = Master Mean

len = size(n);
lenT = len(1,2);
arrayRt = zeros(lenT,256);
    for i = 1:length(n)
compare = sum(min(j(:,1),n));
end

x = 10 Trial Images
y = 193 control images
M1 = min(size(x));
M2 = min(size(y));

C = cell(M1,M2);

for m = 1:1:M1;
    for j = 1:1:M2
```

```

    C{m,j} = sum(min(x(:,m),y(:,j)));
end
end

```

6.1.5 Comparison of 24 vs 12-hour plots of data

Previous work by Truax et al. (2022) documented images of moss response to Cu treatment using LIF every 24 hours, which allowed for clear documentation of color changes in moss appearing within minutes of dosing with the metal. In the current study imaging was performed every 12 hours and Figure A.4 shows plots of moss difference from control after being treated with metals over the 7 days of the experiment for all color channels and comparing profiles of metal response at both 24-hour and 12-hour intervals. Both plots show clear indication of increased color change in the moss on treatment days, but the 12-hour plots show a more nuanced response also indicating in some instances that the response at the 12-hour mark after treatment is still elevated but subsides by 24 hours. The response at 12 and 36 hours represent the beginning and end of photoperiod. For each instance, hour 24 after dosing, however, is the lowest recorded response and happens to correlate to after the night cycle or period of sustained darkness. Only the 12-hour results are presented in the main body of the paper, while 24-hour results are used throughout the Appendices to show general trends.

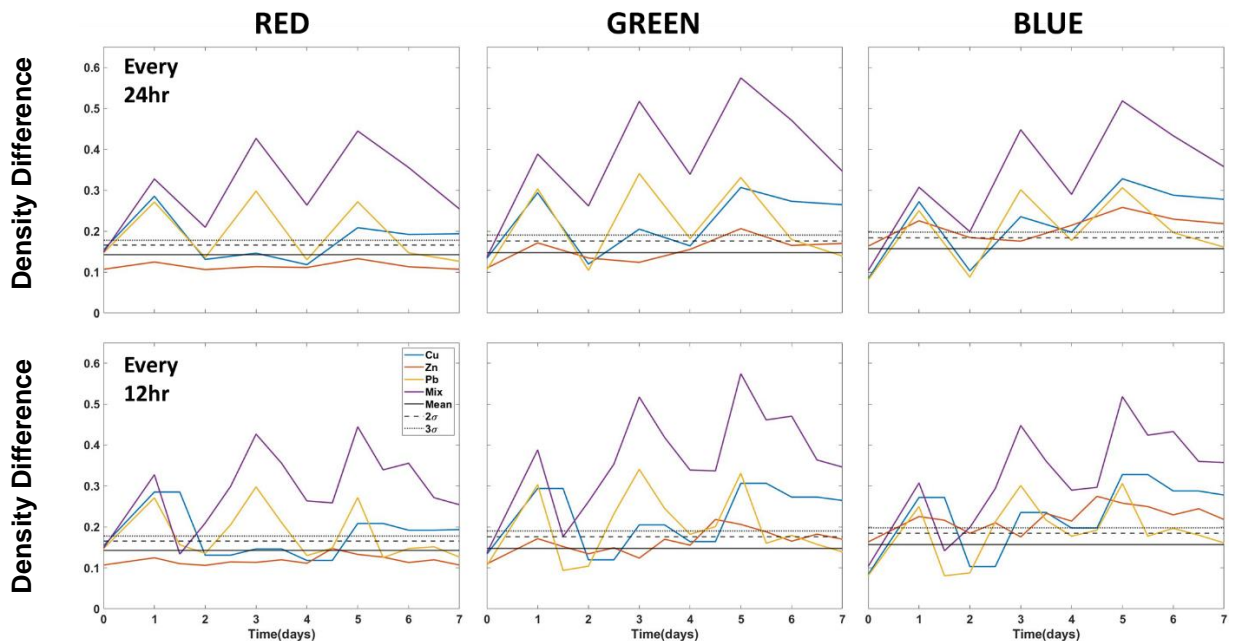


Figure A.4: Comparison of density difference analysis using images collected every 24 hours (top) and every 12 hours (bottom) for each color channel.

6.1.6 Notes on gain level and methods used when collected images with Green Laser

Images were taken at 3 gain levels (5, 10, and 15) for just the green laser. Five shots were taken from the front of the moss tray (each corner and the center), and then rotated 180° so the back of the moss could be imaged, producing 10 images in total.



Figure A.5: Single-color density difference comparison of images of mosses collected using only the Green Laser (532 nm) treated with metals to the control. Plots are first sorted vertically by gain (5, 10, and 15), then by analysis method (MMM - left or BMM – right), and finally by color (R,G,B). X-axis for all figures is in time (days) and the y-axis is the density difference between images of metal treated and control moss as determined by individual colors. Purple (metal mix), yellow (Pb), blue (Cu), and orange (Zn).

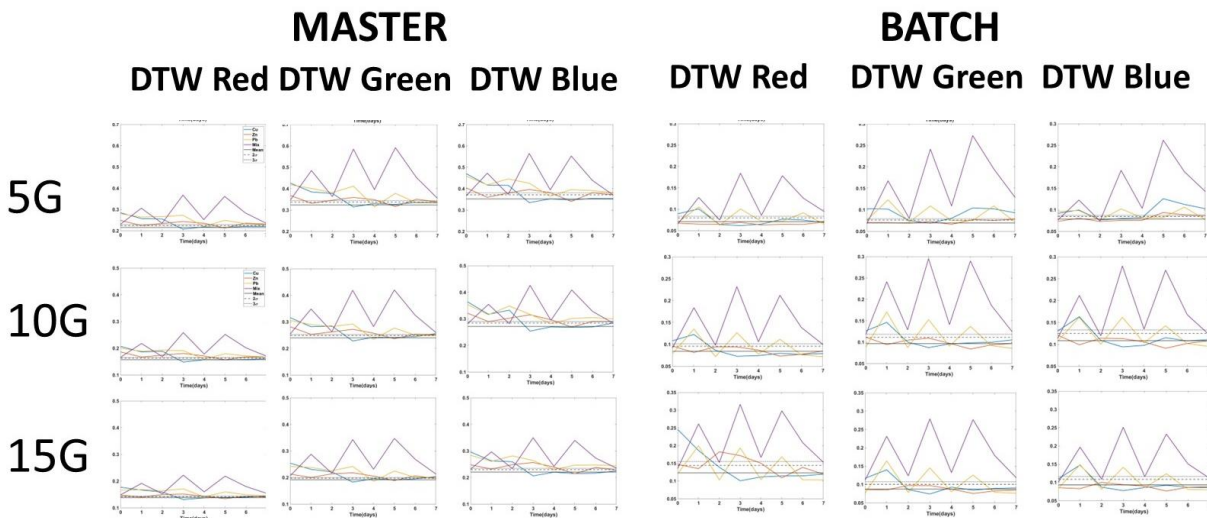


Figure A.6: Single-color DTW comparison of images of mosses collected using only the Green Laser (532 nm) treated with metals to the control. Plots are first sorted vertically by gain (5, 10, and 15), then by analysis method (MMM - left or BMM – right), and finally by color (R,G,B). X-axis for all figures is in

time (days) and the y-axis is the density difference between images of metal treated and control moss as determined by individual colors. Purple (metal mix), yellow (Pb), blue (Cu), and orange (Zn).

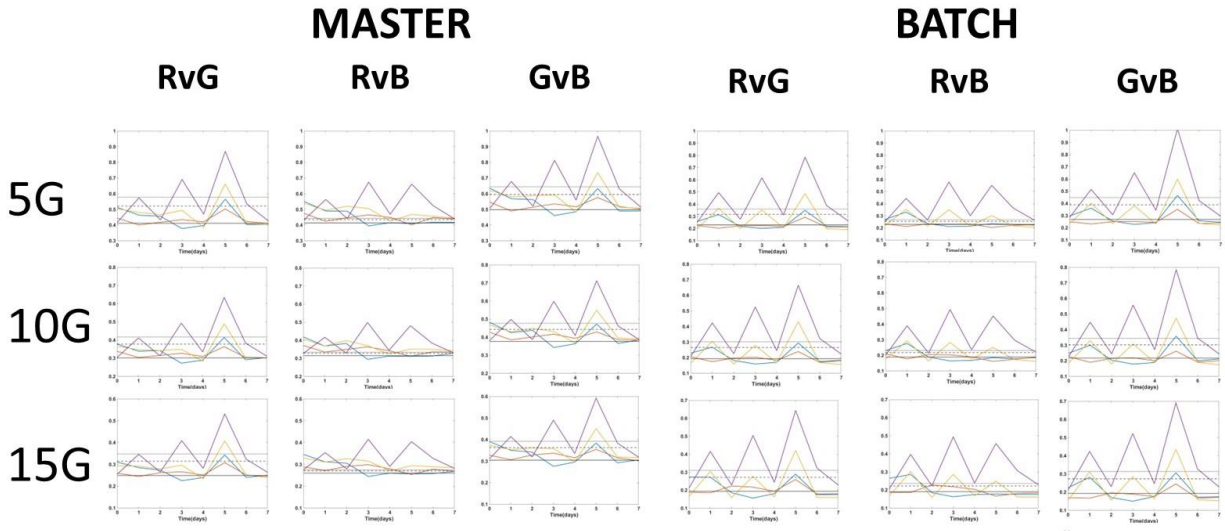


Figure A.7: two-color DTW comparison of images of mosses collected using only the Green Laser (532 nm) treated with metals to the control. Plots are first sorted vertically by gain (5, 10, and 15), then by analysis method (MMM - left or BMM – right), and finally by color (R,G,B). X-axis for all figures is in time (days) and the y-axis is the density difference between images of metal treated and control moss as determined by individual colors. Purple (metal mix), yellow (Pb), blue (Cu), and orange (Zn).

6.1.7 UV Laser Summary

6.1.7.1 Notes on gain Level and methods used when collecting images with UV Laser

Images were taken at 3 gain levels (15, 30, and 45) for just the UV laser. Five shots were taken from the front of the moss tray (each corner and the center), and then rotated 180° so the back of the moss could be imaged, producing 10 images in total.

6.1.7.2 Results of Batch processing for UV Laser

The benefit of batch processing is most observable when reviewing its application to UV LIF images. The master mean comparison is consistent with the match mean in its results for Zn identification but can only be interpreted for all metal identification at the highest treatment level. Batch processing on the other hand shows clear peaks for all color channels and metals. Previous work did not find a significant impact in using just LIF images of UV response (Truax et al., 2020), which was assumed to result from UV being more applicable to hydrocarbons and microbe detection. The observed profiles of Zn from the UV plots may indicate a secondary

process of metal interaction with protein or lipid structure, or batch processing may have helped to reveal subtle differences that the CoCoBi now picks up on due to the introduction of the short pass filter to the camera used for imaging. Regardless of the color channel, each metal presents a peak at time of dosing when compared to the control using the density difference method. There are instances where the UV laser at a gain of 30 fails to detect lower thresholds of metals that could fall within the natural environmental background which could be useful for delineating between higher and lower detection limits.

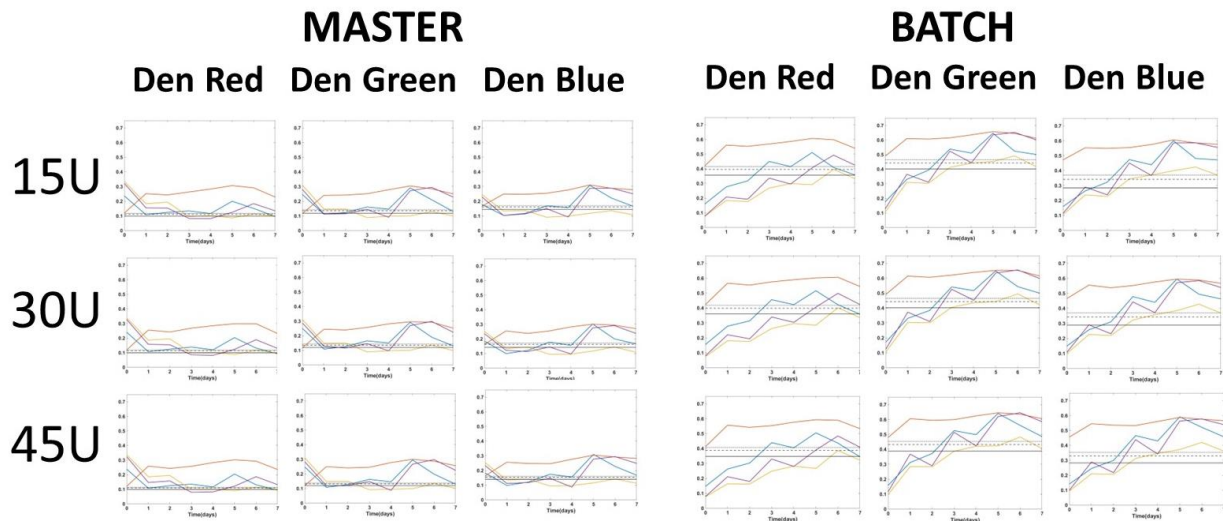


Figure A.8: Single-color density difference comparison of images of mosses collected using only the UV Laser (355 nm) treated with metals to the control. Plots are first sorted vertically by gain (5, 10, and 15), then by analysis method (MMM - left or BMM – right), and finally by color (R,G,B). X-axis for all figures is in time (days) and the y-axis is the density difference between images of metal treated and control moss as determined by individual colors. Purple (metal mix), yellow (Pb), blue (Cu), and orange (Zn).

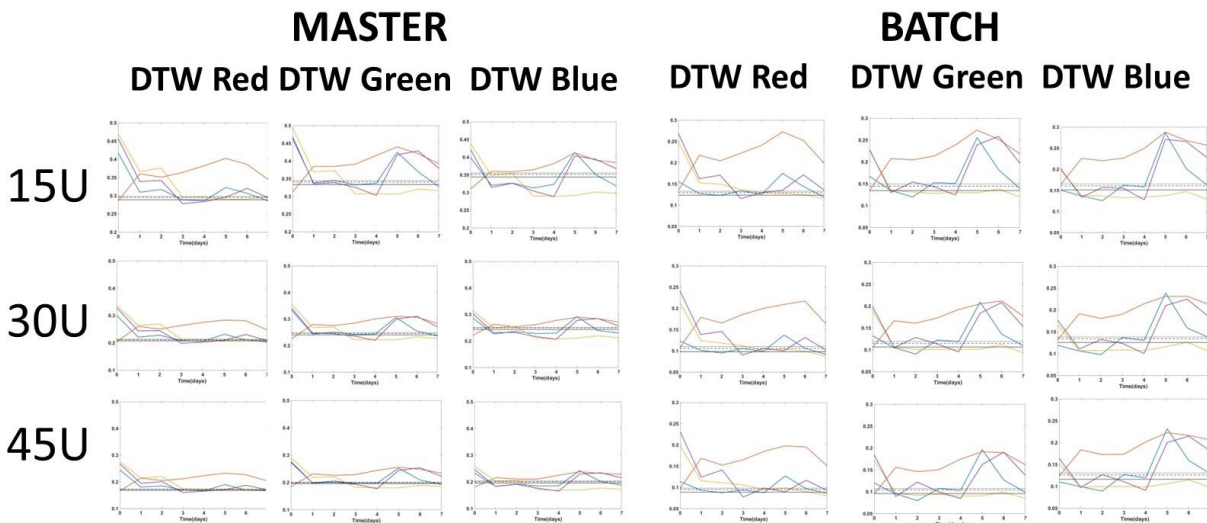


Figure A.9: Single-color DTW comparison of images of mosses collected using only the UV Laser (355 nm) treated with metals to the control. Plots are first sorted vertically by gain (5, 10, and 15), then by analysis method (MMM - left or BMM – right), and finally by color (R,G,B). X-axis for all figures is in time (days) and the y-axis is the density difference between images of metal treated and control moss as determined by individual colors. Purple (metal mix), yellow (Pb), blue (Cu), and orange (Zn).

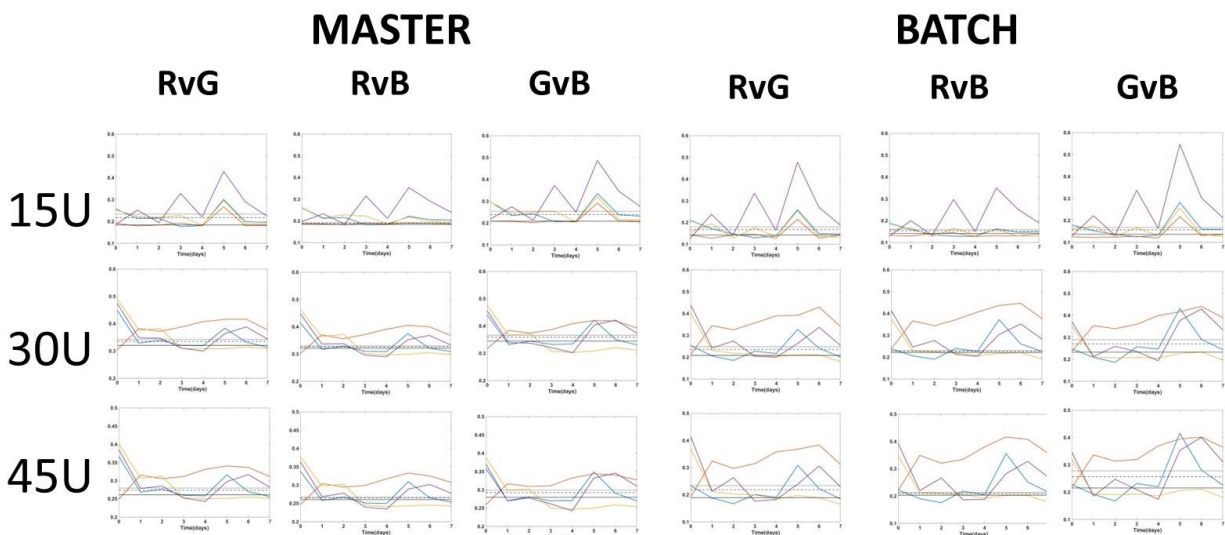


Figure A.10: Two-color DTW difference comparison of images of mosses collected using only the UV Laser (355 nm) treated with metals to the control. Plots are first sorted vertically by gain (5, 10, and 15), then by analysis method (MMM - left or BMM – right), and finally by color (R,G,B). X-axis for all figures is in time (days) and the y-axis is the density difference between images of metal treated and control moss as determined by individual colors. Purple (metal mix), yellow (Pb), blue (Cu), and orange (Zn).

6.1.7.3 Results of UV Laser Density Difference analysis for environmental and photoperiod

Though the UV laser images captured at a gain of 30 appeared useful for identification of metals, Figure 10 reveals the UV laser was also capable of assessing environmental and photoperiod stressors regardless of color channel. UV appears less sensitive to long photoperiods, but performs poorly when attempting to identify differences between other photoperiods or environmental stressors. Though a peak is present at the time of metal dosing, the profiles cannot be statistically distinguished from photoperiod or environmental stressors. UV proves useful in the identification of Zn, but its inability to distinguish between other stressors types limits UV application. It also raises the question of potential secondary processes of metal interactions with plants with lipid or protein structures. Because the CoCoBi is designed as a broad-spectrum detector for biologicals and organics more processes than just

photosynthesis and chlorophyll may be responding to the laser wavelengths being utilized. The possible explanations are numerous and would require further exploration. Review of the t-test results in Table A.2 in regards to the UV data confirms that stressors types are likely to be indistinguishable.

UV Laser – Gain 30

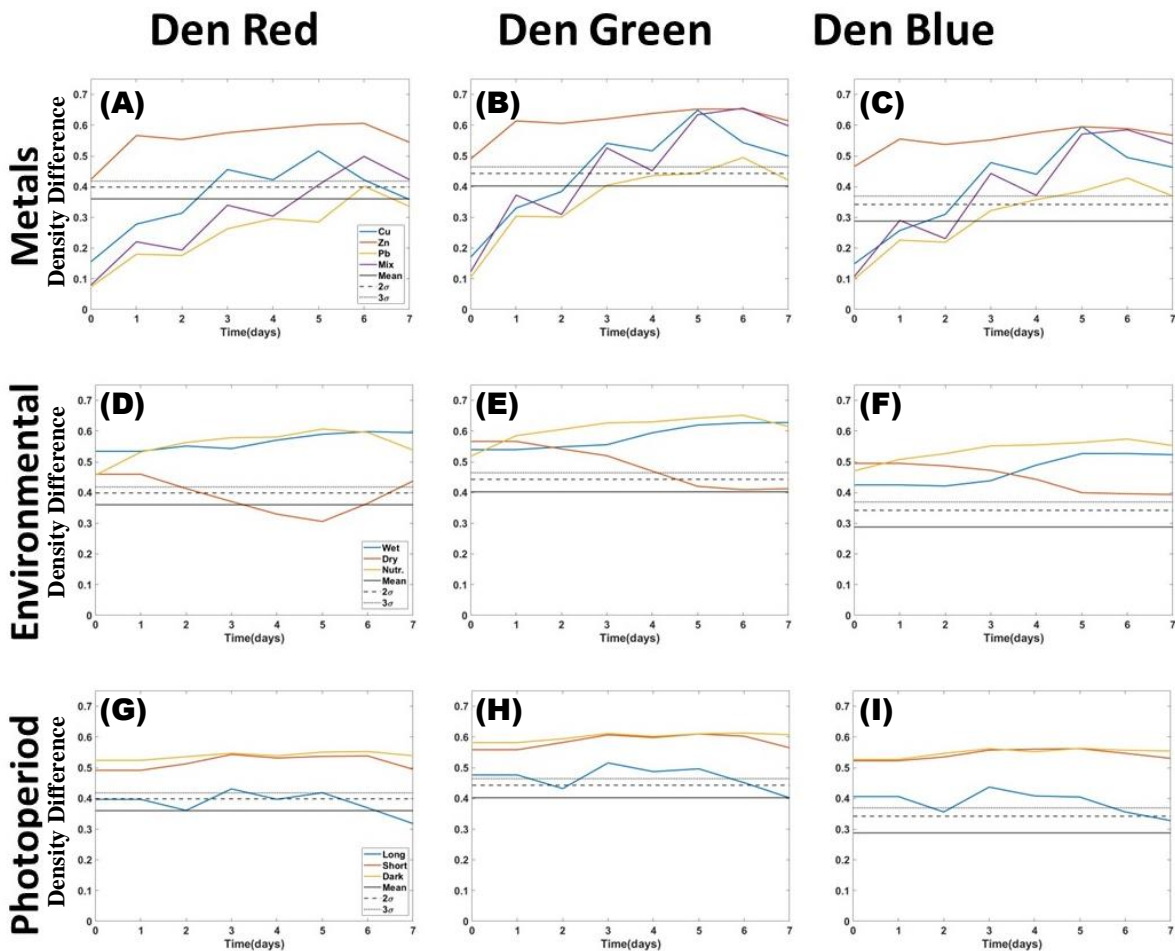


Figure A.11: Single color density difference using BMM analysis for all color channels of images taken just the UV laser, of metal, environmental, and photoperiod trials with the control mean and confidence intervals included.

Table A.2: Welch's t-test applied to the density difference analysis values for images collected using the UV laser at a gain of 30. Columns are separated into trial, then by color channel (red, green, blue). The left column shows the t-value for the trial while the right column shows the t-value for the control for

each day. Cells shaded in grey represent *t*-values that exceed the critical *t*-value to be considered similar to the control.

		Copper						Zinc					
day	red		green		blue		red		green		blue		
0	6.88	1.74	5.35	1.74	2.70	1.75	1.40	1.74	2.24	1.77	2.24	1.77	
1	3.57	1.76	1.96	1.79	0.25	1.79	6.92	1.78	5.89	1.82	5.89	1.82	
2	0.93	1.73	0.11	1.77	0.73	1.78	7.52	1.76	5.99	1.81	5.99	1.81	
3	4.63	1.76	4.59	1.76	4.88	1.77	9.61	1.79	7.53	1.82	7.53	1.82	
4	2.04	1.74	2.73	1.75	3.01	1.76	7.95	1.78	6.45	1.82	6.45	1.82	
5	6.47	1.79	6.37	1.80	6.61	1.78	9.79	1.79	6.73	1.82	6.73	1.82	
6	1.06	1.73	2.43	1.74	3.42	1.76	7.29	1.79	6.06	1.82	6.06	1.82	
7	0.32	1.75	1.66	1.78	2.49	1.78	5.13	1.76	4.66	1.80	4.66	1.80	
		Lead						Mix					
day	red		green		blue		red		green		blue		
0	11.96	1.82	7.86	1.78	7.86	1.78	11.64	1.81	7.77	1.81	7.77	1.81	
1	5.52	1.73	2.47	1.76	2.47	1.76	4.06	1.74	0.69	1.74	0.69	1.74	
2	5.07	1.73	1.86	1.76	1.86	1.76	4.77	1.74	1.72	1.77	1.72	1.77	
3	2.02	1.74	0.76	1.75	0.76	1.75	0.42	1.74	4.40	1.79	4.40	1.79	
4	1.44	1.73	0.83	1.75	0.83	1.75	1.48	1.74	1.32	1.78	1.32	1.78	
5	2.07	1.73	1.09	1.75	1.09	1.75	1.55	1.73	5.81	1.78	5.81	1.78	
6	0.60	1.74	1.46	1.75	1.46	1.75	3.31	1.74	5.63	1.77	5.63	1.77	
7	0.93	1.74	0.24	1.76	0.24	1.76	1.43	1.74	4.08	1.78	4.08	1.78	
		Wet						Dry					
day	red		green		blue		red		green		blue		
0	5.66	1.77	3.59	1.78	3.59	1.78	2.52	1.74	4.48	1.80	4.48	1.80	
1	5.66	1.77	3.59	1.78	3.59	1.78	2.52	1.74	4.48	1.80	4.48	1.80	
2	7.23	1.75	4.25	1.78	4.25	1.78	2.20	1.74	4.26	1.80	4.26	1.80	
3	7.67	1.76	5.26	1.79	5.26	1.79	1.28	1.73	4.05	1.77	4.05	1.77	
4	6.32	1.74	4.88	1.77	4.88	1.77	0.68	1.74	1.77	1.78	1.77	1.78	
5	8.73	1.76	5.72	1.80	5.72	1.80	1.54	1.74	0.64	1.79	0.64	1.79	
6	6.65	1.77	5.01	1.78	5.01	1.78	0.39	1.77	0.58	1.80	0.58	1.80	
7	6.52	1.75	4.71	1.77	4.71	1.77	2.11	1.78	0.47	1.80	0.47	1.80	
		Nutrients						Long					
day	red		green		blue		red		green		blue		
0	2.30	1.74	2.94	1.77	2.94	1.77	0.55	1.74	1.87	1.77	1.87	1.77	
1	4.92	1.74	5.03	1.81	5.03	1.81	0.55	1.74	1.87	1.77	1.87	1.77	
2	7.21	1.74	5.92	1.80	5.92	1.80	0.54	1.74	1.34	1.79	1.34	1.79	
3	8.41	1.74	7.43	1.79	7.43	1.79	3.62	1.75	4.17	1.80	4.17	1.80	
4	6.38	1.74	6.06	1.80	6.06	1.80	1.35	1.75	2.30	1.80	2.30	1.80	
5	8.27	1.74	6.26	1.80	6.26	1.80	2.28	1.74	2.50	1.78	2.50	1.78	
6	6.13	1.75	5.83	1.80	5.83	1.80	0.26	1.77	0.53	1.80	0.53	1.80	
7	4.46	1.74	4.46	1.78	4.46	1.78	1.55	1.76	0.74	1.80	0.74	1.80	
		Short						Dark					

day	red		green		blue		red		green		blue	
0	3.72	1.75	4.03	1.77	4.03	1.77	3.56	1.74	4.37	1.75	4.37	1.75
1	3.72	1.75	4.03	1.77	4.03	1.77	3.56	1.74	4.37	1.75	4.37	1.75
2	5.76	1.75	5.10	1.78	5.10	1.78	4.35	1.75	4.87	1.75	4.87	1.75
3	7.30	1.75	6.70	1.78	6.70	1.78	5.33	1.74	6.35	1.76	6.35	1.76
4	5.50	1.75	4.93	1.77	4.93	1.77	4.52	1.74	5.12	1.78	5.12	1.78
5	6.21	1.74	5.45	1.80	5.45	1.80	4.82	1.74	4.95	1.76	4.95	1.76
6	4.68	1.76	4.47	1.79	4.47	1.79	3.79	1.74	4.35	1.76	4.35	1.76
7	3.41	1.74	3.24	1.78	3.24	1.78	3.78	1.74	4.17	1.77	4.17	1.77

Review of color channel ratios for the UV laser at a gain of 30 using the density difference method, proves to be just as muddled as Figure A.12 and Table A.3. In Figure A.12 it becomes clear that the green color channel is the most dominate in all of the trials. The control does appear to have a lower blue channel values and some of the metals appear to have lower red channel values, but each is difficult to discern from one another at first glance. Results comparing the trials to the control's 3σ for each color channel (Table A.3) reveals that the blue channel is the most reliable for detecting deviation from the control. However, the blue channel shows deviation in all trials but the over wetting. Only Pb and the mixture of metals show deviation in the green channel. Therefore, if wanting to detect Pb or a mixture of metals in the environment, use of just the UV laser would be advisable. It cannot be recommended for use with other metals or monitoring environmental or photoperiod stressors based on these results.

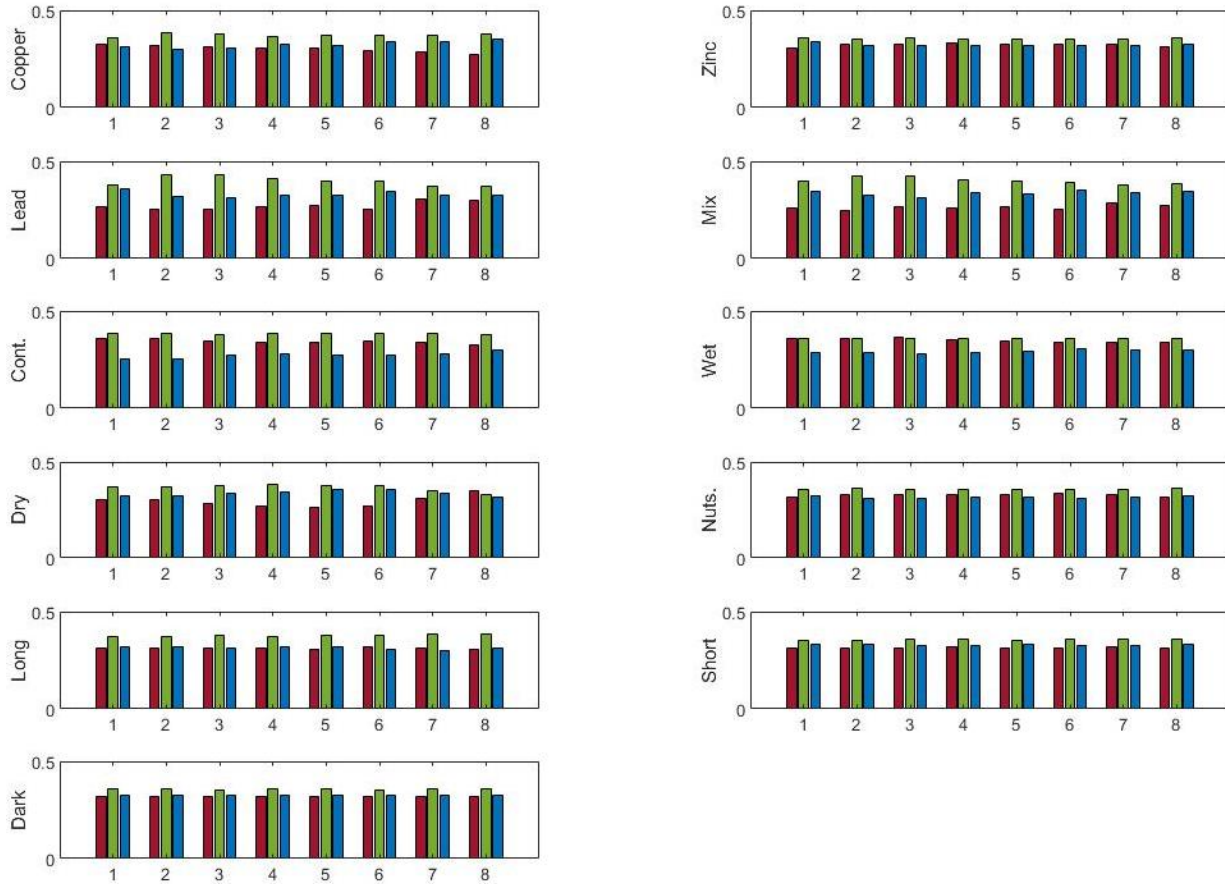


Figure A.12: Use of color ratios from density difference (UV laser) analysis to compare the 11 trials using BMM. Values used are listed in Table A.2 and calculated from dividing individual color channels (R,G,B) by the sum of their difference from the control.

Table A.3 Values plotted in Figure A.12 and calculated from density difference analysis of images collected using a UV laser at a gain of 30. Shaded cells are values that exceed 3σ confidence interval for the control (statistically different).

day	Copper			Zinc			Lead			Mix		
	red	green	blue	red	green	blue	red	green	blue	red	green	blue
0	0.156	0.171	0.149	0.423	0.490	0.466	0.074	0.105	0.099	0.080	0.124	0.107
1	0.278	0.330	0.257	0.566	0.614	0.555	0.180	0.303	0.226	0.221	0.372	0.290
2	0.314	0.384	0.310	0.553	0.606	0.537	0.176	0.301	0.219	0.194	0.310	0.231
3	0.456	0.541	0.478	0.575	0.620	0.552	0.263	0.404	0.322	0.340	0.526	0.443
4	0.422	0.516	0.440	0.589	0.638	0.576	0.296	0.436	0.358	0.304	0.452	0.372
5	0.516	0.649	0.596	0.602	0.652	0.595	0.285	0.443	0.385	0.406	0.634	0.571
6	0.422	0.543	0.495	0.606	0.652	0.589	0.401	0.495	0.428	0.498	0.655	0.585
7	0.358	0.499	0.463	0.544	0.614	0.567	0.335	0.421	0.369	0.423	0.598	0.539
day	Wet			Dry			Nutrients			Control		
	red	green	blue	red	green	blue	red	green	blue	red	green	blue
0	0.534	0.539	0.425	0.460	0.566	0.495	0.456	0.518	0.471	0.379	0.403	0.267
1	0.534	0.539	0.425	0.460	0.566	0.495	0.532	0.585	0.508	0.379	0.403	0.267
2	0.551	0.549	0.421	0.413	0.542	0.487	0.563	0.605	0.527	0.344	0.380	0.274
3	0.543	0.556	0.439	0.371	0.520	0.472	0.579	0.626	0.552	0.326	0.375	0.271
4	0.571	0.594	0.489	0.330	0.470	0.443	0.580	0.630	0.555	0.354	0.400	0.286
5	0.590	0.620	0.527	0.306	0.420	0.400	0.607	0.642	0.563	0.352	0.395	0.282
6	0.598	0.627	0.527	0.365	0.409	0.396	0.596	0.651	0.574	0.378	0.431	0.315
7	0.595	0.628	0.523	0.437	0.413	0.394	0.538	0.615	0.553	0.370	0.431	0.342
day	Long			Short			Dark			mean per color combo		
	red	green	blue	red	green	blue	red	green	blue			
0	0.397	0.476	0.406	0.492	0.558	0.523	0.524	0.582	0.527			
1	0.397	0.476	0.406	0.492	0.558	0.523	0.524	0.582	0.527			
2	0.361	0.432	0.356	0.512	0.582	0.535	0.536	0.594	0.546	mean		
3	0.431	0.515	0.437	0.543	0.607	0.557	0.547	0.611	0.562			
4	0.397	0.487	0.408	0.531	0.598	0.560	0.539	0.602	0.552	red	0.360	0.414
5	0.419	0.496	0.404	0.537	0.610	0.562	0.551	0.610	0.563	green	0.402	0.460
6	0.369	0.451	0.356	0.538	0.602	0.547	0.553	0.613	0.557	blue	0.288	0.364
	0.318	0.402	0.328	0.495	0.565	0.530	0.539	0.607	0.554			

6.1.7.4 Discussion of UV laser application

The same techniques used with just the UV laser at a gain of 30 were found to be much less conclusive. Figure displays photoperiod as similar to the control, but environmental stressors have more separated profiles, and reverse of the density difference for both lasers at a gain of 10. Though metal profiles are difficult to distinguish, UV could be a better indicator of plant health as a monitor of metal contamination. It is assumed that the UV is revealing other biological processes besides those occurring with chlorophyll. However, more work would need to be done to research the possible interactions if they can be effectively determined or controlled in the laboratory. The t-test could be used to determine Pb or the mixture of metals due to deviation occurring in both the green and blue color channels. Ratios are less useful here with deviation for all stressors occurring in the blue channel. It is recommended that use of just the UV laser only be utilized when determining if a contaminant is comprised of single or multiple metals.

6.1.7.5 All gains tested using both lasers for metal stress



Figure A.13: Single-color density difference comparison of images of mosses collected using both lasers treated with metals to the control. Plots are first sorted vertically by gain (5, 10, and 15), then by analysis method (MMM - left or BMM – right), and finally by color (R,G,B). X-axis for all figures is in time (days) and the y-axis is the density difference between images of metal treated and control moss as determined by individual colors. Purple (metal mix), yellow (Pb), blue (Cu), and orange (Zn).

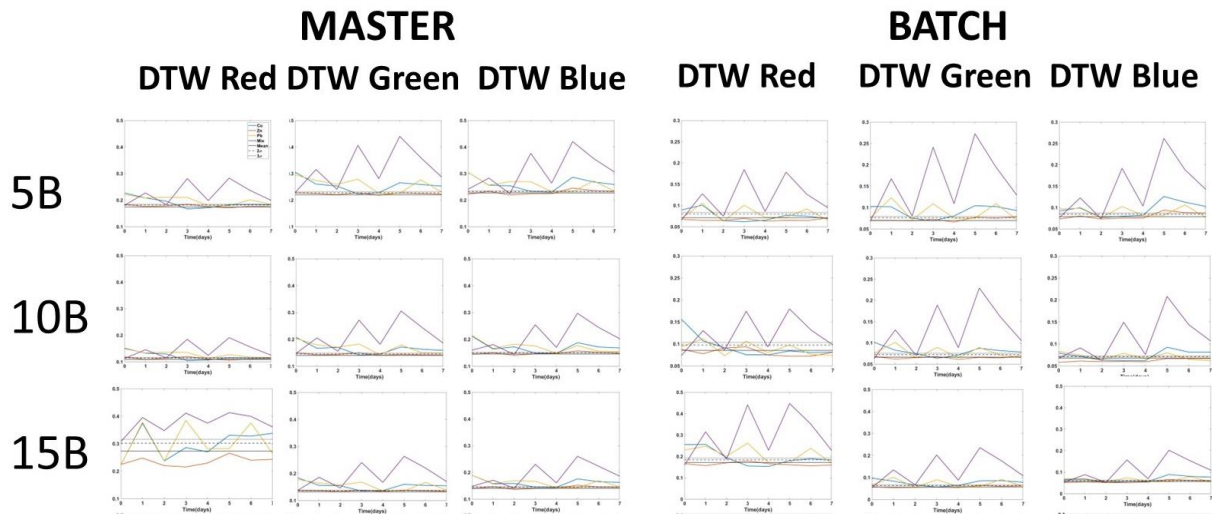


Figure A.14: Single-color DTW comparison of images of mosses collected using both lasers treated with metals to the control. Plots are first sorted vertically by gain (5, 10, and 15), then by analysis method (MMM - left or BMM – right), and finally by color (R,G,B). X-axis for all figures is in time (days) and the y-axis is the density difference between images of metal treated and control moss as determined by individual colors. Purple (metal mix), yellow (Pb), blue (Cu), and orange (Zn).

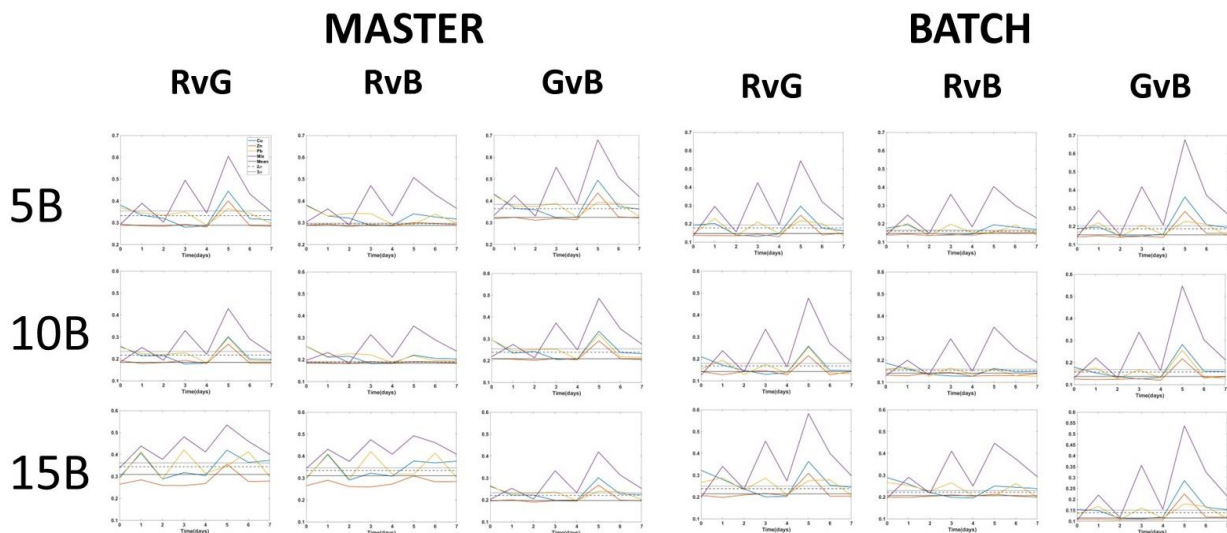


Figure A.15: Two-color DTW comparison of images of mosses collected using both lasers treated with metals to the control. Plots are first sorted vertically by gain (5, 10, and 15), then by analysis method (MMM - left or BMM – right), and finally by color (R,G,B). X-axis for all figures is in time (days) and the y-axis is the density difference between images of metal treated and control moss as determined by individual colors. Purple (metal mix), yellow (Pb), blue (Cu), and orange (Zn).

6.1.8 Tables associated with Figures in Main Text

Table A.4: Values for all trials calculated from using the Density Difference batch method of comparison to the control for single color analysis. Shaded cells represent those that deviate from the 3σ interval for the control trial.

day	Copper			Zinc			Lead			Mix		
	red	green	blue	red	green	blue	red	green	blue	red	green	blue
0.0	0.154	0.134	0.084	0.107	0.110	0.163	0.147	0.106	0.081	0.149	0.136	0.104
1.0	0.285	0.294	0.272	0.125	0.171	0.226	0.271	0.303	0.250	0.328	0.388	0.307
1.5	0.285	0.294	0.272	0.110	0.152	0.216	0.156	0.094	0.081	0.134	0.177	0.142
2.0	0.131	0.120	0.103	0.106	0.134	0.184	0.136	0.104	0.088	0.210	0.262	0.199
2.5	0.131	0.120	0.103	0.115	0.149	0.210	0.206	0.232	0.213	0.299	0.353	0.294
3.0	0.146	0.205	0.235	0.114	0.124	0.176	0.298	0.341	0.301	0.427	0.517	0.448
3.5	0.146	0.205	0.235	0.120	0.170	0.233	0.211	0.245	0.217	0.356	0.419	0.361
4.0	0.118	0.164	0.197	0.111	0.156	0.214	0.130	0.182	0.178	0.264	0.339	0.290
4.5	0.118	0.164	0.197	0.148	0.218	0.275	0.148	0.201	0.192	0.259	0.337	0.297
5.0	0.209	0.307	0.328	0.133	0.206	0.258	0.272	0.331	0.306	0.445	0.574	0.518
5.5	0.209	0.307	0.328	0.126	0.188	0.250	0.125	0.160	0.178	0.339	0.461	0.424
6.0	0.192	0.273	0.288	0.113	0.165	0.230	0.147	0.180	0.197	0.356	0.471	0.433
6.5	0.192	0.273	0.288	0.120	0.182	0.245	0.152	0.157	0.180	0.272	0.364	0.360
7.0	0.194	0.265	0.278	0.107	0.170	0.218	0.127	0.139	0.161	0.254	0.346	0.357
day	Nutrients			Over Wetting			Drought			Control		
	red	green	blue	red	green	blue	red	green	blue	red	green	blue
0.0	0.144	0.179	0.227	0.158	0.181	0.201	0.118	0.195	0.213	0.127	0.128	0.141
1.0	0.186	0.227	0.276	0.158	0.181	0.201	0.118	0.195	0.213	0.127	0.128	0.141
1.5	0.151	0.192	0.250	0.162	0.188	0.228	0.123	0.190	0.220	0.140	0.139	0.159
2.0	0.134	0.166	0.236	0.170	0.189	0.223	0.104	0.142	0.171	0.141	0.140	0.142
2.5	0.167	0.200	0.269	0.201	0.223	0.247	0.115	0.175	0.202	0.182	0.168	0.177
3.0	0.164	0.199	0.267	0.173	0.206	0.231	0.111	0.145	0.174	0.151	0.155	0.162
3.5	0.166	0.210	0.275	0.205	0.239	0.271	0.109	0.157	0.195	0.168	0.160	0.162
4.0	0.158	0.200	0.271	0.182	0.222	0.251	0.105	0.122	0.147	0.146	0.154	0.164
4.5	0.232	0.290	0.337	0.192	0.237	0.286	0.112	0.162	0.204	0.140	0.154	0.175
5.0	0.205	0.247	0.307	0.177	0.222	0.266	0.104	0.124	0.165	0.161	0.166	0.164

5.5	0.209	0.277	0.322	0.219	0.262	0.303	0.127	0.142	0.204	0.179	0.186	0.185	
6.0	0.163	0.209	0.277	0.195	0.243	0.279	0.133	0.124	0.186	0.148	0.161	0.176	
6.5	0.202	0.260	0.308	0.191	0.243	0.283	0.200	0.171	0.261	0.127	0.147	0.176	
7.0	0.183	0.240	0.287	0.206	0.261	0.291	0.239	0.177	0.286	0.138	0.147	0.166	
day	Long			Short			Dark						
	red	green	blue	red	green	blue	red	green	blue				
0.0	0.198	0.241	0.241	0.176	0.223	0.289	0.238	0.294	0.341				
1.0	0.198	0.241	0.241	0.176	0.223	0.289	0.238	0.294	0.341				
1.5	0.186	0.237	0.250	0.157	0.199	0.262	0.157	0.218	0.275				
2.0	0.244	0.271	0.255	0.180	0.227	0.282	0.218	0.271	0.327				
2.5	0.250	0.272	0.249	0.178	0.217	0.271	0.156	0.223	0.266				
3.0	0.184	0.236	0.237	0.191	0.245	0.301	0.260	0.309	0.364				
3.5	0.237	0.265	0.250	0.182	0.223	0.281	0.170	0.235	0.290				
4.0	0.238	0.283	0.266	0.187	0.243	0.294	0.220	0.276	0.339				
4.5	0.196	0.261	0.263	0.190	0.241	0.294	0.186	0.258	0.306				
5.0	0.261	0.306	0.276	0.189	0.244	0.299	0.234	0.293	0.352				
5.5	0.273	0.304	0.272	0.197	0.242	0.294	0.163	0.232	0.293	mean	0.148	0.152	0.164
6.0	0.281	0.315	0.269	0.205	0.254	0.306	0.221	0.281	0.338	1 sig	0.167	0.168	0.178
6.5	0.304	0.328	0.274	0.255	0.295	0.331	0.141	0.208	0.267	2 sig	0.185	0.184	0.192
7.0	0.272	0.301	0.262	0.203	0.245	0.295	0.225	0.278	0.341	3sig	0.203	0.200	0.206

Table A.5: Welch's t-test applied to the density difference analysis values for images collected using both lasers at a gain of 10. Columns are separated into trial, then by color channel (red, green, blue). The left column shows the t-value for the trial while the right column shows the t-value for the control for each day. Cells shaded in grey represent t-values that exceed the critical t-value to be considered similar to the control.

day	Copper						Zinc						Lead						Mix					
	red		green		blue		red		green		blue		red		green		blue		red		green		blue	
0.0	1.06	1.73	0.23	1.74	3.34	1.75	1.03	1.78	0.82	1.74	0.82	1.74	0.99	1.77	1.03	1.74	1.03	1.74	0.99	1.75	0.45	1.77	0.45	1.77
1.0	6.44	1.73	6.78	1.73	6.84	1.74	0.11	1.75	2.07	1.74	2.07	1.74	5.39	1.73	7.80	1.74	7.80	1.74	8.01	1.73	12.23	1.74	12.23	1.74
1.5	4.79	1.75	6.11	1.73	6.61	1.73	1.08	1.77	0.55	1.74	0.55	1.74	0.58	1.78	2.05	1.75	2.05	1.75	0.21	1.74	1.58	1.74	1.58	1.74
2.0	0.44	1.76	0.86	1.75	1.94	1.74	1.56	1.77	0.20	1.74	0.20	1.74	0.26	1.79	1.52	1.75	1.52	1.75	2.47	1.73	4.95	1.74	4.95	1.74
2.5	1.80	1.78	2.08	1.75	3.65	1.74	2.32	1.77	0.77	1.74	0.77	1.74	0.71	1.74	2.42	1.74	2.42	1.74	3.60	1.74	7.81	1.75	7.81	1.75

3.0	0.15	1.75	1.81	1.73	3.64	1.74	1.41	1.78	1.22	1.74	1.22	1.74	4.97	1.74	7.63	1.74	7.63	1.74	10.13	1.76	16.48	1.77	16.48	1.77
3.5	0.75	1.75	1.83	1.74	3.83	1.74	1.81	1.77	0.43	1.73	0.43	1.73	1.32	1.73	3.38	1.74	3.38	1.74	6.55	1.75	12.50	1.73	12.50	1.73
4.0	1.03	1.76	0.41	1.73	1.88	1.75	1.32	1.77	0.07	1.74	0.07	1.74	0.49	1.73	1.03	1.74	1.03	1.74	4.06	1.75	7.96	1.74	7.96	1.74
4.5	0.96	1.75	0.44	1.74	1.48	1.74	0.30	1.75	3.32	1.74	3.32	1.74	0.33	1.74	2.12	1.74	2.12	1.74	4.25	1.73	8.03	1.74	8.03	1.74
5.0	1.49	1.74	5.38	1.73	8.69	1.74	0.97	1.75	1.72	1.74	1.72	1.74	3.45	1.74	6.27	1.74	6.27	1.74	9.62	1.74	17.17	1.74	17.17	1.74
5.5	0.88	1.74	4.86	1.74	7.57	1.74	1.70	1.75	0.10	1.73	0.10	1.73	1.79	1.76	1.10	1.73	1.10	1.73	5.69	1.79	14.02	1.74	14.02	1.74
6.0	1.40	1.74	3.59	1.74	5.46	1.74	1.29	1.77	0.19	1.75	0.19	1.75	0.01	1.76	0.75	1.73	0.75	1.73	6.87	1.74	11.98	1.73	11.98	1.73
6.5	2.48	1.74	4.39	1.77	5.69	1.74	0.33	1.73	1.62	1.74	1.62	1.74	1.15	1.74	0.48	1.74	0.48	1.74	6.92	1.74	11.61	1.73	11.61	1.73
7.0	1.83	1.73	3.56	1.73	4.67	1.75	1.24	1.77	0.88	1.76	0.88	1.76	0.39	1.74	0.26	1.74	0.26	1.74	3.81	1.73	6.09	1.73	6.09	1.73
	Nutrients						Over Wetting						Draught											
day	red		green		blue		red		green		blue		red		green		blue							
0.0	0.79	1.75	2.04	1.73	2.04	1.73	1.08	1.74	1.93	1.74	1.93	1.74	0.39	1.74	2.58	1.74	2.58	1.74						
1.0	1.95	1.74	3.24	1.75	3.24	1.75	1.08	1.74	1.93	1.74	1.93	1.74	0.39	1.74	2.58	1.74	2.58	1.74						
1.5	0.31	1.74	1.79	1.74	1.79	1.74	0.61	1.73	1.72	1.74	1.72	1.74	0.59	1.75	1.73	1.74	1.73	1.74						
2.0	0.27	1.74	0.98	1.73	0.98	1.73	0.92	1.74	1.70	1.74	1.70	1.74	1.63	1.77	0.07	1.73	0.07	1.73						
2.5	0.49	1.75	1.21	1.73	1.21	1.73	0.48	1.74	1.67	1.74	1.67	1.74	2.34	1.78	0.25	1.73	0.25	1.73						
3.0	0.40	1.74	1.43	1.74	1.43	1.74	0.70	1.74	1.85	1.73	1.85	1.73	1.47	1.77	0.32	1.74	0.32	1.74						
3.5	0.07	1.74	2.01	1.74	2.01	1.74	1.16	1.73	3.52	1.73	3.52	1.73	2.12	1.76	0.13	1.74	0.13	1.74						
4.0	0.37	1.73	1.59	1.74	1.59	1.74	1.03	1.73	2.71	1.73	2.71	1.73	1.52	1.77	1.24	1.73	1.24	1.73						
4.5	3.01	1.74	5.84	1.74	5.84	1.74	1.77	1.74	4.23	1.73	4.23	1.73	1.23	1.75	0.35	1.74	0.35	1.74						
5.0	1.30	1.73	2.73	1.74	2.73	1.74	0.43	1.74	1.95	1.74	1.95	1.74	2.24	1.78	1.77	1.74	1.77	1.74						
5.5	0.93	1.74	3.63	1.74	3.63	1.74	1.15	1.74	3.41	1.73	3.41	1.73	1.82	1.79	1.84	1.74	1.84	1.74						
6.0	0.45	1.73	1.64	1.74	1.64	1.74	1.32	1.73	3.12	1.73	3.12	1.73	0.58	1.79	1.78	1.76	1.78	1.76						
6.5	2.49	1.75	4.44	1.75	4.44	1.75	2.42	1.74	4.47	1.74	4.47	1.74	4.02	1.77	1.37	1.74	1.37	1.74						
7.0	1.60	1.74	2.76	1.73	2.76	1.73	2.05	1.73	3.91	1.74	3.91	1.74	3.73	1.75	1.22	1.78	1.22	1.78						
	Long						Short						Dark											
day	red		green		blue		red		green		blue		red		green		blue							
0.0	3.24	1.75	5.46	1.75	5.46	1.75	1.77	1.74	3.40	1.74	3.40	1.74	4.89	1.74	7.30	1.74	7.30	1.74						
1.0	3.24	1.75	5.46	1.75	5.46	1.75	1.77	1.74	3.40	1.74	3.40	1.74	4.89	1.74	7.30	1.74	7.30	1.74						
1.5	1.65	1.77	4.12	1.74	4.12	1.74	0.53	1.74	2.37	1.73	2.37	1.73	0.57	1.76	3.54	1.75	3.54	1.75						
2.0	3.84	1.74	5.35	1.74	5.35	1.74	1.48	1.74	3.83	1.75	3.83	1.75	3.57	1.79	5.86	1.75	5.86	1.75						
2.5	2.45	1.79	4.77	1.77	4.77	1.77	0.15	1.75	1.87	1.74	1.87	1.74	0.94	1.78	2.61	1.78	2.61	1.78						

3.0	1.20	1.76	3.46	1.75	3.46	1.75	1.27	1.74	3.19	1.73	3.19	1.73	4.35	1.80	6.58	1.75	6.58	1.75				
3.5	2.66	1.78	5.44	1.74	5.44	1.74	0.50	1.74	2.97	1.73	2.97	1.73	0.10	1.76	4.33	1.76	4.33	1.76				
4.0	3.12	1.74	5.20	1.73	5.20	1.73	1.30	1.74	3.41	1.73	3.41	1.73	2.93	1.79	5.56	1.75	5.56	1.75				
4.5	2.23	1.74	4.99	1.73	4.99	1.73	2.04	1.74	4.44	1.73	4.44	1.73	2.16	1.77	6.17	1.76	6.17	1.76				
5.0	3.54	1.75	6.09	1.74	6.09	1.74	1.00	1.76	3.62	1.75	3.62	1.75	2.77	1.78	5.24	1.73	5.24	1.73				
5.5	3.36	1.79	6.32	1.75	6.32	1.75	0.57	1.75	2.77	1.74	2.77	1.74	0.56	1.78	2.32	1.74	2.32	1.74				
6.0	5.10	1.78	7.38	1.76	7.38	1.76	1.64	1.73	3.22	1.74	3.22	1.74	2.76	1.78	5.47	1.75	5.47	1.75	mean	1.75	1.74	1.74
6.5	10.48	1.80	12.08	1.76	12.08	1.76	2.40	1.80	2.72	1.81	2.72	1.81	0.71	1.75	2.89	1.74	2.89	1.74	2 σ	1.79	1.77	1.76
7.0	5.19	1.76	6.15	1.77	6.15	1.77	2.38	1.75	3.71	1.76	3.71	1.76	3.73	1.81	5.20	1.77	5.20	1.77	3 σ	1.81	1.74	1.77

Table A.6: Values for all trials calculated from using the DTW batch method of comparison to the control for two color analysis. Shaded cells represent those that deviate from the 3σ interval for the control trial.

day	Copper			Zinc			Lead			Mix		
	rvg	rvb	gvb	rvg	rvb	gvb	rvg	rvb	gvb	rvg	rvb	gvb
0	0.192	0.176	0.189	0.138	0.138	0.141	0.145	0.159	0.165	0.134	0.139	0.141
1	0.202	0.195	0.196	0.136	0.143	0.148	0.229	0.202	0.219	0.295	0.248	0.288
1.5	0.160	0.153	0.163	0.140	0.153	0.156	0.142	0.146	0.154	0.150	0.146	0.157
2	0.139	0.137	0.148	0.134	0.136	0.140	0.134	0.134	0.143	0.155	0.147	0.152
2.5	0.138	0.140	0.150	0.132	0.140	0.145	0.154	0.152	0.155	0.221	0.193	0.211
3	0.131	0.139	0.146	0.142	0.142	0.146	0.209	0.198	0.206	0.425	0.361	0.418
3.5	0.150	0.160	0.173	0.140	0.151	0.160	0.162	0.155	0.162	0.296	0.261	0.285
4	0.145	0.143	0.158	0.130	0.137	0.140	0.147	0.151	0.154	0.195	0.183	0.206
4.5	0.159	0.157	0.166	0.144	0.160	0.169	0.141	0.141	0.146	0.199	0.186	0.211
5	0.181	0.194	0.222	0.142	0.156	0.169	0.147	0.151	0.154	0.447	0.404	0.498
5.5	0.169	0.182	0.208	0.145	0.155	0.166	0.142	0.141	0.148	0.320	0.303	0.373
6	0.177	0.181	0.209	0.140	0.151	0.162	0.201	0.194	0.211	0.320	0.301	0.370
6.5	0.177	0.181	0.217	0.136	0.150	0.157	0.150	0.158	0.164	0.249	0.259	0.303
7	0.162	0.169	0.193	0.149	0.155	0.163	0.136	0.139	0.146	0.224	0.232	0.266
day	Nutrients			Over Wetting			Drought			Control		
	rvg	rvb	gvb	rvg	rvb	gvb	rvg	rvb	gvb	rvg	rvb	gvb
0	0.148	0.149	0.158	0.149	0.146	0.151	0.144	0.146	0.148	0.133	0.142	0.143

1	0.154	0.165	0.163	0.149	0.146	0.151	0.144	0.146	0.148	0.133	0.142	0.143	
1.5	0.145	0.156	0.163	0.150	0.155	0.156	0.143	0.145	0.158	0.128	0.130	0.130	
2	0.156	0.157	0.170	0.165	0.171	0.172	0.148	0.145	0.152	0.150	0.150	0.149	
2.5	0.144	0.168	0.170	0.172	0.177	0.180	0.139	0.141	0.146	0.126	0.136	0.133	
3	0.152	0.170	0.167	0.147	0.151	0.156	0.150	0.149	0.151	0.146	0.156	0.151	
3.5	0.144	0.162	0.167	0.150	0.158	0.161	0.141	0.140	0.145	0.130	0.139	0.138	
4	0.152	0.175	0.209	0.144	0.150	0.154	0.145	0.142	0.138	0.142	0.153	0.150	
4.5	0.176	0.199	0.209	0.151	0.167	0.165	0.131	0.135	0.141	0.138	0.142	0.139	
5	0.161	0.182	0.204	0.155	0.167	0.172	0.166	0.160	0.161	0.135	0.143	0.138	
5.5	0.171	0.187	0.204	0.172	0.199	0.210	0.143	0.135	0.147	0.157	0.156	0.155	
6	0.152	0.173	0.188	0.160	0.170	0.176	0.155	0.135	0.155	0.139	0.146	0.146	
6.5	0.159	0.178	0.188	0.157	0.168	0.177	0.141	0.145	0.150	0.136	0.141	0.142	
7	0.154	0.170	0.187	0.157	0.172	0.178	0.161	0.182	0.170	0.149	0.152	0.149	
day	Long			Short			Dark						
	rvg	rvb	gvb	rvg	rvb	gvb	rvg	rvb	gvb				
0	0.162	0.164	0.172	0.153	0.168	0.172	0.160	0.183	0.194				
1	0.162	0.164	0.172	0.153	0.168	0.172	0.160	0.183	0.194				
1.5	0.149	0.151	0.163	0.150	0.161	0.163	0.160	0.157	0.160				
2	0.184	0.181	0.187	0.150	0.167	0.172	0.142	0.168	0.179				
2.5	0.181	0.174	0.179	0.144	0.157	0.162	0.142	0.173	0.181				
3	0.149	0.151	0.159	0.158	0.176	0.183	0.174	0.201	0.210				
3.5	0.188	0.182	0.190	0.142	0.155	0.161	0.174	0.158	0.165				
4	0.167	0.162	0.173	0.155	0.172	0.181	0.147	0.178	0.188				
4.5	0.157	0.155	0.169	0.143	0.162	0.173	0.147	0.163	0.171				
5	0.204	0.194	0.211	0.140	0.158	0.166	0.156	0.186	0.198		RVG	RVB	GVB
5.5	0.195	0.184	0.197	0.147	0.167	0.175	0.156	0.166	0.174	mean	0.139	0.145	0.143
6	0.202	0.185	0.197	0.176	0.196	0.203	0.151	0.179	0.192	1 sig	0.148	0.153	0.151
6.5	0.206	0.183	0.194	0.157	0.170	0.179	0.151	0.147	0.150	2 sig	0.157	0.160	0.158
7	0.186	0.176	0.185	0.145	0.159	0.165	0.150	0.185	0.191	3sig	0.166	0.168	0.165

Table A.7: Welch's *t*-test applied to the DTW analysis values for images collected using both lasers at a gain of 5. Columns are separated into trial, then by color channel (red, green, blue). The left column shows the *t*-value for the trial while the right column shows the *t*-value for the control for each day. Cells shaded in grey represent *t*-values that exceed the critical *t*-value to be considered similar to the control.

day	Copper						Zinc						Lead						Mix					
	rvg		rvb		gvb		rvg		rvb		gvb		rvg		rvb		gvb		rvg		rvb		gvb	
0.0	1.55	1.76	0.96	1.76	1.21	1.75	0.17	1.74	0.15	1.73	0.09	1.73	0.38	1.74	0.50	1.75	0.62	1.75	0.02	1.73	0.13	1.73	0.08	1.73
1.0	2.06	1.75	1.79	1.74	1.67	1.74	0.10	1.73	0.06	1.74	0.19	1.74	2.57	1.76	1.87	1.75	2.17	1.75	3.66	1.77	2.91	1.76	3.47	1.76
1.5	1.07	1.74	0.81	1.74	1.14	1.73	0.50	1.73	0.95	1.74	0.99	1.74	0.47	1.74	0.52	1.74	0.77	1.74	0.84	1.73	0.63	1.73	1.04	1.74
2.0	0.35	1.74	0.46	1.73	0.05	1.73	0.55	1.73	0.52	1.73	0.32	1.74	0.56	1.73	0.55	1.73	0.20	1.73	0.19	1.74	0.12	1.74	0.10	1.73
2.5	0.47	1.73	0.17	1.73	0.67	1.74	0.21	1.73	0.20	1.73	0.49	1.73	1.04	1.73	0.68	1.73	0.84	1.73	2.71	1.76	2.04	1.74	2.37	1.75
3.0	0.52	1.74	0.63	1.74	0.15	1.74	0.13	1.73	0.50	1.74	0.18	1.74	1.82	1.74	1.36	1.73	1.63	1.73	5.35	1.78	4.42	1.77	5.11	1.77
3.5	0.85	1.73	0.92	1.73	1.35	1.73	0.44	1.74	0.52	1.73	0.86	1.73	1.19	1.74	0.69	1.73	0.93	1.73	3.87	1.77	3.43	1.76	3.69	1.77
4.0	0.14	1.73	0.38	1.73	0.31	1.74	0.43	1.74	0.63	1.73	0.39	1.74	0.20	1.73	0.07	1.74	0.16	1.74	1.61	1.75	1.12	1.74	1.73	1.74
4.5	0.83	1.74	0.63	1.74	1.08	1.74	0.21	1.74	0.75	1.74	1.11	1.73	0.11	1.74	0.03	1.74	0.27	1.74	1.90	1.74	1.66	1.73	2.31	1.74
5.0	1.72	1.73	2.03	1.73	2.56	1.74	0.29	1.74	0.57	1.74	1.09	1.74	0.47	1.73	0.35	1.73	0.60	1.74	6.20	1.79	5.64	1.78	6.67	1.78
5.5	0.45	1.74	1.00	1.74	1.74	1.75	0.53	1.73	0.07	1.73	0.45	1.73	0.58	1.74	0.65	1.74	0.25	1.73	3.69	1.78	3.82	1.78	4.70	1.78
6.0	1.36	1.73	1.37	1.73	2.07	1.74	0.02	1.74	0.23	1.74	0.61	1.73	1.82	1.75	1.62	1.74	1.94	1.75	4.11	1.77	3.99	1.77	4.88	1.78
6.5	1.53	1.73	1.63	1.73	2.23	1.74	0.01	1.74	0.37	1.74	0.54	1.74	0.50	1.74	0.62	1.74	0.77	1.74	2.88	1.75	3.25	1.75	3.75	1.76
7.0	0.45	1.73	0.64	1.73	1.45	1.74	0.03	1.73	0.12	1.74	0.52	1.73	0.48	1.73	0.53	1.74	0.14	1.73	2.15	1.75	2.45	1.74	3.13	1.76
day	Nutrients						Over Wetting						Draught											
	rvg		rvb		gvb		rvg		rvb		gvb		rvg		rvb		gvb							
0.0	0.58	1.73	0.30	1.74	0.60	1.74	0.65	1.74	0.17	1.74	0.29	1.74	0.42	1.73	0.17	1.73	0.18	1.74						
1.0	0.83	1.74	0.95	1.73	0.78	1.74	0.65	1.74	0.17	1.74	0.29	1.74	0.42	1.73	0.17	1.73	0.18	1.74						
1.5	0.73	1.74	1.11	1.74	1.33	1.74	0.94	1.74	1.05	1.74	1.05	1.74	0.61	1.74	0.63	1.74	1.06	1.74						
2.0	0.23	1.74	0.30	1.74	0.76	1.74	0.60	1.74	0.83	1.74	0.84	1.74	0.05	1.73	0.19	1.73	0.10	1.74						
2.5	0.74	1.74	1.43	1.74	1.46	1.74	1.84	1.73	1.70	1.73	1.80	1.73	0.49	1.73	0.21	1.73	0.50	1.74						
3.0	0.25	1.74	0.52	1.74	0.56	1.74	0.06	1.74	0.20	1.74	0.17	1.74	0.13	1.73	0.25	1.74	0.01	1.74						
3.5	0.60	1.74	1.03	1.73	1.15	1.73	0.83	1.74	0.84	1.73	0.94	1.73	0.41	1.73	0.06	1.73	0.27	1.73						
4.0	0.42	1.74	0.94	1.74	1.91	1.74	0.08	1.74	0.10	1.74	0.15	1.74	0.11	1.74	0.37	1.74	0.44	1.73						
4.5	1.35	1.73	2.09	1.73	2.28	1.74	0.50	1.74	1.05	1.74	0.98	1.74	0.26	1.73	0.29	1.73	0.06	1.74						
5.0	1.07	1.74	1.57	1.73	2.15	1.73	0.83	1.74	0.99	1.73	1.23	1.74	0.98	1.74	0.60	1.74	0.75	1.73						

Table A.8: Ratio values plotted in Figures 8 and 9 calculated from density difference analysis of images collected using both lasers at a gain of 10. Shaded cells represent values that exceed the 3σ confidence interval for the control and therefore are statistically different.

day	Copper			Zinc			Lead			Mix		
	red	green	blue	red	green	blue	red	green	blue	red	green	blue
0	0.415	0.359	0.226	0.281	0.289	0.430	0.440	0.317	0.242	0.382	0.351	0.267
1	0.335	0.345	0.320	0.239	0.329	0.432	0.329	0.368	0.303	0.320	0.380	0.300
1.5	0.335	0.345	0.320	0.230	0.318	0.452	0.472	0.284	0.244	0.296	0.390	0.314
2	0.370	0.338	0.292	0.250	0.316	0.434	0.414	0.318	0.268	0.313	0.391	0.297
2.5	0.370	0.338	0.292	0.242	0.315	0.443	0.316	0.357	0.327	0.316	0.373	0.310
3	0.249	0.349	0.401	0.275	0.300	0.425	0.317	0.363	0.321	0.307	0.372	0.322
3.5	0.249	0.349	0.401	0.229	0.325	0.446	0.314	0.364	0.322	0.314	0.369	0.318
4	0.246	0.342	0.411	0.231	0.323	0.445	0.266	0.372	0.362	0.295	0.380	0.325
4.5	0.246	0.342	0.411	0.230	0.341	0.429	0.274	0.371	0.355	0.290	0.378	0.332
5	0.247	0.364	0.389	0.223	0.345	0.432	0.299	0.364	0.337	0.289	0.374	0.337
5.5	0.247	0.364	0.389	0.224	0.333	0.443	0.270	0.346	0.384	0.277	0.377	0.346
6	0.255	0.363	0.382	0.223	0.325	0.452	0.281	0.343	0.376	0.282	0.374	0.344
6.5	0.255	0.363	0.382	0.219	0.334	0.447	0.310	0.322	0.368	0.273	0.365	0.362
7	0.263	0.360	0.377	0.216	0.343	0.440	0.296	0.326	0.377	0.265	0.361	0.373
	Nutrients			Over Wetting			Drought			Control		
day	red	green	blue	red	green	blue	red	green	blue	red	green	blue
0	0.262	0.325	0.413	0.293	0.335	0.372	0.224	0.372	0.404	0.321	0.323	0.357
1	0.270	0.330	0.400	0.293	0.335	0.372	0.224	0.372	0.404	0.321	0.323	0.357
1.5	0.254	0.324	0.421	0.280	0.325	0.395	0.230	0.357	0.413	0.320	0.317	0.363
2	0.250	0.310	0.440	0.291	0.325	0.384	0.250	0.340	0.410	0.334	0.330	0.335
2.5	0.263	0.315	0.422	0.300	0.332	0.369	0.234	0.356	0.410	0.345	0.319	0.336
3	0.260	0.316	0.425	0.284	0.337	0.379	0.259	0.337	0.404	0.322	0.332	0.346
3.5	0.255	0.323	0.422	0.287	0.334	0.379	0.236	0.341	0.423	0.342	0.327	0.331
4	0.251	0.318	0.430	0.278	0.339	0.383	0.281	0.325	0.394	0.315	0.332	0.354
4.5	0.270	0.338	0.392	0.269	0.332	0.399	0.235	0.339	0.427	0.299	0.328	0.373
5	0.270	0.325	0.405	0.266	0.334	0.400	0.264	0.316	0.420	0.328	0.338	0.334
5.5	0.259	0.343	0.398	0.279	0.334	0.387	0.270	0.300	0.431	0.325	0.338	0.337

6	0.251	0.323	0.426	0.272	0.339	0.389	0.300	0.280	0.420	0.305	0.332	0.363	
6.5	0.263	0.338	0.400	0.266	0.339	0.395	0.316	0.271	0.413	0.283	0.327	0.390	
7	0.258	0.338	0.405	0.272	0.344	0.384	0.340	0.252	0.408	0.306	0.326	0.368	
day	red	Long green	blue	red	Short green	blue	red	Dark green	blue				
0	0.291	0.354	0.354	0.256	0.325	0.420	0.272	0.336	0.391				
1	0.291	0.354	0.354	0.256	0.325	0.420	0.272	0.336	0.391				
1.5	0.277	0.352	0.371	0.254	0.322	0.423	0.241	0.336	0.423				
2	0.317	0.352	0.331	0.261	0.330	0.409	0.267	0.332	0.401				
2.5	0.324	0.353	0.323	0.267	0.326	0.407	0.241	0.346	0.413				
3	0.280	0.360	0.361	0.260	0.332	0.408	0.278	0.331	0.391				
3.5	0.314	0.352	0.333	0.265	0.325	0.409	0.245	0.338	0.417				
4	0.303	0.359	0.338	0.259	0.336	0.406	0.264	0.330	0.406				
4.5	0.272	0.363	0.366	0.262	0.333	0.405	0.248	0.344	0.408				
5	0.310	0.363	0.328	0.258	0.333	0.409	0.266	0.333	0.401				
5.5	0.322	0.358	0.320	0.269	0.330	0.402	0.237	0.337	0.426				
6	0.324	0.365	0.311	0.268	0.332	0.400	0.263	0.334	0.403	mean	red	green	blue
6.5	0.335	0.362	0.303	0.289	0.335	0.376	0.229	0.338	0.433	2 sig	0.319	0.328	0.353
7	0.326	0.360	0.314	0.273	0.329	0.397	0.267	0.330	0.404	3 sig	0.351	0.340	0.386
											0.367	0.346	0.403

6.2 APPENDIX B

6.2.1 Image Analysis Results for all laser wavelengths and comparison methods

6.2.1.1 CoCoBi Single and Dual Laser

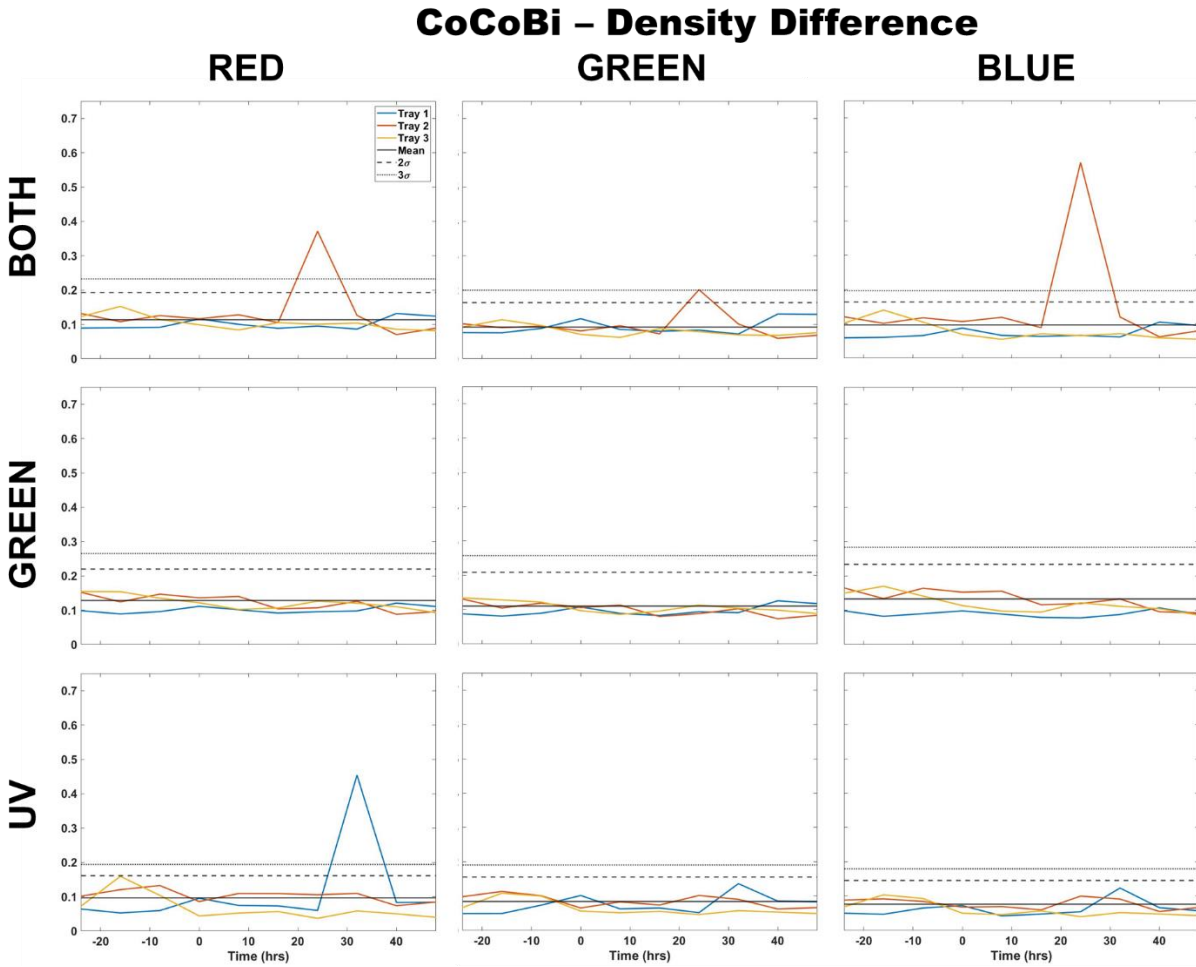


Figure B.1: Comparison of moss response to all lasers of the CoCoBi using single-color density difference image analysis. Images were collected every 8 hours over three days. Control images were collected for the first 24 hours. At time 0 three Cu treatments were given at 1 nmol/cm² for Tray 1 (blue), 10 nmol/cm² for Tray 2 (red), and 100 nmol/cm² for Tray 3 (yellow).

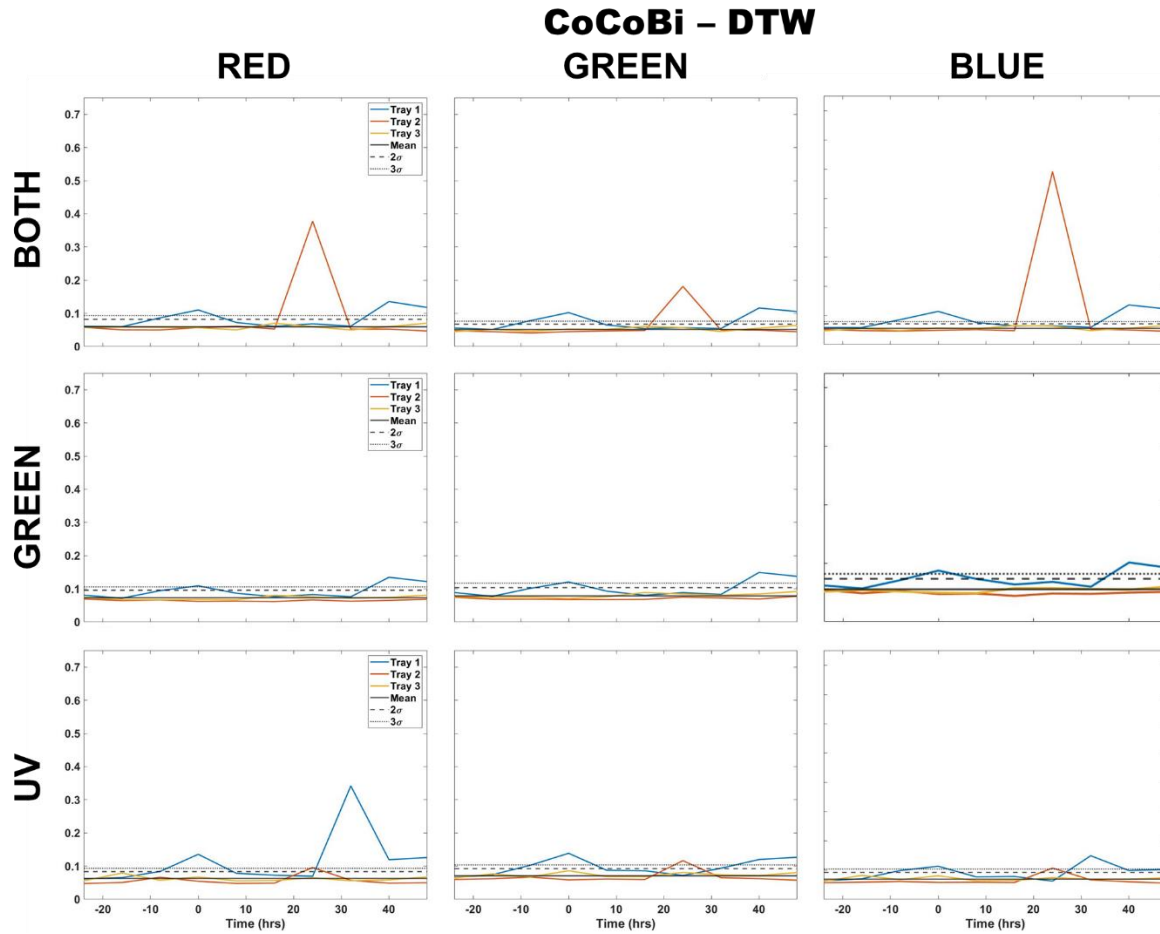


Figure B.2: Comparison of moss response to all lasers of the CoCoBi using single-color DTW image analysis. Images were collected every 8 hours over three days. Control images were collected for the first 24 hours. At time 0 three Cu treatments were given at 1 nmol/cm^2 for Tray 1 (blue), 10 nmol/cm^2 for Tray 2 (red), and 100 nmol/cm^2 for Tray 3 (yellow).

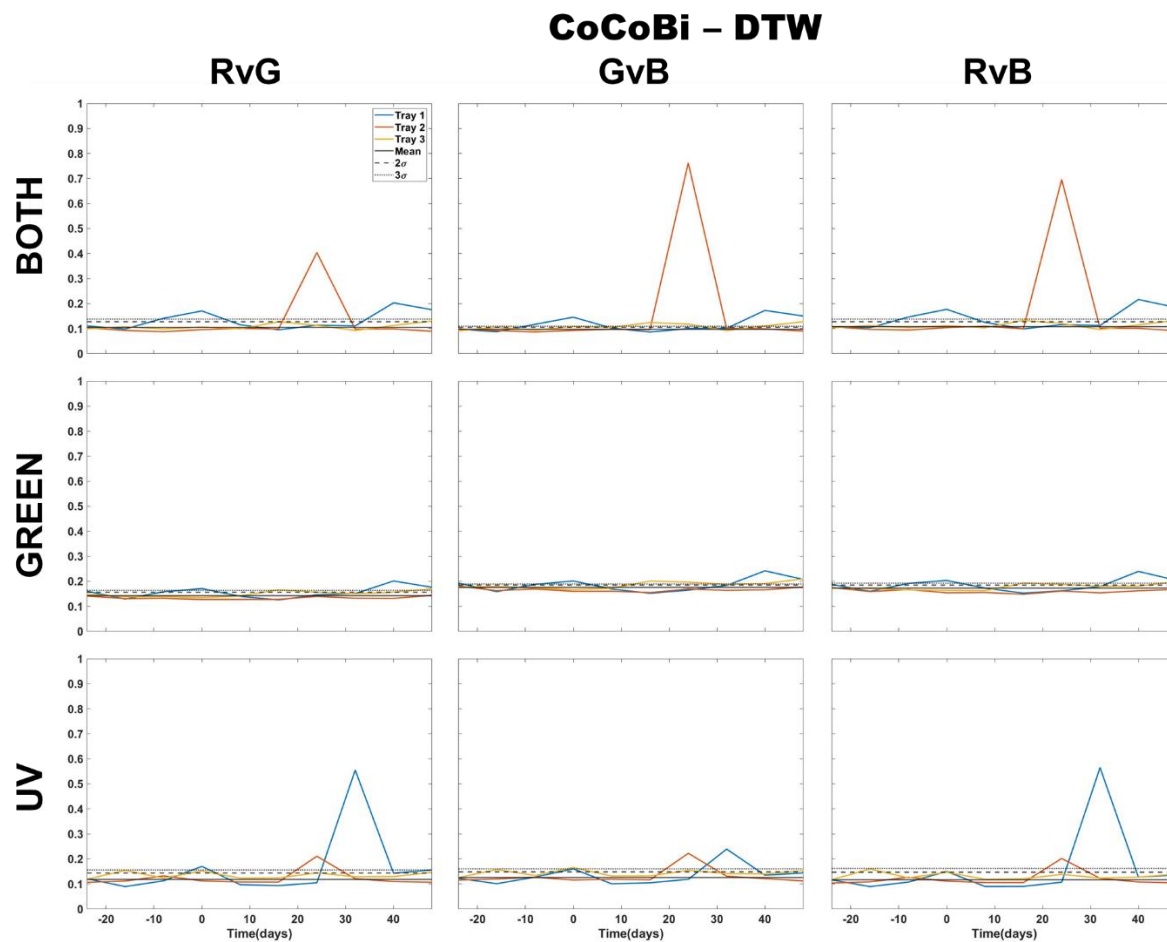


Figure B.3: Comparison of moss response to all lasers of the CoCoBi using two-color DTW image analysis. Images were collected every 8 hours over three days. Control images were collected for the first 24 hours. At time 0 three Cu treatments were given at 1 nmol/cm^2 for Tray 1 (blue), 10 nmol/cm^2 for Tray 2 (red), and 100 nmol/cm^2 for Tray 3 (yellow).

6.2.1.2 Chl-A Laser Results with and without filters

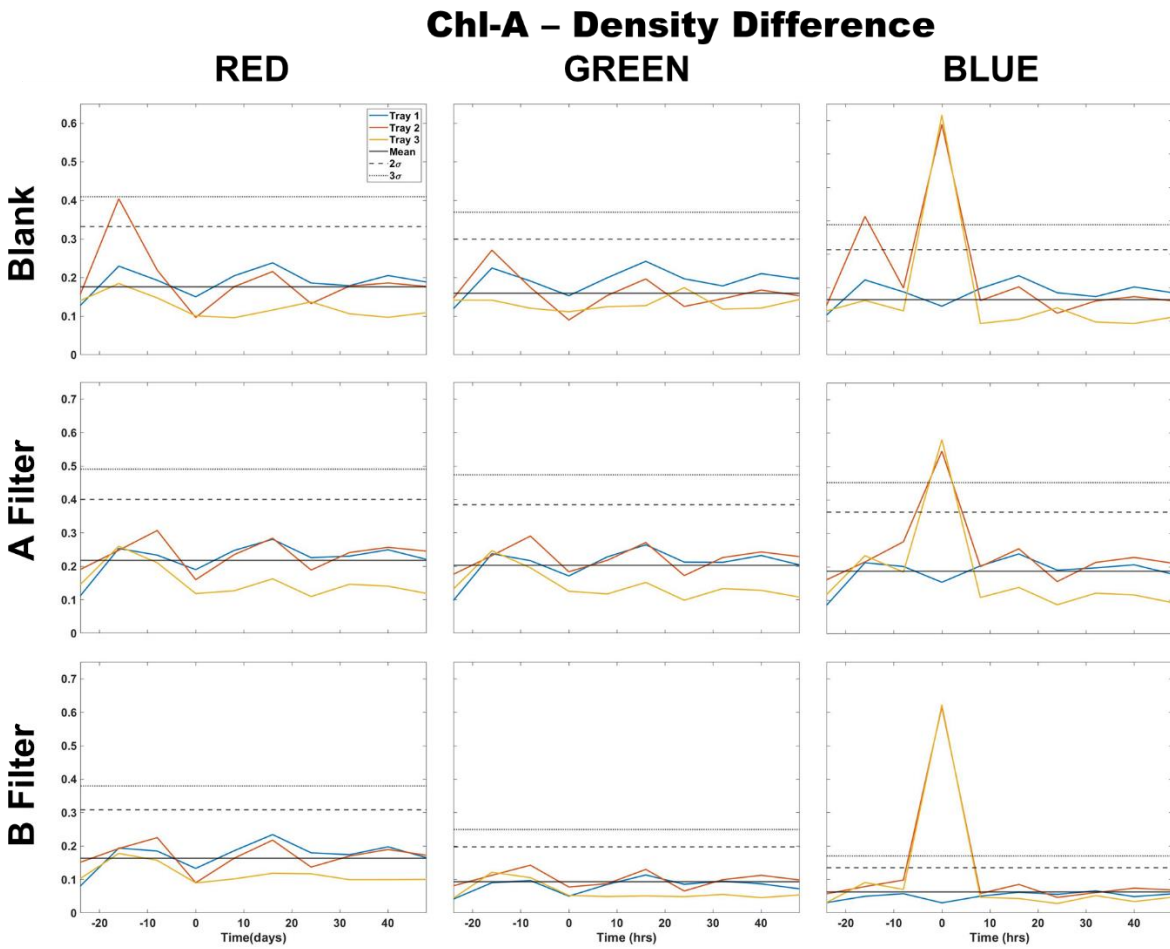


Figure B.4: Comparison of moss response to all filter options on the Chl-A laser using single-color density difference image analysis. Images were collected every 8 hours over three days. Control images were collected for the first 24 hours. At time 0 three Cu treatments were given at 1 nmol/cm² for Tray 1 (blue), 10 nmol/cm² for Tray 2 (red), and 100 nmol/cm² for Tray 3 (yellow).

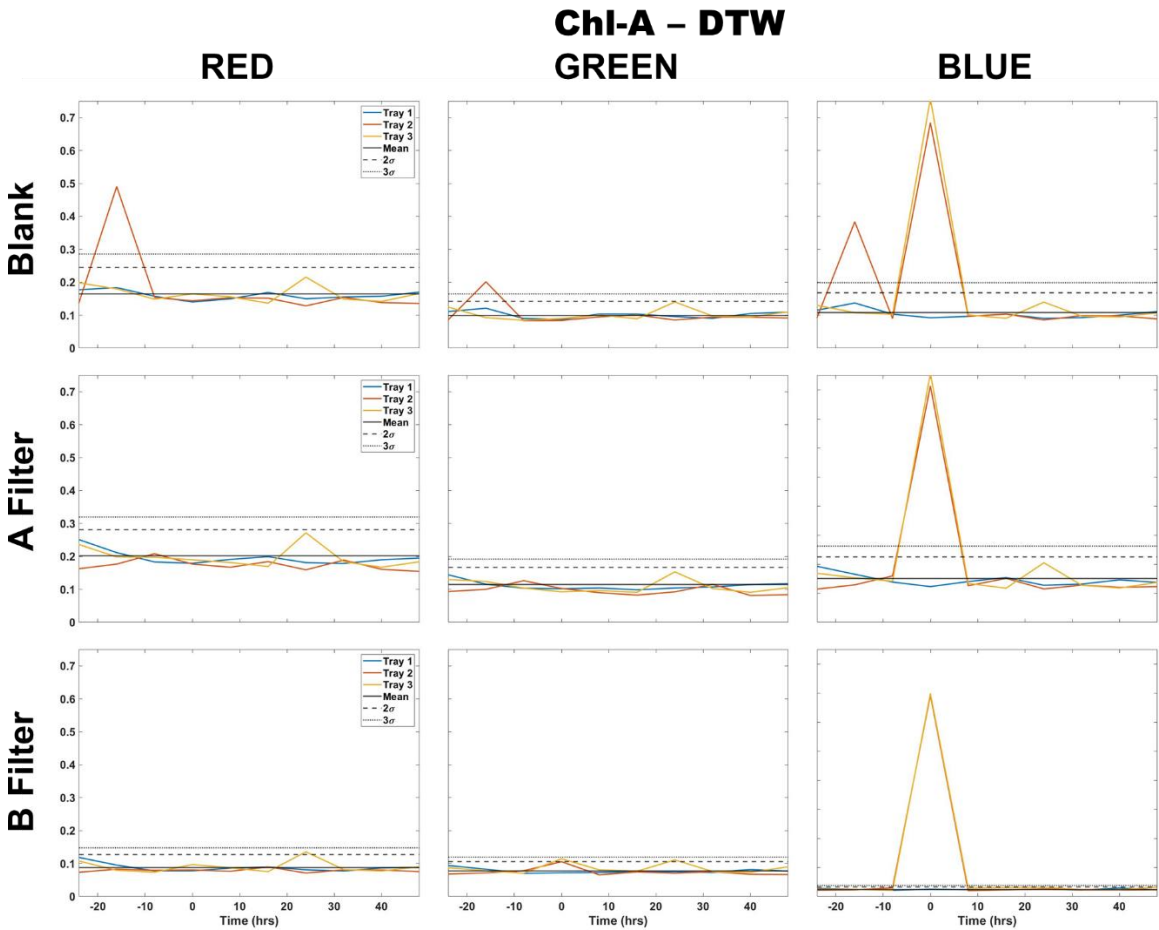


Figure B.5: Comparison of moss response to all filter options on the Chl-A laser using single-color DTW image analysis. Images were collected every 8 hours over three days. Control images were collected for the first 24 hours. At time 0 three Cu treatments were given at 1 nmol/cm² for Tray 1 (blue), 10 nmol/cm² for Tray 2 (red), and 100 nmol/cm² for Tray 3 (yellow).

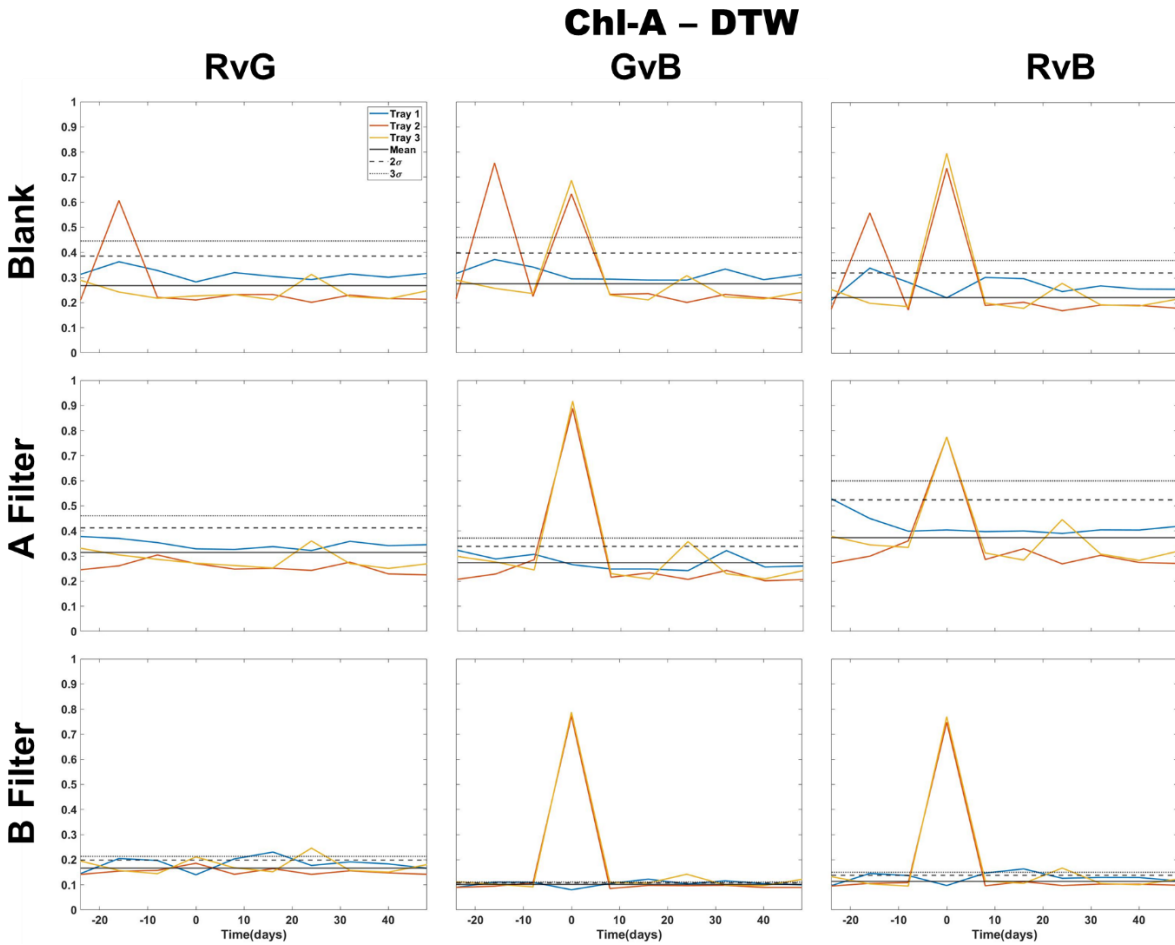


Figure B.6: Comparison of moss response to all filter options on the Chl-A laser using two-color DTW image analysis. Images were collected every 8 hours over three days. Control images were collected for the first 24 hours. At time 0 three Cu treatments were given at 1 nmol/cm² for Tray 1 (blue), 10 nmol/cm² for Tray 2 (red), and 100 nmol/cm² for Tray 3 (yellow).

6.2.1.3 Chl-B Laser Results with and without a filter

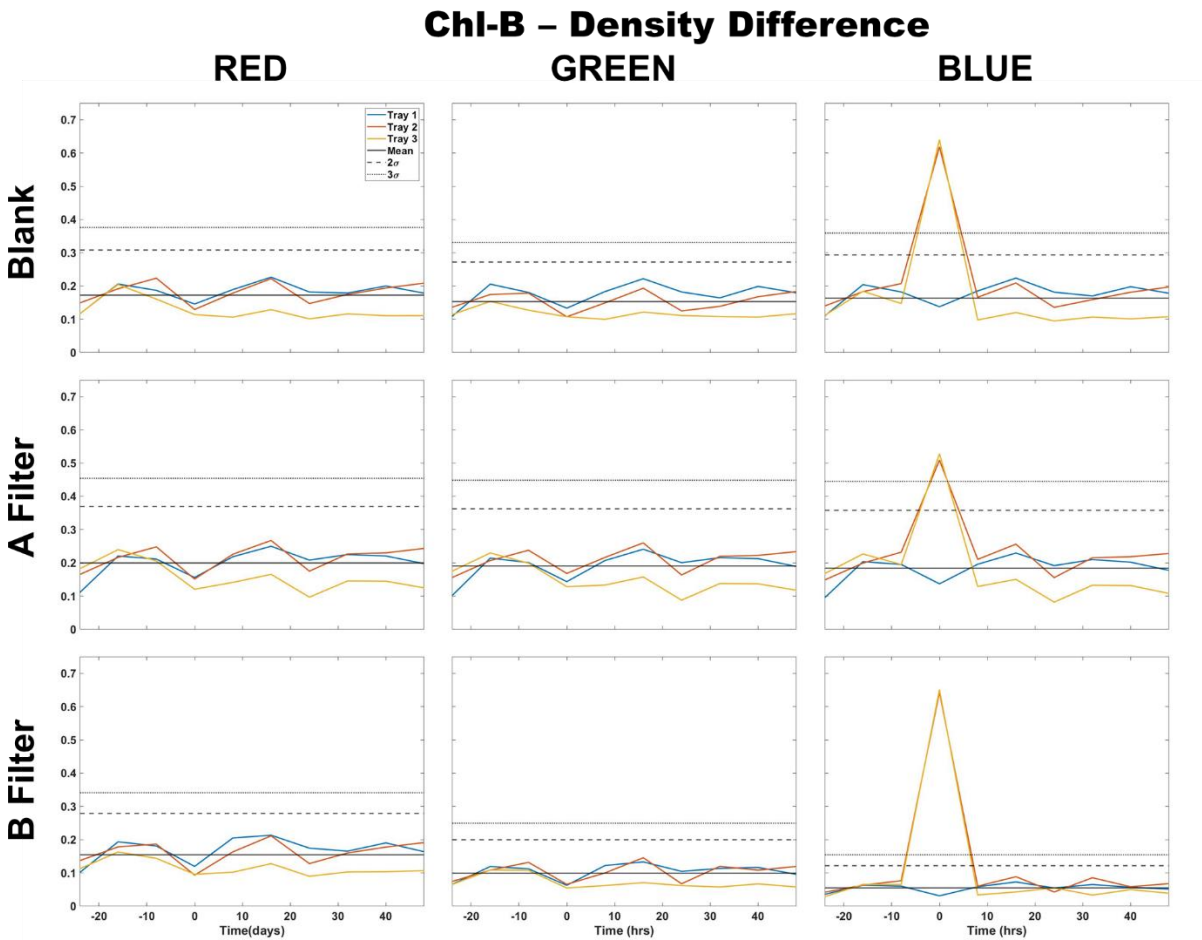


Figure B.7: Comparison of moss response to all filter options on the Chl-B laser using single-color density difference image analysis. Images were collected every 8 hours over three days. Control images were collected for the first 24 hours. At time 0 three Cu treatments were given at 1 nmol/cm² for Tray 1 (blue), 10 nmol/cm² for Tray 2 (red), and 100 nmol/cm² for Tray 3 (yellow).

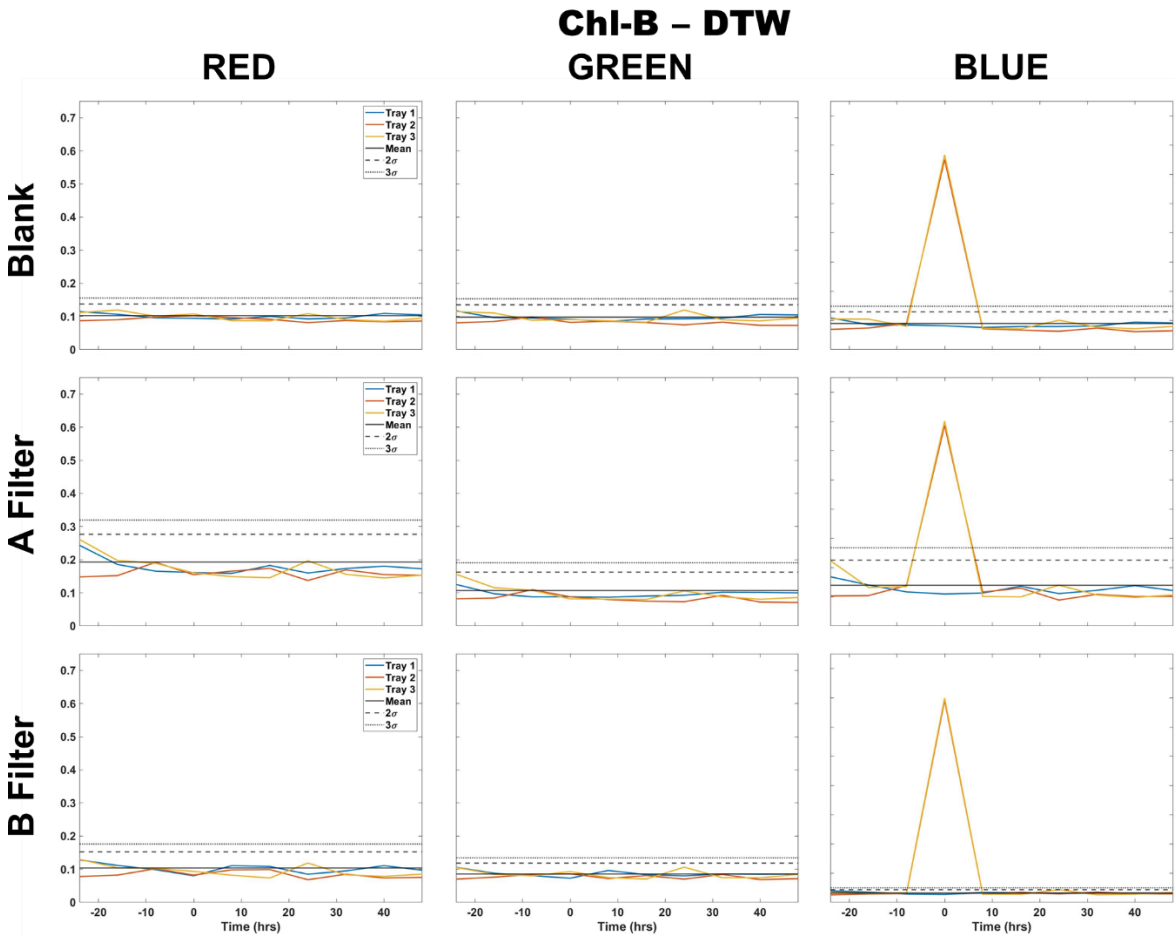


Figure B.8: Comparison of moss response to all filter options on the Chl-B laser using single-color DTW image analysis. Images were collected every 8 hours over three days. Control images were collected for the first 24 hours. At time 0 three Cu treatments were given at 1 nmol/cm^2 for Tray 1 (blue), 10 nmol/cm^2 for Tray 2 (red), and 100 nmol/cm^2 for Tray 3 (yellow).

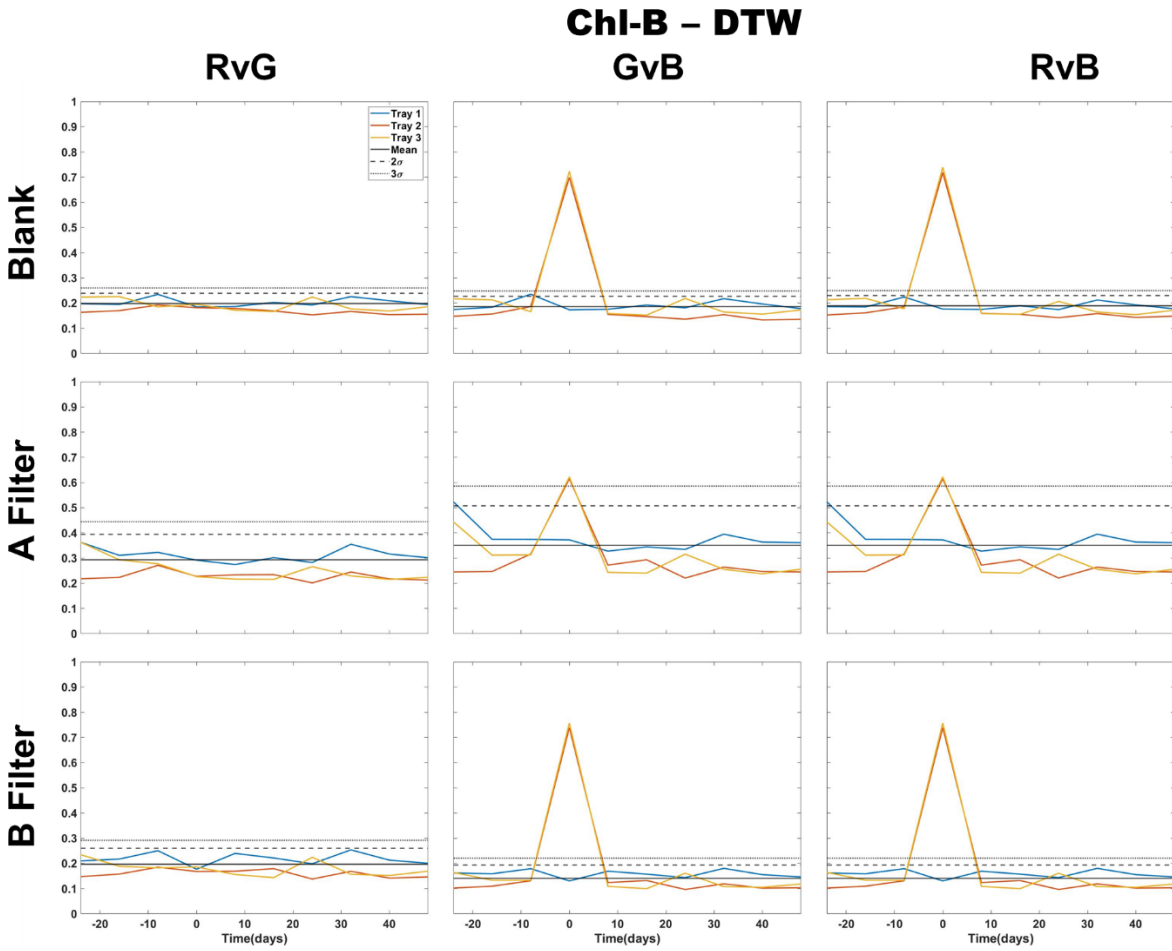


Figure B.9: Comparison of moss response to all filter options on the Chl-B laser using two-color DTW image analysis. Images were collected every 8 hours over three days. Control images were collected for the first 24 hours. At time 0 three Cu treatments were given at 1 nmol/cm² for Tray 1 (blue), 10 nmol/cm² for Tray 2 (red), and 100 nmol/cm² for Tray 3 (yellow).

6.2.2 Tables corresponding to Appendix 6.2.1 Figures

6.2.2.1 CoCoBi Comparison Results

Table B.1: Comparison of moss response to all lasers of the CoCoBi using single-color density difference image analysis. Images were collected every 8 hours over three days. Control images were collected for the first 24 hours. At time 0 three Cu treatments were given at 1 nmol/cm² for Tray 1, 10 nmol/cm² for Tray 2, and 100 nmol/cm² for Tray 3. Light gray shading indicates a 2 sigma deviation from the control. Dark gray shading indicates a 3 sigma deviation from the control.

CoCoBi Density Difference Results - Both Lasers												
Time (hrs)	Tray 1			Tray 2			Tray 3			Red	Green	Blue
	Red	Green	Blue	Red	Green	Blue	Red	Green	Blue			
-24	0.089	0.076	0.059	0.132	0.102	0.120	0.123	0.092	0.102	Mean		
-16	0.090	0.076	0.060	0.108	0.091	0.101	0.152	0.114	0.140	0.112	0.092	0.093
-8	0.092	0.088	0.066	0.126	0.095	0.118	0.114	0.097	0.105			
0	0.116	0.117	0.087	0.117	0.081	0.106	0.099	0.071	0.069	2 Sigma		
8	0.100	0.085	0.066	0.128	0.096	0.119	0.084	0.062	0.055	0.153	0.114	0.147
16	0.089	0.080	0.063	0.105	0.072	0.089	0.105	0.088	0.071			
24	0.095	0.083	0.066	0.371	0.201	0.570	0.101	0.079	0.065	3 Sigma		
32	0.086	0.072	0.062	0.126	0.101	0.120	0.104	0.069	0.071	0.173	0.125	0.174
40	0.132	0.130	0.105	0.070	0.059	0.062	0.086	0.068	0.059			
48	0.124	0.129	0.095	0.089	0.068	0.080	0.082	0.076	0.055			
CoCoBi Density Difference Results - Green Laser												
Time (hrs)	Tray 1			Tray 2			Tray 3			Red	Green	Blue
	Red	Green	Blue	Red	Green	Blue	Red	Green	Blue			
-24	0.099	0.088	0.098	0.152	0.131	0.165	0.155	0.134	0.150	Mean		
-16	0.089	0.081	0.082	0.124	0.105	0.134	0.154	0.128	0.170	0.125	0.109	0.128
-8	0.096	0.090	0.090	0.147	0.119	0.164	0.135	0.122	0.141			
0	0.112	0.108	0.098	0.136	0.106	0.153	0.122	0.097	0.114	2 Sigma		
8	0.101	0.089	0.089	0.140	0.113	0.156	0.102	0.086	0.098	0.176	0.148	0.193
16	0.092	0.083	0.079	0.104	0.080	0.116	0.107	0.096	0.095			
24	0.096	0.094	0.078	0.107	0.088	0.120	0.126	0.113	0.122	3 Sigma		
32	0.098	0.091	0.088	0.126	0.102	0.133	0.121	0.104	0.111	0.201	0.167	0.225

40	0.121	0.126	0.107	0.088	0.073	0.096	0.110	0.098	0.104			
48	0.111	0.117	0.088	0.096	0.084	0.092	0.093	0.089	0.086			
CoCoBi Density Difference Results - UV Laser												
Time (hrs)	Tray 1			Tray 2			Tray 3			Red	Green	Blue
	Red	Green	Blue	Red	Green	Blue	Red	Green	Blue			
-24	0.064	0.049	0.050	0.102	0.098	0.088	0.072	0.067	0.069	Mean		
-16	0.053	0.049	0.047	0.121	0.113	0.092	0.159	0.108	0.104	0.090	0.081	0.074
-8	0.060	0.074	0.065	0.133	0.101	0.084	0.104	0.100	0.093			
0	0.095	0.102	0.072	0.086	0.065	0.068	0.044	0.056	0.050	2 Sigma		
8	0.075	0.063	0.042	0.109	0.083	0.069	0.052	0.051	0.046	0.159	0.128	0.112
16	0.073	0.065	0.048	0.109	0.074	0.060	0.057	0.055	0.057			
24	0.060	0.052	0.054	0.106	0.102	0.100	0.037	0.046	0.040	3 Sigma		
32	0.454	0.136	0.124	0.110	0.091	0.091	0.059	0.058	0.052	0.194	0.152	0.131
40	0.083	0.085	0.066	0.074	0.062	0.055	0.050	0.053	0.048			
48	0.084	0.084	0.057	0.085	0.066	0.067	0.040	0.049	0.043			

Table B.2: Comparison of moss response to all lasers of the CoCoBi using single-color DTW image analysis. Images were collected every 8 hours over three days. Control images were collected for the first 24 hours. At time 0 three Cu treatments were given at 1 nmol/cm² for Tray 1, 10 nmol/cm² for Tray 2, and 100 nmol/cm² for Tray 3. Light gray shading indicates a 2 sigma deviation from the control. Dark gray shading indicates a 3 sigma deviation from the control.

CoCoBi Single Color DTW Results - Both Lasers												
Time	Tray 1			Tray 2			Tray 3			Red	Green	Blue
	Red	Green	Blue	Red	Green	Blue	Red	Green	Blue			
-24	0.061	0.056	0.059	0.058	0.048	0.052	0.057	0.045	0.047	Mean		
-16	0.060	0.051	0.058	0.050	0.045	0.048	0.059	0.051	0.055	0.059	0.050	0.055
-8	0.086	0.078	0.085	0.050	0.041	0.047	0.058	0.047	0.049			
0	0.110	0.102	0.114	0.057	0.045	0.049	0.057	0.053	0.057	2 Sigma		
8	0.072	0.065	0.076	0.061	0.047	0.051	0.050	0.051	0.054	0.079	0.071	0.077
16	0.061	0.054	0.064	0.053	0.048	0.048	0.070	0.061	0.065			
24	0.068	0.057	0.065	0.378	0.181	0.591	0.060	0.057	0.063	3 Sigma		

32	0.061	0.054	0.059	0.052	0.050	0.053	0.050	0.045	0.048	0.089	0.082	0.089
40	0.136	0.116	0.136	0.052	0.049	0.050	0.060	0.055	0.056			
48	0.118	0.105	0.122	0.047	0.045	0.046	0.070	0.064	0.065			
CoCoBi Single Color DTW Results - Green Laser												
Time	Tray 1			Tray 2			Tray 3			Red	Green	Blue
	Red	Green	Blue	Red	Green	Blue	Red	Green	Blue			
-24	0.081	0.089	0.124	0.069	0.075	0.109	0.074	0.077	0.103	Mean		
-16	0.072	0.077	0.114	0.064	0.069	0.097	0.067	0.074	0.108	0.072	0.078	0.111
-8	0.094	0.102	0.142	0.066	0.069	0.105	0.067	0.075	0.103			
0	0.109	0.121	0.175	0.062	0.068	0.095	0.068	0.071	0.099	2 Sigma		
8	0.086	0.093	0.146	0.063	0.067	0.096	0.067	0.076	0.097	0.090	0.098	0.137
16	0.076	0.080	0.127	0.061	0.068	0.088	0.080	0.089	0.115			
24	0.083	0.089	0.136	0.067	0.075	0.096	0.076	0.084	0.115	3 Sigma		
32	0.076	0.083	0.119	0.062	0.072	0.095	0.072	0.081	0.112	0.099	0.107	0.149
40	0.135	0.149	0.202	0.065	0.069	0.099	0.074	0.084	0.110			
48	0.122	0.137	0.185	0.068	0.078	0.102	0.081	0.092	0.120			
CoCoBi Single Color DTW Results - UV Laser												
Time	Tray 1			Tray 2			Tray 3			Red	Green	Blue
	Red	Green	Blue	Red	Green	Blue	Red	Green	Blue			
-24	0.061	0.065	0.063	0.047	0.060	0.056	0.056	0.064	0.061	Mean		
-16	0.065	0.074	0.070	0.050	0.062	0.058	0.079	0.076	0.081	0.062	0.070	0.067
-8	0.084	0.103	0.098	0.066	0.067	0.061	0.057	0.067	0.067			
0	0.136	0.139	0.113	0.054	0.058	0.057	0.067	0.086	0.080	2 Sigma		
8	0.078	0.087	0.076	0.048	0.061	0.058	0.055	0.068	0.064	0.085	0.095	0.093
16	0.072	0.086	0.078	0.049	0.059	0.057	0.056	0.068	0.064			
24	0.069	0.072	0.062	0.095	0.116	0.107	0.065	0.081	0.074	3 Sigma		
32	0.342	0.094	0.149	0.057	0.065	0.066	0.056	0.073	0.068	0.096	0.107	0.105
40	0.119	0.120	0.098	0.048	0.062	0.060	0.058	0.071	0.069			
48	0.126	0.127	0.102	0.050	0.057	0.055	0.067	0.080	0.073			

Table B.3: Comparison of moss response to all lasers of the CoCoBi using two-color DTW image analysis. Images were collected every 8 hours over three days. Control images were collected for the first 24 hours. At time 0 three Cu treatments were given at 1 nmol/cm² for Tray 1, 10 nmol/cm² for Tray 2, and 100 nmol/cm² for Tray 3. Light gray shading indicates a 2 sigma deviation from the control. Dark gray shading indicates a 3 sigma deviation from the control.

CoCoBi Two Color DTW Results - Both Lasers												
Time	Tray 1			Tray 2			Tray 3			RvG	GvB	RvB
	RvG	GvB	RvB	RvG	GvB	RvB	RvG	GvB	RvB			
-24	0.111	0.098	0.108	0.103	0.099	0.108	0.099	0.091	0.103	Mean		
-16	0.098	0.087	0.103	0.093	0.092	0.097	0.107	0.105	0.112	0.103	0.096	0.107
-8	0.141	0.117	0.146	0.087	0.086	0.094	0.099	0.094	0.104	2 Sigma		
0	0.171	0.146	0.177	0.096	0.093	0.104	0.106	0.108	0.111	2 Sigma		
8	0.115	0.102	0.125	0.101	0.097	0.109	0.099	0.105	0.103	0.133	0.115	0.136
16	0.095	0.086	0.099	0.099	0.096	0.099	0.127	0.124	0.133	3 Sigma		
24	0.114	0.100	0.116	0.404	0.762	0.696	0.113	0.118	0.120	3 Sigma		
32	0.111	0.101	0.113	0.098	0.101	0.102	0.093	0.092	0.096	0.147	0.124	0.151
40	0.203	0.173	0.216	0.099	0.099	0.101	0.112	0.111	0.115	3 Sigma		
48	0.176	0.150	0.184	0.089	0.090	0.091	0.130	0.127	0.133	3 Sigma		
CoCoBi Two Color DTW Results - Green Laser												
Time	Tray 1			Tray 2			Tray 3			RvG	GvB	RvB
	RvG	GvB	RvB	RvG	GvB	RvB	RvG	GvB	RvB			
-24	0.160	0.193	0.188	0.141	0.181	0.176	0.148	0.176	0.174	Mean		
-16	0.129	0.159	0.160	0.131	0.163	0.159	0.138	0.178	0.172	0.141	0.175	0.172
-8	0.158	0.188	0.191	0.132	0.169	0.167	0.139	0.174	0.166	2 Sigma		
0	0.171	0.201	0.203	0.127	0.160	0.154	0.135	0.167	0.164	2 Sigma		
8	0.140	0.169	0.173	0.127	0.160	0.155	0.141	0.172	0.163	0.163	0.196	0.193
16	0.126	0.152	0.153	0.128	0.155	0.148	0.166	0.201	0.192	3 Sigma		
24	0.146	0.164	0.162	0.140	0.169	0.161	0.156	0.197	0.188	3 Sigma		
32	0.151	0.183	0.179	0.132	0.164	0.154	0.150	0.189	0.180	0.174	0.207	0.204
40	0.201	0.242	0.239	0.132	0.166	0.162	0.156	0.191	0.181	3 Sigma		
48	0.176	0.207	0.204	0.144	0.177	0.168	0.170	0.210	0.198	3 Sigma		
CoCoBi Two Color DTW Results - UV Laser												

Time	Tray 1			Tray 2			Tray 3			RvG	GvB	RvB
	RvG	GvB	RvB	RvG	GvB	RvB	RvG	GvB	RvB			
-24	0.121	0.123	0.117	0.107	0.116	0.104	0.119	0.125	0.117	Mean		
-16	0.090	0.101	0.090	0.112	0.120	0.109	0.154	0.158	0.160	0.118	0.125	0.116
-8	0.113	0.128	0.108	0.132	0.128	0.127	0.124	0.134	0.124			
0	0.170	0.161	0.150	0.112	0.116	0.112	0.152	0.166	0.147	2 Sigma		
8	0.097	0.101	0.090	0.108	0.119	0.106	0.123	0.132	0.119	0.151	0.154	0.153
16	0.094	0.105	0.090	0.108	0.117	0.106	0.124	0.132	0.121			
24	0.105	0.119	0.107	0.211	0.223	0.202	0.145	0.155	0.139	3 Sigma		
32	0.555	0.240	0.565	0.121	0.131	0.123	0.129	0.142	0.124	0.168	0.168	0.172
40	0.143	0.135	0.128	0.110	0.122	0.108	0.130	0.140	0.127			
48	0.156	0.144	0.136	0.107	0.112	0.105	0.147	0.153	0.140			

6.2.2.2 Chl-A Laser Comparison Results

Table B.4: Comparison of moss response to all filter options for the Chl-A laser using single-color density difference image analysis. Images were collected every 8 hours over three days. Control images were collected for the first 24 hours. At time 0 three Cu treatments were given at 1 nmol/cm² for Tray 1, 10 nmol/cm² for Tray 2, and 100 nmol/cm² for Tray 3. Light gray shading indicates a 2 sigma deviation from the control. Dark gray shading indicates a 3 sigma deviation from the control.

Chl-A Laser Density Difference Results – Blank												
Time(hrs)	Tray 1			Tray 2			Tray 3			Red	Green	Blue
	Red	Green	Blue	Red	Green	Blue	Red	Green	Blue			
-24	0.128	0.119	0.118	0.157	0.147	0.147	0.140	0.142	0.131	Mean		
-16	0.229	0.225	0.224	0.404	0.271	0.413	0.185	0.141	0.162	0.188	0.164	0.177
-8	0.193	0.191	0.188	0.219	0.174	0.199	0.147	0.120	0.131			
0	0.150	0.153	0.145	0.096	0.090	0.689	0.101	0.111	0.716	2 Sigma		
8	0.204	0.199	0.198	0.176	0.153	0.162	0.096	0.125	0.093	0.347	0.260	0.348
16	0.238	0.242	0.236	0.215	0.196	0.203	0.116	0.127	0.106			
24	0.186	0.197	0.185	0.132	0.125	0.124	0.137	0.174	0.140	3 Sigma		
32	0.179	0.178	0.174	0.178	0.145	0.161	0.106	0.118	0.098	0.426	0.308	0.433
40	0.205	0.210	0.203	0.186	0.168	0.174	0.097	0.121	0.093			

48	0.188	0.196	0.185	0.177	0.153	0.161	0.109	0.143	0.112			
Chl-A Laser Density Difference Results - A Filter												
Time(hrs)	Tray 1			Tray 2			Tray 3			Red	Green	Blue
	Red	Green	Blue	Red	Green	Blue	Red	Green	Blue			
-24	0.112	0.098	0.085	0.191	0.176	0.162	0.146	0.132	0.117	Mean		
-16	0.253	0.238	0.213	0.248	0.232	0.215	0.260	0.246	0.233	0.209	0.194	0.178
-8	0.233	0.217	0.201	0.307	0.290	0.275	0.211	0.196	0.184			
0	0.190	0.171	0.154	0.160	0.184	0.546	0.119	0.125	0.580	2 Sigma		
8	0.247	0.228	0.203	0.235	0.218	0.201	0.127	0.117	0.109	0.323	0.306	0.288
16	0.281	0.264	0.239	0.284	0.271	0.254	0.163	0.152	0.139			
24	0.226	0.213	0.190	0.189	0.172	0.156	0.110	0.099	0.087	3 Sigma		
32	0.230	0.212	0.197	0.241	0.226	0.213	0.146	0.133	0.121	0.381	0.363	0.343
40	0.249	0.232	0.206	0.257	0.243	0.228	0.141	0.128	0.116			
48	0.221	0.204	0.178	0.245	0.229	0.211	0.119	0.108	0.093			
Chl-A Laser Density Difference Results - B Filter												
Time(hrs)	Tray 1			Tray 2			Tray 3			Red	Green	Blue
	Red	Green	Blue	Red	Green	Blue	Red	Green	Blue			
-24	0.081	0.041	0.031	0.151	0.081	0.057	0.103	0.044	0.031	Mean		
-16	0.194	0.090	0.050	0.193	0.113	0.079	0.178	0.122	0.091	0.156	0.086	0.058
-8	0.185	0.097	0.058	0.225	0.143	0.098	0.157	0.106	0.070			
0	0.133	0.050	0.030	0.090	0.078	0.616	0.090	0.052	0.622	2 Sigma		
8	0.186	0.085	0.050	0.164	0.087	0.058	0.102	0.049	0.047	0.243	0.150	0.104
16	0.234	0.113	0.062	0.218	0.130	0.085	0.119	0.051	0.043			
24	0.180	0.086	0.056	0.137	0.066	0.046	0.117	0.049	0.028	3 Sigma		
32	0.174	0.095	0.066	0.170	0.099	0.061	0.100	0.055	0.052	0.286	0.181	0.126
40	0.198	0.087	0.049	0.190	0.112	0.074	0.100	0.046	0.034			
48	0.165	0.072	0.057	0.172	0.099	0.069	0.100	0.054	0.047			

Table B.5: Comparison of moss response to all filter options for the Chl-A laser using single-color DTW image analysis. Images were collected every 8 hours over three days. Control images were collected for the first 24 hours. At time 0 three Cu treatments were given at 1 nmol/cm² for

Tray 1, 10 nmol/cm² for Tray 2, and 100 nmol/cm² for Tray 3. Light gray shading indicates a 2 sigma deviation from the control. Dark gray shading indicates a 3 sigma deviation from the control.

Chl-A Laser Single Color DTW Results - Blank												
Time(hrs)	Tray 1			Tray 2			Tray 3			Red	Green	Blue
	Red	Green	Blue	Red	Green	Blue	Red	Green	Blue			
-24	0.177	0.111	0.115	0.137	0.086	0.092	0.198	0.125	0.130	Mean		
-16	0.184	0.121	0.137	0.491	0.201	0.384	0.180	0.093	0.108	0.187	0.106	0.125
-8	0.157	0.090	0.103	0.154	0.083	0.090	0.149	0.084	0.103			
0	0.140	0.087	0.092	0.144	0.084	0.684	0.165	0.090	0.758	2 Sigma		
8	0.150	0.104	0.096	0.153	0.095	0.096	0.156	0.100	0.101	0.394	0.177	0.300
16	0.169	0.103	0.103	0.152	0.101	0.103	0.136	0.089	0.091			
24	0.150	0.096	0.090	0.128	0.085	0.085	0.216	0.140	0.140	3 Sigma		
32	0.155	0.090	0.093	0.154	0.094	0.099	0.149	0.097	0.097	0.497	0.212	0.387
40	0.157	0.105	0.100	0.138	0.094	0.098	0.142	0.095	0.094			
48	0.170	0.109	0.111	0.136	0.091	0.089	0.166	0.110	0.107			
Chl-A Laser Single Color DTW Results - A Filter												
Time(hrs)	Tray 1			Tray 2			Tray 3			Red	Green	Blue
	Red	Green	Blue	Red	Green	Blue	Red	Green	Blue			
-24	0.251	0.144	0.193	0.163	0.093	0.114	0.236	0.130	0.169	Mean		
-16	0.212	0.116	0.165	0.177	0.100	0.129	0.198	0.124	0.153	0.201	0.115	0.150
-8	0.183	0.103	0.138	0.208	0.126	0.160	0.197	0.104	0.141			
0	0.179	0.102	0.123	0.177	0.103	0.813	0.190	0.092	0.857	2 Sigma		
8	0.191	0.104	0.140	0.167	0.090	0.126	0.181	0.096	0.134	0.254	0.146	0.194
16	0.199	0.099	0.154	0.184	0.082	0.151	0.169	0.091	0.117			
24	0.181	0.104	0.127	0.159	0.092	0.115	0.272	0.153	0.205	3 Sigma		
32	0.178	0.107	0.131	0.189	0.115	0.128	0.184	0.103	0.127	0.280	0.162	0.216
40	0.190	0.114	0.146	0.161	0.081	0.120	0.167	0.091	0.118			
48	0.195	0.117	0.137	0.154	0.084	0.123	0.184	0.105	0.137			
Chl-A Laser Single Color DTW Results - B Filter												
Time(hrs)	Tray 1			Tray 2			Tray 3			Red	Green	Blue
	Red	Green	Blue	Red	Green	Blue	Red	Green	Blue			

-24	0.119	0.094	0.028	0.073	0.068	0.022	0.108	0.087	0.025	Mean		
-16	0.095	0.083	0.025	0.083	0.072	0.023	0.079	0.078	0.025	0.086	0.077	0.024
-8	0.078	0.070	0.021	0.079	0.078	0.030	0.074	0.071	0.021			
0	0.078	0.072	0.025	0.080	0.106	0.693	0.097	0.114	0.698	2 Sigma		
8	0.086	0.073	0.023	0.076	0.066	0.020	0.087	0.081	0.029	0.117	0.094	0.030
16	0.090	0.075	0.023	0.090	0.075	0.023	0.075	0.077	0.030			
24	0.081	0.075	0.026	0.071	0.071	0.026	0.135	0.111	0.031	3 Sigma		
32	0.077	0.073	0.022	0.081	0.075	0.023	0.082	0.076	0.024	0.132	0.102	0.032
40	0.087	0.082	0.029	0.080	0.067	0.022	0.077	0.074	0.023			
48	0.089	0.077	0.023	0.076	0.067	0.023	0.091	0.090	0.032			

Table B.6: Comparison of moss response to all filter options for the Chl-A laser using two-color DTW image analysis. Images were collected every 8 hours over three days. Control images were collected for the first 24 hours. At time 0 three Cu treatments were given at 1 nmol/cm² for Tray 1, 10 nmol/cm² for Tray 2, and 100 nmol/cm² for Tray 3. Light gray shading indicates a 2 sigma deviation from the control. Dark gray shading indicates a 3 sigma deviation from the control.

Chl-A Laser Two Color DTW Results - Blank												
Time(hrs)	Tray 1			Tray 2			Tray 3			RvG	GvB	RvB
	RvG	GvB	RvB	RvG	GvB	RvB	RvG	GvB	RvB			
-24	0.312	0.212	0.316	0.210	0.177	0.215	0.289	0.254	0.290	Mean		
-16	0.363	0.340	0.372	0.607	0.560	0.756	0.242	0.200	0.257	0.293	0.246	0.309
-8	0.328	0.283	0.342	0.221	0.173	0.225	0.218	0.186	0.236			
0	0.282	0.222	0.295	0.211	0.737	0.633	0.227	0.797	0.687	2 Sigma		
8	0.320	0.303	0.294	0.232	0.191	0.233	0.232	0.201	0.230	0.527	0.479	0.625
16	0.304	0.298	0.290	0.232	0.204	0.236	0.211	0.179	0.211			
24	0.292	0.246	0.290	0.201	0.170	0.201	0.312	0.279	0.307	3 Sigma		
32	0.314	0.269	0.334	0.230	0.193	0.233	0.224	0.194	0.223	0.644	0.596	0.782
40	0.301	0.256	0.291	0.216	0.191	0.219	0.215	0.189	0.215			
48	0.316	0.256	0.312	0.213	0.180	0.209	0.247	0.216	0.242			
Chl-A Laser Two Color DTW Results - A Filter												
	Tray 1			Tray 2			Tray 3					

Time(hrs)	RvG	GvB	RvB	RvG	GvB	RvB	RvG	GvB	RvB	RvG	GvB	RvB
-24	0.378	0.323	0.528	0.245	0.207	0.272	0.331	0.299	0.379	Mean		
-16	0.370	0.289	0.450	0.261	0.229	0.300	0.304	0.277	0.345	0.312	0.271	0.367
-8	0.354	0.307	0.399	0.304	0.286	0.361	0.287	0.245	0.334			
0	0.329	0.266	0.404	0.270	0.888	0.774	0.272	0.917	0.775	2 Sigma		
8	0.326	0.248	0.397	0.248	0.216	0.286	0.262	0.230	0.312	0.400	0.343	0.515
16	0.338	0.249	0.400	0.251	0.233	0.329	0.253	0.208	0.284			
24	0.322	0.242	0.390	0.243	0.207	0.269	0.360	0.358	0.445	3 Sigma		
32	0.359	0.322	0.404	0.276	0.243	0.303	0.270	0.230	0.308	0.444	0.380	0.588
40	0.342	0.256	0.404	0.229	0.202	0.275	0.251	0.209	0.283			
48	0.345	0.260	0.418	0.225	0.206	0.271	0.269	0.242	0.319			
Chl-A Laser Two Color DTW Results - B Filter												
Time(hrs)	Tray 1			Tray 2			Tray 3			RvG	GvB	RvB
	RvG	GvB	RvB	RvG	GvB	RvB	RvG	GvB	RvB	RvG	GvB	RvB
-24	0.145	0.090	0.097	0.142	0.090	0.095	0.195	0.112	0.133	Mean		
-16	0.205	0.111	0.145	0.155	0.095	0.106	0.157	0.102	0.104	0.165	0.101	0.112
-8	0.197	0.110	0.137	0.157	0.108	0.109	0.144	0.092	0.095			
0	0.140	0.080	0.097	0.186	0.773	0.748	0.211	0.788	0.770	2 Sigma		
8	0.203	0.105	0.147	0.142	0.085	0.096	0.168	0.109	0.116	0.212	0.119	0.149
16	0.231	0.123	0.164	0.164	0.098	0.113	0.152	0.107	0.106			
24	0.177	0.104	0.126	0.142	0.097	0.097	0.246	0.142	0.167	3 Sigma		
32	0.192	0.116	0.130	0.156	0.098	0.103	0.158	0.099	0.106	0.236	0.128	0.167
40	0.183	0.105	0.129	0.148	0.090	0.103	0.151	0.097	0.100			
48	0.166	0.100	0.116	0.142	0.090	0.099	0.181	0.122	0.123			

6.2.2.3 Chl-B Laser Comparison Results

Table B.7: Comparison of moss response to all filter options for the Chl-B laser using single-color density difference image analysis. Images were collected every 8 hours over three days. Control images were collected for the first 24 hours. At time 0 three Cu treatments were given at 1 nmol/cm² for Tray 1, 10 nmol/cm² for Tray 2, and 100 nmol/cm² for Tray 3. Light gray shading indicates a 2 sigma deviation from the control. Dark gray shading indicates a 3 sigma deviation from the control.

ChI-B Laser Density Difference Results - Blank												
Time(hrs)	Tray 1			Tray 2			Tray 3			Red	Green	Blue
	Red	Green	Blue	Red	Green	Blue	Red	Green	Blue			
-24	0.117	0.109	0.110	0.149	0.136	0.140	0.117	0.114	0.112	Mean		
-16	0.206	0.206	0.204	0.192	0.175	0.183	0.205	0.154	0.184	0.169	0.150	0.159
-8	0.187	0.181	0.182	0.224	0.179	0.207	0.161	0.127	0.147			
0	0.146	0.133	0.138	0.130	0.107	0.618	0.114	0.108	0.640	2 Sigma		
8	0.189	0.183	0.185	0.179	0.149	0.166	0.106	0.100	0.098	0.242	0.213	0.229
16	0.227	0.222	0.224	0.222	0.193	0.209	0.129	0.122	0.120			
24	0.182	0.182	0.182	0.147	0.125	0.136	0.101	0.111	0.095	3 Sigma		
32	0.179	0.164	0.170	0.175	0.139	0.159	0.116	0.108	0.107	0.279	0.245	0.264
40	0.200	0.199	0.198	0.194	0.168	0.181	0.111	0.107	0.101			
48	0.179	0.180	0.178	0.209	0.183	0.197	0.111	0.117	0.108			
ChI-B Laser Density Difference Results - A Filter												
Time(hrs)	Tray 1			Tray 2			Tray 3			Red	Green	Blue
	Red	Green	Blue	Red	Green	Blue	Red	Green	Blue			
-24	0.111	0.101	0.095	0.165	0.156	0.148	0.182	0.175	0.168	Mean		
-16	0.221	0.214	0.204	0.216	0.207	0.199	0.240	0.230	0.227	0.195	0.186	0.179
-8	0.211	0.201	0.195	0.248	0.238	0.232	0.206	0.199	0.195			
0	0.156	0.143	0.137	0.151	0.168	0.509	0.121	0.128	0.528	2 Sigma		
8	0.218	0.207	0.196	0.226	0.216	0.210	0.141	0.133	0.129	0.275	0.265	0.259
16	0.250	0.241	0.229	0.267	0.260	0.256	0.165	0.158	0.150			
24	0.208	0.200	0.192	0.175	0.163	0.156	0.097	0.088	0.082	3 Sigma		
32	0.225	0.215	0.210	0.227	0.219	0.215	0.146	0.138	0.133	0.314	0.305	0.299
40	0.221	0.213	0.202	0.230	0.222	0.218	0.145	0.137	0.132			
48	0.197	0.189	0.177	0.243	0.234	0.228	0.125	0.118	0.108			
ChI-B Laser Density Difference Results - B Filter												
Time(hrs)	Tray 1			Tray 2			Tray 3			Red	Green	Blue
	Red	Green	Blue	Red	Green	Blue	Red	Green	Blue			
-24	0.101	0.065	0.036	0.137	0.074	0.042	0.113	0.065	0.029	Mean		
-16	0.193	0.119	0.063	0.178	0.108	0.063	0.163	0.109	0.065	0.152	0.096	0.053
-8	0.181	0.112	0.060	0.187	0.132	0.077	0.144	0.108	0.065			

0	0.120	0.063	0.031	0.093	0.066	0.643	0.096	0.055	0.651	2 Sigma		
8	0.205	0.122	0.058	0.163	0.100	0.060	0.102	0.062	0.034	0.215	0.142	0.083
16	0.213	0.133	0.073	0.211	0.145	0.089	0.128	0.071	0.043	3 Sigma		
24	0.174	0.105	0.055	0.128	0.067	0.043	0.090	0.062	0.055	3 Sigma		
32	0.165	0.114	0.065	0.160	0.120	0.085	0.103	0.058	0.033	0.246	0.166	0.098
40	0.190	0.116	0.057	0.178	0.108	0.058	0.103	0.067	0.050			
48	0.164	0.096	0.051	0.191	0.119	0.068	0.107	0.058	0.039			

Table B.8: Comparison of moss response to all filter options for the Chl-B laser using single-color DTW image analysis. Images were collected every 8 hours over three days. Control images were collected for the first 24 hours. At time 0 three Cu treatments were given at 1 nmol/cm² for Tray 1, 10 nmol/cm² for Tray 2, and 100 nmol/cm² for Tray 3. Light gray shading indicates a 2 sigma deviation from the control. Dark gray shading indicates a 3 sigma deviation from the control.

Chl-B Laser Single Color DTW Results - Blank												
Time(hrs)	Tray 1			Tray 2			Tray 3			Red	Green	Blue
	Red	Green	Blue	Red	Green	Blue	Red	Green	Blue			
-24	0.115	0.117	0.108	0.087	0.081	0.069	0.112	0.115	0.104	Mean		
-16	0.106	0.096	0.085	0.090	0.085	0.074	0.119	0.110	0.104	0.102	0.098	0.088
-8	0.095	0.095	0.084	0.098	0.098	0.090	0.101	0.088	0.080			
0	0.094	0.091	0.081	0.102	0.082	0.650	0.107	0.090	0.666	2 Sigma		
8	0.092	0.085	0.075	0.097	0.085	0.071	0.087	0.087	0.073	0.123	0.122	0.114
16	0.100	0.092	0.079	0.091	0.082	0.067	0.087	0.082	0.071			
24	0.092	0.093	0.079	0.081	0.075	0.063	0.108	0.119	0.100	3 Sigma		
32	0.095	0.094	0.081	0.088	0.083	0.073	0.091	0.090	0.077	0.134	0.135	0.128
40	0.109	0.106	0.094	0.084	0.073	0.061	0.085	0.087	0.071			
48	0.104	0.104	0.091	0.086	0.073	0.064	0.095	0.095	0.079			
Chl-B Laser Single Color DTW Results - A Filter												
Time(hrs)	Tray 1			Tray 2			Tray 3			Red	Green	Blue
	Red	Green	Blue	Red	Green	Blue	Red	Green	Blue			
-24	0.243	0.125	0.168	0.148	0.082	0.102	0.261	0.156	0.223	Mean		
-16	0.185	0.097	0.140	0.152	0.084	0.104	0.197	0.116	0.132	0.189	0.105	0.136
-8	0.165	0.088	0.116	0.192	0.109	0.138	0.189	0.108	0.134			

0	0.161	0.088	0.109	0.154	0.088	0.686	0.160	0.082	0.700	2 Sigma		
8	0.159	0.087	0.112	0.165	0.080	0.116	0.149	0.081	0.101	0.262	0.149	0.206
16	0.183	0.090	0.136	0.174	0.075	0.129	0.145	0.080	0.099			
24	0.160	0.093	0.111	0.137	0.073	0.088	0.196	0.106	0.139	3 Sigma		
32	0.173	0.102	0.122	0.169	0.092	0.108	0.156	0.088	0.106	0.298	0.172	0.242
40	0.180	0.101	0.138	0.155	0.072	0.100	0.145	0.081	0.097			
48	0.172	0.100	0.121	0.153	0.071	0.101	0.153	0.086	0.106			
Chl-B Laser Single Color DTW Results - B Filter												
Time(hrs)	Tray 1			Tray 2			Tray 3			Red	Green	Blue
	Red	Green	Blue	Red	Green	Blue	Red	Green	Blue			
-24	0.128	0.106	0.039	0.078	0.070	0.025	0.129	0.105	0.035	Mean		
-16	0.111	0.088	0.035	0.082	0.076	0.028	0.104	0.085	0.030	0.103	0.085	0.031
-8	0.098	0.080	0.028	0.101	0.084	0.030	0.103	0.080	0.031			
0	0.080	0.073	0.027	0.082	0.086	0.691	0.093	0.093	0.698	2 Sigma		
8	0.110	0.096	0.033	0.098	0.072	0.027	0.082	0.074	0.028	0.136	0.108	0.039
16	0.108	0.083	0.033	0.099	0.081	0.034	0.073	0.070	0.027			
24	0.085	0.080	0.030	0.068	0.070	0.029	0.118	0.106	0.043	3 Sigma		
32	0.095	0.086	0.032	0.085	0.084	0.035	0.083	0.074	0.026	0.153	0.120	0.043
40	0.110	0.085	0.031	0.073	0.068	0.029	0.078	0.074	0.028			
48	0.097	0.085	0.032	0.075	0.071	0.029	0.085	0.084	0.034			

Table B.9: Comparison of moss response to all filter options for the Chl-B laser using two-color DTW image analysis. Images were collected every 8 hours over three days. Control images were collected for the first 24 hours. At time 0 three Cu treatments were given at 1 nmol/cm² for Tray 1, 10 nmol/cm² for Tray 2, and 100 nmol/cm² for Tray 3. Light gray shading indicates a 2 sigma deviation from the control. Dark gray shading indicates a 3 sigma deviation from the control.

Chl-B Laser Two Color DTW Results - Blank												
Time(hrs)	Tray 1			Tray 2			Tray 3			RvG	GvB	RvB
	RvG	GvB	RvB	RvG	GvB	RvB	RvG	GvB	RvB			
-24	0.198	0.175	0.186	0.163	0.148	0.153	0.224	0.217	0.213	Mean		
-16	0.195	0.184	0.185	0.170	0.157	0.161	0.226	0.213	0.219	0.197	0.185	0.188

-8	0.235	0.235	0.224	0.193	0.186	0.185	0.185	0.166	0.177			
0	0.186	0.173	0.176	0.182	0.699	0.718	0.195	0.723	0.739	2 Sigma		
8	0.186	0.175	0.175	0.179	0.155	0.160	0.172	0.159	0.158	0.244	0.240	0.235
16	0.203	0.192	0.189	0.169	0.147	0.156	0.167	0.152	0.156			
24	0.192	0.181	0.174	0.153	0.136	0.142	0.224	0.218	0.207	3 Sigma		
32	0.226	0.218	0.212	0.167	0.154	0.159	0.177	0.165	0.165	0.268	0.268	0.258
40	0.209	0.196	0.193	0.154	0.133	0.143	0.169	0.156	0.154			
48	0.194	0.178	0.177	0.156	0.136	0.148	0.186	0.173	0.172			

Chi-B Laser Two Color DTW Results - A Filter

Time(hrs)	Tray 1			Tray 2			Tray 3			RvG	GvB	RvB
	RvG	GvB	RvB	RvG	GvB	RvB	RvG	GvB	RvB			
-24	0.363	0.295	0.523	0.218	0.184	0.245	0.363	0.378	0.443	Mean		
-16	0.311	0.228	0.375	0.223	0.187	0.247	0.293	0.247	0.312	0.289	0.248	0.340
-8	0.323	0.278	0.374	0.271	0.247	0.316	0.277	0.241	0.313			
0	0.292	0.232	0.372	0.228	0.749	0.614	0.226	0.757	0.622	2 Sigma		
8	0.274	0.209	0.328	0.234	0.195	0.272	0.217	0.182	0.243	0.388	0.360	0.511
16	0.302	0.216	0.345	0.234	0.204	0.293	0.216	0.179	0.240			
24	0.283	0.220	0.335	0.202	0.161	0.221	0.266	0.244	0.316	3 Sigma		
32	0.355	0.322	0.395	0.245	0.200	0.264	0.229	0.193	0.256	0.438	0.416	0.596
40	0.316	0.236	0.364	0.217	0.172	0.247	0.215	0.178	0.238			
48	0.301	0.233	0.361	0.213	0.172	0.245	0.224	0.192	0.256			

Chi-B Laser Two Color DTW Results - B Filter

Time(hrs)	Tray 1			Tray 2			Tray 3			RvG	GvB	RvB
	RvG	GvB	RvB	RvG	GvB	RvB	RvG	GvB	RvB			
-24	0.210	0.101	0.162	0.147	0.095	0.102	0.235	0.140	0.164	Mean	rmean	0.195
-16	0.217	0.139	0.159	0.158	0.104	0.110	0.189	0.114	0.134	0.195	0.117	0.139
-8	0.251	0.148	0.179	0.185	0.114	0.131	0.183	0.111	0.133			
0	0.177	0.095	0.131	0.168	0.747	0.739	0.186	0.761	0.757	2 Sigma		
8	0.240	0.145	0.169	0.169	0.099	0.124	0.156	0.102	0.109	0.259	0.153	0.189
16	0.222	0.157	0.158	0.179	0.115	0.132	0.144	0.097	0.100			
24	0.199	0.123	0.144	0.138	0.099	0.097	0.224	0.149	0.161	3 Sigma		
32	0.254	0.153	0.180	0.169	0.119	0.119	0.157	0.100	0.108	0.291	0.171	0.213

40	0.213	0.128	0.155	0.142	0.097	0.102	0.152	0.102	0.105	
48	0.201	0.119	0.146	0.147	0.100	0.103	0.169	0.118	0.118	

6.2.3 Tables corresponding to Figures in Main Body

Table B.10: Comparison of moss response to all analysis method using both lasers of the CoCoBi. Images were collected every 8 hours over three days. Control images were collected for the first 24 hours. At time 0 three Cu treatments were given at 1 nmol/cm² for Tray 1, 10 nmol/cm² for Tray 2, and 100 nmol/cm² for Tray 3. Light gray shading indicates a 2 sigma deviation from the control. Dark gray shading indicates a 3 sigma deviation from the control.

CoCoBi Density Difference Results - Both Lasers												
Time(hrs)	Tray 1			Tray 2			Tray 3			Red	Green	Blue
	Red	Green	Blue	Red	Green	Blue	Red	Green	Blue			
-24	0.089	0.076	0.059	0.132	0.102	0.120	0.123	0.092	0.102	Mean		
-16	0.090	0.076	0.060	0.108	0.091	0.101	0.152	0.114	0.140	0.112	0.092	0.093
-8	0.092	0.088	0.066	0.126	0.095	0.118	0.114	0.097	0.105			
0	0.116	0.117	0.087	0.117	0.081	0.106	0.099	0.071	0.069	2 Sigma		
8	0.100	0.085	0.066	0.128	0.096	0.119	0.084	0.062	0.055	0.153	0.114	0.147
16	0.089	0.080	0.063	0.105	0.072	0.089	0.105	0.088	0.071			
24	0.095	0.083	0.066	0.371	0.201	0.570	0.101	0.079	0.065	3 Sigma		
32	0.086	0.072	0.062	0.126	0.101	0.120	0.104	0.069	0.071	0.173	0.125	0.174
40	0.132	0.130	0.105	0.070	0.059	0.062	0.086	0.068	0.059			
48	0.124	0.129	0.095	0.089	0.068	0.080	0.082	0.076	0.055			
CoCoBi Single Color DTW Results - Both Lasers												
Time(hrs)	Tray 1			Tray 2			Tray 3			Red	Green	Blue
	Red	Green	Blue	Red	Green	Blue	Red	Green	Blue			
-24	0.061	0.056	0.059	0.058	0.048	0.052	0.057	0.045	0.047	Mean		
-16	0.060	0.051	0.058	0.050	0.045	0.048	0.059	0.051	0.055	0.059	0.050	0.055
-8	0.086	0.078	0.085	0.050	0.041	0.047	0.058	0.047	0.049			
0	0.110	0.102	0.114	0.057	0.045	0.049	0.057	0.053	0.057	2 Sigma		
8	0.072	0.065	0.076	0.061	0.047	0.051	0.050	0.051	0.054	0.079	0.071	0.077
16	0.061	0.054	0.064	0.053	0.048	0.048	0.070	0.061	0.065			

24	0.068	0.057	0.065	0.378	0.181	0.591	0.060	0.057	0.063	3 Sigma		
32	0.061	0.054	0.059	0.052	0.050	0.053	0.050	0.045	0.048	0.089	0.082	0.089
40	0.136	0.116	0.136	0.052	0.049	0.050	0.060	0.055	0.056			
48	0.118	0.105	0.122	0.047	0.045	0.046	0.070	0.064	0.065			
CoCoBi Two Color DTW Results - Both Lasers												
Time(hrs)	Tray 1			Tray 2			Tray 3			RvG	GvB	RvB
	RvG	GvB	RvB	RvG	GvB	RvB	RvG	GvB	RvB			
-24	0.111	0.098	0.108	0.103	0.099	0.108	0.099	0.091	0.103	Mean		
-16	0.098	0.087	0.103	0.093	0.092	0.097	0.107	0.105	0.112	0.103	0.096	0.107
-8	0.141	0.117	0.146	0.087	0.086	0.094	0.099	0.094	0.104			
0	0.171	0.146	0.177	0.096	0.093	0.104	0.106	0.108	0.111	2 Sigma		
8	0.115	0.102	0.125	0.101	0.097	0.109	0.099	0.105	0.103	0.133	0.115	0.136
16	0.095	0.086	0.099	0.099	0.096	0.099	0.127	0.124	0.133			
24	0.114	0.100	0.116	0.404	0.762	0.696	0.113	0.118	0.120	3 Sigma		
32	0.111	0.101	0.113	0.098	0.101	0.102	0.093	0.092	0.096	0.147	0.124	0.151
40	0.203	0.173	0.216	0.099	0.099	0.101	0.112	0.111	0.115			
48	0.176	0.150	0.184	0.089	0.090	0.091	0.130	0.127	0.133			

Table B.11: Comparison of moss response to all analysis method using the Chl-B Filter with the Chl-A laser. Images were collected every 8 hours over three days. Control images were collected for the first 24 hours. At time 0 three Cu treatments were given at 1 nmol/cm² for Tray 1, 10 nmol/cm² for Tray 2, and 100 nmol/cm² for Tray 3. Light gray shading indicates a 2 sigma deviation from the control. Dark gray shading indicates a 3 sigma deviation from the control.

Chl-A Laser Density Difference Results - B Filter												
Time(hrs)	Tray 1			Tray 2			Tray 3			Red	Green	Blue
	Red	Green	Blue	Red	Green	Blue	Red	Green	Blue			
-24	0.081	0.041	0.031	0.151	0.081	0.057	0.103	0.044	0.031	Mean		
-16	0.194	0.090	0.050	0.193	0.113	0.079	0.178	0.122	0.091	0.156	0.086	0.058
-8	0.185	0.097	0.058	0.225	0.143	0.098	0.157	0.106	0.070			
0	0.133	0.050	0.030	0.090	0.078	0.616	0.090	0.052	0.622	2 Sigma		
8	0.186	0.085	0.050	0.164	0.087	0.058	0.102	0.049	0.047	0.243	0.150	0.104

16	0.234	0.113	0.062	0.218	0.130	0.085	0.119	0.051	0.043			
24	0.180	0.086	0.056	0.137	0.066	0.046	0.117	0.049	0.028	3 Sigma		
32	0.174	0.095	0.066	0.170	0.099	0.061	0.100	0.055	0.052	0.286	0.181	0.126
40	0.198	0.087	0.049	0.190	0.112	0.074	0.100	0.046	0.034			
48	0.165	0.072	0.057	0.172	0.099	0.069	0.100	0.054	0.047			

ChI-A Laser Single Color DTW Results - B Filter

Time(hrs)	Tray 1			Tray 2			Tray 3			Red	Green	Blue
	Red	Green	Blue	Red	Green	Blue	Red	Green	Blue			
-24	0.119	0.094	0.028	0.073	0.068	0.022	0.108	0.087	0.025	Mean		
-16	0.095	0.083	0.025	0.083	0.072	0.023	0.079	0.078	0.025	0.086	0.077	0.024
-8	0.078	0.070	0.021	0.079	0.078	0.030	0.074	0.071	0.021			
0	0.078	0.072	0.025	0.080	0.106	0.693	0.097	0.114	0.698	2 Sigma		
8	0.086	0.073	0.023	0.076	0.066	0.020	0.087	0.081	0.029	0.117	0.094	0.030
16	0.090	0.075	0.023	0.090	0.075	0.023	0.075	0.077	0.030			
24	0.081	0.075	0.026	0.071	0.071	0.026	0.135	0.111	0.031	3 Sigma		
32	0.077	0.073	0.022	0.081	0.075	0.023	0.082	0.076	0.024	0.132	0.102	0.032
40	0.087	0.082	0.029	0.080	0.067	0.022	0.077	0.074	0.023			
48	0.089	0.077	0.023	0.076	0.067	0.023	0.091	0.090	0.032			

ChI-A Laser Two Color DTW Results - B Filter

Time(hrs)	Tray 1			Tray 2			Tray 3			RvG	GvB	RvB
	RvG	GvB	RvB	RvG	GvB	RvB	RvG	GvB	RvB			
-24	0.145	0.090	0.097	0.142	0.090	0.095	0.195	0.112	0.133	Mean		
-16	0.205	0.111	0.145	0.155	0.095	0.106	0.157	0.102	0.104	0.165	0.101	0.112
-8	0.197	0.110	0.137	0.157	0.108	0.109	0.144	0.092	0.095			
0	0.140	0.080	0.097	0.186	0.773	0.748	0.211	0.788	0.770	2 Sigma		
8	0.203	0.105	0.147	0.142	0.085	0.096	0.168	0.109	0.116	0.212	0.119	0.149
16	0.231	0.123	0.164	0.164	0.098	0.113	0.152	0.107	0.106			
24	0.177	0.104	0.126	0.142	0.097	0.097	0.246	0.142	0.167	3 Sigma		
32	0.192	0.116	0.130	0.156	0.098	0.103	0.158	0.099	0.106	0.236	0.128	0.167
40	0.183	0.105	0.129	0.148	0.090	0.103	0.151	0.097	0.100			
48	0.166	0.100	0.116	0.142	0.090	0.099	0.181	0.122	0.123			

Table B.12: Comparison of moss response to all analysis method using the Chl-B Filter with the Chl-B laser. Images were collected every 8 hours over three days. Control images were collected for the first 24 hours. At time 0 three Cu treatments were given at 1 nmol/cm² for Tray 1, 10 nmol/cm² for Tray 2, and 100 nmol/cm² for Tray 3. Light gray shading indicates a 2 sigma deviation from the control. Dark gray shading indicates a 3 sigma deviation from the control.

Chl-B Laser Density Difference Results - B Filter												
Time(hrs)	Tray 1			Tray 2			Tray 3			Red	Green	Blue
	Red	Green	Blue	Red	Green	Blue	Red	Green	Blue			
-24	0.101	0.065	0.036	0.137	0.074	0.042	0.113	0.065	0.029	Mean		
-16	0.193	0.119	0.063	0.178	0.108	0.063	0.163	0.109	0.065	0.152	0.096	0.053
-8	0.181	0.112	0.060	0.187	0.132	0.077	0.144	0.108	0.065			
0	0.120	0.063	0.031	0.093	0.066	0.643	0.096	0.055	0.651	2 Sigma		
8	0.205	0.122	0.058	0.163	0.100	0.060	0.102	0.062	0.034	0.215	0.142	0.083
16	0.213	0.133	0.073	0.211	0.145	0.089	0.128	0.071	0.043			
24	0.174	0.105	0.055	0.128	0.067	0.043	0.090	0.062	0.055	3 Sigma		
32	0.165	0.114	0.065	0.160	0.120	0.085	0.103	0.058	0.033	0.246	0.166	0.098
40	0.190	0.116	0.057	0.178	0.108	0.058	0.103	0.067	0.050			
48	0.164	0.096	0.051	0.191	0.119	0.068	0.107	0.058	0.039			
Chl-B Laser Single Color DTW Results - B Filter												
Time(hrs)	Tray 1			Tray 2			Tray 3			Red	Green	Blue
	Red	Green	Blue	Red	Green	Blue	Red	Green	Blue			
-24	0.128	0.106	0.039	0.078	0.070	0.025	0.129	0.105	0.035	Mean		
-16	0.111	0.088	0.035	0.082	0.076	0.028	0.104	0.085	0.030	0.103	0.085	0.031
-8	0.098	0.080	0.028	0.101	0.084	0.030	0.103	0.080	0.031			
0	0.080	0.073	0.027	0.082	0.086	0.691	0.093	0.093	0.698	2 Sigma		
8	0.110	0.096	0.033	0.098	0.072	0.027	0.082	0.074	0.028	0.136	0.108	0.039
16	0.108	0.083	0.033	0.099	0.081	0.034	0.073	0.070	0.027			
24	0.085	0.080	0.030	0.068	0.070	0.029	0.118	0.106	0.043	3 Sigma		
32	0.095	0.086	0.032	0.085	0.084	0.035	0.083	0.074	0.026	0.153	0.120	0.043
40	0.110	0.085	0.031	0.073	0.068	0.029	0.078	0.074	0.028			
48	0.097	0.085	0.032	0.075	0.071	0.029	0.085	0.084	0.034			
Chl-B Laser Two Color DTW Results - B Filter												

Time(hrs)	Tray 1			Tray 2			Tray 3			RvG	GvB	RvB
	RvG	GvB	RvB	RvG	GvB	RvB	RvG	GvB	RvB			
-24	0.210	0.101	0.162	0.147	0.095	0.102	0.235	0.140	0.164	Mean	rmean	0.195
-16	0.217	0.139	0.159	0.158	0.104	0.110	0.189	0.114	0.134	0.195	0.117	0.139
-8	0.251	0.148	0.179	0.185	0.114	0.131	0.183	0.111	0.133			
0	0.177	0.095	0.131	0.168	0.747	0.739	0.186	0.761	0.757	2 Sigma		
8	0.240	0.145	0.169	0.169	0.099	0.124	0.156	0.102	0.109	0.259	0.153	0.189
16	0.222	0.157	0.158	0.179	0.115	0.132	0.144	0.097	0.100	3 Sigma		
24	0.199	0.123	0.144	0.138	0.099	0.097	0.224	0.149	0.161			
32	0.254	0.153	0.180	0.169	0.119	0.119	0.157	0.100	0.108	0.291	0.171	0.213
40	0.213	0.128	0.155	0.142	0.097	0.102	0.152	0.102	0.105			
48	0.201	0.119	0.146	0.147	0.100	0.103	0.169	0.118	0.118			

Table B.13: Moss tray images compared to the control and validated using a Welch t-test Time starts at the initial dosing (time 0) and continues 48 hours to compare the 3 laser systems (CoCoBi, Chl-A, and Chl-B with all 3 analysis methods (density difference, single color DTW, and two color DTW) in the blue or RvB color channel.

Tray 1	CoCoBi - Both Lasers						Chl-A w/ B Filter						Chl-B w/ B Filter					
Time (hrs)	DD		DTW-1		DTW-2		DD		DTW-1		DTW-2		DD		DTW-1		DTW-2	
0	0.22	1.74	12.41	1.80	9.57	1.77	0.52	1.74	2.80	1.73	0.09	1.73	0.67	1.74	8.17	1.80	2.78	1.79
8	0.17	1.75	5.35	1.78	5.29	1.75	0.05	1.75	1.91	1.73	0.10	1.74	0.16	1.75	0.64	1.77	0.74	1.74
16	0.54	1.74	5.92	1.76	12.03	1.74	0.35	1.73	2.47	1.73	1.52	1.74	0.57	1.74	3.66	1.77	1.25	1.75
24	0.40	1.74	1.83	1.78	1.78	1.73	0.91	1.74	2.09	1.74	3.04	1.76	1.27	1.74	5.83	1.79	1.63	1.79
32	0.75	1.74	0.38	1.74	1.75	1.74	0.13	1.74	2.99	1.74	1.11	1.73	0.02	1.74	1.26	1.75	1.23	1.75
40	1.35	1.73	8.60	1.75	8.18	1.80	0.60	1.74	5.42	1.80	0.60	1.75	0.36	1.74	2.06	1.77	1.39	1.75
48	0.95	1.73	18.61	1.78	8.77	1.78	0.35	1.73	5.91	1.73	2.52	1.74	0.72	1.73	4.30	1.75	1.65	1.77
Tray 2	CoCoBi - Both Lasers						Chl-A w/ B Filter						Chl-B w/ B Filter					
Time (hrs)	DD		DTW-1		DTW-2		DD		DTW-1		DTW-2		DD		DTW-1		DTW-2	
0	26.08	1.79	2.31	1.75	0.15	1.74	3.54	1.75	367.40	1.82	26.05	1.74	6.11	1.75	368.10	1.83	22.75	1.74
8	3.04	1.83	2.74	1.75	0.50	1.73	1.18	1.75	5.68	1.79	0.38	1.73	2.03	1.76	0.64	1.74	0.51	1.74
16	3.00	1.74	0.80	1.78	0.22	1.74	1.62	1.75	4.11	1.78	0.12	1.73	1.46	1.75	3.21	1.76	0.03	1.73

24	1.10	1.76	28.50	1.83	15.08	1.75	0.85	1.75	3.79	1.80	0.10	1.73	0.88	1.75	4.65	1.79	0.21	1.73
32	3.07	1.81	4.24	1.75	0.21	1.74	1.00	1.74	0.55	1.73	0.11	1.74	1.81	1.74	2.83	1.79	0.32	1.74
40	3.67	1.73	3.56	1.76	0.32	1.74	2.56	1.74	4.64	1.80	0.21	1.74	2.47	1.74	0.73	1.78	0.84	1.74
48	0.06	1.76	4.87	1.76	0.68	1.75	0.41	1.74	1.68	1.78	0.14	1.74	0.42	1.74	3.61	1.81	0.03	1.74
Tray 3	CoCoBi - Both Lasers						Chl-A w/ B Filter						Chl-B w/ B Filter					
Time (hrs)	DD		DTW-1		DTW-2		DD		DTW-1		DTW-2		DD		DTW-1		DTW-2	
0	19.05	1.77	5.49	1.81	0.41	1.74	7.93	1.74	393.00	1.78	20.18	1.74	10.98	1.74	303.50	1.75	14.77	1.74
8	3.62	1.77	0.73	1.75	0.33	1.77	3.06	1.76	1.88	1.75	0.48	1.73	2.97	1.75	1.41	1.79	0.79	1.73
16	4.47	1.74	5.42	1.81	1.71	1.74	2.81	1.74	6.44	1.79	0.49	1.74	2.61	1.74	2.93	1.76	1.18	1.74
24	1.07	1.74	7.10	1.82	0.84	1.74	1.36	1.73	4.86	1.76	1.05	1.74	1.50	1.73	2.91	1.78	0.07	1.73
32	3.20	1.74	4.73	1.76	0.58	1.77	2.89	1.75	0.73	1.80	0.07	1.73	2.85	1.75	2.80	1.81	0.82	1.73
40	4.05	1.73	4.49	1.77	0.62	1.73	3.09	1.74	2.63	1.74	0.23	1.74	2.94	1.74	2.58	1.77	0.95	1.73
48	0.57	1.74	8.08	1.82	1.34	1.73	0.47	1.73	4.63	1.77	0.35	1.73	0.51	1.73	0.68	1.74	1.18	1.74

6.2.4 Additional Metal and Chlorophyll Plots

6.2.4.1 Two color DTW versus wet Metals

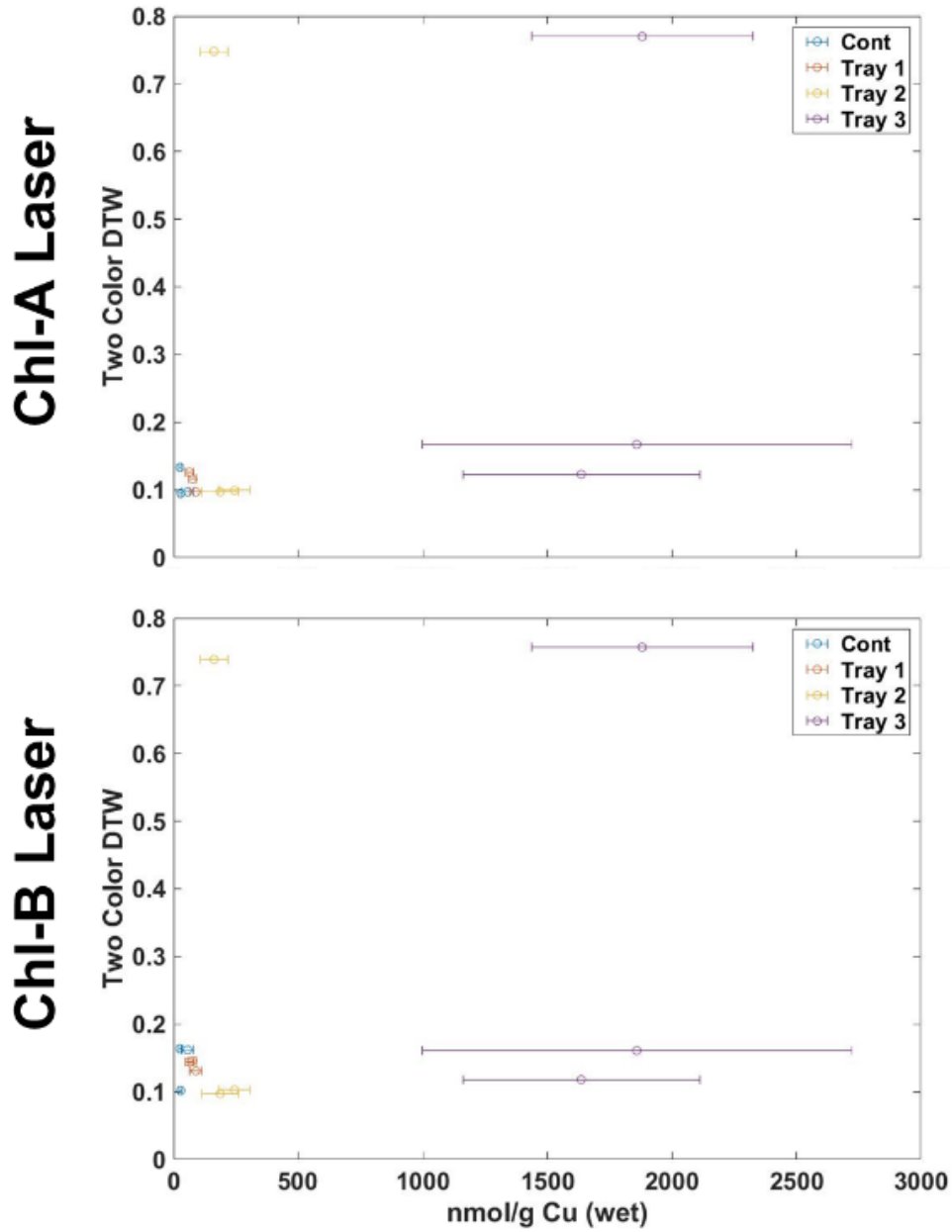


Figure B.10: Metal extraction results and wet weight of 10 pairs of fronds collected every 24 hours compared to Chl-A and Chl-B two color DTW results.

6.2.4.2 Chl versus two color DTW

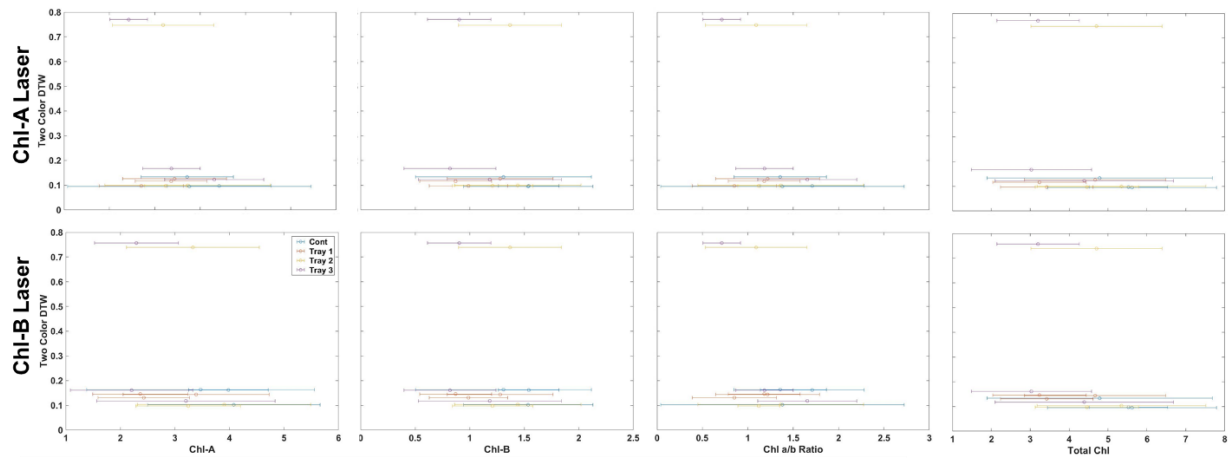


Figure B.11: Chlorophyll extraction results as Total Chl, chl-a and -b , and chl a/b ratio, compared to two color DTW results from images collected using the Chl-A (top) and Chl-B lasers (bottom) using the B filter.

6.2.4.3 Chl versus Cu wet weight

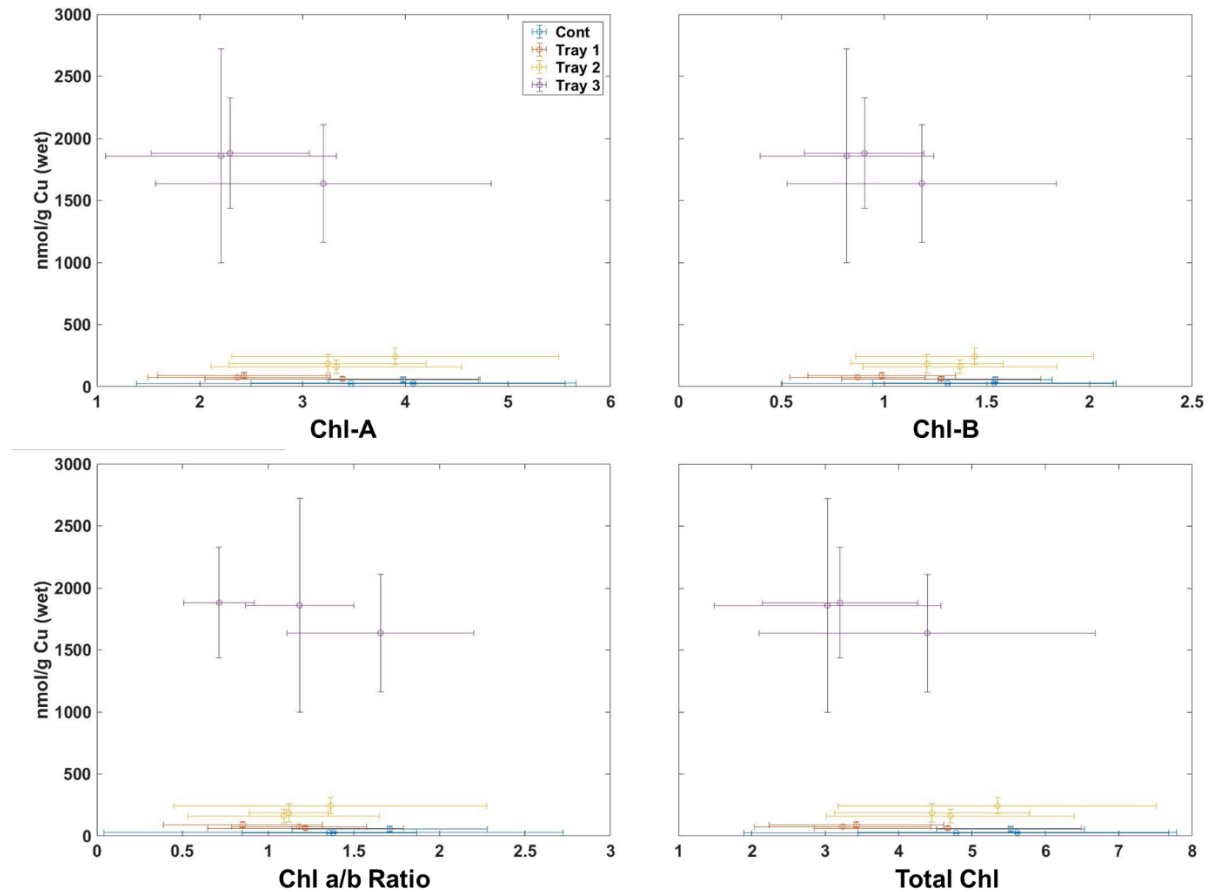


Figure B.12: Chlorophyll extraction versus metal extraction wet weight collected every 24 hrs. Time 0 samples are marked with a black circle.

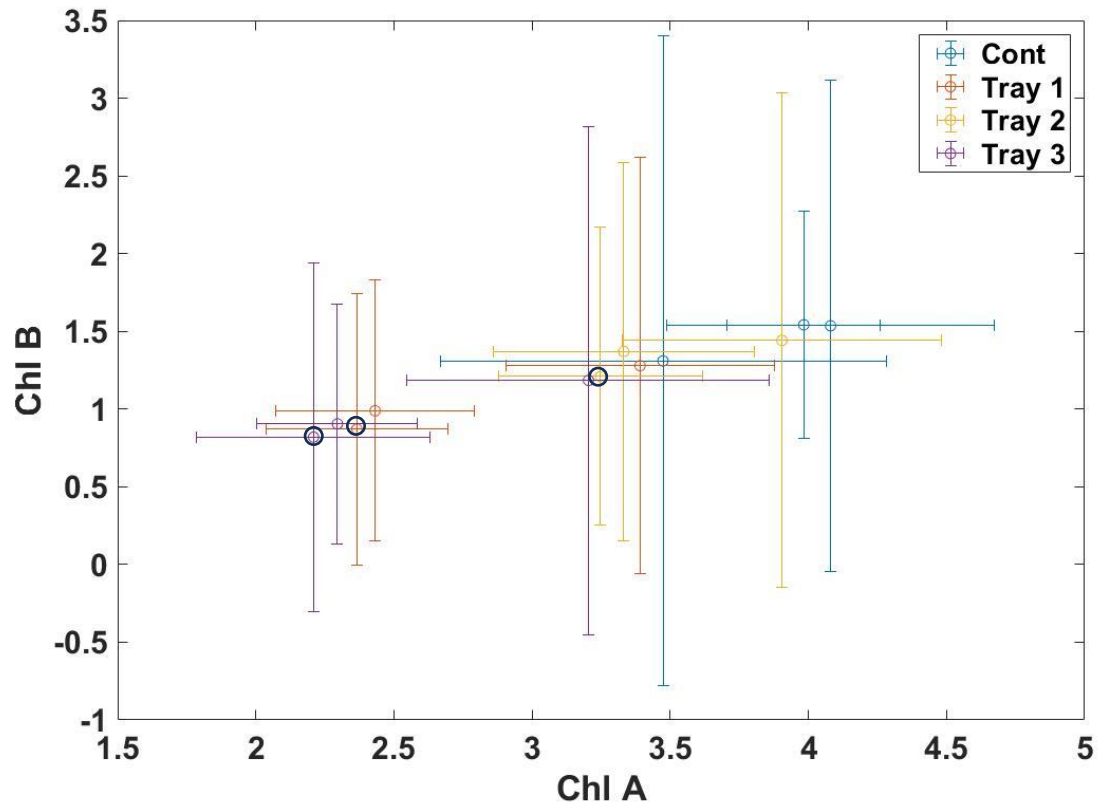


Figure B.13: Chl-a moss content versus chl-b moss content over the duration of the experiment. Black circles represent each moss tray at time 0 when dosed with Cu.

6.3 APPENDIX C

6.3.1 Image Analysis Results for all laser wavelengths and comparison methods

6.3.1.1 CoCoBi Single and Dual Laser

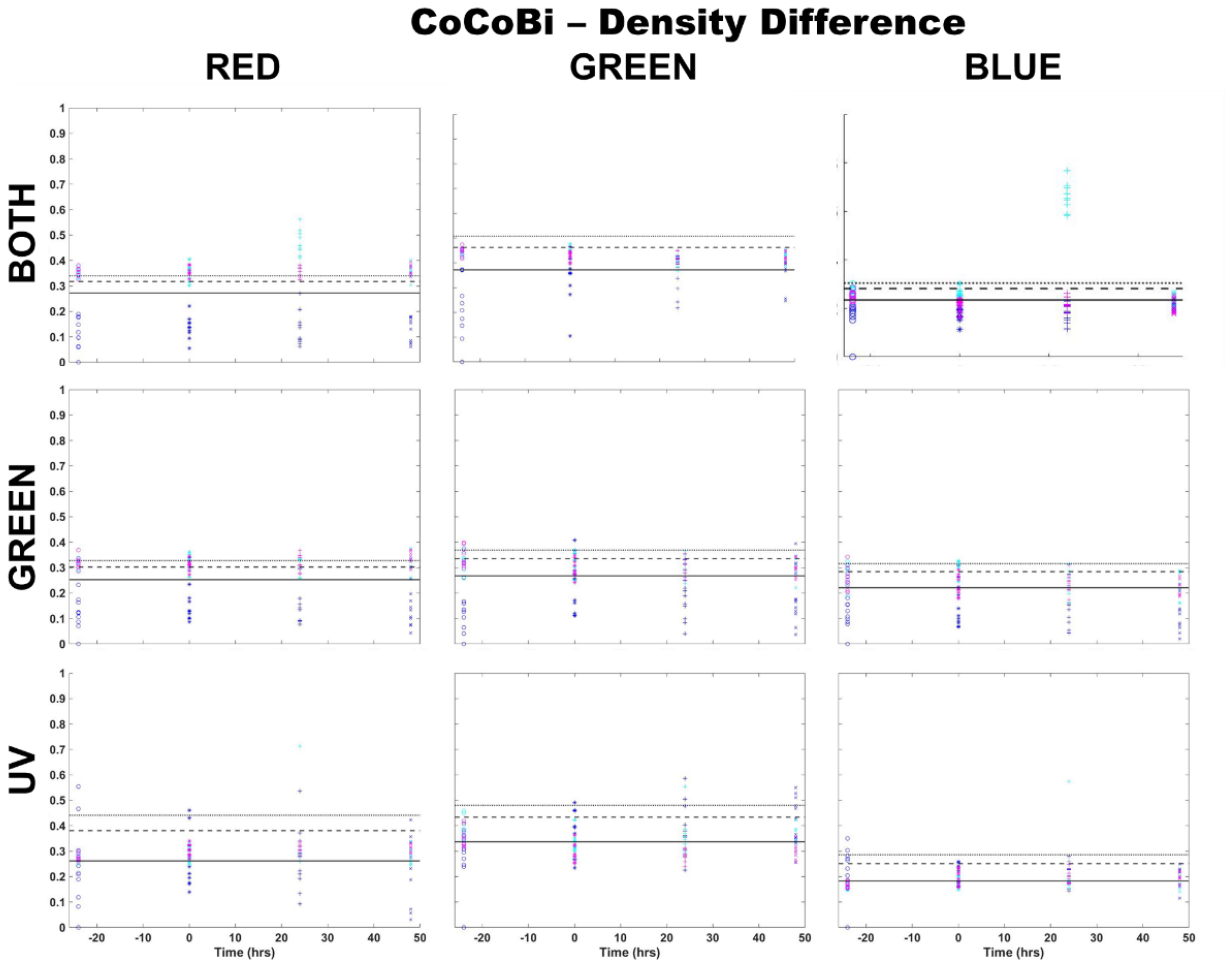


Figure C.1: Comparison of moss response to all lasers of the CoCoBi using single-color density difference to compare all color channels (R,G,B). Images of fronds were collected every 24 hours over three days. At time 0 three Cu treatments were given at 1 nmol/cm² for Tray 1 (blue), 10 nmol/cm² for Tray 2 (cyan), and 100 nmol/cm² for Tray 3 (magenta).

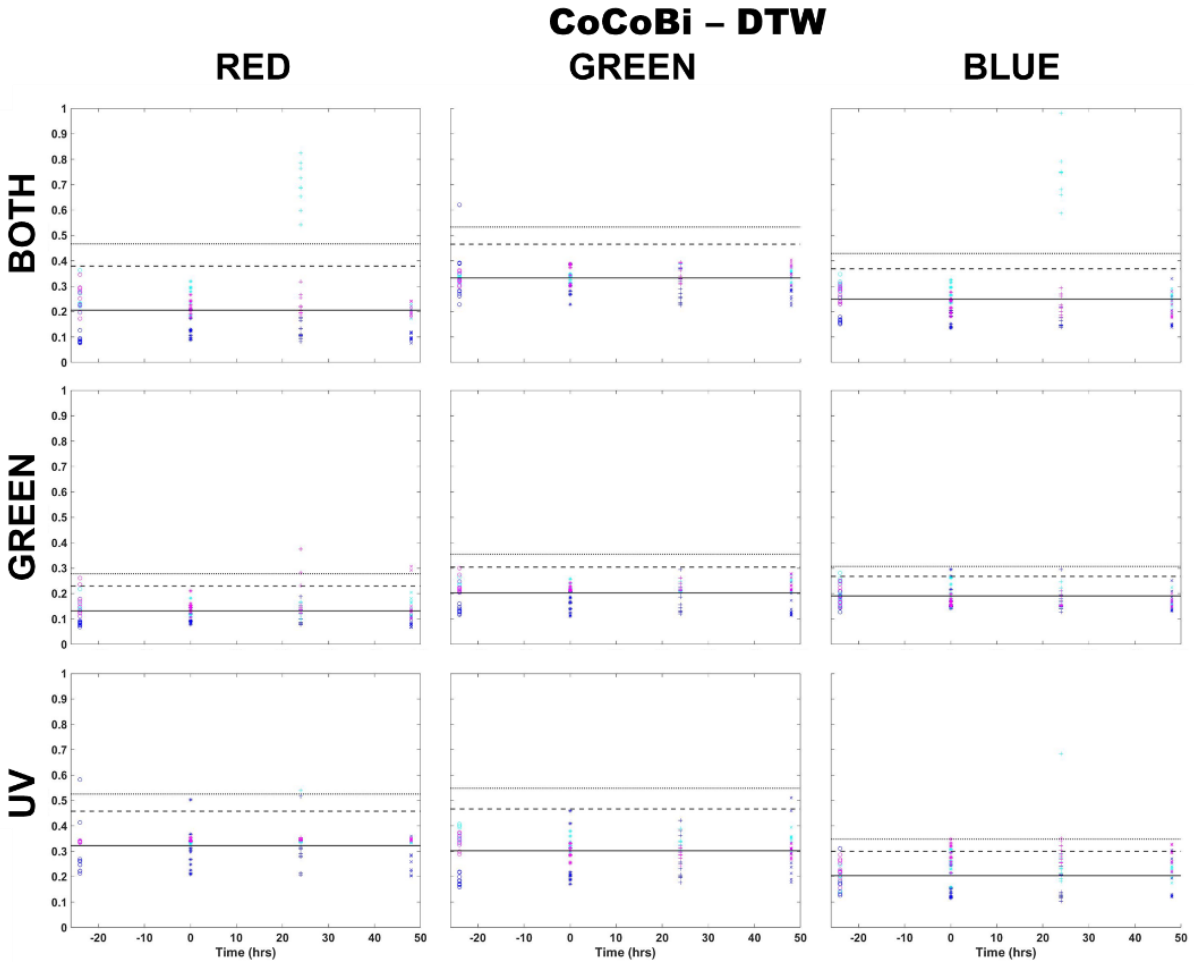


Figure C.2: Comparison of moss response to all lasers of the CoCoBi using single-color DTW to compare all color channels (R,G,B). Images of fronds were collected every 24 hours over three days. At time 0 three Cu treatments were given at 1 nmol/cm² for Tray 1 (blue), 10 nmol/cm² for Tray 2 (cyan), and 100 nmol/cm² for Tray 3 (magenta).

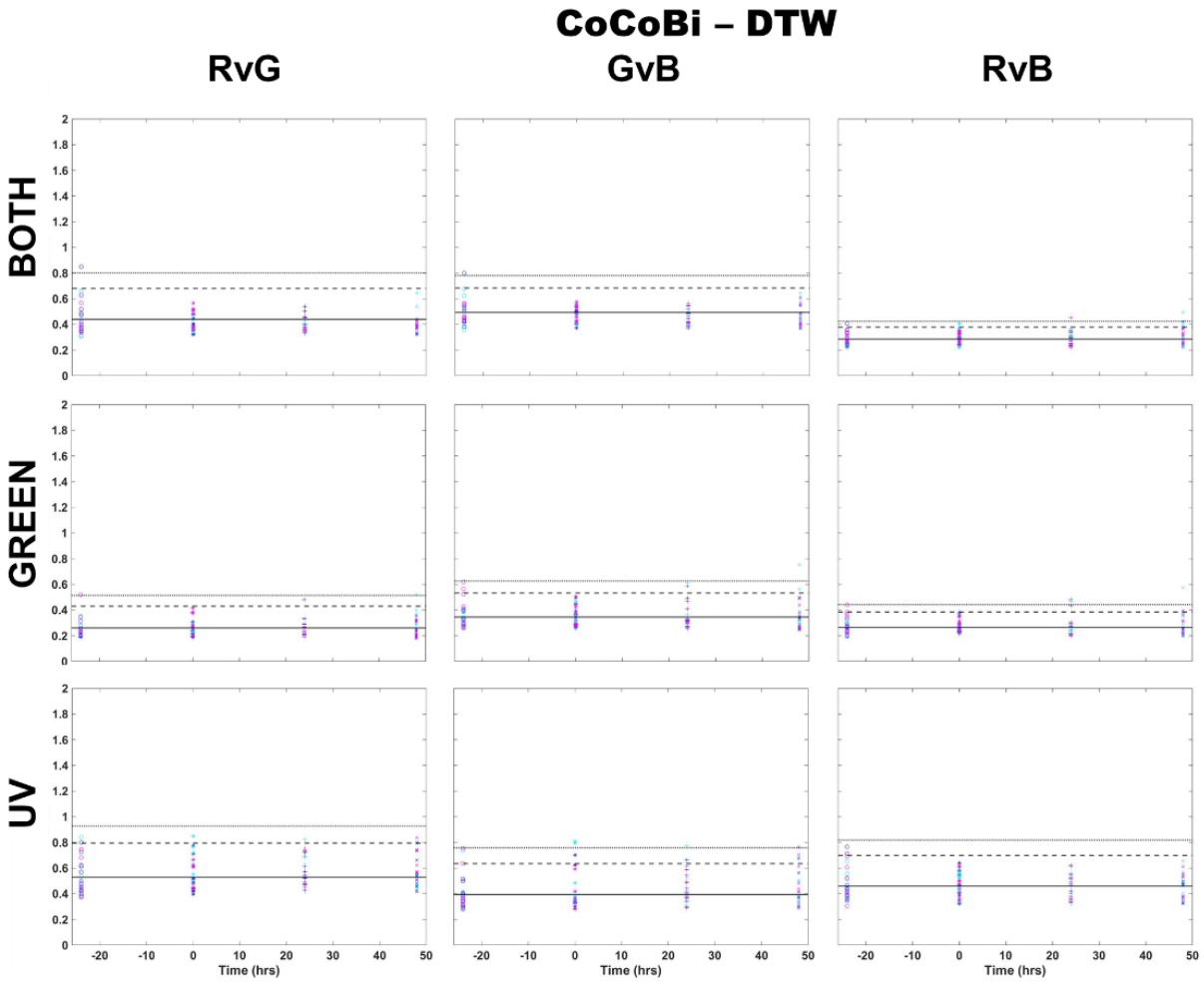


Figure C.3: Comparison of moss response to all lasers of the CoCoBi using two-color DTW to compare all color channels (R,G,B). Images of fronds were collected every 24 hours over three days. At time 0 three Cu treatments were given at 1 nmol/cm² for Tray 1 (blue), 10 nmol/cm² for Tray 2 (cyan), and 100 nmol/cm² for Tray 3 (magenta).

6.3.1.2 Chl-A with and without filter

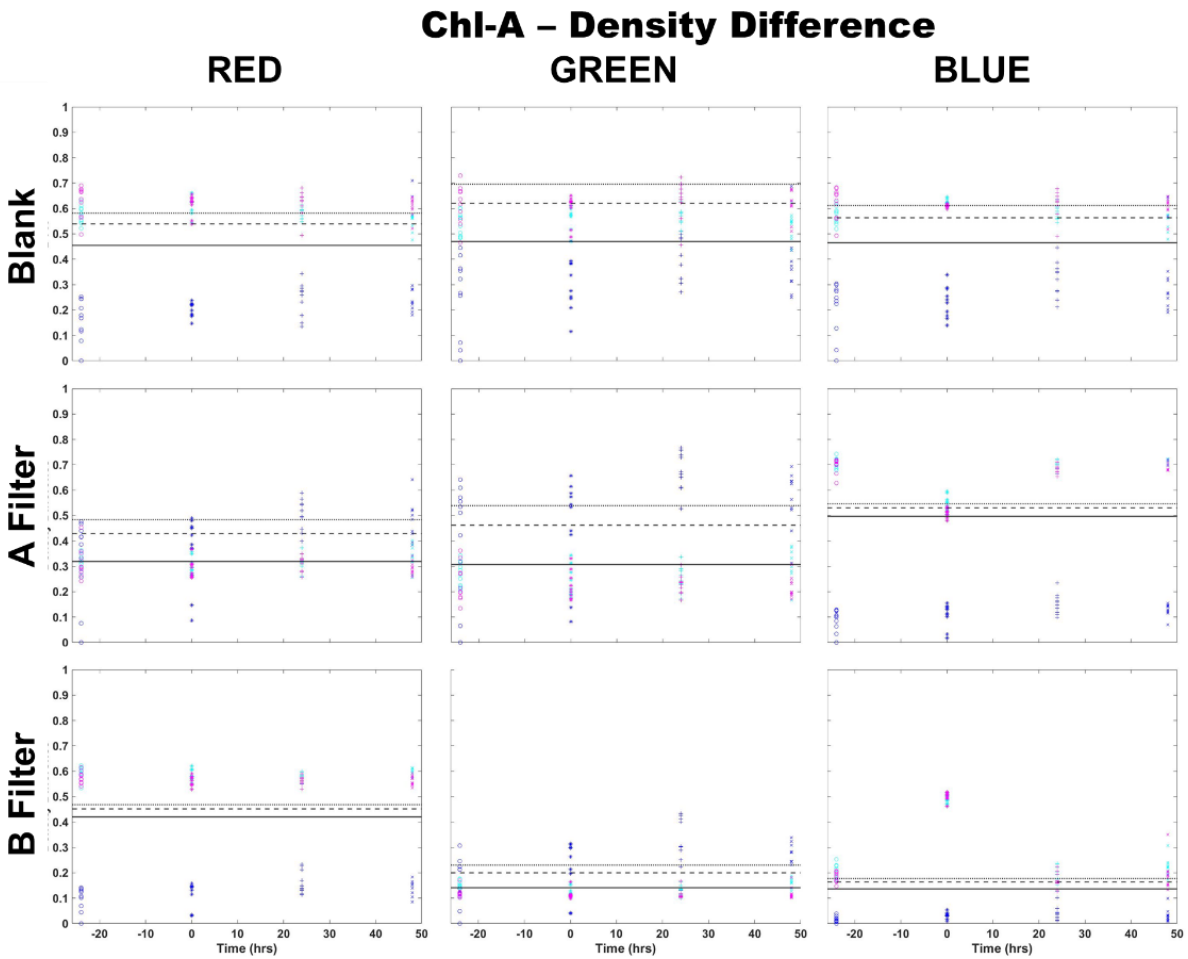


Figure C.4: Comparison of moss response to all filter options for the Chl-A laser using single-color density difference to compare all color channels (R,G,B). Images of fronds were collected every 24 hours over three days. At time 0 three Cu treatments were given at 1 nmol/cm² for Tray 1 (blue), 10 nmol/cm² for Tray 2 (cyan), and 100 nmol/cm² for Tray 3 (magenta).

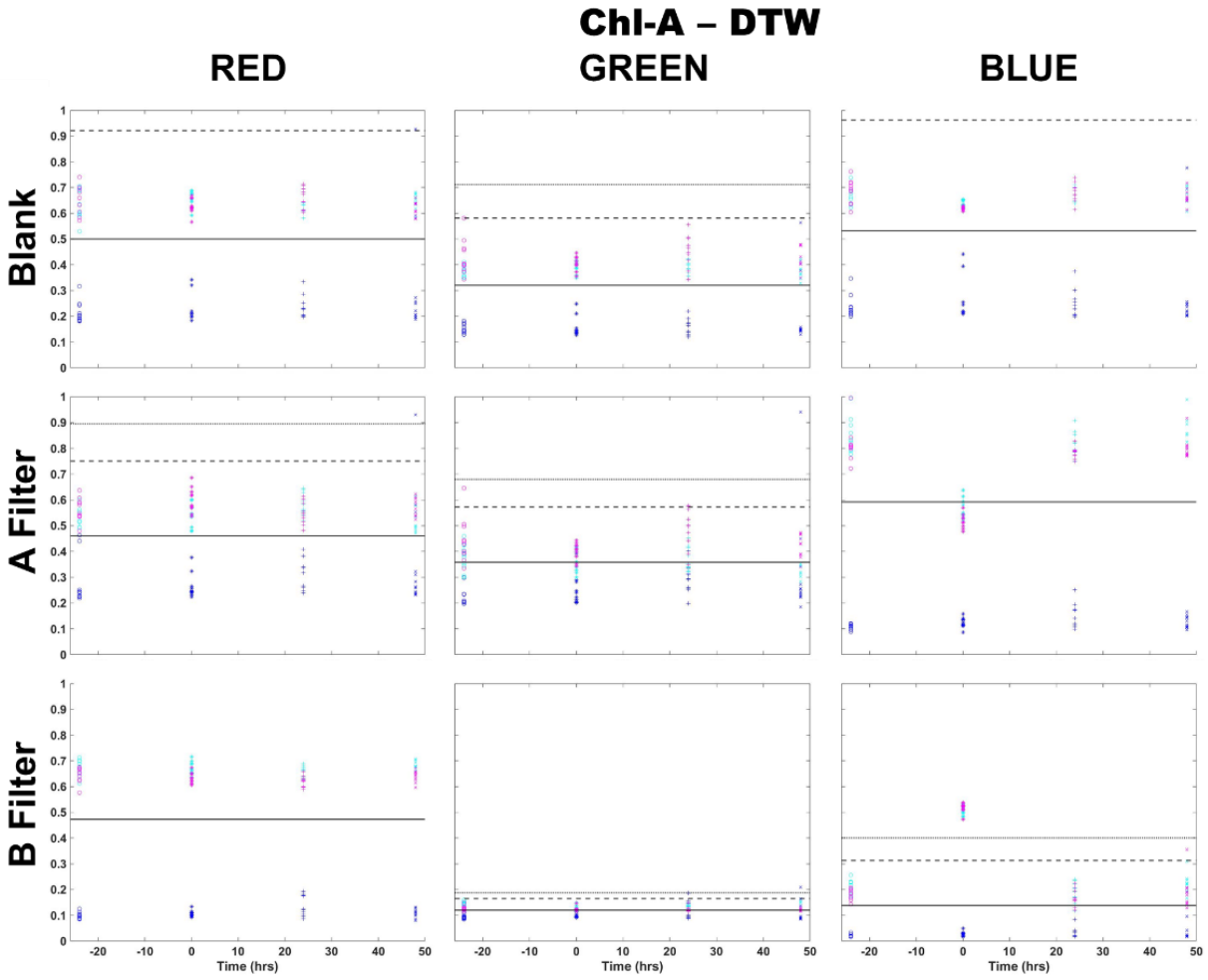


Figure C.5: Comparison of moss response to all filter options for the Chl-A laser using single-color DTW to compare all color channels (R,G,B). Images of fronds were collected every 24 hours over three days. At time 0 three Cu treatments were given at 1 nmol/cm^2 for Tray 1 (blue), 10 nmol/cm^2 for Tray 2 (cyan), and 100 nmol/cm^2 for Tray 3 (magenta).

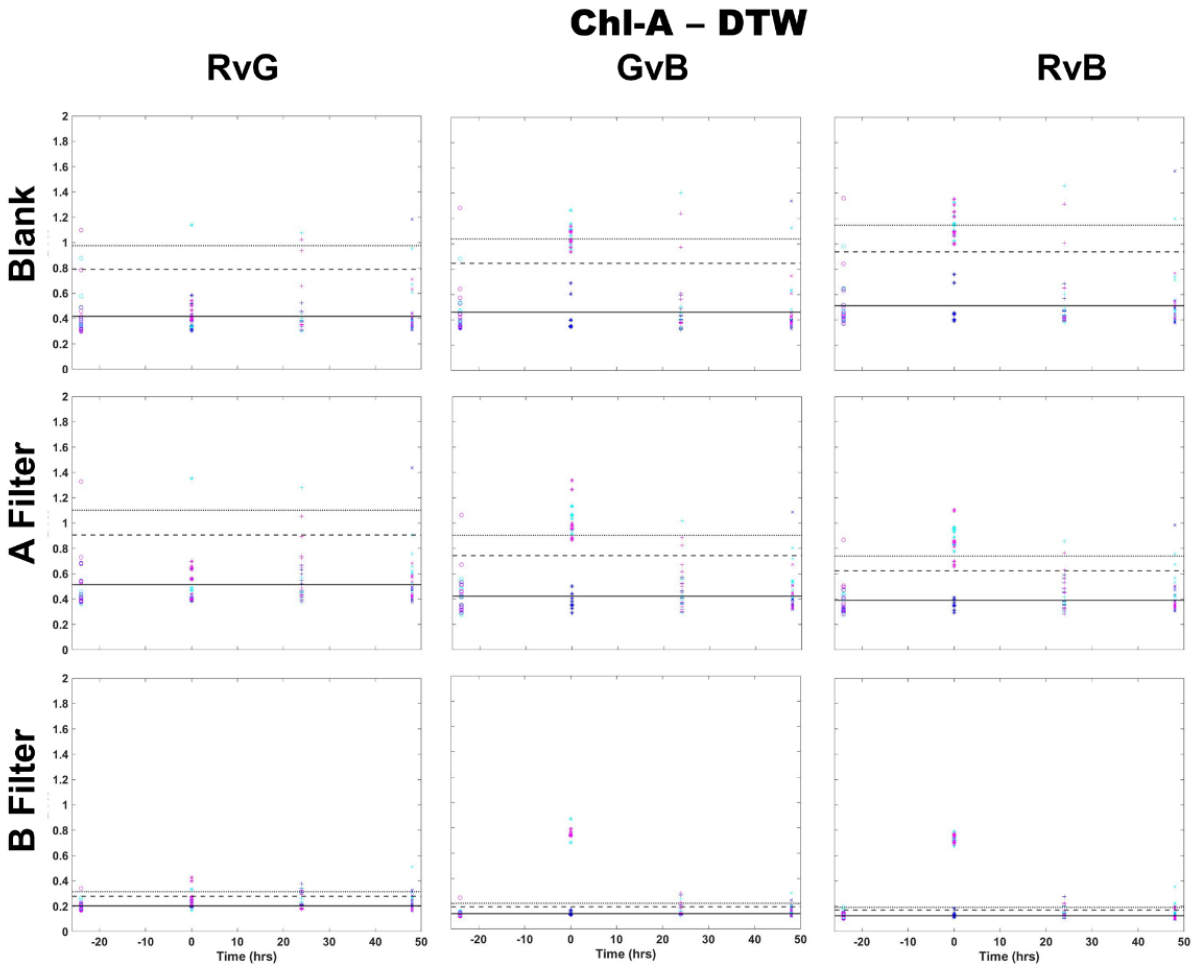


Figure C.6: Comparison of moss response to all filter options for the Chl-A laser using two-color DTW to compare all color channels (R,G,B). Images of fronds were collected every 24 hours over three days. At time 0 three Cu treatments were given at 1 nmol/cm² for Tray 1 (blue), 10 nmol/cm² for Tray 2 (cyan), and 100 nmol/cm² for Tray 3 (magenta).

6.3.1.3 Chl-B with and without filter

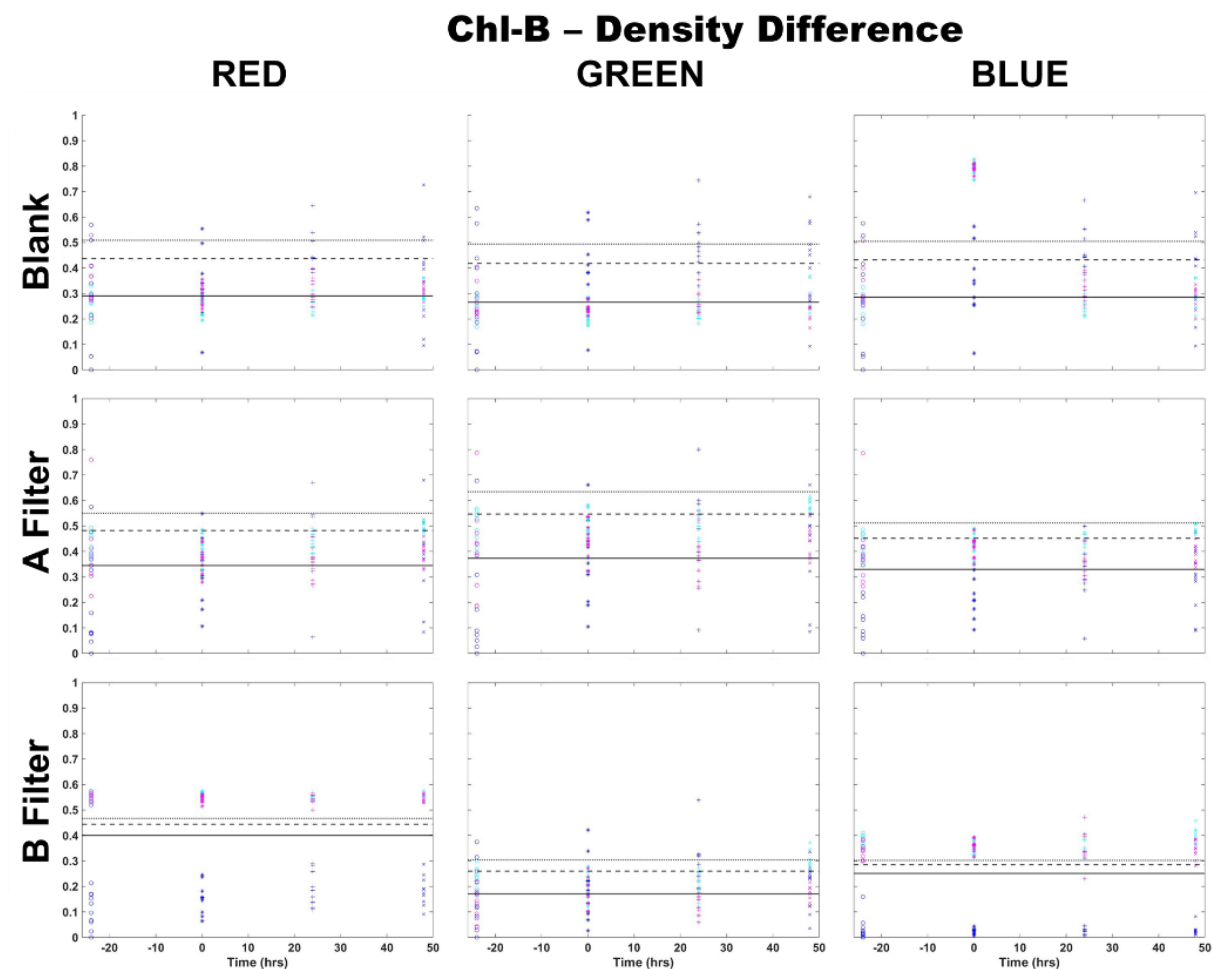


Figure C.7: Comparison of moss response to all filter options for the Chl-B laser using single-color density difference to compare all color channels (R,G,B). Images of fronds were collected every 24 hours over three days. At time 0 three Cu treatments were given at 1 nmol/cm² for Tray 1 (blue), 10 nmol/cm² for Tray 2 (cyan), and 100 nmol/cm² for Tray 3 (magenta).

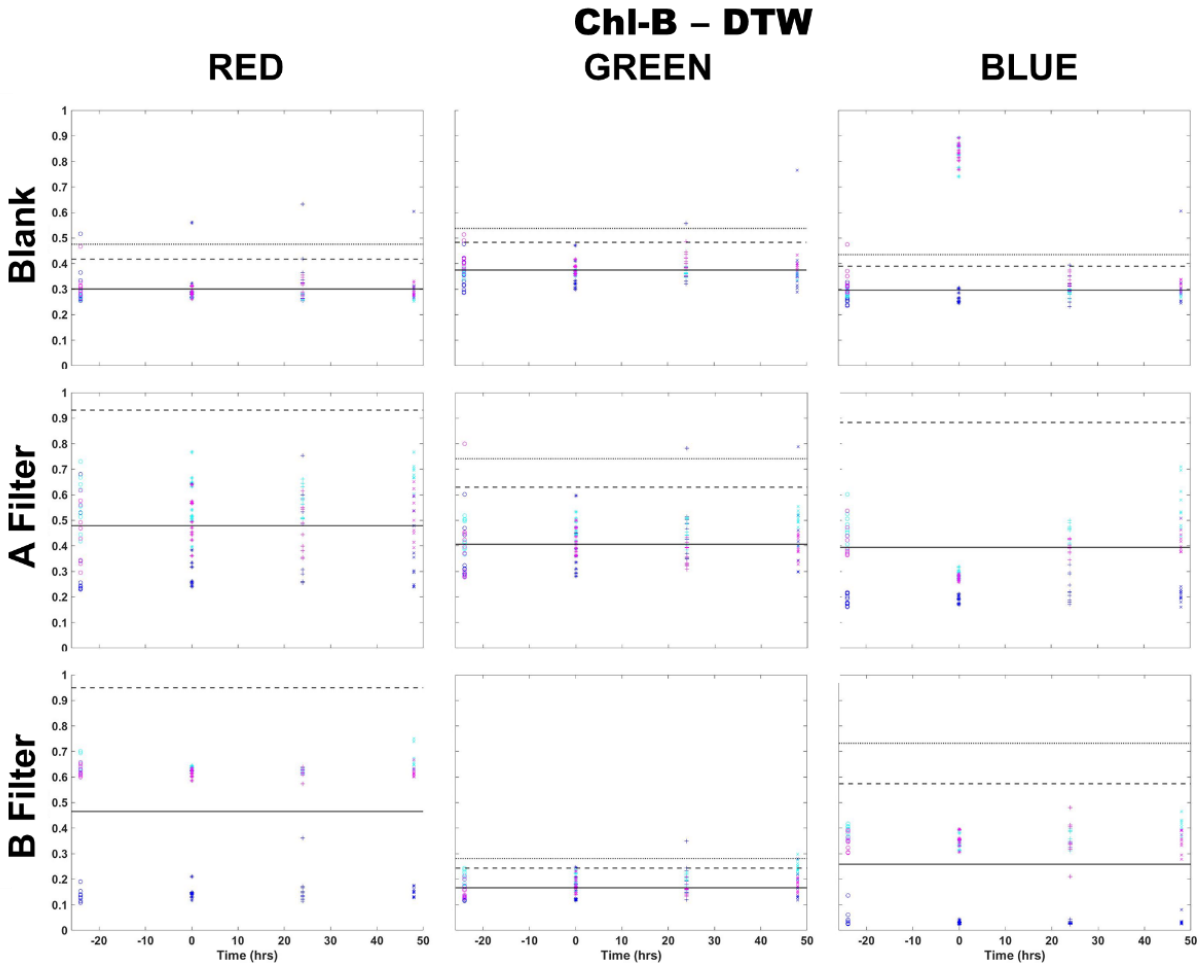


Figure C.8: Comparison of moss response to all filter options for the Chl-B laser using single-color DTW to compare all color channels (R,G,B). Images of fronds were collected every 24 hours over three days. At time 0 three Cu treatments were given at 1 nmol/cm² for Tray 1 (blue), 10 nmol/cm² for Tray 2 (cyan), and 100 nmol/cm² for Tray 3 (magenta).

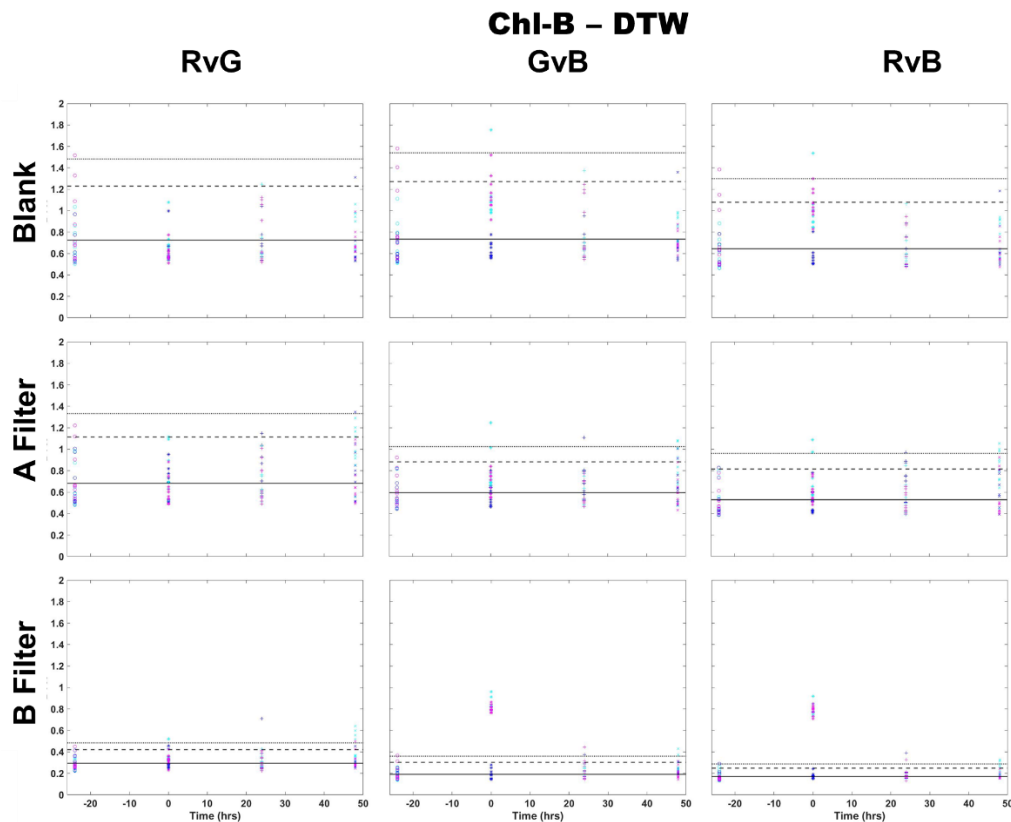


Figure C.9: Comparison of moss response to all filter options for the Chl-B laser using two-color DTW to compare all color channels (R,G,B). Images of fronds were collected every 24 hours over three days. At time 0 three Cu treatments were given at 1 nmol/cm^2 for Tray 1 (blue), 10 nmol/cm^2 for Tray 2 (cyan), and 100 nmol/cm^2 for Tray 3 (magenta).

6.3.2 Chlorophyll and Metal Results

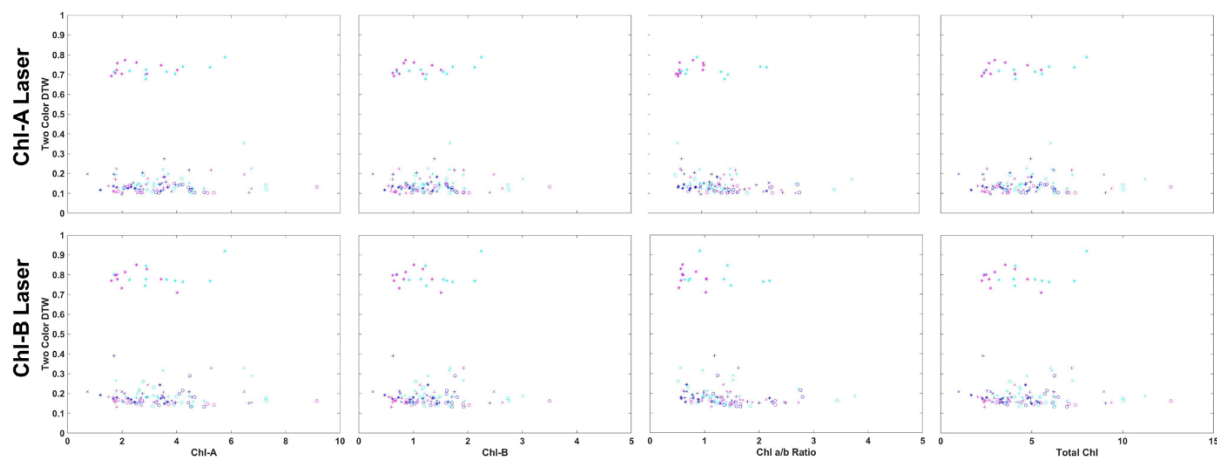


Figure C.10: Chlorophyll extraction results of Total Chl, chl-a and -b, and chl a/b ratio, compared to two color DTW (RvB) results from images collected using the Chl-A (top) and Chl-B lasers (bottom) using the B filter.

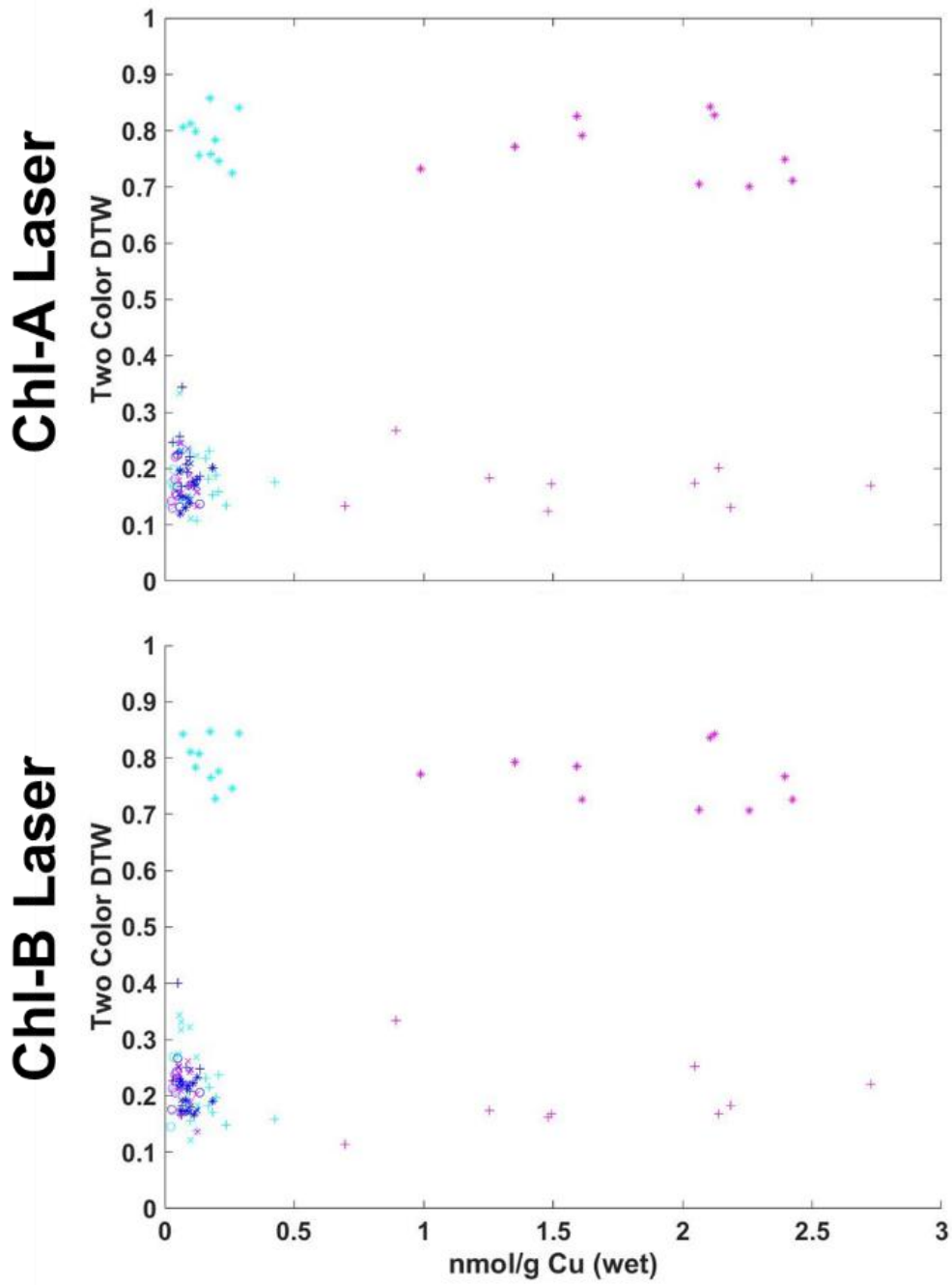


Figure C.11: Metal extraction results of Cu wet weight of fronds collected every 24 hours compared to Chl-A and Chl-B two color DTW results.

7 REFERENCES

- Aboal, J. R., Fernández, J. A., Boquete, T., & Carballeira, A. (2010). Is it possible to estimate atmospheric deposition of heavy metals by analysis of terrestrial mosses?. *Science of the Total Environment*, 408(24), 6291-6297. <https://doi.org/10.1016/j.scitotenv.2010.09.013>
- Al-Radady, A. S., Davies, B. E., & French, M. J. (1993). A new design of moss bag to monitor metal deposition both indoors and outdoors. *Science of the Total Environment*, 133, 275–283. [https://doi.org/10.1016/0048-9697\(93\)90249-6](https://doi.org/10.1016/0048-9697(93)90249-6)
- Bangare, S. L., Dubal, A., Bangare, P. S., & Patil, S. (2015). Reviewing Otsu's method for image thresholding. *International Journal of Applied Engineering Research*, 10(9), 21777-21783. <https://dx.doi.org/10.37622/IJAER/10.9.2015.21777-21783>
- Bardi, U. (2010). Extracting minerals from seawater: an energy analysis. *Sustainability*, 2, 980–992. <https://doi.org/10.3390/su2040980>
- Bates, J. W. (1992). Mineral nutrient acquisition and retention by bryophytes. *Journal of Bryology*, 17(2), 223-240. <https://doi.org/10.1179/jbr.1992.17.2.223>
- Berg, T., Røyset, O., Steinnes, E., & Vadset, M. (1995). Atmospheric trace element deposition: Principal component analysis of ICP-MS data from moss samples. *Environmental Pollution*, 88(1), 67–77. [http://doi.org/10.1016/0269-7491\(95\)91049-q](http://doi.org/10.1016/0269-7491(95)91049-q)
- Berg, T., & Steinnes E. (1997). Use of mosses (*Hylocomium splendens* and *Pleuroziumschreberi*) as biomonitors of heavy metal deposition: from relative to absolute deposition values. *Environmental Pollution*, 98, 61–71. [https://doi.org/10.1016/S0269-7491\(97\)00103-6](https://doi.org/10.1016/S0269-7491(97)00103-6)
- Bidwell, A. L., Callahan, S. T., Tobin, P. C., Nelson, B. K., & DeLuca, T. H. (2019). Quantifying the elemental composition of mosses in western Washington USA. *Science of the Total Environment*, 693, 133404. <https://doi.org/10.1016/j.scitotenv.2019.07.210>
- Blagnytè, R., & Paliulis, D. (2010). Research into heavy metals pollution of atmosphere applying moss as bioindicator: a literature review. *Environmental Research, Engineering and Management*, 54(4), 26-33. ISSN 2029-2139
- Brach, E. J., Molnar, J. M., & Jasmin, J. J. (1977). Detection of lettuce maturity and variety by remote sensing techniques. *Journal of Agricultural Engineering Research*, 22, 45–54. [https://doi.org/10.1016/0021-8634\(77\)90092-0](https://doi.org/10.1016/0021-8634(77)90092-0)
- Buschmann, C. (2007). Variability and application of the chlorophyll fluorescence emission ratio red/far red of leaves. *Photosynthesis Research*, 92, 261–271. <https://doi.org/10.1007/s11120-007-9187-8>
- Brooks, M. D., & Niyogi, K. K. (2011). Use of a pulse-amplitude modulated chlorophyll fluorometer to study the efficiency of photosynthesis in Arabidopsis plants. *Methods in Molecular Biology*, 775, 299-310. https://doi.org/10.1007/978-1-61779-237-3_16

- Brown, D. H., & Wells, J. M. (1988). Sequential elution technique for determining the cellular location of cations. In Glime, J.M. (Ed.). *Methods in bryology. Proceedings of the Bryological Methods*, 227-233. Nichinan: Hattori Botanical Laboratory. ISBN 493816310X
- Čeburnis, D., Rühling, Å., & Kvietkus, K. (1999). Extended study of atmospheric heavy metal deposition in Lithuania based on moss analysis. *Environmental Monitoring and Assessment*, 47, 135-152. <https://doi.org/10.1023/A:1005779101732>
- Čeburnis, D., Šakalys, J., Armolaitis, K., Valiulis, D., Kvietkus, K. (2002). In-stack emissions of heavy metals estimated by moss biomonitoring method and snow-pack analysis. *Atmospheric Environment*, 36, 1465 – 1474. [https://doi.org/10.1016/S1352-2310\(01\)00577-5](https://doi.org/10.1016/S1352-2310(01)00577-5)
- Chakraborty, S., & Paratkar, G. T. (2006). Biomonitoring of trace element air pollution using mosses. *Aerosol and Air Quality Research*, 6, 247–258. <https://doi.org/10.4209/aaqr.2006.09.0002>
- Chappelle, E. W., Wood, F. M., McMurtrey, J. E., & Newcomb, W. W. (1984). Laser-induced fluorescence of green plants. 1: A technique for the remote detection of plant stress and species differentiation. *Applied Optics*, 23, 134-138. <https://doi.org/10.1364/ao.23.000134>
- Chappelle, E. W., Wood, F. M., Newcomb, W. W., & McMurtrey, J. E. (1985). Laser-induced fluorescence of green plants. 3: LIF spectral signatures of five major plant types. *Applied Optics*, 24, 74-80. <https://doi.org/10.1364/ao.24.000074>
- Chaudhry, V., Runge, P., Sengupta, P., Doehlemann, G., Parker, J. E., & Kemen, E. (2021). Shaping the leaf microbiota: plant–microbe–microbe interactions. *Journal of Experimental Botany*, 72(1), 36–56. <https://doi.org/10.1093/jxb/eraa417>
- Choudhury, S., & Panda S. K. (2005). Toxic effects, oxidative stress and ultrastructural changes in moss *Taxithelium nepalense* (Schwaegr.) both under chromium and lead phytotoxicity. *Water, Air, Soil Pollution*, 167, 73–90. <https://doi.org/10.1007/s11270-005-8682-9>
- Colman, J. A., Rice, K. C., & Willoughby, T. C. (2001). Methodology and significance of studies of atmospheric deposition in highway runoff. Open-File Report 01-259. *US Geological Survey, Northborough, Massachusetts*. <https://pubs.usgs.gov/of/2001/ofr01-259/pdf/ofr01259.pdf>
- Crum, H., & Mueller-Dombois, D. (1968). Two new mosses from Hawaii. *Journal of the Hattori Botanical Laboratory*, 31, 293–296. <https://doi.org/10.11646/bde.25.1.7>
- Cui, X., Gu, S., Wu, J., & Tang, Y. 2009. Photosynthetic response to dynamic changes of light and air humidity in two moss species from the Tibetan Plateau. *Ecological Research*, 24, 645–653. <https://doi.org/10.1007/s11284-008-0535-8>
- Degola, F., De Benedictis, M., Petraglia, A., Massimi, A., Fattorini, L., Sorbo, S., Basile, A., & di Toppi, L. S. (2014). A Cd/Fe/Zn responsive phytochelatin synthase is constitutively present in

- the ancient liverwort *Luruciatenularia cruciata* (L.) Dumort. *Plant and Cell Physiology*, 55, 1884–1891. <https://doi.org/10.1093/pcp/pcu117>
- Dragovič, S., & Mihailovič, N. (2009). Analysis of mosses and topsoils for detecting sources of heavy metal pollution: multivariate and enrichment factor analysis. *Environmental Monitoring and Assessment*, 157, 383–390. <https://doi.org/10.1007/s10661-008-0543-8>
- de Temmerman, L., Bell, N. B., Garrec, J. P., Klumpp, A., Krause, G. H. M., & Tonneijck, A. E. G. (2001). Biomonitoring of air pollutants with plants - Considerations for the future. *Urban Air Pollution, bioindication and Environmental Awareness*. https://www.researchgate.net/publication/40798218_Biomonitoring_of_air_pollutants_with_plants_-_Considerations_for_the_future
- Fedotov, Y. V, Kravtsov, D. A., Belov, M. L., Cherpakova, A. A., & Gorodnichev, V. A. (2019). Experimental studies of laser-induced fluorescence spectra of plants under man-made soil pollution. *25th International Symposium on Atmospheric and Ocean Optics: Atmospheric Physics.*, 112083L. <https://doi.org/10.1117/12.2540100>
- Gameiro, C., Utkin, A. B., Cartaxana, P., Marques da Silva, J., & Matos, A.R. (2016). The use of laser induced chlorophyll fluorescence (LIF) as a fast and non-destructive method to investigate water deficit in Arabidopsis. *Agriculture Water Management*, 164, 127–136. <https://doi.org/10.1016/j.agwat.2015.09.008>
- García-Sánchez, F., Galvez-Sola, L., Martínez-Nicolás, J. J., Muelas-Domingo, R., & Nieves, M. (2017). Using Near-Infrared Spectroscopy in Agricultural Systems. *InTech*. <https://doi.org/10.5772/67236>
- Gatziolis, D., Jovan, S., Donovan, G. H., Amacher, M. C., & Monleon-Moscardo, V. J. (2016). Elemental atmospheric pollution assessment via moss-based measurements in Portland, Oregon. United States Department of Agriculture, Forest Service, Pacific Northwest Research Station. <https://doi.org/10.2737/PNW-GTR-938>
- Giannakoula, A., Therios, I., & Chatzissavvidis, C. (2021). Effect of lead and copper on photosynthetic apparatus in citrus (*Citrus aurantium* L.) plants. The role of antioxidants in oxidative damage as a response to heavy metal stress. *Plants*, 10(1), 155. <https://doi.org/10.3390/plants10010155>
- Gjengedal, E., & Steinnes, E. (1990). Uptake of metal ions in moss from artificial precipitation. *Environmental Monitoring and Assessment*, 14(1), 77-87. <https://doi.org/10.1007/BF00394359>
- González, A. G., & Pokrovsky, O. S. (2014). Metal adsorption on mosses: toward a universal adsorption model. *Journal of Colloid and Interface Science*, 415, 169-178. <https://doi.org/10.1016/j.jcis.2013.10.028>
- Haidekker, M. A., Dong, K., Mattos, E., & van Iersel, M. W. (2022). A very low-cost pulse-amplitude modulated chlorophyll fluorometer. *Computers and Electronics in Agriculture*, 203, 107438. <https://doi.org/10.1016/j.compag.2022.107438>

Hall J. L. (2002). Cellular mechanisms for heavy metal detoxification and tolerance. *Journal of Experimental Biology*, 53, 1-11. <https://doi.org/10.1093/jexbot/53.366.1>

Han, S. G., Kang, S. B., Moon, Y. I., Park J. H., Park. K. J., & Choi, Y. H. (2014). Establishment of analytical method for chlorophyll using the N,N-dimethylformamide and dimethylsulfoxide in citrus leaves. *Korean Journal of Environmental Agriculture*, 33(4), 344–349. <http://dx.doi.org/10.5338/KJEA.2014.33.4.344>

Heckathorn, S. A., Mueller, J. K., LaGuidice, S., Zhu, B., Barrett, T., Blair, B., Dong, Y. (2004). Chloroplast small heat-shock proteins protect photosynthesis during heavy metal stress. *American Journal of Botany*, 91, 1312–1318. <https://doi.org/10.3732/ajb.91.9.1312>

Hedimbi, M., Singh, S., & Kent, A. (2012). Laser induced fluorescence study on the growth of maize plants. *Natural Science*, 4, 395-401. <https://doi.org/10.4236/ns.2012.46054>.

Hoe, W.J. (1974). Annotated checklist of Hawaiian mosses. *Lyonia*, 1(1): 1–45. <http://hdl.handle.net/10125/10729>

Israsena Na Ayudhya, T., Posey, F. T., Tyus, J. C., & Dingra, N. N. (2015). Using a microscale approach to rapidly separate and characterize three photosynthetic pigment species from fern. *Journal of Chemical Education*, 92(5), 920-923. <https://doi.org/10.1021/ed500344c>

Jameson, D. M. (2014). Introduction to Fluorescence (1st ed.). CRC Press. <https://doi.org/10.1201/b16502>

Jeffrey, S. W., Mantoura, R. F. C., & Wright, S. W. (1997). Phytoplankton pigments in oceanography: Guidelines to modern methods. Paris: UNESCO Pub. ISBN 9231032755

Jeffrey, T. R., Schuerger, A. C., Capelle, G., & Guikema, J. A. (2003). Laser-induced fluorescence spectroscopy of dark-and light-adapted bean (*Phaseolus vulgaris* L.) and wheat (*Triticum aestivum* L.) plants grown under three irradiance levels and subjected to fluctuating lighting conditions. *Remote Sensing of Environment*, 84, 323–341 [https://doi.org/10.1016/S0034-4257\(02\)00115-3](https://doi.org/10.1016/S0034-4257(02)00115-3)

Jekel, C. F., Venter, G., Venter, M. P., Stander, N., & Haftka, R. T. (2018). Similarity measures for identifying material parameters from hysteresis loops using inverse analysis. *International Journal of Material Forming*. <https://doi.org/10.1007/s12289-018-1421-8>

Jiang, Y., Fan, M., Hu, R., Zhao, J., & Wu, Y. (2018). Mosses Are Better than Leaves of Vascular Plants in Monitoring Atmospheric Heavy Metal Pollution in Urban Areas. *International Journal of Environmental Research and Public Health*, 15(6), 1105. <https://doi.org/10.3390/ijerph15061105>.

Kinsey, J. L. (1977). Laser-Induced Fluorescence. *Annual Review of Physical Chemistry*, 28(1), 349–372. <https://doi.org/10.1146/annurev.pc.28.100177.002025>

Klimov, D., Ananyev, G., Rascher, U., Berry, J., & Osmond, B. (2005). Measuring photosynthetic parameters at a distance: Laser induced fluorescence transient (LIFT) method for

remote measurements of photosynthesis in terrestrial vegetation. *Photosynthesis Research*, 84, 121–129. <https://doi.org/10.1007/s11120-005-5092-1>

Kolber, Z., Klimov, D., Ananyev, G., Rascher, U., Berry, J., & Osmond, B. (2005). Measuring photosynthetic parameters at a distance: laser induced fluorescence transient (LIFT) method for remote measurements of photosynthesis in terrestrial vegetation. *Photosynthesis Research*, 84(1-3), 121–129. <https://doi.org/10.1007/s11120-005-5092-1>

Krause, G. H., & Weis, E. (1991). Chlorophyll fluorescence and photosynthesis: the basics. *Annual Review of Plant Physiology and Plant Molecular Biology*, 42, 313–349. <https://doi.org/10.1146/annurev.pp.42.060191.001525>

Kuang, Y. W., Zhou, G. Y., Wen, D. Z., & Liu, S. Z. (2007). Heavy metals in bark of *Pinus massoniana* (Lamb.) as an indicator of atmospheric deposition near a smeltery at Qujiang, China. *Environmental Science Pollution Research International*, 14(4), 270 – 275. <https://doi.org/10.1065/espr2006.09.344>

Lakowicz, J. R. (Ed.) (2006). Principles of fluorescence spectroscopy. Boston, MA: Springer US. <https://doi.org/10.1007/978-0-387-46312-4>

Lavrov, A., Utkin, A. B., Marques da Silva, J., Vilar, R., Santos, N. M., & Alves, B. (2012). Water stress assessment of cork oak leaves and maritime pine needles based on LIF spectra. *Optical Spectroscopy*, 112(2), 271–279. <https://doi.org/10.1134/S0030400X12020166>

Lefsrud, M. G., Kopsell, D. A., Augé, R. M., & Both, A.J. (2006). Biomass Production and Pigment Accumulation in Kale Grown Under Increasing Photoperiods. *HortScience*, 41(3), 603-606. <https://doi.org/10.21273/HORTSCI.41.3.603>

Lichtenthaler, H. K., Hák, R., & Rinderle, U. (1990). The chlorophyll fluorescence ratio F690/F730 in leaves of different chlorophyll contents. *Photosynthesis Research*, 25, 295–298. <https://doi.org/10.1007/BF00033170>

Maarek, J. I., & Kim, S. (2001). Multispectral excitation of time-resolved fluorescence of biological compounds: variation of fluorescence lifetime with excitation and emission wavelengths. *Proc. SPIE 4252, Advances in Fluorescence Sensing Technology V*. <https://doi.org/10.1117/12.426734>

Macedo-Miranda, G., Avila-Pérez, P., Gil-Vargas, P., Zarazúa, G., Sánchez-Meza, J. C., Zepeda-Gómez, C., & Tejeda, S. (2016). Accumulation of heavy metals in mosses: a biomonitoring study. *SpringerPlus*, 5(715). <https://doi.org/10.1186/s40064-016-2524-7>

Malenovský, Z., Turnbull, J. D., Lucieer, A., & Robinson, S. A. (2015). Antarctic moss stress assessment based on chlorophyll content and leaf density retrieved from imaging spectroscopy data. *New Phytologist*, 208(2), 608-624. <https://doi.org/10.1111/nph.13524>

Manzar Abbas, M., Melesse, A. M., Scinto, L. J., & Rehage, J. S. (2019). Satellite Estimation of Chlorophyll-a Using Moderate Resolution Imaging Spectroradiometer (MODIS) Sensor in

Shallow Coastal Water Bodies: Validation and Improvement. *Water*, 11(8), 1621. MDPI AG. <http://dx.doi.org/10.3390/w11081621>

Marques da Silva, Jorge; Borissovitch Utkin, Andrei (2018). Application of Laser-Induced Fluorescence in Functional Studies of Photosynthetic Biofilms. *Processes*, 6(11), 227. <https://doi.org/10.3390/pr6110227>

MATLAB Release 2021a, The MathWorks, Inc., Natick, Massachusetts, United States.

McMurtrey, J. E., Chappelle, E. W., Kim, M. S., Meisinger, J. J., & Corp, L. A. (1994). Distinguishing nitrogen fertilization levels in field corn (*Zea mays L.*) with actively induced fluorescence and passive reflectance measurements. *Remote Sensing of Environment*, 47(1), 36-44. [https://doi.org/10.1016/0034-4257\(94\)90125-2](https://doi.org/10.1016/0034-4257(94)90125-2)

Misra, A. K., Acosta-Maeda, T. E., Porter, J. N., Egan, M. J., Sandford, M., Gasda, P. J., Sharma, S. K., Lucey, P., Garmire, D., Zhou, J., Oyama, T., Acosta, N., McKay, C. P., Wiens, R. C., Clegg, S. M., Ollila, A. M., & Abedin, N. (2018). Standoff Biofinder: powerful search for life instrument for planetary exploration. *Lidar Remote Sensing for Environmental Monitoring XVI*. <https://doi.org/10.1117/12.2324201>

Misra, A. K., Acosta-Maeda, T. E., Zhou, J., Egan, M. J., Dasilveira, L., Porter, J. N., Rowley, S. J., Trimble, A. Z., Boll, P., Sandford, M. W., McKay, C. P., & Abedin, M. N. (2021). Compact Color Biofinder (CoCoBi): Fast, Standoff, Sensitive Detection of Biomolecules and Polyaromatic Hydrocarbons for the Detection of Life. *Applied Spectroscopy*, 75(11), 1427–1436. <https://doi.org/10.1177/00037028211033911>

Nagajyoti, P. C., Lee, K. D., & Sreekanth, T. V. M. (2010). Heavy metals, occurrence and toxicity for plants: a review. *Environmental Chemistry Letters*, 8, 199–216. <https://doi.org/10.1007/s10311-010-0297-8>

Nriagu, O. A. (1996). A history of global metal pollution. *Science*, 272(5259), 223. <https://doi.org/10.1126/science.272.5259.223>

Otsu, N. (1979). A Threshold Selection Method from Gray-Level Histograms. *IEEE Transactions on Systems, Man, and Cybernetics*, 9(1), 62-66. <https://doi.org/10.1109/TSMC.1979.4310076>.

Paode, R. D., Sofuoglu, S. C., Sivadechathep, J., Noll, K. E., Holsen, T. M., & Keeler, G. J. (1998). Dry deposition fluxes and mass size distributions of Pb, Cu, and Zn measured in Southern Lake Michigan during AEOLUS. *Environmental Science and Technology*, 32, 1629–1635. <https://doi.org/10.1021/es970892b>

Papenfus, M., Schaeffer, B., Pollard, A. I., & Loftin, K. (2020). Exploring the potential value of satellite remote sensing to monitor chlorophyll-a for US lakes and reservoirs. *Environmental Monitoring and Assessment*, 192, 808. <https://doi.org/10.1007/s10661-020-08631-5>

- Pérez-Llamazares, Alicia, Galbán-Malagón, Cristóbal J., Aboal, Jesús R., Fernández, J. Ángel and Carballeira, Alejo (2010). Evaluation of cations and chelating agents as extracellular extractants for Cu, Pb, V and Zn in the sequential elution technique applied to the terrestrial moss *Pseudoscleropodium purum*. *Ecotoxicology and Environmental Safety*, 73(4), 507-514. <https://doi.org/10.1016/j.ecoenv.2009.12.019>
- Peters K., Gorzolka K., Bruelheide H., & Neumann S. (2018). Seasonal variation of secondary metabolites in nine different bryophytes. *Ecology and Evolution*, 8(17), 9105-9117. <https://doi.org/10.1002/ece3.4361>
- Petschinger, K., Adlassnig, W., Sabovljevic, M. S., & Lang, I. (2021). Lamina Cell Shape and Cell Wall Thickness Are Useful Indicators for Metal Tolerance-An Example in Bryophytes. *Plants*, 10(2), 274. <https://doi.org/10.3390/plants10020274>.
- Porra, R.J. (2002). The chequered history of the development and use of simultaneous equations for the accurate determination of chlorophylls a and b. *Photosynthesis Research*, 73, 149–156. <https://doi.org/10.1023/A:1020470224740>
- Rai, P.K. (2016). Impacts of particulate matter pollution on plants: Implications for environmental biomonitoring. *Ecotoxicology and Environmental Safety*, 129, 120–136. <https://doi.org/10.1016/j.ecoenv.2016.03.012>
- Ram, S. S., Majumder, S., Chaudhuri, P., Chanda, S., Santra, S.C., Chakraborty, A., & Sudarshan, M. (2015). A review on air pollution monitoring and management using plants with special reference to foliar dust adsorption and physiological stress responses. *Critical Reviews in Environmental Science and Technology*, 45, 2489–2522. <https://doi.org/10.1080/10643389.2015.1046775>.
- Rastogi, A., Antala, M., Gąbka, M., Rosadziński, S., Stróżecki, M., Brestic, M., & Juszczak, R. (2020). Impact of warming and reduced precipitation on morphology and chlorophyll concentration in peat mosses (*Sphagnum angustifolium* and *S. fallax*). *Scientific Reports*, 10, 8592. <https://doi.org/10.1038/s41598-020-65032-x>
- Rocchetta, I., & Küpper, H. (2009). Chromium and copper induced inhibition of photosynthesis in *Euglena gracilis* analysed on the single-cell level by fluorescence kinetic microscopy. *New Phytologist*, 182, 405–420. <https://doi.org/10.1111/j.1469-8137.2009.02768.x>
- Rosman, K. J., Ly, C., & Steinnes, E. (1998). Spatial and temporal variation in isotopic composition of atmospheric lead in Norwegian moss. *Environmental Science and Technology*, 32, 2542-2546. <https://doi.org/10.1021/es9710215>
- Sarkar, P., Bosneaga, E., & Auer, M. (2009). Plant cell walls throughout evolution: Towards a molecular understanding of their design principles. *Journal of Experimental Botany*, 60, 3615–3635. <https://doi.org/10.1093/jxb/erp245>.
- Schreiber, U., Bilger, W., & Shliwa, U. (1986). Continuous recording of photochemical and non-photochemical quenching with a new type of modulation fluorometer. *Photosynthesis Research*, 10, 51–62. <https://doi.org/10.1007/BF00024185>

- Schreiber, U., & Bilger, W. (1993). Progress in Chlorophyll Fluorescence Research: Major Developments During the Past Years in Retrospect. Behnke, HD., Lüttge, U., Esser, K., Kadereit, J.W., Runge, M. (eds). *Progress in Botany*, 54. Springer, Berlin, Heidelberg. https://doi.org/10.1007/978-3-642-78020-2_8
- Schreiber, U. (2004). Pulse-Amplitude-Modulation (PAM) Fluorometry and Saturation Pulse Method: An Overview. In: Papageorgiou, G.C., Govindjee (eds) Chlorophyll a Fluorescence. *Advances in Photosynthesis and Respiration*, 19. Springer, Dordrecht. https://doi.org/10.1007/978-1-4020-3218-9_11
- Segura, A., de Wit, P., & Preston, G. M. (2009). Life of microbes that interact with plants. *Microbial Biotechnology*, 2(4), 412-5. <https://doi.org/10.1111/j.1751-7915.2009.00129.x>
- Serbula, M. S., Miljkovic, D. D., Kovacevic, M. R., & Ilic, A. A. (2012). Assessment of airborne heavy metal pollution using plant parts and topsoil. *Ecotoxicology and Environmental Safety*, 76, 209–214. <https://doi.org/10.1016/j.ecoenv.2011.10.009>
- Shakya, K., Chettri, M. K., & Sawidis, T. (2008). Impact of heavy metals (copper, zinc, and lead) on the chlorophyll content of some mosses. *Archives of Environmental Contamination and Toxicology*, 54, 412–421. <https://doi.org/10.1007/s00244-007-9060-y>
- Subhash, N., & Mohanan, C. N. (1997). Curve fit analysis of chlorophyll fluorescence spectra: Application to nutrient stress detection in sunflower. *Remote Sensing of Environment*, 60, 347–356. [https://doi.org/10.1016/S0034-4257\(96\)00217-9](https://doi.org/10.1016/S0034-4257(96)00217-9)
- Suchara, I., Sucharova, J., Hola, M., Reimann, C., Boyd, R., Filzmoser, P., & Englmaier, P. (2011). The performance of moss, grass, and 1- and 2-year old spruce needles as bioindicators of contamination: a comparative study at the scale of the Czech Republic. *Science of the Total Environment*, 409, 2281–2297. <https://doi.org/10.1016/j.scitotenv.2011.02.003>
- Sun, S. Q., He, M., Cao, T., Zhang, Y. C., & Han, W. (2009). Response mechanisms of antioxidants in bryophyte (*Hypnum plumaeforme*) under the stress of single or combined Pb and/or Ni. *Environmental Monitoring and Assessment*, 149, 291–302. <https://doi.org/10.1007/s10661-008-0203-z>
- Sun, H., Liu, S., Chen, K., & Li, G. (2021). Spectrophotometric determination of chlorophylls in different solvents related to the leaf traits of the main tree species in Northeast China. IOP Conference Series, Bristol. *Earth and Environmental Science*, 836(1). <https://doi.org/10.1088/1755-1315/836/1/012008>
- Stanković, J. D., Sabovljević, A. D., & Sabovljević, M. S. (2018). Bryophytes and heavy metals: a review. *Acta Botanica Croatica*, 77(2), 109–118. <https://doi.org/10.2478/botcro-2018-0014>
- Staples, G.W., Imada, C.T., Hoe, W.J., & Smith, C.W. (2004). A revised checklist of Hawaiian mosses. *Tropical Bryology*, 25, 35–69. <https://doi.org/10.11646/bde.25.1.7>

- Swain, M. J., Ballard, D. H. (1992). Indexing via Color Histograms. In: Sood, A.K., Wechsler, H. (eds) *Active Perception and Robot Vision*. NATO ASI Series, 83. Springer, Berlin, Heidelberg. https://doi.org/10.1007/978-3-642-77225-2_13
- Świsłowski, P., Nowak, A., & Rajfur, M. (2021a). Is Your Moss Alive during Active Biomonitoring Study?. *Plants*, *10*(11), 2389. <http://dx.doi.org/10.3390/plants10112389>
- Świsłowski, P., Nowak, A., & Rajfur, M. (2021b). The influence of environmental conditions on the lifespan of mosses under long-term active biomonitoring. *Atmospheric Pollution Research*, *12*(10), 101203. <https://doi.org/10.1016/j.apr.2021.101203>
- Swoczyna, T., Kalaji, H. M., Bussotti, F., Mojski, J., & Pollastrini, M. (2022). Environmental stress - what can we learn from chlorophyll a fluorescence analysis in woody plants? A review. *Frontiers in Plant Science*, *13*, 1048582. <https://doi.org/10.3389/fpls.2022.1048582>
- Szczepaniak, K., & Biziuk, M. (2003). Aspects of the biomonitoring studies using mosses and lichens as indicators of metal pollution. *Environmental Research*, *93*, 221–230. [https://doi.org/10.1016/S0013-9351\(03\)00141-5](https://doi.org/10.1016/S0013-9351(03)00141-5).
- Tan, J. Y., Ker, P. J., Lau, K. Y., Hannan, M. A., & Tang, S. G. H. (2019). Applications of Photonics in Agriculture Sector: A Review. *Molecules*, *24*(10), 2025. <https://doi.org/10.3390/molecules24102025>
- The Plant List (2013). Version 1.1. <http://www.theplantlist.org/>. accessed 1st July 2023.
- Touw, A. (2001). A taxonomic revision of the Thuidiaceae (Musci) of tropical Asia, the western Pacific, and Hawaii. *Journal of the Hattori Botanical Laboratory*, *91*, 1–136. https://doi.org/10.18968/jhbl.91.0_1
- Tremper, A. H., Agneta, M., Burton, S., & Higgs, D. E. (2004). Field and laboratory exposures of two moss species to low level metal pollution. *Journal of Atmospheric Chemistry*, *49*, 111–120. <https://doi.org/10.1007/s10874-004-1218-7>
- Truax, K., Dulai, H., Misra, A., Kuhne, W., & Fulkey, P. (2020). Quantifying Moss Response to Contaminant Exposure using Laser Induced Fluorescence (Master's thesis, University of Hawaii at Manoa, Honolulu, Hawaii, USA). <http://hdl.handle.net/10125/73329>
- Truax, K., Dulai, H., Misra, A., Kuhne, W., and Fulkey, P. (2022). Quantifying Moss Response to Metal Contaminant Exposure using Laser Induced Fluorescence. *Applied Sciences*, *12*(22), 11580. <https://doi.org/10.3390/app122211580>
- Valeur, B., & Berberan-Santos, M. N. (2011). A brief history of fluorescence and phosphorescence before the emergence of quantum theory. *Journal of Chemistry Education*, *88* (6), 731–738. <https://doi.org/10.1021/ed100182h>

- van Dobben, H. F., Wolterbeek, H. T., Wamelink, G. W. W., & Ter Braak, C. J. F. (2001). Relationship between epiphytic lichens, trace elements and gaseous atmospheric pollutants. *Environmental Pollution*, 112 (2), 163-169. [https://doi.org/10.1016/S0269-7491\(00\)00121-4](https://doi.org/10.1016/S0269-7491(00)00121-4)
- Vázquez, M. D., Lopez, J., & Carballeira, A. (1999a). Uptake of heavy metals to the extracellular and intracellular compartments in three species of aquatic bryophyte. *Ecotoxicology and Environmental Safety*, 44, 12–24. <http://doi.org/10.1006/eesa.1999.1798>
- Vázquez, M.D., Lopez, J., and Carballeira, A. (1999b). Modification of the sequential elution technique for the extraction of heavy metals from bryophytes. *Science of The Total Environment*, 241. [https://doi.org/10.1016/S0048-9697\(99\)00337-X](https://doi.org/10.1016/S0048-9697(99)00337-X)
- Vermette, S. J., Peden, M. E., Willoughby, T. C., Lindberg, S. E. and Weiss, A. D. (1995). Methodology for the sampling of metals in precipitation: results of the national atmospheric deposition pilot network. *Atmospheric Environment*, 29, 1221–1229. [https://doi.org/10.1016/1352-2310\(94\)00207-2](https://doi.org/10.1016/1352-2310(94)00207-2)
- Vernon, L.P. (1960). Spectrophotometric Determination of Chlorophylls and Pheophytins in Plant Extracts. *Analytical Chemistry*, 32 (9), 1144-1150. <https://doi.org/10.1021/ac60165a029>
- Wang, Q., Wu, N., Luo, P., Yi, S., Bao, W., & Shi, F. (2008). Growth rate of mosses and their environmental determinants in subalpine coniferous forests and clear-cuts at the eastern edge of the Qinghai-Tibetan Plateau, China. *Frontiers for Forestry in China*, 3(2), 171–176. <https://doi.org/10.1007/s11461-008-0030-y>
- Willoughby, T. C. (1995). Quality of wet deposition in the Grand Calumet River watershed, northwestern Indiana, June 30, 1992–August 31, 1993: U.S. Geological Survey Water-Resources Investigations Report 95- 4172, 55. <https://pubs.usgs.gov/wri/1995/4172/report.pdf>
- Wolterbeek, B. (2002). Biomonitoring of trace element air pollution: principles, possibilities and perspectives. *Environmental Pollution*, 120, 11–21. [https://doi.org/10.1016/S0269-7491\(02\)00124-0](https://doi.org/10.1016/S0269-7491(02)00124-0)
- Wong, C. S. C., Li, X., & Thornton, I. (2006). Urban environmental geochemistry of trace metals: a review. *Environmental Pollution*, 142, 1–16. <https://doi.org/10.1016/j.envpol.2005.09.004>
- WHO (2007) Health risks of heavy metals from long-range transboundary air pollution. World Health Organization 2007. WHO Regional Office for Europe Copenhagen, Denmark ISBN 978 92 890 7179 6
- World Flora Online (June 2023). *Thuidium Schimp.* <https://wfoplantlist.org/plant-list/taxon/wfo-4000038297-2023-06?page=1>. accessed July 1st, 2023.
- Yang-Er, C., Zhong-Wei, Z., Ming, Y., & Shu, Y. (2019). Perspective of Monitoring Heavy Metals by Moss Visible Chlorophyll Fluorescence Parameters. *Frontiers in Plant Science*, 10(35). <https://doi.org/10.3389/fpls.2019.00035>

Zhang, A., Cortés, V., Phelps, B., Van Ryswyk, H., & Srebotnjak, T. (2018). Experimental Analysis of Soil and Mandarin Orange Plants Treated with Heavy Metals Found in Oilfield-Produced Wastewater. *Sustainability*, *10*, 1493. <https://doi.org/10.3390/su10051493>.

Zhang, J., & Hu, J. (2008). Image Segmentation Based on 2D Otsu Method with Histogram Analysis. *International Conference on Computer Science and Software Engineering*. 105-108. Wuhan, China. <https://doi.org/10.1109/CSSE.2008.206>.